

This volume is the property of the University of Oklahoma, but the literary rights of the author are a separate property and must be respected. Passages must not be copied or closely paraphrased without the previous written consent of the author. If the reader obtains any assistance from this volume, he or she must give proper credit in his own work.

I grant the University of Oklahoma Libraries permission to make a copy of my thesis/dissertation upon the request of individuals or libraries. This permission is granted with the understanding that a copy will be provided for research purposes only, and that requestors will be informed of these restrictions.

NAME

[REDACTED]

DATE

05/10/2013

A library which borrows this thesis/dissertation for use by its patrons is expected to secure the signature of each user.

This thesis/dissertation by EMILIO JOSE TORRES PARADA has been used by the following persons, whose signatures attest their acceptance of the above restrictions.

NAME AND ADDRESS

DATE

UNIVERSITY OF OKLAHOMA  
GRADUATE COLLEGE

UNCONVENTIONAL GAS SHALE ASSESSMENT OF LA LUNA FORMATION,  
IN THE CENTRAL AND SOUTH AREAS OF THE MIDDLE MAGDALENA  
VALLEY BASIN, COLOMBIA.

A THESIS  
SUBMITTED TO THE GRADUATE FACULTY  
in partial fulfillment of the requirements for the  
Degree of  
MASTER OF SCIENCE

By

EMILIO JOSE TORRES PARADA  
Norman, Oklahoma  
2013

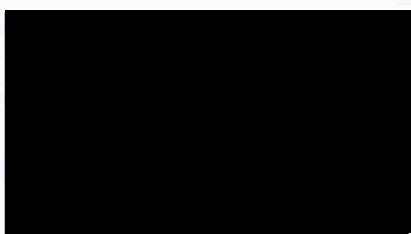


THESIS  
OR  
OP.3

UNCONVENTIONAL GAS SHALE ASSESSMENT OF LA LUNA FORMATION,  
IN THE CENTRAL AND SOUTH AREAS OF THE MIDDLE MAGDALENA  
VALLEY BASIN, COLOMBIA.

A THESIS APPROVED FOR THE  
CONOCOPHILLIPS SCHOOL OF GEOLOGY AND GEOPHYSICS

BY



Dr. R. Paul Philp, Chair



Dr. Roger M. Slatt



MSc. Brian J. Cardott

Copyright by ENGLAD 2013  
All Rights Reserved



## ACKNOWLEDGEMENTS

I would like to express my highest gratitude to many different people who supported and encouraged me throughout my goals and dreams.

I would like to express my deepest gratitude to Dr. K. Paul Filly who very generously accepted to be my advisor, for his guidance, counseling, friendship and support throughout my studies, especially providing funding for my maintenance and this research project. He is the best.

I also would like thank Dr. Roger M. Slav, who very kindly advised and helped my family and I throughout my studies and during the past two years, and who kindly accepted to be part of my committee and supported the research I am conducting during this research. He is the best friend and mentor.

I would like to thank my family for always being at my side, especially my mother, preparing and supporting me throughout my studies, and taking the time and effort to read my manuscript. I would like to thank my friends for always being there for me, especially my friends: *To Heydi, Simón and Lorenzo*  
*In Memoriam, Jose M. Torres Mantilla (1954-2012), my beloved Dad*  
*“Con Dios todo y sin el nada”.*

I would like to thank my gratitude to Dr. Neil O'Brien from the State University of New York at Binghamton, for his kindly support and help for the SEM images writing and editing.

I would like to thank to the people from the Spanish Government Library, in particular to Mr. Juan Carlos for his helpful technical support, to Dr. Thanh Nguyen, Dr. Corinne Blache, Dr. Alexander Alkhalaf, Mr. Tang Wang, Mr. Nicolas Sabin, Mr. Larry Hayes and Mrs. Brenda Van Alphen for their assistance, to Mrs. Andrea Martínez-Rodrigo for her time, advice and recommendations.

## ACKNOWLEDGEMENTS

I would like to express my highest gratitude to many different people who supported and encouraged me to pursue my goals and dreams.

I would like to express my deepest gratitude to Dr. R. Paul Philp who very generously accepted to be my advisor, for his guidance, mentoring, friendship and support throughout my Masters, and for providing funding for my assistantship and this research project.

I also want to thank Dr. Roger M. Slatt, who very kindly advised and helped my family and I for coming to OU and during the past two years, and also nicely accepted to be part of my committee and supported the reservoir characterization part of this research. He is more than a friend and mentor.

To Mr. Brian Cardott for serving on my committee, for his kindly help for preparing and measuring the vitrinite reflectance on my samples and for his great suggestions and interest, and taking the time and dedication in reviewing this manuscript.

I wish to extend my gratitude to Dr Neil O'Brien from the State University of New York at Potsdam, for his kindly support and help for the SEM images training and analysis.

My appreciation to the people from the Organic Geochemistry Laboratory, in particular to Mr. Jon Allen for his helpful technical support; to Dr. Than Nguyen, Dr Coralie Biache, Dr Alsharif Albaghdady, Mr. Ting Wang, Mr Kirellos Sefein, Mr. Larry Hayde and Mrs. Brandi Van Alphen for their assistance; to Mrs. Andrea Miceli-Romero for her time, advices and recommendations.

My appreciation to the OU Institute of Reservoir Characterization (IRC) for the financial and technical support. Also I would like to thank to IRC current and former members, for all the technical discussions and recommendations during my thesis research experience.

I want to acknowledge the entire faculty and staffs of the School of Geology and Geophysics, for helping me grow as a professional and contributing in achieving my Master's degree. I also would like to show my special appreciation to Mrs. Nancy Leonard.

Many thanks to all my friends who have accompanied me during this journey, for their joy, help and support, to The Colombian and Venezuelan "Mafia": Jean Amorocho, Luz Angela Guzman, Andrea Serna, Carlos Molinares, Adriana Gomez, Rafael Sierra, Andrea Cadena, Luis Castillo, Andrea Miceli, Oswaldo Davogusto, Richard Brito, Alfredo Fernandez and Carlos Cerón.

My most special thanks are extended to my Mom, Dad and Brother who are the dearest people in my life. Thank you for your love, patience, and support. For always trust in me. In the loving memory of my father, who always believed and supported my goals.

A special dedication to my lovely and wonderful wife, Heydi Rodriguez, for her priceless love and support, for believing that coming to OU has been the best journey of our lives and for always encouraging me through each step of the way, and for giving me the best thing I ever had, our son Simon. Also thanks to Heydi for her important technical support with the SEM porosity calculations, without her nothing could be done. To our puppy Lorenzo. Thank you all very much.



## TABLE OF CONTENTS

<b>ABSTRACT .....</b>	<b>XIV</b>
<b>CHAPTER I.....</b>	<b>1</b>
<b>1. INTRODUCTION.....</b>	<b>1</b>
1.1.    BACKGROUND OF THESIS TOPIC.....	5
1.1.1.    Thesis Scientific Problem.....	7
1.1.2.    Regional Framework .....	7
1.2.    GEOLOGIC FRAMEWORK.....	8
1.2.1.    Regional Basin Geology.....	8
1.2.2.    Basin Boundaries (ANH, 2008). .....	9
1.2.3.    Basin Development and Petroleum System .....	11
1.2.4.    Petroleum System Elements of MMVB .....	13
1.2.5.    La Luna Formation. Previous geological description studies.....	15
1.3.    THESIS RESEARCH GOAL AND OBJECTIVES .....	16
<b>CHAPTER II .....</b>	<b>18</b>
<b>2. METHODOLOGY.....</b>	<b>18</b>
2.1.    STUDY AREAS AND SAMPLE LOCATIONS.....	18
2.1.1.    South East MMVB Stratigraphic Section, OUTCROP A. ....	18
2.1.2.    Central MMVB Stratigraphic Section, OUTCROP B. ....	21
2.2.    EXPERIMENTAL .....	32
2.3.    SOURCE ROCK CHARACTERIZATION.....	32
2.3.1.    Preliminary Sample Treatment.....	37
2.3.2.    Total Organic Carbon (TOC) and Rock Eval Pyrolysis.....	37
2.3.3.    Vitrinite Reflectance.....	37
2.3.4.    Extraction and Fractionation .....	38
2.3.5.    Gas Chromatography (GC).....	39
2.3.6.    Gas Chromatography-Mass Spectrometry (GC-MS) .....	39
2.3.7.    Micro-Scale Sealed Vessel( MSSV). ....	41
2.4.    RESERVOIR ROCK CHARACTERIZATION .....	42
2.4.1.    Scanning Electron Microscopy (SEM).....	42
2.4.2.    Thin section analysis .....	43
2.4.3.    XRD.....	44
2.4.4.    Organic Geochemistry TOC and RHP Profiling.....	44

<b>CHAPTER III.....</b>	<b>46</b>
<b>3. RESULTS AND DISCUSSIONS .....</b>	<b>46</b>
3.1. SOURCE ROCK CHARACTERIZATION.....	46
3.1.1. Organic Richness.....	46
3.1.2. Kerogen Type .....	56
3.1.2.1. OUTCROP A Kerogen Type.....	56
3.1.2.2. OUTCROP B Kerogen Type.....	59
3.1.3. Thermal Maturity.....	63
3.2. BIOMARKER ANALYSIS.....	78
3.2.1. n-Alkanes.....	78
3.2.2. Pristane and Phytane.....	86
3.2.3. Steranes.....	88
3.2.3.1. Diasteranes .....	96
3.2.3.2. Pregnane and homopregnane.....	97
3.2.4. Terpanes .....	99
3.2.5. Biodegradation .....	112
3.3. LITHOFACIES CHARACTERIZATION.....	116
3.3.1. Lithofacies Definition, outcrop and thin Section descriptions. ....	116
3.3.1.1. Lithofacies and Organic Facies in the Salada member. ....	116
3.3.1.2. Lithofacies and Organic Facies in the Pujamana member. ....	117
3.3.1.3. Lithofacies and Organic Facies in the Galembo member. ....	127
3.3.2. XRD Results.....	129
3.3.3. SEM Analysis.....	134
3.3.3.1. Pore Classification.....	134
3.3.3.2. SEM microfabric and porosity characterization.....	136
3.4. PALEOENVIRONMENTAL INTERPRETATION.....	153
3.5. SEQUENCE STRATIGRAPHY INTERPRETATION.....	155
<b>CONCLUSIONS. UNCONVENTIONAL ASSESMENT.....</b>	<b>161</b>
<b>RECOMMENDED FUTURE WORK .....</b>	<b>165</b>
<b>BIBLIOGRAPHY.....</b>	<b>166</b>
<b>APPENDICES.....</b>	<b>188</b>



## LIST OF FIGURES

<b>Figure 1.</b>	U.S. shale gas plays, lower 48 states (EIA, May 9, 2011). Source: Energy Information Administration, 2012. ....	2
<b>Figure 2.</b>	Geographic map of Colombia, showing the 2012 Open bid leasing blocks (Dark blue polygons). Source: ANH 2012. ....	6
<b>Figure 3.</b>	Map of Colombia with its main tectonic domains. ....	10
<b>Figure 4.</b>	Location of the Middle Magdalena Valley Basin, Colombia. ....	10
<b>Figure 5.</b>	General stratigraphic column and Petroleum System elements of the Middle Magdalena Valley Basin, Colombia. ANH, 2008. ....	14
<b>Figure 6.</b>	Map showing the location of the Cretaceous outcrops in MMVB. ....	20
<b>Figure 7.</b>	Erosive contact of la Luna Fm top and Umir Fm base, OUTCROP A. ....	23
<b>Figure 8.</b>	Contact of la Luna Fm top and Umir Fm basal coalbed, OUTCROP A. ....	23
<b>Figure 9.</b>	La Luna Fm Galembo member, OUTCROP A. ....	24
<b>Figure 10.</b>	Contact of Galembo and Pujamana members, OUTCROP A. ....	25
<b>Figure 11.</b>	Salada member, OUTCROP A. ....	26
<b>Figure 12.</b>	Stratigraphic column of the Galembo member in OUTCROP A. ....	27
<b>Figure 13.</b>	Contact of La Luna Fm top contact with Umir Fm base, OUTCROP B. ....	28
<b>Figure 14.</b>	La Luna Fm Salada outcrop in a quarry, OUTCROP B. ....	28
<b>Figure 15.</b>	Pujamana member in OUTCROP B. ....	29
<b>Figure 16.</b>	Bitumen layers between cherts, claystone and siliceous mudstone beds of the Pujamana member, in OUTCROP B. ....	29
<b>Figure 17.</b>	Galembo section at “La Azufrada” Creek, OUTCROP B. ....	30
<b>Figure 18.</b>	Galembo section, calcareous nodules at “La Azufrada” Creek. OUTCROP B. ....	30
<b>Figure 19.</b>	Measured stratigraphic column of La Luna Formation at OUTCROP B. ....	31
<b>Figure 20.</b>	Schematic workflow used in the laboratory analysis. ....	40
<b>Figure 21.</b>	Diagram showing how the samples were prepared for viewing with the SEM. .	43
<b>Figure 22.</b>	Diagram showing how the samples were mounted onto the aluminum stub. ....	43
<b>Figure 23.</b>	Comparison of relative sea level and RHP curves for the Barnett Shale. ....	45
<b>Figure 24.</b>	Geochemical log showing TOC vs Depth for the OUTCROP A. ....	54
<b>Figure 25.</b>	Geochemical log showing TOC vs Depth for the OUTCROP B. ....	55
<b>Figure 26.</b>	Modified Van Krevelen diagram for the OUTCROP A. ....	57

<b>Figure 27.</b>	Rock Eval Remaining Hydrocarbon Potential ( $S_2$ ) vs. TOC plot for determination of kerogen type and maturity of the OUTCROP A.....	58
<b>Figure 28.</b>	Modified Van Krevelen diagram for the OUTCROP B.....	60
<b>Figure 29.</b>	Rock Eval Remaining Hydrocarbon Potential ( $S_2$ ) vs. TOC plot for determination of kerogen type and maturity of the OUTCROP B La Luna samples.....	61
<b>Figure 30.</b>	Geochemical log of HI variation with stratigraphic depth for OUTCROP B.....	62
<b>Figure 31.</b>	$S_1$ vs. TOC plot for identifying the hydrocarbon staining and/or contamination of La Luna OUTCROP A samples.....	64
<b>Figure 32.</b>	$T_{max}$ vs. Production Index (PI) plot for estimating thermal maturity of La Luna OUTCROP A samples.....	65
<b>Figure 33.</b>	HI vs. $T_{max}$ plot showing maturity and kerogen type of the La Luna Formation OUTCROP A samples.....	67
<b>Figure 34.</b>	Geochemical log showing normalized oil content for the OUTCROP A.....	68
<b>Figure 35.</b>	$S_1$ vs. TOC plot for identifying hydrocarbon staining and/or contamination of La Luna OUTCROP B samples.....	69
<b>Figure 36.</b>	$T_{max}$ vs. Production Index (PI) plot for estimating thermal maturity of La Luna OUTCROP B samples.....	69
<b>Figure 37.</b>	HI vs. $T_{max}$ plot showing maturity and kerogen type of the La Luna Formation OUTCROP B samples.....	70
<b>Figure 38.</b>	Geochemical log showing normalized oil content for the OUTCROP B.....	71
<b>Figure 39.</b>	Geochemical log showing calculated vitrinite reflectance ( $\%R_o$ ) for OUTCROP A section.....	74
<b>Figure 40.</b>	Geochemical log showing calculated vitrinite reflectance ( $\%R_o$ ) for OUTCROP B section (plot template modified from Humble Geochemical Services).....	75
<b>Figure 41.</b>	Measured vitrinite reflectance ( $\%R_o$ ) map for La Luna formation in MMVB (Garcia and Parra, 2003).....	77
<b>Figure 42.</b>	Gas chromatogram of Zumberge (1984) showing the aliphatic-hydrocarbon fraction of a Salada member sample from the La Luna Formation nearby OUTCROP B location.....	81
<b>Figure 43.</b>	Gas chromatogram showing the aliphatic-hydrocarbon fraction of OUTCROP B Salada member sample CAR M-3 after MSSV.....	81



<b>Figure 44.</b>	Gas chromatograms of saturate fractions from bitumen extracts of the La Luna Formation OUTCROP A Galembo and Salada members. Note the heavy biodegradation level evidenced by big the humps and the removal of n-alkane and depletion of isoprenoids.....	82
<b>Figure 45.</b>	Gas chromatograms of saturate fractions from bitumen extracts of the La Luna Formation OUTCROP B Galembo member. Note the high level of biodegradation as evidenced by the big humps and the removal of lighter n-alkane and depletion of isoprenoids. ....	83
<b>Figure 46.</b>	Gas chromatograms of saturate fractions from bitumen extracts of the La Luna Formation OUTCROP B Pujamana member. Note the high level of biodegradation as evidenced by the big humps, the removal of lighter n-alkane and depletion of isoprenoids. ....	84
<b>Figure 47.</b>	Gas chromatograms of saturate fractions from bitumen extracts of the La Luna Formation OUTCROP B Salada member. Note the heavy level of biodegradation as evidenced by the big humps and the removal of n-alkane and depletion of isoprenoids.....	85
<b>Figure 48.</b>	Micro-scale Sealed Vessel analysis for the Salada member CAR M-3 sample. .	86
<b>Figure 49.</b>	Partial fragmentograms of the m/z 217 ion showing steranes distribution in the saturate fractions of the OUTCROP A Galembo member P2M1 sample. Peak identification is presented in Table 10. ....	92
<b>Figure 50.</b>	Partial fragmentograms of the m/z 217 ion showing steranes distribution in the saturate fractions of the OUTCROP A Salada member P4M2 sample. Peak identification is presented in Table 10. ....	92
<b>Figure 51.</b>	Partial fragmentograms of the m/z 217 ion showing steranes distribution in the saturate fractions of the OUTCROP B Galembo member QLS M-3 sample. Peak identification is presented in Table 10.....	93
<b>Figure 52.</b>	Partial fragmentograms of the m/z 217 ion showing steranes distribution in the saturate fractions of the OUTCROP B Pujamana member CAN M-15 sample. Peak identification is presented in Table 10.....	93
<b>Figure 53.</b>	Partial fragmentograms of the m/z 217 ion showing steranes distribution in the saturate fractions of the OUTCROP B Salada member CAR M-14 sample. Peak identification is presented in Table 10. ....	94
<b>Figure 54.</b>	Partial fragmentograms of the m/z 217 ion showing steranes distribution in the saturate fractions of the OUTCROP B Salada member CAR M-2 sample. Peak identification is presented in Table 10. ....	94
<b>Figure 55.</b>	Ternary diagram of C <sub>27</sub> , C <sub>28</sub> and C <sub>29</sub> steranes for the La Luna Formation samples. ....	95

<b>Figure 56.</b>	Proposed geochemical log of sterane biomarker ratios and TOC vs. depth for the La Luna OUTCROP B. ....	98
<b>Figure 57.</b>	m/z 191 fragmentograms showing terpanes distribution in the saturate fractions of the OUTCROP A Galemba member P2M1 sample. Peaks identification is presented in Table 12. ....	101
<b>Figure 58.</b>	m/z 191 fragmentograms showing terpanes distribution in the saturate fractions of the OUTCROP A Salada member P4M2 sample. Peaks identification is presented in Table 12 ....	101
<b>Figure 59.</b>	m/z 191 fragmentograms showing terpanes distribution in the saturate fractions of the OUTCROP B Galemba member QLS M-3 sample. Peaks identification is presented in Table 12. ....	102
<b>Figure 60.</b>	m/z 191 fragmentograms showing terpanes distribution in the saturate fractions of the OUTCROP B Pujamana member CAN M-15 sample. Peaks identification is presented in Table 12. ....	102
<b>Figure 61.</b>	m/z 191 fragmentograms showing terpanes distribution in the saturate fractions of the OUTCROP B Salada member CAR M-14 sample. Peaks identification is presented in Table 12. ....	103
<b>Figure 62.</b>	m/z 191 fragmentograms showing terpanes distribution in the saturate fractions of the OUTCROP B Salada member CAR M-2 sample. Peaks identification is presented in Table 12. ....	103
<b>Figure 63.</b>	Geochemical logs of biomarker ratios from terpanes for the La Luna formation OUTCROP B. Values in table 13. ....	111
<b>Figure 64.</b>	m/z 191 and 177 for CAR M-2 sample indicating the occurrence of 25-norhopanes indicated by n-carbon number notation and the degradation of the tricyclic terpanes. ....	114
<b>Figure 65.</b>	Ranking of biodegradation levels proposed by Wenger et al. (2002). ....	115
<b>Figure 66.</b>	Lithological facies Salada-i. Outcrop sample and thin section in parallel nichols (parallel polarized light). ....	122
<b>Figure 67.</b>	Lithological facies Salada-ii. Outcrop sample and thin section in parallel nichols (parallel polarized light). ....	123
<b>Figure 68.</b>	Lithological facies Pujamana iii, iv and v. Outcrop sample and thin section in parallel nichols (parallel polarized light). ....	124



<b>Figure 69.</b>	Lithological facies Galembo vi. Outcrop sample and thin section in parallel nichols (parallel polarized light). .....	125
<b>Figure 70.</b>	Lithological facies Galembo vii. Outcrop sample and thin section in parallel nichols (parallel polarized light). .....	126
<b>Figure 71.</b>	Ternary plot from XRD analysis of OUTRCOP B samples. ....	132
<b>Figure 72.</b>	XRD mineralogy variation vs. stratigraphic depth of OUTCROP B section. ....	133
<b>Figure 73.</b>	Brittleness Index (BI) for OUTCROP B section. ....	133
<b>Figure 74.</b>	Pore classification for shales recognized under SEM analysis. ....	135
<b>Figure 75.</b>	SEM analysis of sample CAR M-3 corresponding to lithofacies S-i. ....	137
<b>Figure 76.</b>	Calculation of total porosity for sample CAR M-3. ....	138
<b>Figure 77.</b>	Total porosity calculation and histograms for sample CAR M-3. ....	139
<b>Figure 78.</b>	SEM analysis of sample CAR M-5 corresponding to lithofacies S-ii. ....	140
<b>Figure 79.</b>	Calculation of total porosity for sample CAR M-5. ....	141
<b>Figure 80.</b>	Total porosity calculation and histograms for sample CAR M-5. ....	142
<b>Figure 81.</b>	SEM analysis of sample QLS M-8 corresponding to lithofacies G-vi. ....	144
<b>Figure 82.</b>	Calculations of total porosity for sample QLS M-8. ....	145
<b>Figure 83.</b>	Total porosity calculation and histograms for sample QLS M-8. ....	146
<b>Figure 84.</b>	SEM analysis of sample QLS M-3 corresponding to lithofacies G-vii. ....	147
<b>Figure 85.</b>	SEM analysis of sample P4M2 corresponding to micritic mudstone. ....	150
<b>Figure 86.</b>	SEM analysis of sample Salada-1 corresponding to a carbonate shale. ....	150
<b>Figure 87.</b>	SEM analysis of sample P2M1 corresponding to micritic Packstone. ....	151
<b>Figure 88.</b>	SEM analysis of sample P4M3 corresponding to carbonate shale. ....	151
<b>Figure 89.</b>	EDX results of OUTCROP B QLS M-3 sample. ....	152
<b>Figure 90.</b>	Sequence stratigraphy cycles of the La Luna Formation based on TOC and relative hydrocarbon potential (RHP) vs depth for OUTCROP B section. ....	159
<b>Figure 91.</b>	TOC, relative hydrocarbon potential (RHP) and Brittleness Index (BI) variation with depth for OUTCROP B section. ....	160

## LIST OF TABLES

<b>Table.1.</b>	List of the La Luna Formation, southeast MMVB, OUTCROP A samples analyzed in this study. ....	33
<b>Table.2.</b>	List of the La Luna Formation, central MMVB, OUTCROP B samples analyzed in this study. ....	35
<b>Table.3.</b>	Parameters and terms derived from Rock Eval pyrolysis (modified from Peters and Cassa, 1994; Jarvie et al., 2005, 2007).....	49
<b>Table.4.</b>	Total Organic Carbon (TOC) and Rock Eval data from La Luna southeast section, OUTCROP A samples used in this study. ....	50
<b>Table.5.</b>	Total Organic Carbon (TOC) and Rock Eval data from La Luna central MMVB section, OUTCROP B samples used in this study.. ....	52
<b>Table.6.</b>	Measured and calculated vitrinite reflectance (%R <sub>o</sub> ) for La Luna samples used in this study. ....	73
<b>Table.7.</b>	Guidelines of calculated vitrinite reflectance values for cuttings and core samples from the Barnett Shale (Jarvie et al., 2005) and Woodford Shale (Miceli-Romero, 2010). ....	73
<b>Table.8.</b>	Biomarkers and chromatograms/fragmentograms used for La Luna Formation OUTCROP A and OUTCROP B samples analysis.. ....	78
<b>Table.9.</b>	Samples for biomarker analysis in OUTCROP A and OUTCROP B. ....	80
<b>Table.10.</b>	Identification of steranes in the partial m/z 217 fragmentogram. ....	90
<b>Table.11.</b>	Steranes data and ratios calculated for the La Luna Formation samples (n.d. = not detected). ....	91
<b>Table.12.</b>	Identification of terpanes in the partial m/z 191 fragmentograms. ....	100
<b>Table.13.</b>	Biomarker ratios for hopanes in the La Luna Formation samples (n.d. = not determined). ....	108
<b>Table.14.</b>	Semi-Quantitative mineral content from XRD analysis, La Luna formation OUTCROP B. ....	130

## ABSTRACT

The La Luna Formation, part of the South American upper Cretaceous sequence, has been recognized as one of the most important hydrocarbon source rocks in Colombian and Venezuelan basins. This formation is described as calcareous shale and limestone, black in color, with high foraminifera (*Globigerina*) content and calcareous and phosphate concretions. Outcrop studies were conducted in the southern part (OUTCROP A) and central part (OUTCROP B) of the Middle Magdalena Valley basin (MMVB) to assess the shale gas potential.

La Luna Formation has been previously sub-divided into three members: upper, middle and lower, recognized respectively as Galembo (calcareous shales with limestone layers and nodules), Pujamana (claystone, mudstone, gray shale and cherts) and Salada (black shales, black mudstones, black calcareous claystone, black limestone layers and concretions with pyrite). Two major stratigraphic sections were measured, one in the OUTCROP B area with a total thickness of 1000 ft., and the other one in the south area of the basin at OUTCROP A 1200 ft. thick.

Based upon 66 samples analyzed, total organic carbon (TOC) values range for the Galembo from 1.09% to 11.90% and for the Salada member from 2.15% to 11.90. Rock Eval pyrolysis data show the La Luna Formation is dominated by Type IIS kerogen, indicating oil and gas prone marine organic matter; thus, these members are excellent source rocks for hydrocarbons. The maturity of this formation increases towards the southeast. Liquid hydrocarbons will be more related to the northern and central part of MMVB and condensates and dry/wet gases will be more related to the



southern MMVB areas. Biomarker analyses reveal variations in redox conditions and a predominant marine organic matter input with anoxic and hypersaline conditions for the Galembo and Salada members.

The SEM analysis identified two major microfabric types in the Salada and Galembo member: 1) organic hash: most of the samples contain common organic matter and the mineral edges are very diffuse; and 2) organic clayey with sharp mineral edges and abundant calcite minerals. The porosity types associated with the Salada and Galembo member are porous floccules, intraparticle porosity, fecal pellet porosity and microchannel porosity. For the Galembo member the average total porosity is 8.5% and for the Salada member average total porosity is 8.11% for the samples analyzed.

The observed facies association and biomarker analysis identified the depositional environment as shallow marine, middle shelf, in a transgressing sea. Four major third order stratigraphic cycles corresponding to the three La Luna Formation members deposition events are proposed. The the lower Salada member is characterized by a major transgression with a maximum flooding surface at Salada member top and a transgressive surface of erosion (TSE) towards the Salada - Pujamana members' boundary. The Pujamana member deposition was interpreted as a HST-TST regional regression, where the observed Pujamana – Galembo boundary corresponds to a third TSE and the Galembo member is mainly a transgression with fluctuations, which indicates that deposition of the Galembo member occurred during a sea level rise towards the La Luna Formation top progradational deposits.

This primary assessment of the La Luna Formation indicates a good potential for a shale gas system, where good organic matter content is present, the formation has reached maturity levels for hydrocarbon generation and has relatively high porosity for oil and/or gas storage. The Salada and Galembo members are good candidates for an unconventional shale gas play, therefore these can be considered as separate operational units, with thicknesses in outcrop from 180-720 ft. for the Galembo member, for the Salada member thickness from 300-400 ft., and approximately 500 ft. of thickness for the transitional Pujamana member, which is very likely to be a possible lithological barrier between the upper and lower La Luna members.

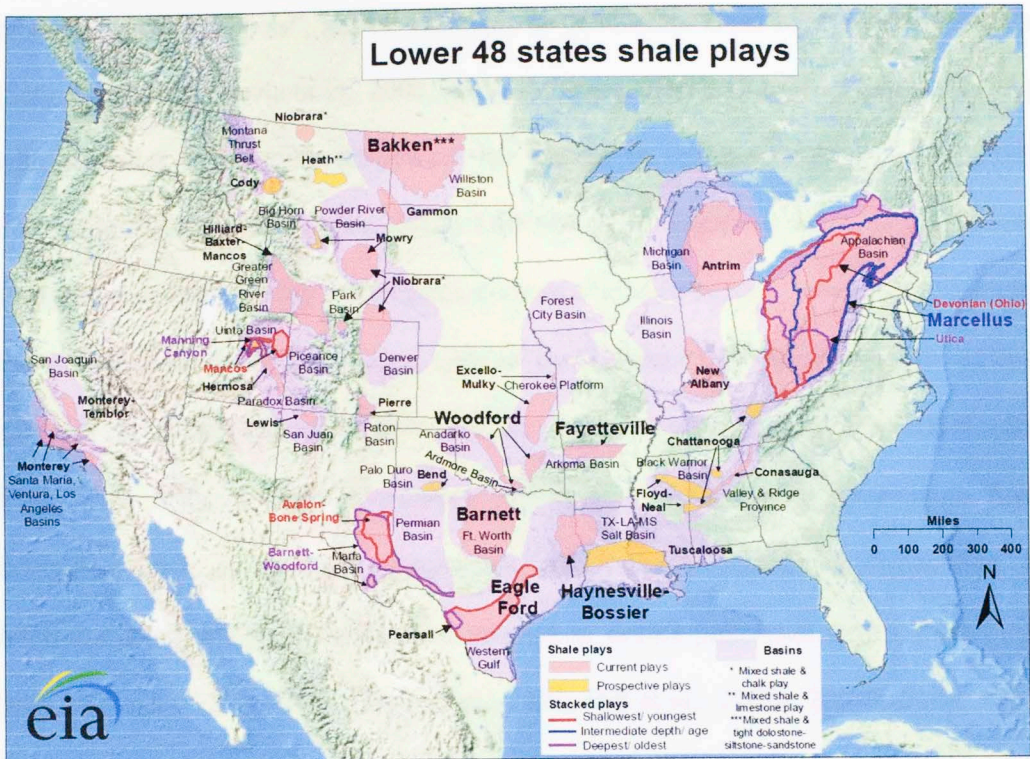
# CHAPTER I

## 1. INTRODUCTION

Over the last decade, unconventional gas resources (coalbed methane, tight gas, shale gas, shale oil, gas hydrates, and deep-basin gas systems) have become significant providers of natural gas and oil in the United States basins (Figure 1). Developed and tested exploratory concepts have been transferred overseas towards new and leading-edge technologies, creating an exploratory boom for these resources.

Unconventional gas/oil shale resources consist of regional and continuous accumulations of light hydrocarbons where migration is not controlled by a buoyancy-driven mechanism. Different than conventional reservoirs, these accumulations are not influenced by hydrodynamic processes. In addition, these reservoirs are not usually related to structural and/or stratigraphic traps and do not show evident traps and seals. Unconventional resources do not have well-defined gas-water and oil-water contacts, and usually show abnormal pressures (high or low). In these plays, natural fractures may be very common and contain high amounts of gas/oil-in-place, with accumulations found adjacent to, or within source rocks (Schmoker et al., 1996; Schmoker, 2002; Law and Curtis, 2002; Schenk, 2005; Jarvie et al., 2005, 2007; Philp, 2007; Pollastro et al., 2007). However, unconventional resources exhibit very low matrix permeability, a low recovery factor with low production of free water, and lower estimated ultimate recovery (EUR) compared to conventional resources (Schmoker et al., 1996; Law and Curtis, 2002; Schenk, 2005).





**Figure 1.** U.S. shale gas plays lower 48 states (EIA, May 9, 2011). Source: Energy Information Administration, 2012.

It has been very common to consider shales as uniform stratigraphic sequences in terms of physical and chemical properties. However, it has been demonstrated that a more detailed analysis of these source/reservoir rocks can provide greater insight about variations in the depositional and environmental factors that influenced source rock deposition and fluids storage (Singh, 2008; Comer, 2009; Slatt et al., 2010, 2012).

The key industry-academia accepted parameters for a shale gas/oil characterization are the primarily identification of lithofacies (shale type), organic content, porosity, permeability, maturity, fracturability, gas content, reservoir thickness, and volumetrics. The integration of these parameters has been established with the aim

of defining “sweet spots”, gas/oil fairways, or producible areas of economic potential (Schmoker, 2002; Jarvie et al., 2005, 2007; Pollastro, 2007). Organic geochemistry tied with sequence stratigraphy framework has played an important role in shale gas/oil evaluation (Slatt and Rodriguez, 2012). Different approaches and techniques have been used to determine maturity and organic content of shales: organic matter type, quantity and provenance; thermal maturity; type of hydrocarbons generated; the role of clay minerals in concentrating organic matter within the reservoirs; and establishing depositional settings. This information has been integrated with information from disciplines such as geology, geophysics, and reservoir/petroleum engineering to determine shale oil/gas potential and attempt to define petroleum systems for these types of plays (Curtis, 2002; Jarvie et al., 2007; Hill et al., 2007a, 2007b; Philp, 2007; Pollastro et al., 2007; Zhao et al., 2007; Kinley et al., 2008).

The present study is focused on the organic geochemistry and reservoir rock characterization of the La Luna Formation in part of the Middle Magdalena Valley Basin (MMVB), Colombia. Two major stratigraphic sections were measured in outcrops of the Eastern Cordillera west flank. The section measured in the southeast area of the MMVB is referred in this study as OUTCROP A, and the second section, measured in the central zone of the basin is referred as OUTCROP B.

The La Luna Formation has been considered to be the main hydrocarbon source rock in the MMVB by Zumberge (1984) and Rangel et al. (1996 and 2000), as well as in other important basins such as the Maracaibo Basin (Talukdar et al., 1986). The existing knowledge about depositional processes controlling the Upper Cretaceous La



Luna Formation deposit in the MMVB is minimal and there are few integrated stratigraphic and geochemical studies on this formation, nor is there any published assessment of this formation as a reservoir. Zumberge (1984) addressed the hydrocarbon potential of the La Luna Formation in the *La Sorda* Creek, central area MMVB, as the most complete stratigraphic outcrop section of this formation. Rangel et al. (1996 and 2000) identified four oil families in the same location using oils from conventional producing reservoirs and La Luna outcrop extracts. Based on oil characteristics, Rangel et al. (1996 and 2000) suggested that two of the oil families in the conventional reservoirs are possibly derived from the La Luna Formation. Ramon and Dzou (1999) used oil-derived parameters to discuss some geochemical processes in the MMVB of the La Luna Formation and associated organic facies, to conclude that La Luna is an effective source rock and makes an oil and gas contribution to Tertiary reservoirs along the basin. There is no study of the storage capacity of this formation as a reservoir.

Sixty-six samples of La Luna Formation outcrop were collected in the field, thirty four from the central MMVB and thirty two from the southeast MMVB. These samples are the main data set of this study, and were analyzed in order to determine the type and quantity of organic matter, maturity, paleoenvironmental conditions, lithological facies, mineral content and porosity. This information has been integrated with published geological data to provide insights regarding source rock depositional history, characteristics and type of hydrocarbons that may be generated from these source rock intervals and storage in the reservoir intervals. The relationship of geochemical parameters to local depositional processes and stratigraphic cycles

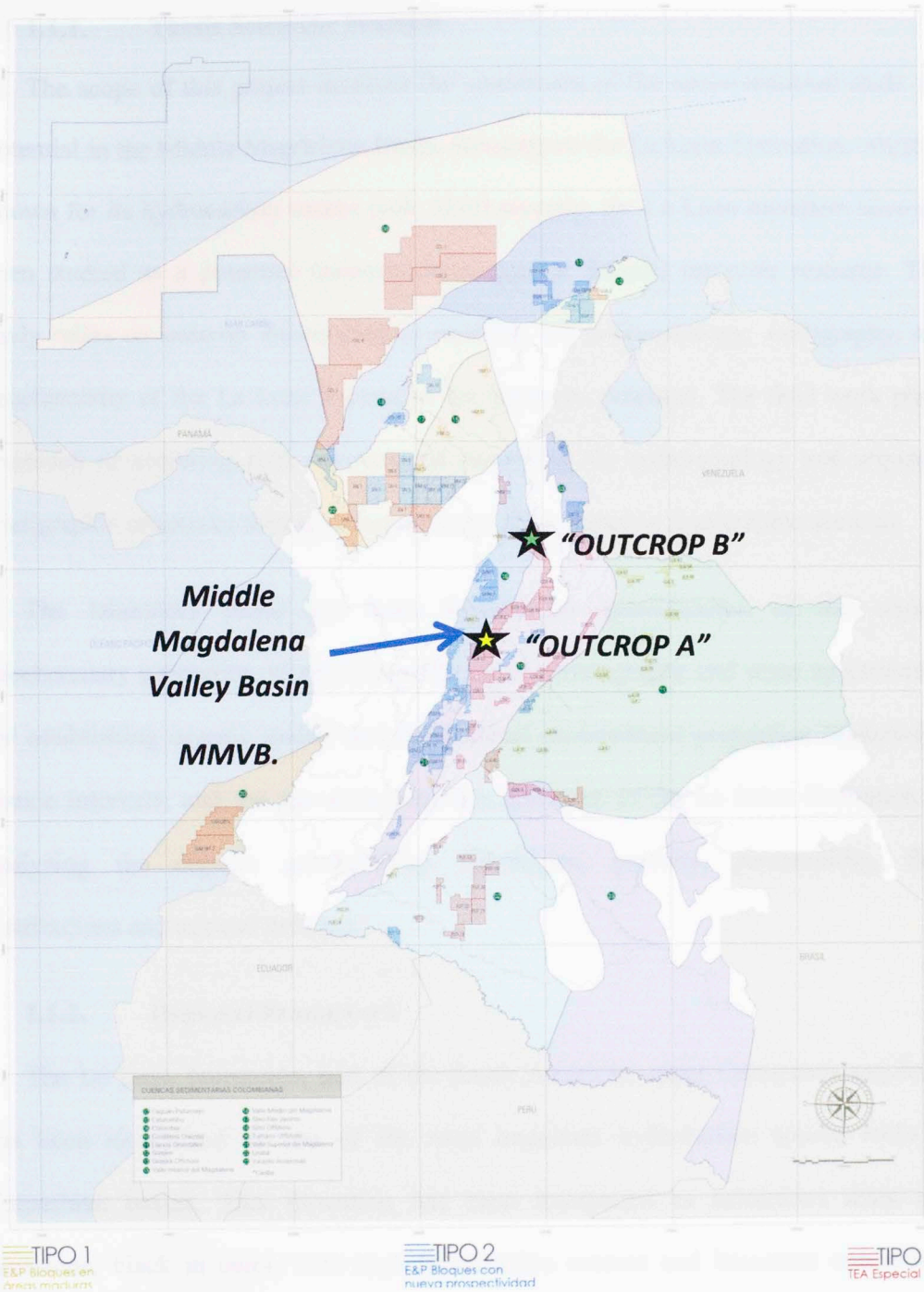
recognized in the basin would help to identify the best source rock intervals and provide a better understanding of the spatial relationship and distribution of the La Luna Formation in the MMVB.

During the past two years, the Colombian Government has considered encouraging the exploration for unconventional oil and gas in Colombia. This is another reason to make this assessment of the La Luna Formation, since it might be an emerging shale play in South America. The Colombian Exploration Blocks offered for the MMVB in the 2012 bidding round are illustrated on Figure 2.

### **1.1. Background of thesis topic.**

In order to assess hydrocarbon prospects, geochemical data, one critical for risk evaluation and petroleum system definition based on oil/gas source rock correlations. In the case of shale gas plays, geochemistry is a very useful tool for establishing potential commercial gas accumulations in terms of origin and characteristics of existing hydrocarbons, source rock thermal maturity, hydrocarbon yield, and burial history modeling.





**Figure 2.** Geographic map of Colombia, showing the 2012 Open bid leasing blocks (Dark blue polygons). Source: ANH 2012.

### **1.1.1. Thesis Scientific Problem**

The scope of this project involves the assessment of the unconventional shale gas potential in the Middle Magdalena Basin, focusing on the La Luna Formation, which is known for its hydrocarbon source rock. Until recently, the La Luna members have not been studied as a potential unconventional gas (or liquids) reservoir resource. This study relies on outcrop information to establish the sedimentology, stratigraphy, and geochemistry of the La Luna Formation for shale gas potential. The field work phase consisted of acquiring rock samples and describing the sedimentology and sequence stratigraphic properties through measurements of key outcrop stratigraphic sections.

The laboratory phase has been focused on quantification of the organic geochemistry properties, biomarkers with gas chromatography and mass spectrometry for establishing organic matter and depositional environment properties, organic-rich anoxic intervals; and the gas shale reservoir attributes of the La Luna Formation by analyzing the organic geochemistry, lithologies, porosity, permeability, fluid distributions and mineral contents.

### **1.1.2. Regional Framework**

The La Luna Formation, part of the South American upper Cretaceous sequence, has been recognized as one of the most important hydrocarbon source rocks in Colombian basins. This formation has been interpreted as calcareous shale and limestone, black in color, with high foraminifera content and limestone concretions (Garner, 1926; Hubach, 1957; Morales, 1958; Julivert, 1968; Ingeominas, 2002). The continuity of this formation has been recognized and extends from the central part of

Colombia towards the Maracaibo Basin, northwest Venezuela (Garner, 1926; Hedberg and Sass, 1937; Renz, 1959; Talukdar et al., 1985; Macellari and DeVries 1987; Perez-Infante et al., 1996; Mann and Stein, 1997; Villamil et al., 1999).

This research focuses on outcrop studies that were made by the author in the southern and middle parts of the Middle Magdalena Valley Basin to assess the shale gas potential of the La Luna Formation. This formation has been sub-divided by previous authors (Garner, 1926; Hedberg and Sass, 1937; Hubach, 1957; Morales, 1958) into upper, middle and lower members, named respectively as Galembó (calcareous shales with limestone layers and nodules), Pujamana (claystone, mudstone, gray shale and cherts) and Salada (black shales, black mudstones, black calcareous claystone, black limestone layers and concretions with pyrite). The field surveys conducted to date involved measuring stratigraphic columns and collecting samples from the three members to preliminarily assess the entire formation's unconventional potential.

## **1.2. Geologic Framework**

### **1.2.1. Regional Basin Geology**

The Middle Magdalena Valley Basin is located in the central area of Colombia, in the northwest corner of South America (Figure 3 and 4). The basin extends along the central reaches of the Magdalena River Valley between the Central and Eastern Cordilleras of the Colombian Andes. This basin has been recognized by ANH (2008) as a Poly-historic, from Rift to Broken Foreland and its area is Area 34,000 km<sup>2</sup> / 7,900,000 acres. The exploratory process has been oriented mainly towards the



identification of structural traps in the Paleogene sequences (ANH, 2008). The sediments that filled the basin are a succession of Jurassic continental deposits overlain by Cretaceous calcareous and siliciclastics sediments that are of transitional to marine origin (ANH, 2008). The Paleogene sequence is made up of siliciclastic rocks deposited mainly under continental conditions with some marine deposition.

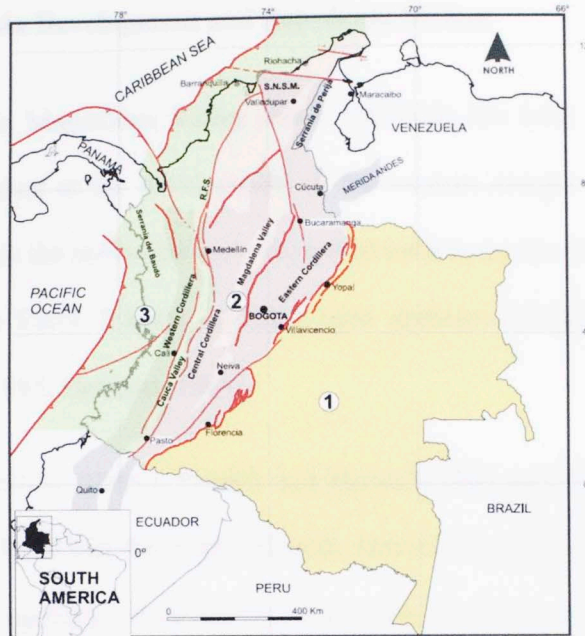
### **1.2.2. Basin Boundaries (ANH, 2008).**

The Middle Magdalena Valley Basin (MMVB) boundaries are illustrated in Figure 4, and are the following:

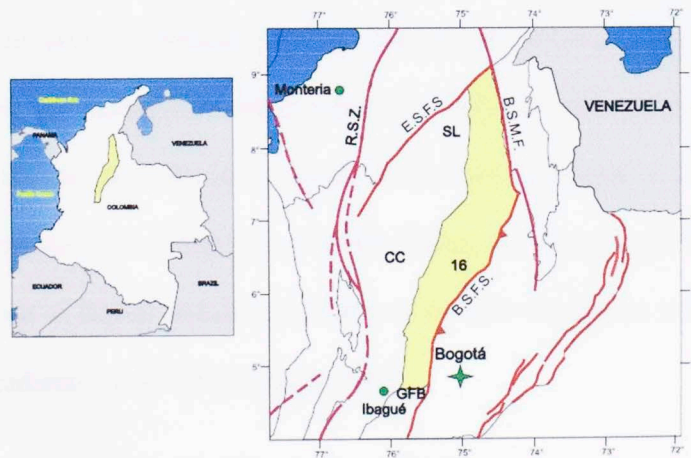
- Southeast: Bituima and La Salina fault systems (B.S.F.S.)
- North: Espíritu Santo fault system (E.S.F.S)
- West: Onlap of Neogene sediments over the “*Serranía de San Lucas*” (SL) and Central Cordillera (CC) basement
- South: Girardot fold belt (GFB)
- Northeast: Bucaramanga-Santa Marta fault system (B.S.M.F.)

In 2008, the Colombian government hydrocarbon management agency, ANH, published the following MMVB factors:

- Wildcat wells 296; Oil field discoveries 41
- Discovered oil reserves 1,900 million barrels of oil (MMBO).
- Discovered gas reserves 2.5 billion cubic feet of gas (BCFG)



**Figure 3.** Map of Colombia with its main tectonic domains. 1) Eastern Region; 2) Central Region; 3) Western Region. In red: regional faults. Gray and shadow areas: Main mountain ranges. Figure notations: R.F.S. Romeral fault system; S.N.S.M. Sierra Nevada de Santa Marta. Note the Magdalena Valley above the area number 2. Illustration from ANH (2008).



**Figure 4.** Location of the Middle Magdalena Valley Basin, Colombia. Figure notations: the Bituima and La Salina fault systems (B.S.F.S.); the *Espirito Santo* fault system (E.S.F.S.); the *Serranía de San Lucas* (SL); the Central Cordillera (CC); the *Girardot* fold belt (GFB); the *Bucaramanga-Santa Marta* fault system (B.S.M.F.). Note that the Yellow polygon corresponds to the MMVB. Figure from ANH, 2008.

### 1.2.3. Basin Development and Petroleum System

The Middle Magdalena Valley Basin (MMVB) has been affected by several tectonic events linked to the development of the western margin of Colombia. Some authors propose that the sediments were deposited initially by the lithospheric extension that started in the Early Triassic, creating tight grabens delimited by normal faults (Fabre, 1983 and 1985; Hebrard, 1985).

Some published studies, Pindell and Barret (1990) and Pindell (1993) among others, have considered that the north of South America was part of the super continent of Pangaea at the beginning of the Mesozoic and then was broken as the product of two possible processes: The first process, proposed by Pindell and Dewey (1982), was an intra-cratonic rift during the Triassic and early Jurassic; it can be applied to the north of Colombia and Venezuela (Sarmiento, 2001) and explains the separation of North America and the proto Caribbean opening. The second process proposed by Tussaint (1995), explains the extension as the product of a back arc rift, which agrees with the existence of volcanic deposits in the south of the basin (Bayona et al., 1994). In the MMVB the development of this type of basin during the Triassic and Jurassic favored the accumulation of fluvial and littoral clastic rocks with subsidence rates of 150 m/My and thermal gradients of 40°C/Km (Fabre, 1981).

All the Cretaceous deposits in the MMVB correspond to a regional mega sequence (Cediel, 1968) with a regional maximum flooding surface at the boundary of the Cenomanian –Turonian (Villamil, 1998). The marine transgression advanced until the Aptian as a product of thermal subsidence and relative increase of base level, until



the basin reached the maximum flooding stage. From the Barremian and during the rest of the Cretaceous, the basin was controlled by thermal subsidence (Fabre, 1981; Dengo and Covey, 1993), the deposits were controlled by eustatic changes and by the transgressions during the Turonian which formed the La Luna formation (Villamil, 1998). Macellari (1988) proposed that during this tectonic phase, the MMVB was a foreland basin and the sediment deposition was also affected by stages of the Santonian and younger Central Colombian Andes cordillera uplift.

According to Pindell and Dewey (1992) and Pindell and Erikson (1993), at the end of the Cretaceous and until the Oligocene, the north of South America was under the tectonic influence of the movement towards the east of the Caribbean plate, the subduction of the *Farallon* plate in the southeast of Colombia, and the late oblique convergence of the *Nazca* plate. During the Paleocene, the relative plate movements created the accretion of oceanic crust in the east of the basin (Cooper et al., 1995; Gomez, 2001) initiating the foreland tectonic setting, including the Eastern Cordillera basin and the *Llanos* basin in Colombia. During the Eocene, the plate convergence rate was higher, and at the west of the MMVB the Central Cordillera was uplifted, creating inversion of ancient normal faults, horsts and folds of the Cretaceous sequence and the development of a regional discordance upon which the clastic Tertiary formations were deposited (Gomez, 2001; Sarmiento, 2001). For the Oligocene and Middle Miocene, the fluvial and lacustrine clastics were deposited in the basin and constitute the principal conventional reservoir targets.



#### 1.2.4. Petroleum System Elements of MMVB

- **Hydrocarbon evidences**

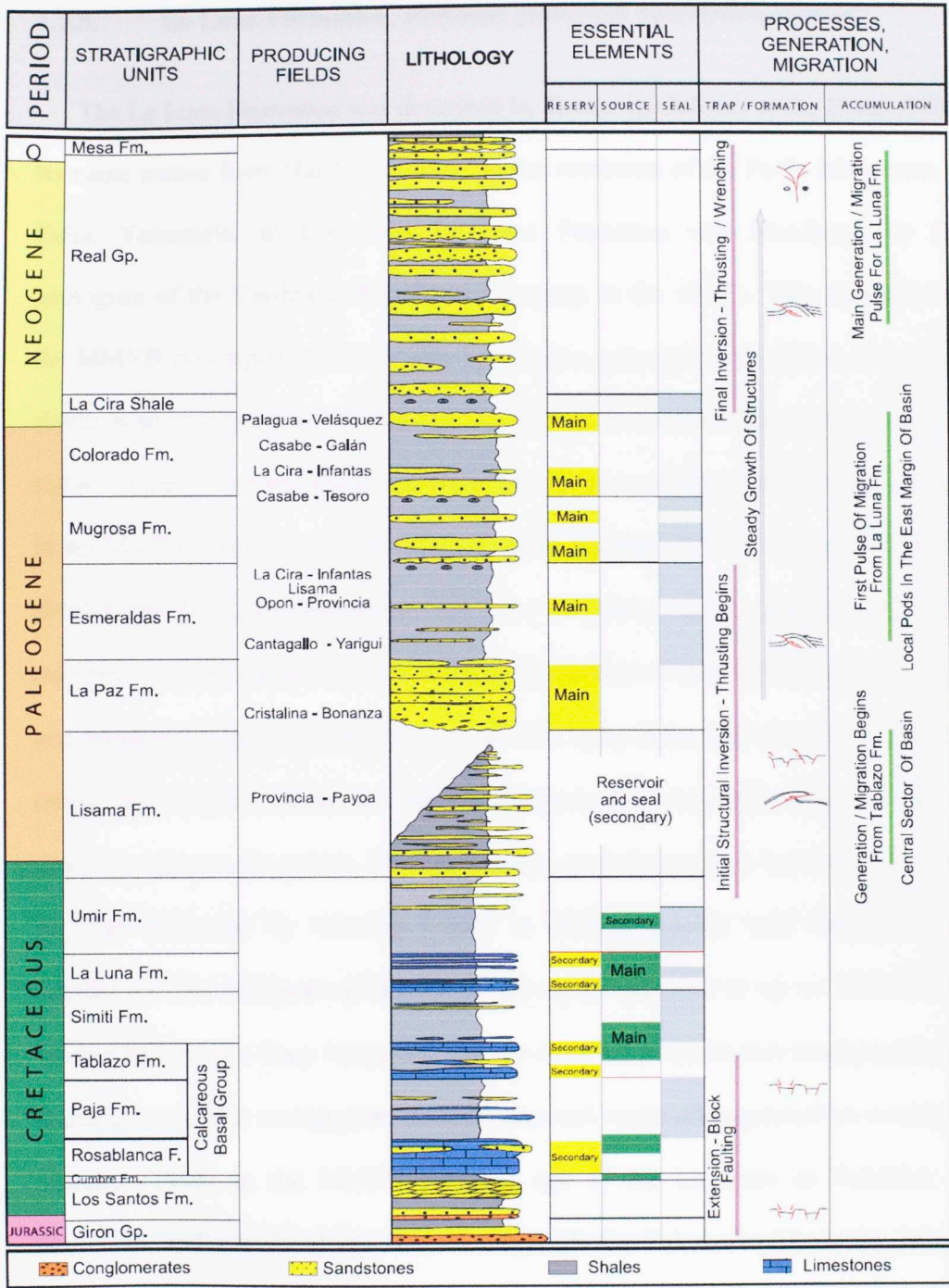
According to ANH (2008), over a century of exploration history in the basin has led to the discovery of about 1,900 MMBO, 2.5 trillion cubic feet of gas (TCF) and a total of 41 fields, including the first giant in Colombia, *La Cira-Infantas* field.

- **Source Rock**

The proposed source rocks are the cretaceous limestones and shales of the La Luna and Tablazo formations are the main source rocks in the basin. TOC values are high (1-12%) and organic matter is essentially Type II, with Ro values reaching 0.6 -3.0 %. (ANH, 2008). According to ANH (2008) these main source rocks were deposited in the basin during two worldwide anoxic events, one at the Early Cretaceous Hauterivian-Barremian and the other at Late Cretaceous Turonian-Santonian.

- **Reservoirs**

As illustrated in Figure 5, conventional reservoirs in the basin are continental Paleogene sandstones (Paleocene-Miocene) of the *Lisama*, *Esmeraldas-La Paz*, and *Colorado-Mugrosa* formations. They have average porosities 15-20% and average permeabilities of 20-600 md. Lightly explored reservoirs are fractured systems of the Cretaceous limestones, *Basal Limestone Group* and La Luna Formation (ANH, 2008).



**Figure 5.** General stratigraphic column and Petroleum System elements of the Middle Magdalena Valley Basin, Colombia. ANH, 2008.

### 1.2.5. La Luna Formation. Previous geological description studies.

The La Luna Formation was described by Garner (in Julivert et al., 1968, 1970). Its name comes from “*La Luna Creek*” at the northwest of the Perija Mountains in Zulia, Venezuela. In Colombia, La Luna Formation was introduced by the geologists of the Caribbean Petroleum Company in the 1920’s. This formation in the MMVB is composed of dark gray limestones, gray and black shales, calcareous shales with intercalations of clay rich limestones, limestone concretions up to two meters in diameter with fossils and black chert layers and phosphatic beds at the top. In the MMVB, previous authors (Garner, 1926; Hubach, 1957; Morales, 1958) have divided the La Luna Formation into three members: upper, middle and lower members, named respectively as Galembo (calcareous shales with limestone layers and nodules), Pujamana (claystone, mudstone, gray shale and cherts) and Salada (black shales, black mudstones, black calcareous claystone, black limestone layers and concretions with pyrite). The depositional environment that has been proposed for this formation by Morales (1958) is shallow marine with bottom water circulation. The thickness of this formation varies from 400 ft. up to 2200 ft. The contact between La Luna Formation and the coaly Umir Formation stratigraphically above is a regional stratigraphic discontinuity and easily distinguished on outcrops. Morales (1958) in the MMVB assigned age of the La Luna as Turonian to Santonian, and correlated this formation towards the Catatumbo-Maracaibo basins in Venezuela.



Zumberge (1984) described, in general, the formation in the central MMVB as lithologically consisting of dark-gray to black calcareous shales with varying amounts of interbedded limestones and some thin chert beds. In thin section, La Luna samples from the Pujamana and Salada Members contain abundant calcareous planktonic foraminifera and other pelagic organisms, suggesting deposition in moderately deep water with restricted bottom circulation. He observed a textural relationship between the organic matter and inorganic minerals (especially the calcite filled *Globigerina* foraminifera) that can be observed within the formation. Zumberge (1984) also mentioned that except for eolian-transported clays, little evidence of land-derived material, such as detrital quartz, was found on foraminiferal tests not filled with calcite, but commonly filled with oil.

### **1.3. Thesis Research Goal and Objectives**

#### **Goal**

The main goal of this thesis is to evaluate the unconventional shale gas/shale oil potential of the Colombian upper Cretaceous La Luna Formation in the Middle Magdalena Basin.

#### **Objectives**

- Evaluate the organic richness of the La Luna Formation.
- Determine organic matter types.
- Assess the hydrocarbon generation potential and thermal maturity across the study area.

- Determine variations in organic matter sources, maturity and depositional environment through biomarker and stratigraphic analysis.
- Address variations in redox conditions in terms of sea-level changes of the depositional environment through linkage of geochemical and geological parameters.
- Characterize the stratigraphy, sedimentology and mineralogy of the La Luna Formation in outcrop samples for determining their potential as shale gas source-reservoir rocks.
- Evaluate the reservoir attributes (porosity, permeability, fluid saturations) in outcrop samples for ranking their shale gas potential.
- Provide a general paleoenvironmental interpretation for deposition of the La Luna Formation in the MMVB.
- Define and correlate the depositional and sequence stratigraphy of the formation for shale gas assessments from field work information.

## CHAPTER II

### 2. METHODOLOGY

#### 2.1. Study Areas and Sample Locations

Two key stratigraphic locations at the MMVB encompass the study area. These sections are located at the central and southeastern MMVB geologic provinces; one is the Eastern Cordillera west flank outcrops in the State of Santander; the other is in the central part of MMVB, on the “*La Sorda*” Creek, which has a complete stratigraphic column of La Luna Formation and presents its three members (Garner, 1926; Hubach, 1957; Morales, 1958; Zumberge, 1984; Rangel et al., 2000). The section measured in the southeast is a new section that has not been reported before and comprises the road between the *Landazuri* and *Cimitarra* townships, towards the province “*Plan de Armas*”. A total of sixty-six outcrop samples for the three La Luna members were collected from eight different locations along these roads and creeks, (Figure 6, Tables 1 and 2).

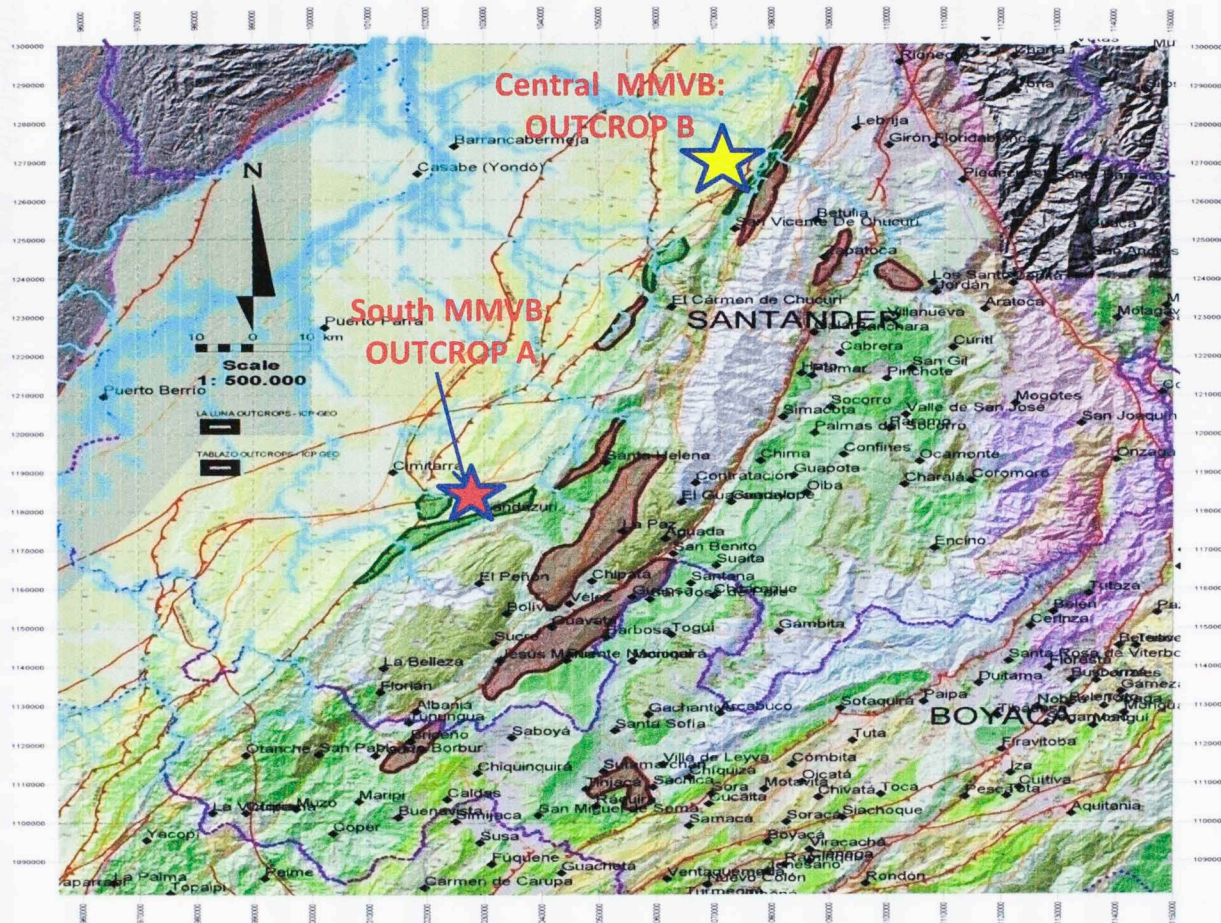
##### 2.1.1. South East MMVB Stratigraphic Section, OUTCROP A.

This section is located 7 km on the road from *Landazuri* to *Cimitarra*, Santander, Colombia (Figure 2 and Figure 6). It is easy to identify the La Luna contact with the overlying Umir Formation because in this area there is an intense exploitation of the Umir coal beds near its contact with the La Luna Formation. The lithologies are intercalations of claystone, very fine sandstone and coaly shale layers (Figures 7 and 8).



This section has 730 ft. of limestones and cherts (Figure 8) of the Galembo member. The details of the measured Galembo stratigraphic column are illustrated on Figure 12. The principal associated lithologies are in the top black shales intercalated with claystones, limestones and calcareous concretions. In the middle part are tabular black shales intercalated with claystones, cherts and calcareous concretions. At the bottom there are intercalations of black shale with very fine sandstones and black mudstones with wavy stratification. Also at the base are black shales with pyrite and calcite concretions, intercalated with black limestones. The outcrop strikes N60°W and dips 70S°W (Figure 9). The La Luna middle Pujamana member is covered by dense vegetation. It is ~500ft thick and consists of claystone and chert interbeds in sharp contact with the Galembo limestones (Figure 10).

The lowermost Salada member is also covered with dense vegetation, but presents some better exposures than the Pujamana member. The principal lithologies are black shales, black marlstones, limestones and cherts. The measured thickness of this member is 480 ft. (Figure 11). Due to heavy rains in 2010 and 2011 in the MMVB, these outcrops were fresh landslides and it was easier to identify the lithologies because they were exposed.



**Figure 6.** Map showing the location of the Cretaceous outcrops in MMVB. La Luna formation outcrops are the dark green polygons.



### 2.1.2. Central MMVB Stratigraphic Section, OUTCROP B.

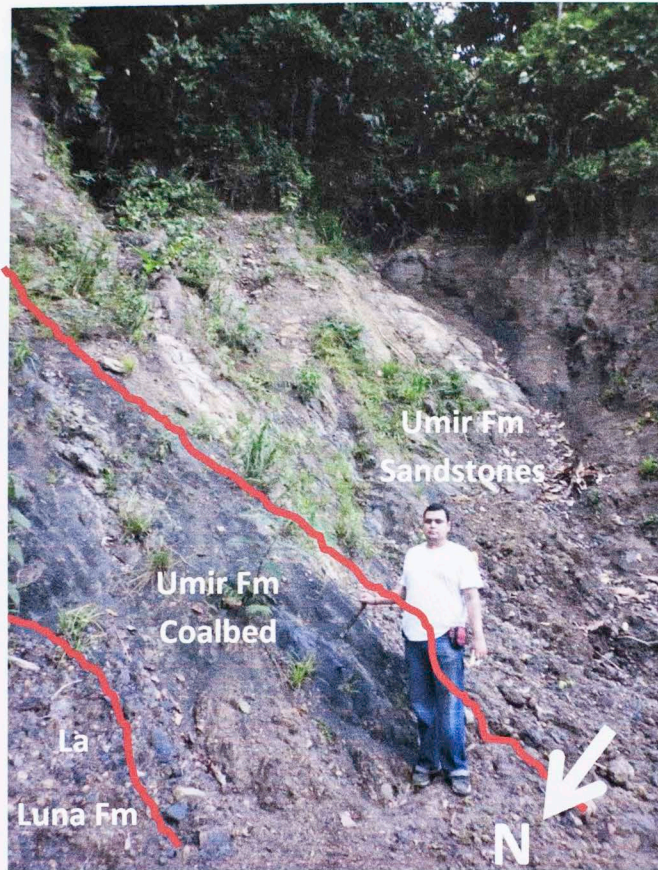
This section is located 7.5 Mi (12 Km) on the road from Lebrija to Barrancabermeja, Santander, Colombia, over the *La Renta* area, in the detour pathway to the “*Uribe-Uribe*” zone (Figure 2 and Figure 6). The elevation is 770-790 m. above sea level. Above the La Luna contact, the Umir Formation is composed of intercalations of claystone, very fine sandstone and coaly shale layers. The contact with La Luna is erosive and unconformable (Figure 13). The basal Salada member occurs on the *Lebrija-Barrancabermeja* road and is exposed 7.5 Mi (12 Km) from *Lebrija* town. The outcrop has dense vegetation on the road, but there is a nice exposure over a quarry that was being blasted for dam construction in the area (Figure 14). The measured thickness is 328ft and part of this member was covered with vegetation. The lithologies associated with this Salada member are compacted black calcareous shales, with planar lamination at the top, and with intercalations of dark limestone beds. The middle part of the Salada member contains intercalations of dark shales with siliceous cherts and claystone lamina. Calcareous nodules around 0.5 in. of diameter are abundant. The bottom of the Salada member contains intercalation of claystones and limestones with calcareous and phosphatic nodules (Figure 19); the outcrop strikes N67°E and dips 27°SE. The identified fracture orientation is N39°W and 71°SW.

The middle Pujamana member was described on the deviation road to the “*Uribe-Uribe*” area. This outcrop is 1.25 Mi (2 Km) towards the northwest of the Salada outcrop through a countrymen pathway. The measured thickness is 508 ft. The

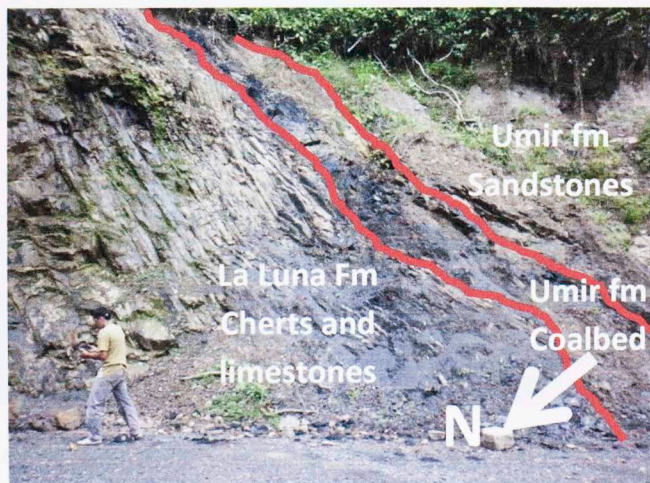


principal lithologies at the top are black, compacted, calcareous shales, with planar laminae (Figure 15). The middle part is composed of intercalations of siliceous and calcareous cherts, with both bitumen filled layers and fractures (Figure 16). Carbonate and phosphatic concretions are randomly distributed. The bottom of the Pujamana member contains calcareous limestone intercalations with gray shales and siliceous claystone layers. The outcrop strikes N40°E and dips 88°SE and the identified filled fracture orientation is N10°W and 88°SW.

The upper Galembo member occurs 2.5 Mi (4 Km) from the Salada outcrop, in the same pathway as the Pujamana outcrop. This member was measured through “*La Azufrada*” Creek (Figure 17). At the top, the associated lithologies are compacted black calcareous shales with planar laminae and intercalated with dark packstones. The middle part consists of dark shales with siliceous cherts and claystone laminae; calcareous nodules around 2-3 ft. in diameter are abundant (Figure 18). The bottom of the Galembo contains intercalations of micritic limestones and dark cherts. Along this creek there used to be a phosphate mine which mined big phosphate concretions and condensate beds from the Galembo member. The total measured thickness of this member is 180.5 ft. The strike and dip are N35°E and 75°SE. Fractures are filled with calcite. Clear calcite fossil shells characterize the limestones as micritic packstones (Figure 19).



**Figure 7.** Erosive contact of la Luna Fm top and Umir Fm base, OUTCROP A.



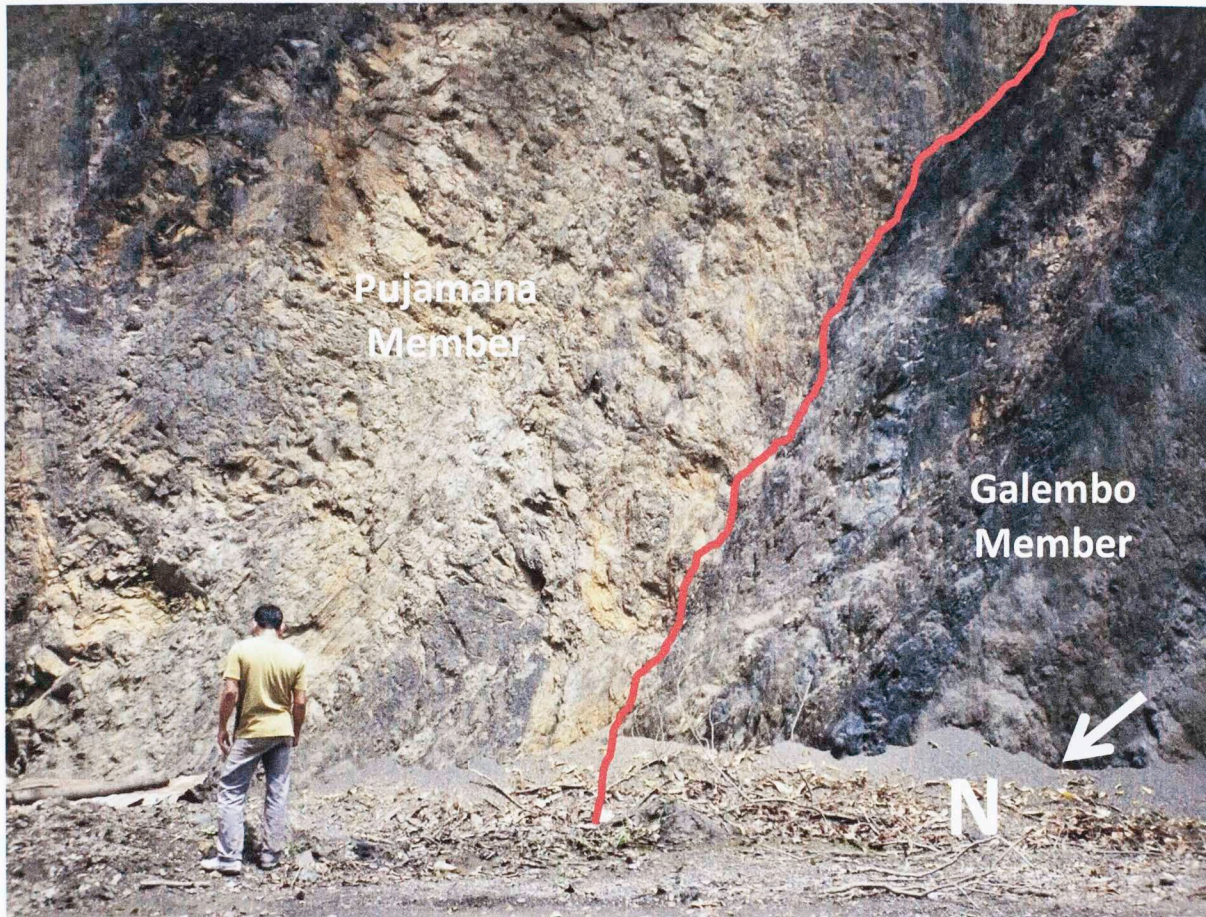
**Figure 8.** Contact of la Luna Fm top and Umir Fm basal coalbed, OUTCROP A.





**Figure 9.** La Luna Fm Galembó member, OUTCROP A.





**Figure 10.** Contact of Galembo and Pujamana members, OUTCROP A. Most of the Pujamana section is covered with vegetation.





**Figure 11.** Salada member, OUTCROP A. Black shales and marlstones are the main lithologies. Most of this member is covered with vegetation.

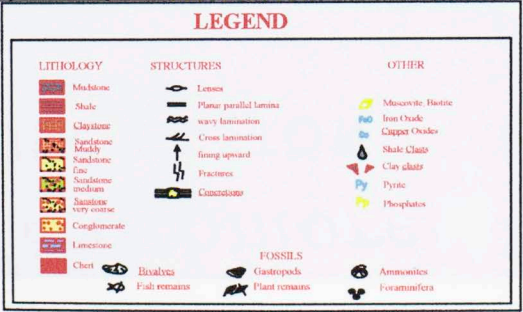
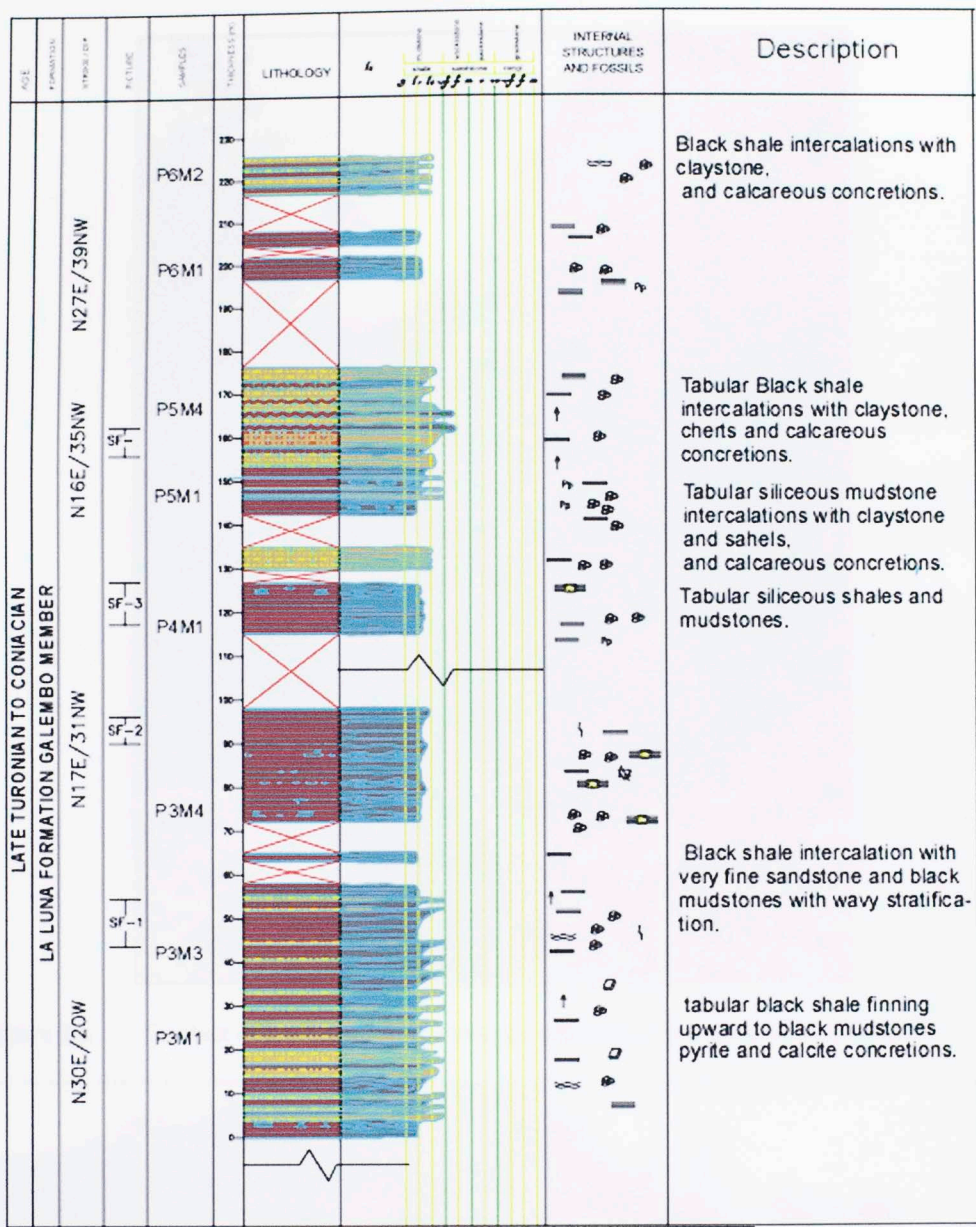
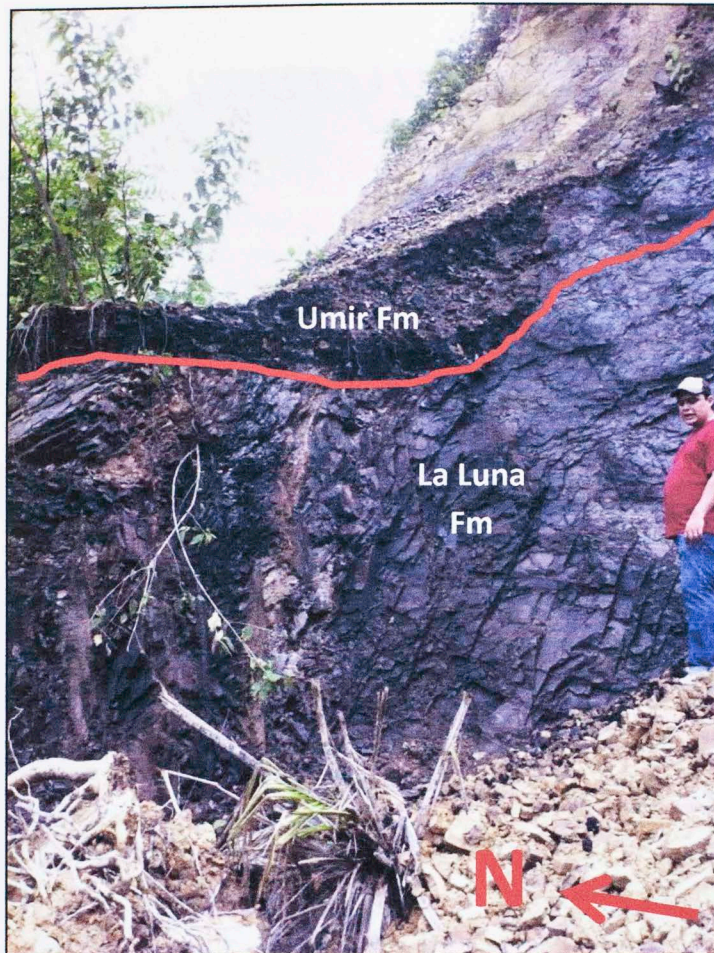


Figure 12. Stratigraphic column of the Galembó member in OUTCROP A.





**Figure 13.** Contact of La Luna Fm top contact with Umir Fm base, OUTCROP B.



**Figure 14.** La Luna Fm Salada outcrop in a quarry, OUTCROP B.





**Figure 15.** Pujamana member in OUTCROP B. More transitional lithofacies compose this member. Cherts, siliceous mudstones and claystones are the principal lithologies, with some light gray limestones towards the contact with the Galembo and Salada members.



**Figure 16.** Bitumen layers between cherts, claystone and siliceous mudstone beds of the Pujamana member, in OUTCROP B.




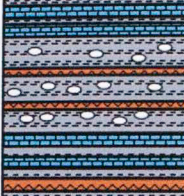
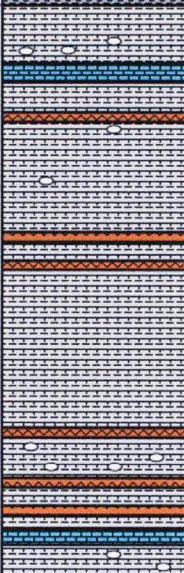
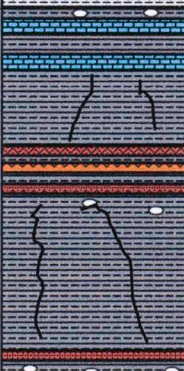


**Figure 17.** Galembo section at “*La Azufrada*” Creek, OUTCROP B. Section is covered by dense vegetation, but the water flowing through the creek allows the exposure of this member.



**Figure 18.** Galembo section, calcareous nodules at “*La Azufrada*” Creek. OUTCROP B.



AGE	Fm	Lithology	Thickness	Description
SANTONIAN CONIACIAN	Umir		9mts 29.57 ft	Coaly Shale lamina.
	La Luna Galebo member		55mts 180.45 ft	Black Calcareous shale, compacted, planar lamination. At the top part, intercalation with dark limestones. At the middle intercalation of dark shale with siliceous cherts and claystone lamina. Calcareous nodules are abundant. At the bottom, intercalation with siliceous limestones and dark cherts.
TURONIAN	La Luna Pujamana member		155mts 508.53 ft	Black Calcareous shale, compacted, planar lamination. At the middle intercalation with siliceous and calcareous cherts. Carbonate and phosphatic concretion are present and distributed arbitrarily. At the bottom calcareous limestones intercalation with gray shales and siliceous claystone layers.
	La Luna Salada member		100mts 328.08 ft	Black Calcareous shale, compacted, planar lamination. At the top part, intercalation with dark limestones. At the middle intercalation of dark shale with siliceous cherts and claystone lamina. Calcareous nodules are abundant and sizes above 50cms diameter. At the bottom, intercalation with claystones and abundance of calcareous and phosphatic nodules.






LEGEND	
	Calcareous Shale
	Coaly Shale Lamina
	Calcareous Limestone
	Chert
	Siltstone
	Black siliceous Shale
	Calcite Nodules

Figure 19. Measured stratigraphic column of La Luna Formation at OUTCROP B.

## **2.2. Experimental**

Sixty-six rock samples from eight different outcrop locations were analyzed in this study. Rock Eval Pyrolysis was conducted for all of these samples as a screening tool, and further cutoff values of Total Organic Carbon (TOC) higher than 2% and S2 higher than 20 mg HC/g rock were the discriminants for conducting biomarker analysis. For thin section, X-Ray diffraction and SEM porosity analysis, samples were chosen based on the pyrolysis results, combining organic rich and organic lean rocks. A list of all the La Luna shale samples analyzed is presented in Table 1 for the Southeast MMVB section (OUTCROP A) and in Table 2 for the Central MMVB section (OUTCROP B).

## **2.3. Source Rock Characterization**

A comprehensive series of geochemical analyses were performed on these samples, including Rock Eval pyrolysis, Total Organic Carbon (TOC), and Vitrinite Reflectance ( $\%R_o$ ). Additionally, crushed rock extracts were subjected to gas chromatography (GC) and gas chromatography-mass spectrometry (GCMS) for biomarker analyses. Rock Eval pyrolysis and TOC determination were performed at Geomark Geochemical Services in Humble, Texas. The other geochemical analyses were performed at the University of Oklahoma Organic Geochemistry Laboratories.

**Table.1.** List of the La Luna Formation, southeast MMVB, OUTCROP A samples analyzed in this study.

<b>Sample Name</b>	<b>Location</b>	<b>Lithology recognized on field</b>	<b>Stratigraphic Depth (ft)</b>	<b>La Luna Fm Member</b>
<b>Balastrearra El Carmen</b>	N 6°14.194' W 73°47.346'	Limestone	28	Galembo
<b>Borrascosa</b>	N 6°14.194' W 73°47.346'	Limestone	56	Galembo
<b>Borrascosa1</b>	N 6°14.194' W 73°47.346'	Black Limestone	84	Galembo
<b>El Balastro</b>	N 6°14.194' W 73°47.346'	Marlstone	112	Galembo
<b>El Carmen</b>	N 6°14.194' W 73°47.346'	Limestone	140	Galembo
<b>Balastreira Dia 3</b>	N 6°14.194' W 73°47.346'	Marlstone	168	Galembo
<b>P1M2</b>	N 6°14.686' W 73°51.777'	Black Shale	196	Galembo
<b>P1M4</b>	N 6°14.686' W 73°51.777'	Limestone	224	Galembo
<b>P1M5</b>	N 6°14.686' W 73°51.777'	Limestone	252	Galembo
<b>P2M1</b>	N 6°14.686' W 73°51.777'	Shale	280	Galembo
<b>P2M1</b>	N 6°14.686' W 73°51.777'	Limestone	308	Galembo
<b>P2M2</b>	N 6°14.686' W 73°51.777'	Limestone	336	Galembo
<b>P2M3</b>	N 6°14.686' W 73°51.777'	Limestone	364	Galembo
<b>P2M3</b>	N 6°14.686' W 73°51.777'	Marlstone	392	Galembo
<b>P2M4</b>	N 6°14.686' W 73°51.777'	Limestone	420	Galembo
<b>P2M5</b>	N 6°14.686' W 73°51.777'	Limestone	448	Galembo
<b>P2M7</b>	N 6°14.686' W 73°51.777'	Limestone	476	Galembo
<b>P3M1</b>	N 6°13.426' W 73°49.657'	Limestone	504	Galembo



**Table 1.** List of the La Luna Formation, southeast MMVB, OUTCROP A samples analyzed in this study. (cont.).

Sample Name	Location	Lithology recognized in field	Stratigraphic Depth (ft)	La Luna Fm Member
P3 M2	N 6°13.426' W 73°49.657''	Limestone	532	Galembo
P4M2	N 6°13.426' W 73°49.657'	Limestone	560	Galembo
P4M3	N 6°13.426' W 73°49.657'	Black Shale	588	Galembo
P4M3	N 6°13.426' W 73°49.657'	Shale	616	Galembo
P4M4	N 6°13.426' W 73°49.657'	Shale	644	Galembo
P5M1	N 6°13.162' W 73°49.343'	Shale	672	Galembo
P5M1	N 6°13.162' W 73°49.343'	Marlstone	700	Galembo
P5M2	N 6°13.162' W 73°49.343'	Limestone	728	Galembo
<b>PUJAMANA MEMBER GAP ~ 500ft</b>				
P2M6	N 6°13.506' W 73°49.841'	Shale	1228	Salada
P4M2	N 6°13.031' W 73°49.147'	Black Shale	1308	Salada
Top Salada	N 6°13.031' W 73°49.147'	Shale	1388	Salada
Salada Shale Top	N 6°13.031' W 73°49.147'	Black Shale	1468	Salada
Salada-1	N 6°13.031' W 73°49.147'	Calcareous Shale	1548	Salada
Salada-2	N 6°13.031' W 73°49.147'	Calcareous Shale	1628	Salada

**Table.2.** List of the La Luna Formation, central MMVB, OUTCROP B samples analyzed in this study.

Sample Name	Location	Lithology recognized in field	Stratigraphic Depth (ft)	La Luna Fm Member
QLS Umir	7°11'1.03"N 73°17'42.94"W	Coaly Shale	0	Galembo
QLS Umir-2	7°11'1.03"N 73°17'42.94"W	Asphaltite	17	Galembo
QLS M-1	7°11'1.03"N 73°17'42.94"W	Marlstone	34	Galembo
QLS M-3	7°11'1.03"N 73°17'42.94"W	Black Shale	51	Galembo
QLS M3-5	7°11'1.03"N 73°17'42.94"W	Limestone	68	Galembo
QLS M-6	7°11'1.03"N 73°17'42.94"W	Marlstone	85	Galembo
QLS M-7	7°11'1.03"N 73°17'42.94"W	Black Shale	102	Galembo
QLS M-7a	7°11'1.03"N 73°17'42.94"W	Limestone	119	Galembo
QLS M-8	7°11'1.03"N 73°17'42.94"W	Marlstone	136	Galembo
QLS M-10	7°11'1.03"N 73°17'42.94"W	Shale	153	Galembo
QLS CHERT-BIT	7°11'1.03"N 73°17'42.94"W	Chert with bitumen	170	Galembo
CAN M-15	7°10'4.62"N 73°18'7.02"W	Black Shale	221	Pujamana
CAN M-13	7°10'4.62"N 73°18'7.02"W	Shale	272	Pujamana
CAN M-11	7°10'4.62"N 73°18'7.02"W	Marlstone	323	Pujamana
CAN M-10	7°10'4.62"N 73°18'7.02"W	Limestone	374	Pujamana
CAN M-8	7°10'4.62"N 73°18'7.02"W	Shale	425	Pujamana
CAN M-7	7°10'4.62"N 73°18'7.02"W	Claystone	476	Pujamana
CAN M-6	7°10'4.62"N 73°18'7.02"W	Chert with bitumen	527	Pujamana
CAN M-5	7°10'4.62"N 73°18'7.02"W	Calcareous mudstone	578	Pujamana

**Table 2.** List of the La Luna Formation, central MMVB, OUTCROP B samples analyzed in this study (cont.)

<b>Sample Name</b>	<b>Location</b>	<b>Lithology recognized in field</b>	<b>Stratigraphic Depth (ft)</b>	<b>La Luna Fm Member</b>
CAN M-1	7°10'4.62"N 73°18'7.02"W	Chert	629	Pujamana
CAN M-1N	7°10'4.62"N 73°18'7.02"W	Claystone	680	Pujamana
CAR M-14	7° 8'57.21"N 73°18'22.96"W	Limestone	706	Salada
CAR M-13	7° 8'57.21"N 73°18'22.96"W	Limestone	732	Salada
CAR M-12	7° 8'57.21"N 73°18'22.96"W	Claystone	758	Salada
CAR M-11	7° 8'57.21"N 73°18'22.96"W	Black Shale	784	Salada
CAR M-9	7° 8'57.21"N 73°18'22.96"W	Limestone	810	Salada
CAR M-8	7° 8'57.21"N 73°18'22.96"W	Limestone	836	Salada
CAR M-5	7° 8'57.21"N 73°18'22.96"W	Marlstone	862	Salada
CAR M-4a	7° 8'57.21"N 73°18'22.96"W	Limestone	888	Salada
CAR M-4	7° 8'57.21"N 73°18'22.96"W	Marlstone	914	Salada
CAR M-3N	7° 8'57.21"N 73°18'22.96"W	Claystone	940	Salada
CAR M-3	7° 8'57.21"N 73°18'22.96"W	Black Shale	966	Salada
CAR M-2	7° 8'57.21"N 73°18'22.96"W	Black Shale	992	Salada
CAR M-1	7° 8'57.21"N 73°18'22.96"W	Claystone	1018	Salada



### **2.3.1. Preliminary Sample Treatment**

All the samples were washed with hot water, distilled water and a 1:1 mixture of dichloromethane ( $\text{CH}_2\text{Cl}_2$ ) and methanol ( $\text{CH}_3\text{OH}$ ) in order to remove any contaminants (e.g. drilling mud, plastic wrap, and handling). After the samples were completely dried, they were crushed with a porcelain mortar and pestle until a fine powder was obtained for screening analysis (TOC and Rock Eval) and soxhlet extraction.

### **2.3.2. Total Organic Carbon (TOC) and Rock Eval Pyrolysis**

Sixty six crushed rock samples were sent to GEOMARK Geochemical Services for TOC determination and Rock Eval pyrolysis. Approximately 2g of each sample were needed to perform these analyses.

### **2.3.3. Vitrinite Reflectance**

To establish the thermal maturity at both stratigraphic sections (OUTCROP A and OUTCROP B), vitrinite reflectance ( $\%R_o$ ) was measured for six samples, three from OUTCROP A (samples: Salada Top, P4M2, P4M3, see Table 1), and two from OUTCROP B (samples: CAR M2, QLS M-8 and UMIR2, see Table 2). These measurements were conducted with the courtesy of Brian Cardott from the Oklahoma Geological Survey.

The vitrinite reflectance values were obtained from pellets prepared at the Oklahoma Geological Survey Organic Petrography Laboratory and measured at the University of Oklahoma Organic Geochemistry Laboratories. The calculated vitrinite

reflectance values from Rock Eval Pyrolysis data (calculated %R<sub>o</sub>) were provided by GEOMARK Geochemical Services. These values are obtained from Rock Eval T<sub>max</sub> data according to the Jarvie et. al., (2007) equation proposed:

$$\text{Calculated \%VR}_o = 0.0180 \times T_{\text{max}} - 7.16$$

#### **2.3.4. Extraction and Fractionation**

A soxhlet extraction device was pre-extracted for 24 hours using a 1:1 mixture of dichloromethane (CH<sub>2</sub>Cl<sub>2</sub>) and methanol (CH<sub>3</sub>OH) in order to remove contaminants. Samples (50g) were extracted with the same solvent mixture for 48 hours. The excess solvent from the bitumen extract was evaporated using a rotary evaporator and the residues were transferred to a glass centrifuge tube for asphaltenes precipitation. The extract was separated into maltenes and asphaltenes by adding an excess of n-pentane. The centrifuge tubes were placed in a freezer overnight to promote complete asphaltene precipitation.

The maltene fractions were transferred to 250mL round bottom flasks to evaporate the solvent and the concentrates were placed in vials, evaporated to dryness and weighed. This fraction was then diluted in a ratio of 2mg sample per 50uL hexane (C<sub>6</sub>) for fractionation into saturates, aromatics, and NSO compounds (resins) by column liquid chromatography using an alumina column. For determining the source rock organic matter type and maturity, the saturate and aromatic fractions were diluted using 1mL of dichloromethane per 3mg of sample.

The n-alkanes were removed from the saturate fraction through molecular sieving. A Pasteur pipette was packed with approximately 2g of HI-SIV 3000 and three bed volumes of pentane were added to remove impurities. The sample was added to the column and it was allowed to stand for 2 minutes. Then, three additional bed volumes of C<sub>5</sub> were used to elute the sample. The n-alkanes were retained in the sieve while the branched and cyclic (B/C) compounds eluted from the column. This fraction was also diluted with 1mL of dichloromethane per 3mg of sample.

### **2.3.5. Gas Chromatography (GC)**

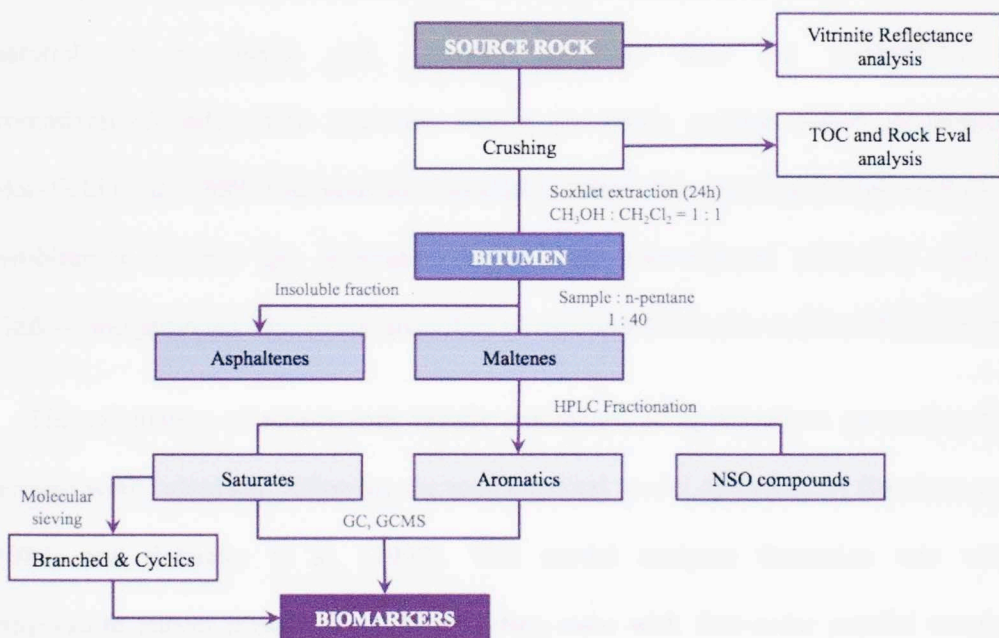
The instrument used for GC analyses was an Agilent 6890 series gas chromatograph with a split/splitless capillary injection system equipped with a 100m x 0.25mm (i.d.) J&D Scientific DB-1 Petro 122-10A6 fused silica capillary column coated with a 0.5µm liquid film. The temperature program for analyses started with an initial temperature of 40°C with 1.5 minutes hold time. The temperature was increased to 310°C at a rate of 4°C per minute followed by an isothermal period of 31 minutes for a total run of 100 minutes. The injector and flame ionization detector (FID) temperatures were set at 300°C and 310°C respectively. Samples were analyzed in splitless mode injection using helium (He) as the carrier gas and a flow rate of 0.5mL/min.

### **2.3.6. Gas Chromatography-Mass Spectrometry (GC-MS)**

GC-MS analyses were carried out with a Varian 3400 GC inlet system. For biomarker analysis, selected ions were chosen to analyze samples in single ion



monitoring (SIM) or multiple ion detection (MID) mode. The mass spectrometer ion source operated in electron impact mode with energy of 70 eV. The GC used a 60m x 0.32mm (i.d.) J&D Scientific DB-5 fused silica capillary column coated with a 0.25 $\mu$ m liquid film. The temperature program for the analyses started at 40°C with 1.5 minutes hold time and was later increased to 310°C at a rate of 4°C per minute and then held isothermal for 31 minutes. The ion source temperature was 200°C, injector temperature was 300°C and transfer line temperature was 310°C. A summary of the laboratory workflow used in this project is illustrated in Figure 20.



**Figure 20.** Schematic workflow used in the laboratory analysis. Methodology from the OU Organic Geochemistry Group (OG2). Diagram modified from Miceli-Romero (2010).

### 2.3.7. Micro-Scale Sealed Vessel( MSSV).

To determine the hydrocarbon generation potential of La Luna formation, the methodology Micro Scale Sealed Vessel Pyrolysis (MSSV-Py) was applied. This is an artificial maturation technique that simulates petroleum generation from a source rock in a closed system (Horsfield et al., 1989).

This method allows the generation of gas and “oil-like” pyrolysates issued from the cracking of the kerogen (primary cracking) and of the generation of gas issued from the cracking of oil and bitumen (secondary cracking). Furthermore, as the source rock is matured in a closed cell, primary products may be recombined by aromatization/condensation reactions into a gas-prone residue called pyrobitumen (Horsfield et al., 1989; Erdmann and Horsfield, 2006). The cracking at high maturity of pyrobitumen extends gas generation beyond the conventional secondary cracking window and provides significant quantities of methane (Erdmann and Horsfield, 2006).

The calculation of source rock kinetic parameters of hydrocarbon generation from kerogen were calculated following the mathematical model described by Burnham et al. (1987) and Schaefer et al. (1990). This model analyses formation rate versus temperature curves measured at three heating rates with first-order parallel reactions with activation energies ( $E_a$ ) regularly spaced between 35 and 80kcal/mol and a single pre-exponential factor  $A$  (s<sup>-1</sup>). As fast heating rates are responsible for heat transfer disturbances (Schenk and Dieckmann, 2004; Warren et al., 2012), the heating rates used were low, namely 0.2, 0.7 and 5°C/min. The curves of hydrocarbon generation of methane ( $C_1$ ), wet gas ( $C_2$ - $C_5$ ), total gas ( $C_1$ - $C_5$ ), and oil-like pyrolysate ( $C_6$ - $C_{30}$ ,  $C_6$ - $C_{14}$ ,

C<sub>15</sub>-C<sub>30</sub>) were processed through the kinetic analysis software package of Schlumberger Petromod 2012 and the results are part of Appendix I.

## **2.4. Reservoir Rock Characterization**

The data obtained for reservoir quality analyses of the outcrop samples include the two measured stratigraphic sections, lithostratigraphy, Scanning Electron Microscopy (SEM) porosity analysis, thin section, X-Ray Diffraction (XRD) mineral content analysis and integrated organic geochemistry (Total Organic Carbon -TOC- and Relative Hydrocarbon Potential -RHP- profiles).

### **2.4.1. Scanning Electron Microscopy (SEM).**

SEM analysis was conducted on seven samples with Dr. Neal O'Brien at the State University of New York, SUNY Potsdam. The seven samples were selected based on their total organic carbon (TOC) content, four for the central MMVB section (OUTCROP B) and three for the south MMVB section (OUTCROP A). The sample selection was made with the representation of each end of the visual properties spectrum as well as samples which fell between the end members. The sample pieces which were analyzed were oriented outcrop samples. Each sample was oriented so the viewing surface would be perpendicular to bedding. The samples were then cut with a diamond disc until they were approximately 3 mm thick. Each sample was then broken by applying pressure from each end with a pair of vice grips (Figure 21). This technique allows for the viewing of a freshly broken surface. After the samples had been broken, they were mounted onto an aluminum stub with the freshly broken surface

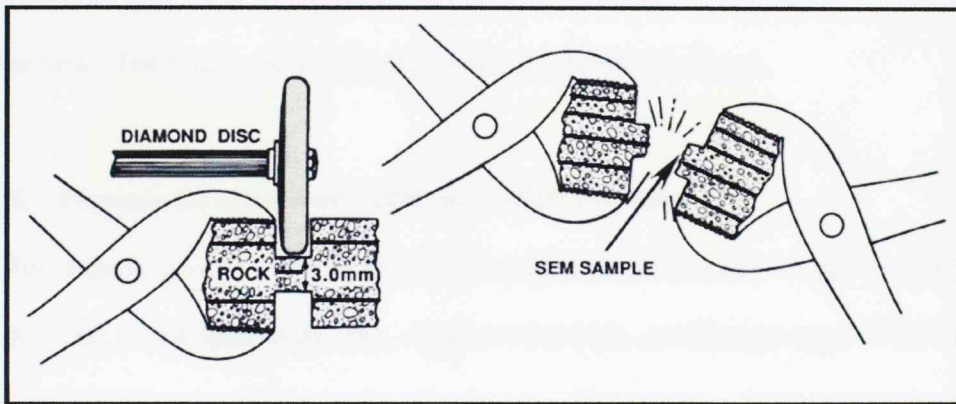
Figure 21. Diagram showing how the samples were oriented into the scanning stub.



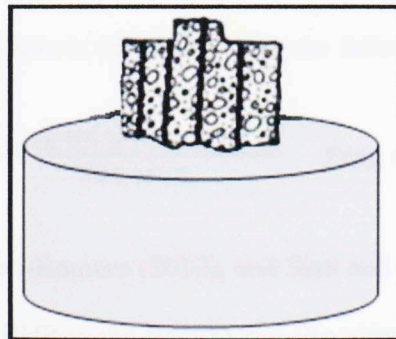
facing upward (Figure 22). After the samples had been prepared, they were then analyzed using an ISI – Topcon SEM. The samples were analyzed at 4,000 times magnification +/- 100 times magnification.

#### 2.4.2. Thin section analysis

Ten thin sections were constructed from the outcrop samples corresponding to Galemba, Pujamana and Salada members. These ten samples provided a guide for analysis of Rock Eval data and XRD data. Thin sections (30 micron thick), all were stained for calcite and were accompanied with cover slips.



**Figure 21.** Diagram showing how the samples were prepared for viewing with the SEM. Black lines in the sample represent bedding planes. Modified from O'Brien and Slatt, (1990).



**Figure 22.** Diagram showing how the samples were mounted onto the aluminum stub.

The thin sections were analyzed using a Zeiss Axio Imager Z1 polarizing microscope with varying degrees of magnification (10 – 100x). Images were captured with a Zeiss AxioCam MRc5 camera in conjunction with the polarizing microscope. Detailed descriptions for each thin section can be found in Appendix II.

### **2.4.3. XRD**

The XRD results are obtained commercially through the OU Institute of Reservoir Characterization (IRC). The results include the amount of quartz, calcite, siderite, pyrite, kaolinite, illite/mica and bulk grain density of the rock. Results were calculated in both weight percentage and volume percentage including the TOC content of the rock. The results were then graphically represented in Excel.

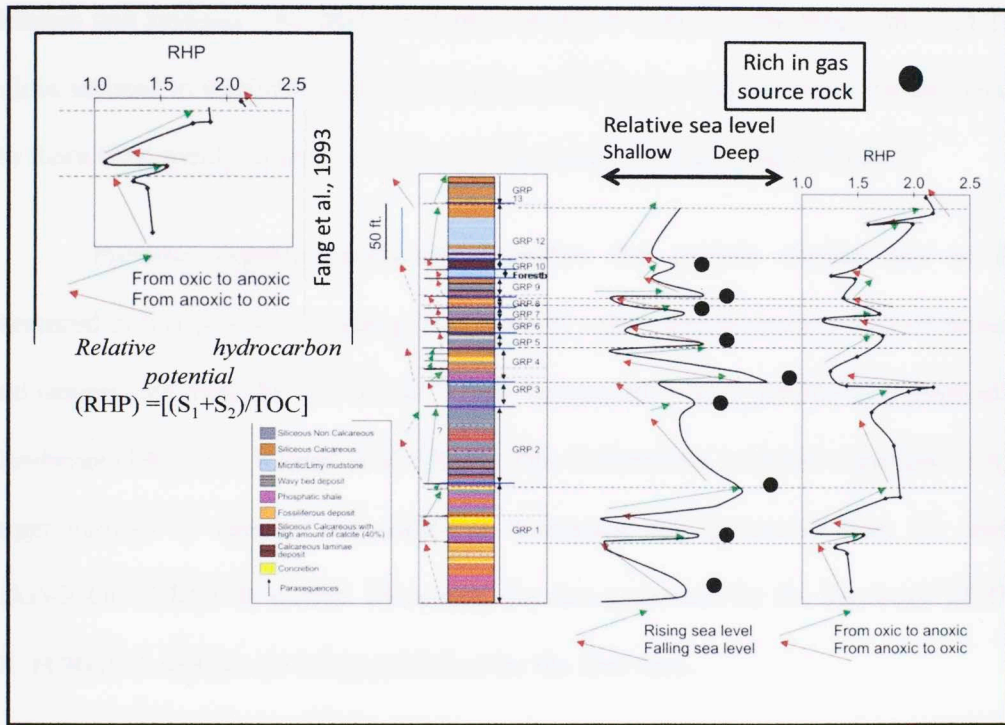
### **2.4.4. Organic Geochemistry TOC and RHP Profiling**

The organic geochemistry Rock Eval Pyrolysis results include weight % TOC, S1, S2, S3, Tmax, hydrogen index (HI), oxygen index (OI), and kerogen type. TOC results were graphically represented in Excel software. The Relative Hydrocarbon Potential (RHP) is an indicator of anoxic and oxic depositional environmental conditions (Fang et al., 1993). Fluctuations in oxygenation conditions are reflected by variations in the relative hydrocarbon potential ratio is calculated using the following equation:

$$\text{RHP} = \frac{\text{S1 mg HC/g} + \text{S2 mg HC/g}}{\text{TOC wt.}\%} \quad \text{Fang et al. (1993),}$$

Fang et al. (1993), Miceli-Romero (2010), and Slatt and Rodriguez (2012), noted stratigraphic variations in the RHP in the Barnett and Woodford shales respectively. In

these cases, it was observed that changes in oxygen levels as indicated by the RHP showed a good correlation with changes in relative sea levels fluctuations derived from the stratigraphic interpretations for the Barnett Shale (Figure 23). Depths with maximum RHP values (anoxic conditions) correspond with interpreted stratigraphic flooding surfaces, while minimum RHP values (oxic conditions) correlate with oxidizing conditions due to lowered sea level (Slatt and Rodriguez, 2012).



**Figure 23.** Comparison of relative sea level and RHP curves for the Barnett Shale. Changes in oxic conditions as indicated by the RHP show a positive correlation with fluctuations in relative sea level. Modified from Miceli-Romero (2010) and Slatt and Rodriguez (2012).



## CHAPTER III

### 3. RESULTS AND DISCUSSIONS

#### 3.1. Source Rock Characterization

Source rock samples were screened on the basis of total organic carbon (TOC) content and Rock Eval pyrolysis. These analyses permit determination of organic richness and kerogen type. Measured and calculated vitrinite reflectance data and  $T_{\max}$  values assisted in establishing thermal maturity for the La Luna samples. Definitions of the Rock Eval pyrolysis terms used in this discussion are presented in Table 3.

Previous organic geochemistry studies that include similar data to that presented in this project, including TOC and HI values and biomarker data of steranes and isoprenoids from the “*La Sorda*” creek section, have been previously published by Zumberge (1984) and Rangel et al. (2000). This information is herein expanded using a larger number of samples and additional biomarker data generated from the central MMVB OUTCROP B section. Moreover, the data generated for the Southeast MMVB OUTCROP A section are being published for the first time.

##### 3.1.1. Organic Richness

The TOC values reflect the amount of organic carbon, including kerogen and bitumen, in a source rock (Peters and Cassa, 1994). The La Luna shale and limestone samples showed TOC values ranging from 1.41% to 11.90% for both OUTCROP A and OUTCROP B sections, indicative of very good to excellent potential source rocks (Peters, 1986; Peters and Cassa, 1994).

Geochemical logs for the central and southeast sections were constructed in order to illustrate the TOC variation with stratigraphic column depth (Figures 24 and 25). In the central section, OUTCROP B, TOC values range between 0.22% and 4.12% for the Galembo member. The lower values are for the transitional deposits such as cherts and siliceous mudstones, and the organic rich sediments are black shales. For the Pujamana member, the TOC values range between 0.24% and 2.54%; the lowest values are for cherts and claystones, and the highest values are for limestones at the contact with the Galembo member. For the Salada member, the TOC values range between 0.25% and 11.90%, with similar characteristics to the Galembo member. The transitional deposits present organic lean characteristics and the black shales being the most organic rich lithologies.

In the south east section, OUTCROP A, TOC values range between 0.31% and 11.90% for the Galembo member; the lower values are for the transitional deposits such as cherts and siliceous mudstones, and the organic rich sediments are for black shales. The low TOC may also be attributed to the high maturity level (average  $T_{max}$  of 511°C, and  $Ro_{Calc}$  2.04%) which transformed the organic matter and dead carbon left within the rock matrix. For the Salada member, the TOC values range between 2.60% and 10.60%, with similar characteristics to the Galembo member. The transitional deposits contain less organic matter, and the marine black shale deposits contain the most organic rich samples. An interesting factor is that despite the high maturity level of the lower member in this area (average  $T_{max}$  of 540;  $Ro_{Calc}$  2.57%), it still has high TOC values, suggesting these values correspond to dead carbon in the rock, and indicating that the original organic content in the rock was much higher.

The breaks that occur in the TOC log for the OUTCROP A and OUTCROP B sections can be attributed to changes in lithological or mineralogical characteristics of the members. Differences between both sections can also be attributed to the dramatic changes in maturity, from an oil window for the Central MMVB OUTCROP B section, to a deep dry gas window for the Southeast MMVB OUTCROP A section. Weathering is also present due to dense vegetation in the area and by fresh water washing by tropical rain storms and streams that might enhance the outcrop organic matter degradation.

The previous organic geochemistry studies by Rangel et al. (1996 and 2000) established important facies changes across the stratigraphic column in the “*La Sorda*” section, that were used also to recognize the upper-middle and middle-lower La Luna Formation boundaries in the field. Zumberge (1984) and Rangel et al. (1996 and 2000), mentioned that the La Luna Formation is a petroleum source rock with good to excellent potential for oil. About 63% of the volume of this formation is composed of phosphatic calcareous shales and laminated mudstones with abundant foraminifers.

Rangel et al. (1996 and 2000), identified three major stratigraphic cycles: (1) a generalized base level fall during deposition of the Salada member; (2) a base level rise or a deepening of the basin during sedimentation of the Pujamana member, and (3) a second base level fall that permitted deposition of the calcareous and phosphatic lithologies of the Galembo member. Zumberge (1984) and Rangel et al. (2000) also recognized that during shallowing stages in carbonate shelves (Salada member and Galembo member) TOC decreases towards the top, and in the siliciclastic shelf, during



shallowing stages, (Pujamana-Salada Member), both TOC values decrease continuously. Because these interpretations are consistent with the geochemical variations observed on the samples from this study, it is proposed that this analysis contains the three La Luna Formation members frequently described in the literature (Garner, 1926; Hubach, 1957; Morales, 1958; Julivert, 1968 and 1970; Zumberge, 1984; Rangel et al., 2000).

**Table.3.** Parameters and terms derived from Rock Eval pyrolysis (modified from Peters and Cassa, 1994; Jarvie et al., 2005, 2007).

<b>TOC</b>	Total Organic Carbon	wt.%
<b>S<sub>1</sub></b>	Free volatile hydrocarbons thermally flushed from a rock sample at 300°C (free oil content)	mg HC/g rock
<b>S<sub>2</sub></b>	Products that crack during standard Rock Eval pyrolysis temperatures (remaining potential)	mg HC/g rock
<b>S<sub>3</sub></b>	Organic carbon dioxide released from rock samples	mg CO <sub>2</sub> /g rock
<b>T<sub>max</sub></b>	Temperature at peak evolution of S <sub>2</sub> hydrocarbons	°C
<b>HI</b>	Hydrogen Index = S <sub>2</sub> x 100/TOC	mg HC/g TOC
<b>OI</b>	Oxygen Index = S <sub>3</sub> x 100/TOC	mg CO <sub>2</sub> /g TOC
<b>S<sub>1</sub>/TOC</b>	Normalized Oil Content = S <sub>1</sub> x 100/TOC	
<b>S<sub>2</sub>/S<sub>3</sub></b>	Describes type of hydrocarbons generated	Values from 0.00 to >5.00
<b>PI</b>	Production Index = S <sub>1</sub> /(S <sub>1</sub> + S <sub>2</sub> ) (or transformation ratio)	Values from 0.00 to 1.00

**Table.4.** Total Organic Carbon (TOC) and Rock Eval data from La Luna southeast section, OUTCROP A samples used in this study.

Sample Name	TOC	S1	S2	S3	Tmax	HI	OI	S2/S3	S1/TOC	PI
Balastreara El Carmen	0.82	0.01	0.07	0.12	n.d.	9	15	1	1.22	0.13
Borrascosa	0.15	0.05	0.02	0.08	n.d.	13	53	0.25	33.33	0.71
Borrascosa1	0.86	0.01	0.08	0.12	n.d.	9	14	1	1.16	0.11
El Balastro	1.09	0.01	0.14	0.03	n.d.	13	3	5	0.92	0.07
El Carmen	1.21	0.03	0.15	0.03	n.d.	12	2	5	2.48	0.17
Balastreira Dia 3	0.97	0.01	0.04	0.11	n.d.	4	11	0.36	1.03	0.20
P1M2	0.48	0.01	0.13	0.11	n.d.	27	23	1	2.08	0.07
P1M4	0.77	0.04	0.31	0.52	505	40	68	1	5.19	0.11
P1M5	1.33	0.03	0.27	0.03	486	20	2	9	2.26	0.10
P2M1	1.51	0.06	0.66	0.07	502	44	5	9.5	3.97	0.08
P2M1	1.14	0.01	0.06	0.31	n.d.	5	27	0.19	0.88	0.14
P2M2	0.68	0.01	0.01	0.07	n.d.	1	10	0.14	1.47	0.50
P2M3	1.76	0.08	0.84	0.08	498	48	5	11	4.55	0.09
P2M3	1.47	0.03	0.11	0.12	n.d.	7	8	1	2.04	0.21
P2M4	1.77	0.04	0.11	0.09	n.d.	6	5	1.22	2.26	0.27
P2M5	0.61	0.01	0.01	0.18	n.d.	2	30	0.06	1.64	0.50
P2M7	1.51	0.02	0.05	0.18	n.d.	3	12	0.28	0.66	0.17
P3M1	0.36	0.03	0.03	0.09	n.d.	8	25	0.33	5.56	0.40

**Table 4.** Total Organic Carbon (TOC) and Rock Eval data from La Luna southeast section, OUCROP A samples used in this study (cont).

Sample Name	TOC	S1	S2	S3	Tmax	HI	OI	S2/S3	S1/TOC	PI
<b>P3 M2</b>	0.31	0.02	0.03	0.51	n.d.	10	165	0.06	6.45	0.40
<b>P4M2</b>	0.64	0.04	0.09	0.10	n.d.	14	16	1	6.25	0.31
<b>P4M3</b>	11.60	0.02	2.65	0.07	537	23	1	38	0.17	0.01
<b>P4M3</b>	11.90	0.02	2.66	0.06	537	22	1	44	0.17	0.01
<b>P4M4</b>	0.64	0.03	0.07	0.35	n.d.	11	55	0.20	4.69	0.30
<b>P5M1</b>	0.36	0.01	0.02	0.12	n.d.	6	33	0.17	2.78	0.33
<b>P5M1</b>	0.36	0.02	0.02	0.13	n.d.	6	36	0.15	5.56	0.50
<b>P5M2</b>	0.45	0.01	0.01	0.01	n.d.	2	2	1	2.22	0.50
<b>PUJAMANA MEMBER GAP ~ 500 ft.</b>										
<b>P2M6</b>	2.70	0.01	0.23	0.12	548	9	4	2	0.37	0.04
<b>P4M2</b>	10.60	0.03	2.78	0.13	535	26	1	21.38	0.28	0.01
<b>Top Salada</b>	4.01	0.01	0.12	0.50	n.d.	3	12	0.24	0.25	0.08
<b>Salada Shale Top</b>	4.49	0.02	0.21	1.35	n.d.	5	30	0.16	0.45	0.09
<b>Salada-1</b>	3.25	0.01	0.10	0.08	n.d.	3	2	1.25	0.31	0.09
<b>Salada-2</b>	8.68	0.02	1.96	0.03	538	23	0	65.33	0.23	0.01

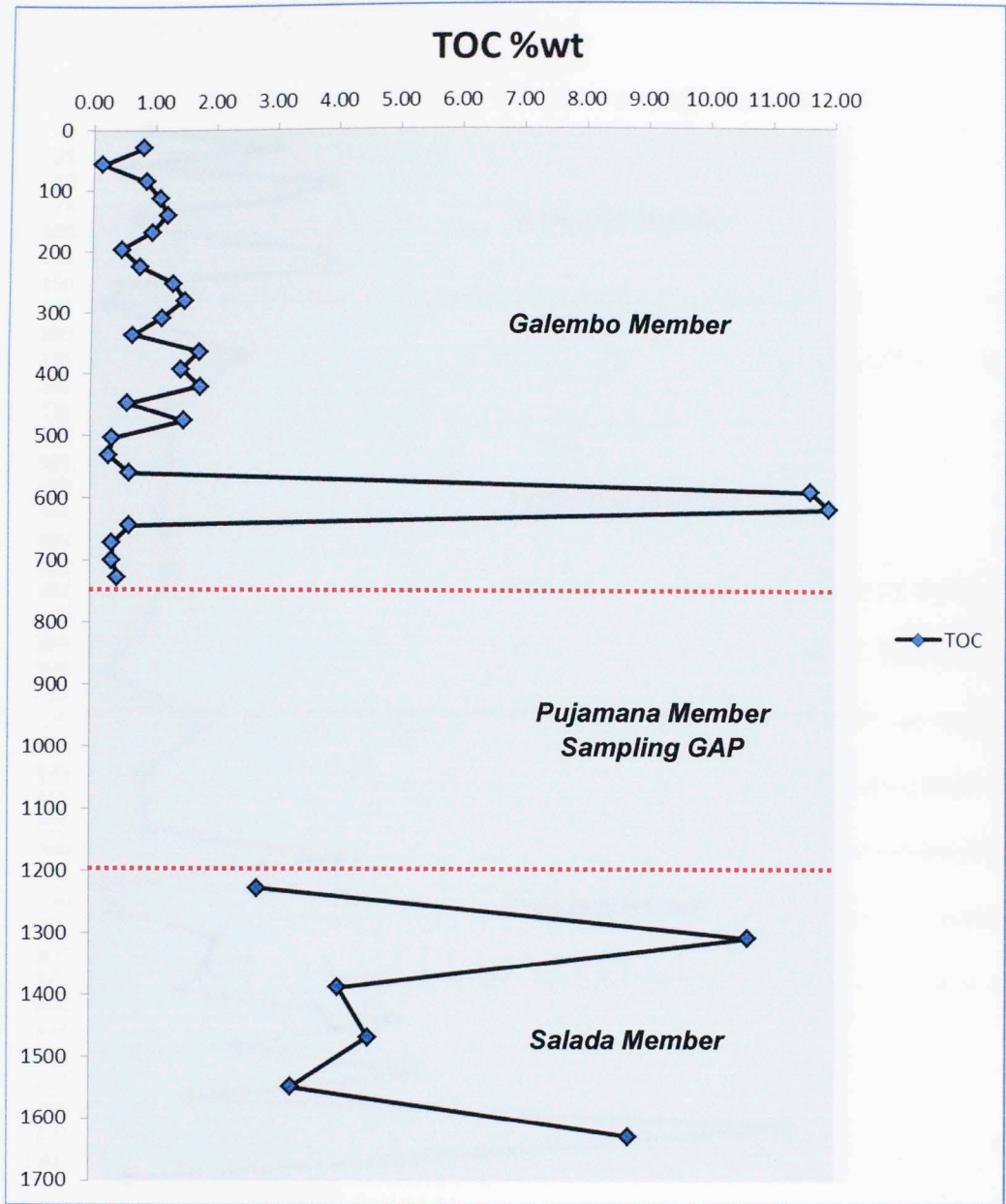


**Table.5.** Total Organic Carbon (TOC) and Rock Eval data from La Luna central MMVB section, OUTCROP B samples used in this study.

Sample Name	TOC	S1	S2	S3	Tmax	HI	OI	S2/S3	S1/TOC	PI
QLS Umir	0.89	0.01	0.45	0.48	437	51	54	1	1	0.02
QLS Umir-2	3.10	1.60	20.83	0.53	418	672	17	39	52	0.07
QLS M-1	0.43	0.04	0.61	0.23	430	141	53	3	9	0.06
QLS M-3	4.09	3.74	17.39	0.28	440	425	7	62	91	0.18
QLS M3-5	3.18	1.44	10.32	0.49	434	325	15	21	45	0.18
QLS M-6	0.77	0.02	0.50	0.46	433	65	60	1	3	0.04
QLS M-7	1.41	0.06	1.77	0.53	432	126	38	3	4	0.03
QLS M-7a	3.94	3.32	16.14	0.37	435	410	9	44	84	0.17
QLS M-8	4.12	4.07	18.10	0.25	435	439	6	72	99	0.18
QLS M-10	0.40	0.06	0.77	0.08	434	193	20	10	15	0.07
QLS CHERT-BIT	0.22	0.02	0.21	0.05	435	97	23	4	9	0.09
CAN M-15	2.54	0.21	4.38	0.57	438	172	22	8	8	0.05
CAN M-13	1.37	0.01	0.47	0.60	437	34	44	1	1	0.02
CAN M-11	1.31	0.48	3.03	0.23	437	231	18	13	37	0.14
CAN M-10	1.17	0.01	0.84	0.77	436	72	66	1	1	0.01
CAN M-8	1.32	0.31	2.50	0.31	437	189	23	8	23	0.11
CAN M-7	0.98	0.05	1.60	0.26	437	163	26	6	5	0.03
CAN M-6	0.24	0.01	0.07	0.14	N.D.	30	59	1	4	0.13
CAN M-5	1.90	0.02	1.11	1.23	438	58	65	1	1	0.02

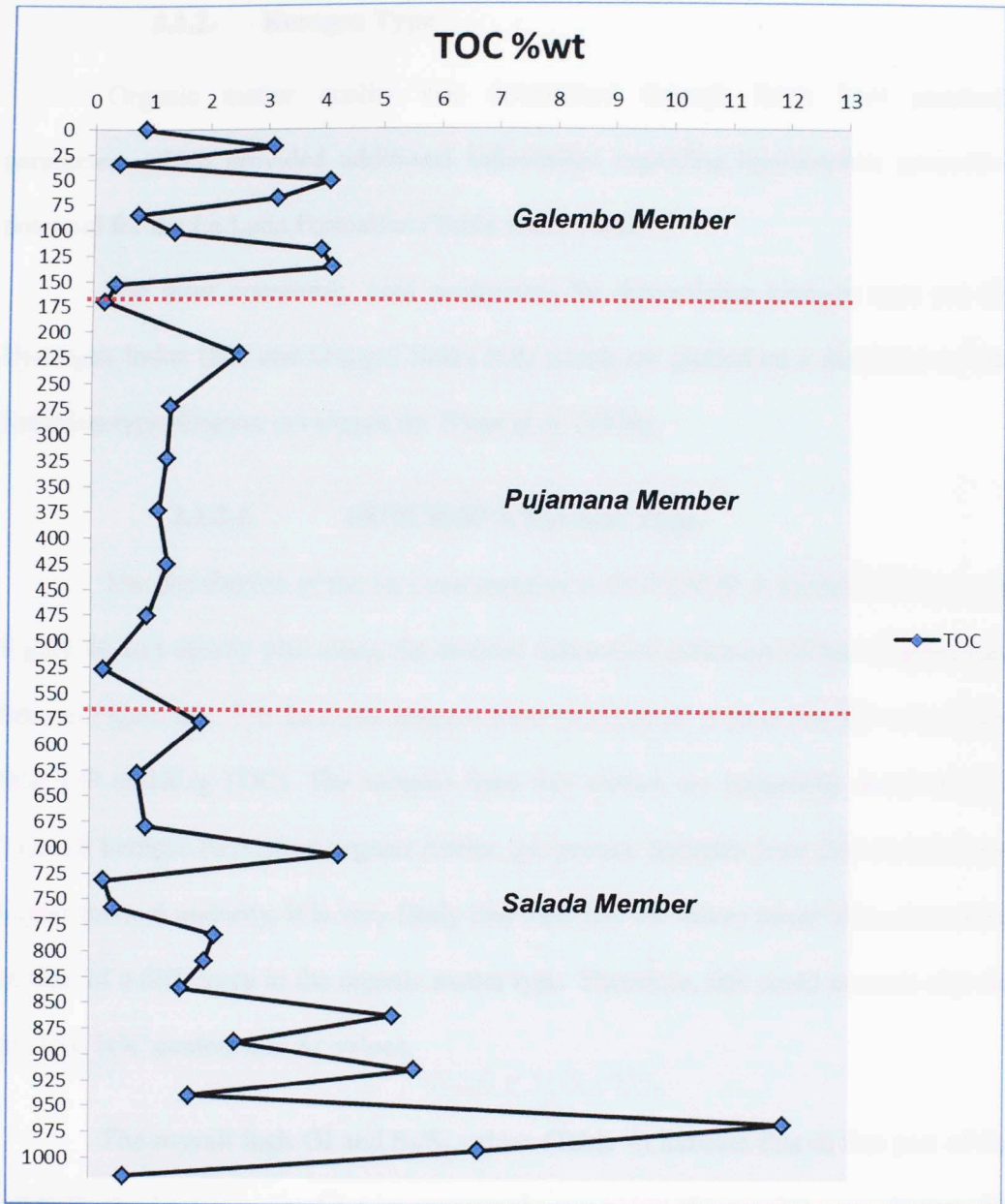
**Table 5.** Total Organic Carbon (TOC) and Rock Eval data from La Luna central MMVB section, OUTCROP B samples used in this study (cont.).

<b>Sample Name</b>	<b>TOC</b>	<b>S1</b>	<b>S2</b>	<b>S3</b>	<b>Tmax</b>	<b>HI</b>	<b>OI</b>	<b>S2/S3</b>	<b>S1/TOC</b>	<b>PI</b>
<b>CAN M-1</b>	0.83	0.01	0.30	0.41	440	36	50	1	1	0.03
<b>CAN M-1N</b>	0.97	0.14	1.48	0.27	435	152	28	5	14	0.09
<b>CAR M-14</b>	4.27	4.26	24.61	0.30	432	576	7	79	100	0.15
<b>CAR M-13</b>	0.25	0.06	0.33	0.10	441	130	39	3	24	0.15
<b>CAR M-12</b>	0.41	0.07	0.78	0.09	436	188	22	9	17	0.08
<b>CAR M-11</b>	2.15	3.46	11.91	0.26	431	554	12	46	161	0.23
<b>CAR M-9</b>	1.98	2.24	8.03	0.21	437	406	11	38	113	0.22
<b>CAR M-8</b>	1.57	0.25	2.97	0.28	433	189	18	11	16	0.08
<b>CAR M-5</b>	5.20	5.18	23.72	0.26	437	456	5	91	100	0.18
<b>CAR M-4a</b>	2.50	0.26	5.25	0.49	439	210	20	11	10	0.05
<b>CAR M-4</b>	5.58	5.81	25.92	0.23	435	465	4	113	104	0.18
<b>CAR M-3N</b>	1.72	0.43	3.90	0.20	436	227	12	20	25	0.10
<b>CAR M-3</b>	11.90	8.36	54.54	0.24	436	458	2	227	70	0.13
<b>CAR M-2</b>	6.68	5.65	29.31	0.24	437	439	4	122	85	0.16
<b>CAR M-1</b>	0.60	0.37	1.83	0.17	434	304	28	11	62	0.17



**Figure 24.** Geochemical log showing TOC vs Depth for the OUTCROP A stratigraphic section.





**Figure 25.** Geochemical log showing TOC vs Depth for the OUTCROP B stratigraphic section.

### 3.1.2. Kerogen Type

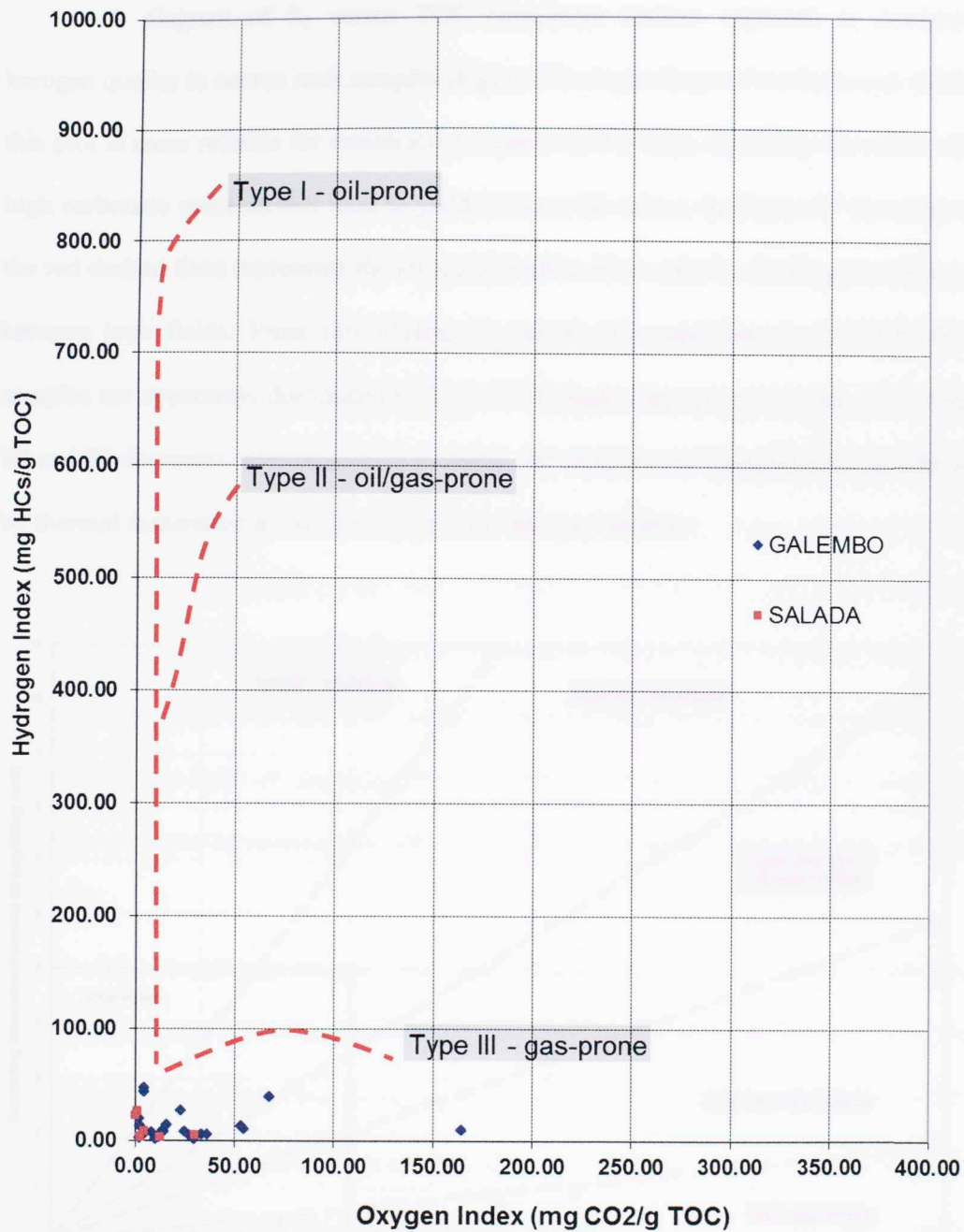
Organic matter quality was determined through Rock Eval pyrolysis parameters which provided additional information regarding hydrocarbon generative potential for the La Luna Formation (Table 4 and Table 5).

The most commonly used parameters for determining kerogen type are the Hydrogen Index (HI) and Oxygen Index (OI) which are plotted on a modified or Van Krevelen-type diagram developed by Tissot et al. (1974).

#### 3.1.2.1. OUTCROP A Kerogen Type.

The distribution of the La Luna samples in OUTCROP A section are shown in Figure 26 and mainly plot along the thermal maturation pathways of the diagram (red lines in Figure 26). The La Luna samples from OUTCROP A have low HI values (less than 100 mgHC/g TOC). The samples from this section are apparently dominated by Type III kerogen (terrestrial organic matter, gas prone). Samples from this section show higher thermal maturity, it is very likely that their low HI values result from maturation instead of a difference in the organic matter type. Therefore, this could account also for the low TOC content and S<sub>2</sub> values.

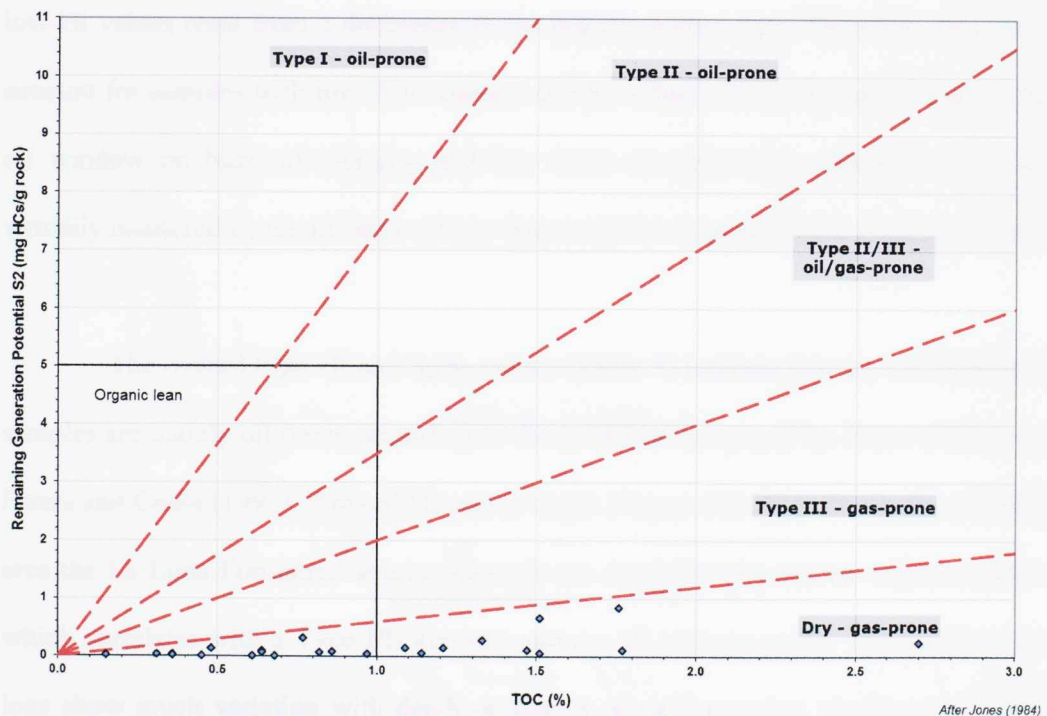
The overall high OI and S<sub>2</sub>/S<sub>3</sub> values (Table 4) indicate that in this part of the MMVB, the La Luna members are apparently gas prone (Figure 26) according to the guidelines proposed by Peters (1986) and Peters and Cassa (1994).



**Figure 26.** Modified Van Krevelen diagram for the OUTCROP A. The interpretations of low HI values are due to depletion by high thermal maturation and secondary cracking where the values yield on an apparent type III kerogen. Average Tmax: 521 °C.



A diagram of  $S_2$  versus TOC constitutes another approach to determine kerogen quality in source rock samples (Figure 27). According to Cornford et al. (1998) this plot is more reliable for establishing organic matter type, especially for rocks with high carbonate contents that tend to yield dubious OI values. In Figure 27 the slope of the red dashed lines represents the HI and therefore they assist in dividing the different kerogen type fields. From this diagram it can be observed that the OUTCROP A samples are apparently dominated by Type IV kerogen, dry gas prone area. Given that HI and  $S_2$  decreases with increasing maturity, the samples are interpreted to be affected by thermal maturation as will be explained in the next section.

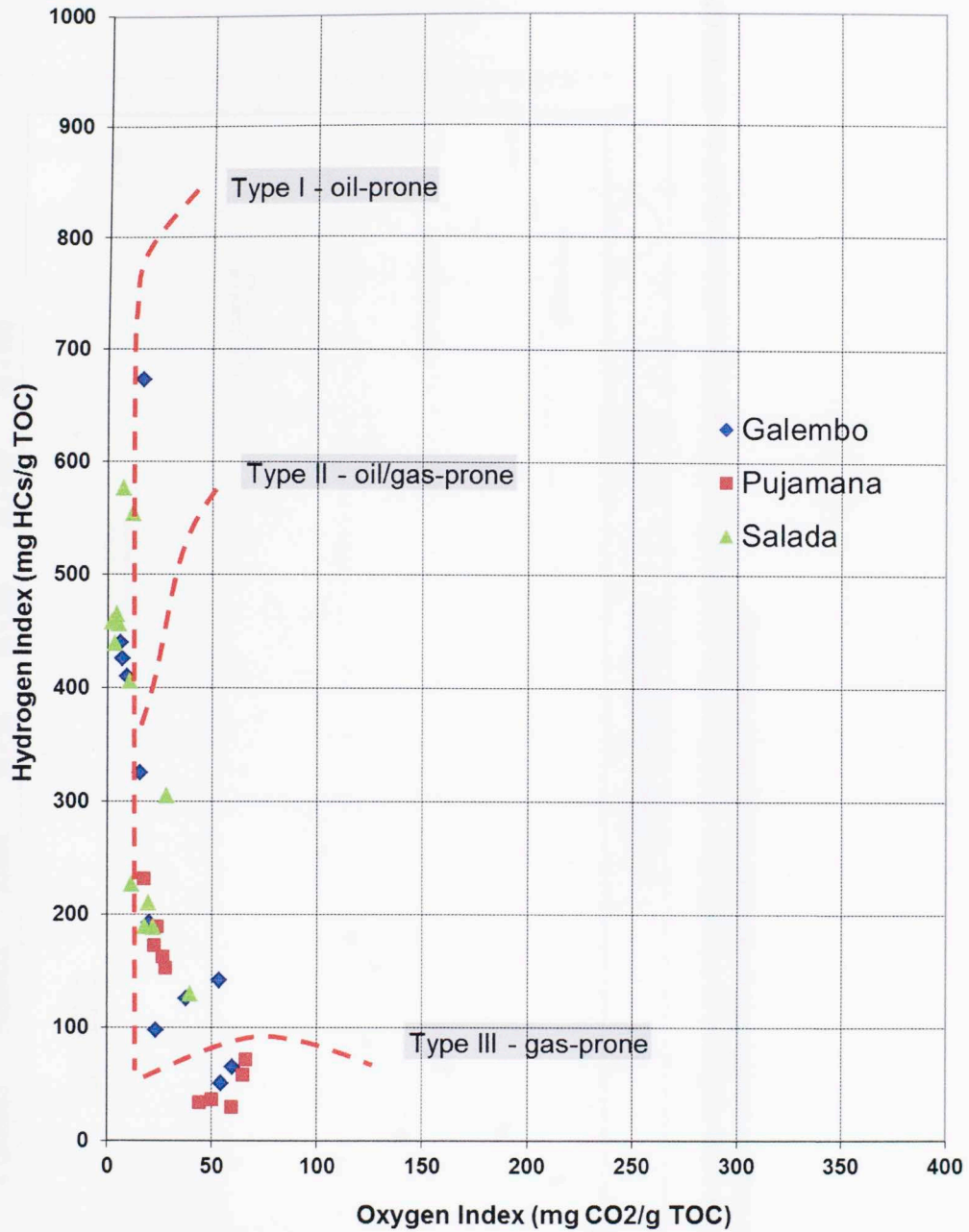


**Figure 27.** Rock Eval Remaining Hydrocarbon Potential ( $S_2$ ) vs. TOC plot for determination of kerogen type and maturity of the OUTCROP A La Luna samples (plot template modified from Geomark Geochemical Services).

### 3.1.2.2. OUTCROP B Kerogen Type.

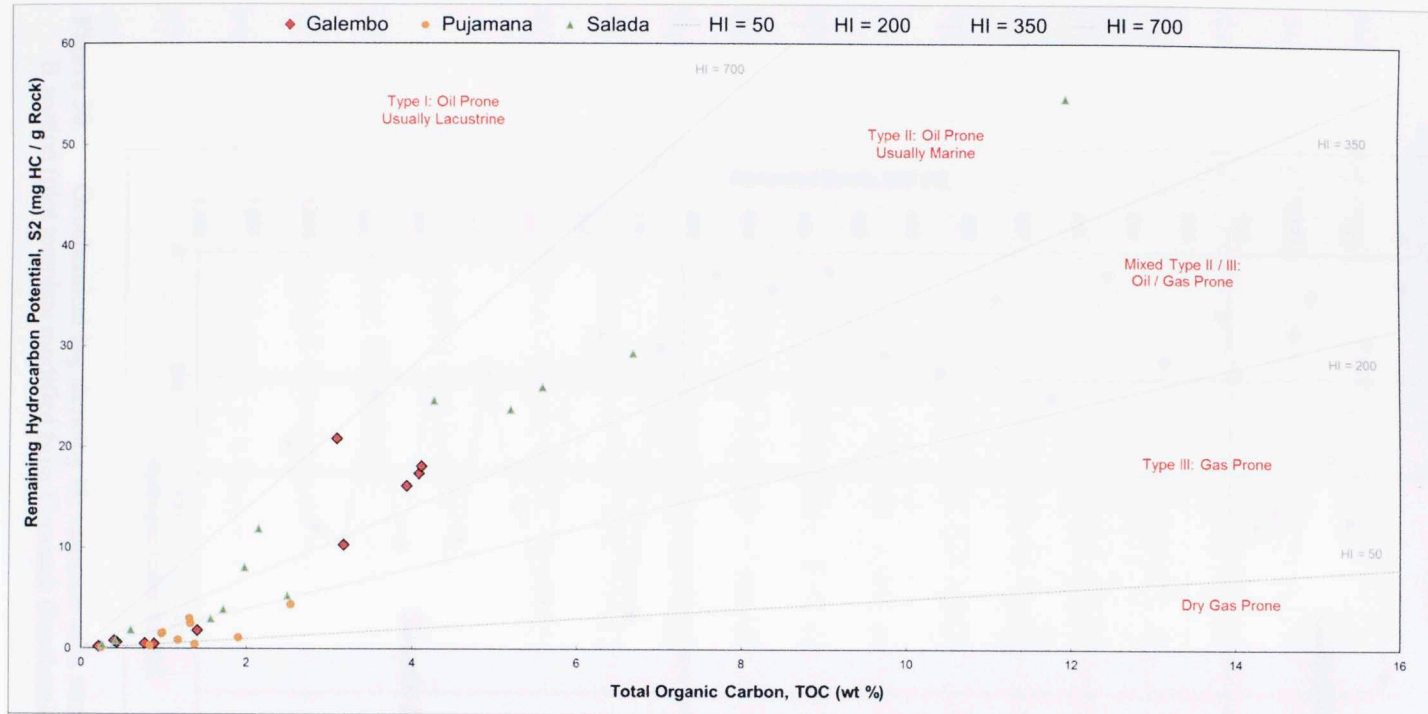
The distribution of the OUTCROP B samples are shown in Figure 28 and 29, which mainly plot along the thermal maturation pathways of the diagram (red dashed lines). The Galembó and Salada members have higher HI values (greater than 300 in most cases). The samples from these members are dominated by Type I and Type II kerogen (marine organic matter, oil and gas prone). The lower HI values are represented by samples mainly from the Pujamana member, but also some Galembó member samples have low values. Because previous studies (Zumberge 1984; Rangel et al., 2000) reported that Pujamana member has a higher terrestrial input and the Galembó member present siliciclastic inputs (also observed in the field), it is very likely that their low HI values result from a difference in the organic matter type. Therefore, this could account for samples with low TOC content and S<sub>2</sub> values. Since the samples are in the oil window on basis of maturity and low level of conversion (Table 5) these are virtually unaltered by temperature effects that could have lowered their organic content.

The overall high HI and S<sub>2</sub>/S<sub>3</sub> values (Table 5) indicate that the OUTCROP B samples are mainly oil prone according to the guidelines proposed by Peters (1986) and Peters and Cassa (1994). Plots of HI versus depth (Figure 30) show that in this MMVB area the La Luna Formation source intervals are dominated by marine organic matter, which correlates with a Type I/II kerogen and are oil and gas prone. The geochemical logs show much variation with depth on breaks of each member, similar to the ones observed on the TOC versus depth plot (Figure 25).

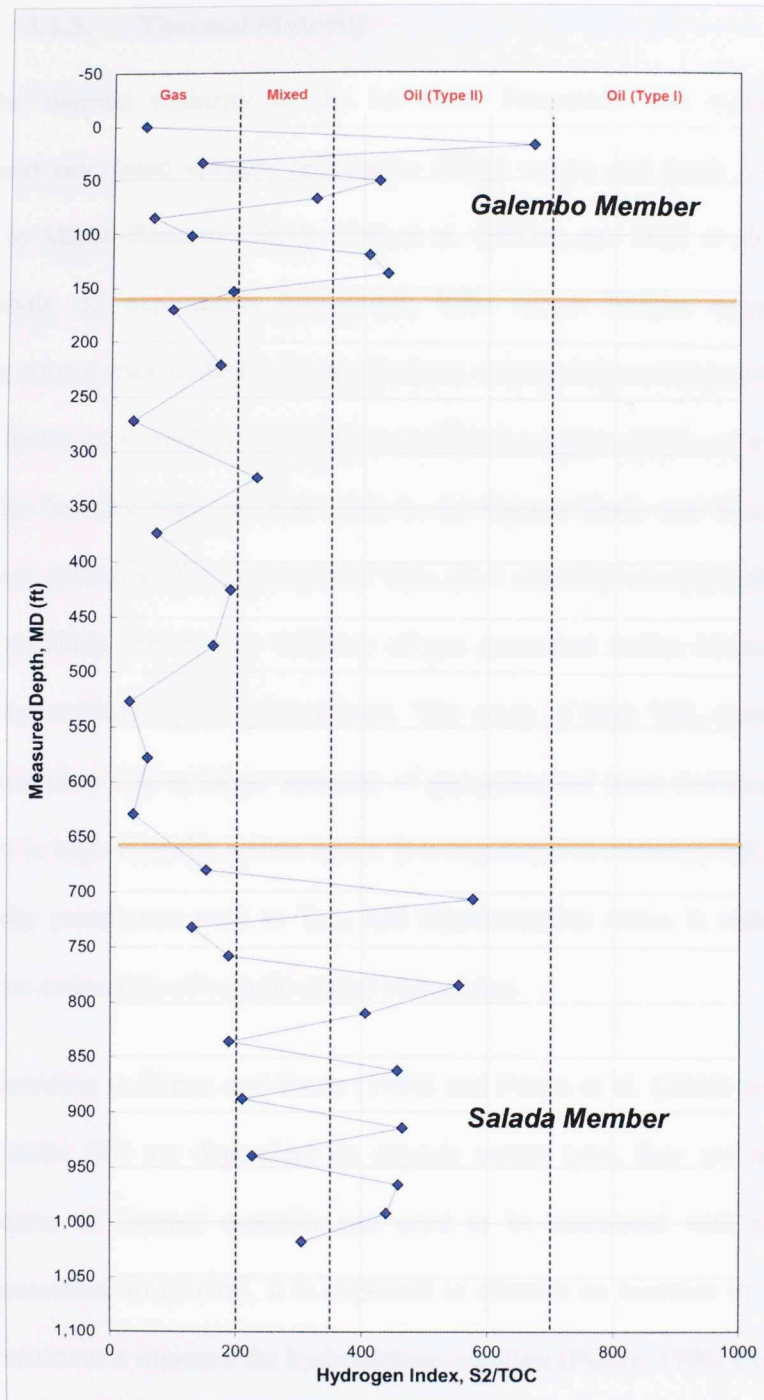


**Figure 28.** Modified pseudo Van Krevelen diagram for the OUTCROP B samples showing the source rock intervals dominated by Type I/II kerogen. Organic poor samples are type III organic matter (Plot template modified from Geomark Geochemical Services). Tmax average 435 °C.





**Figure 29.** Rock Eval Remaining Hydrocarbon Potential ( $S_2$ ) vs. TOC plot for determination of kerogen type and maturity of the OUTCROP B La Luna samples (plot template modified from Geomark Geochemical Services).



**Figure 30.** Geochemical log showing HI variation with stratigraphic depth for OUTCROP B section (plot template modified from Geomark Geochemical Services).

### 3.1.3. Thermal Maturity

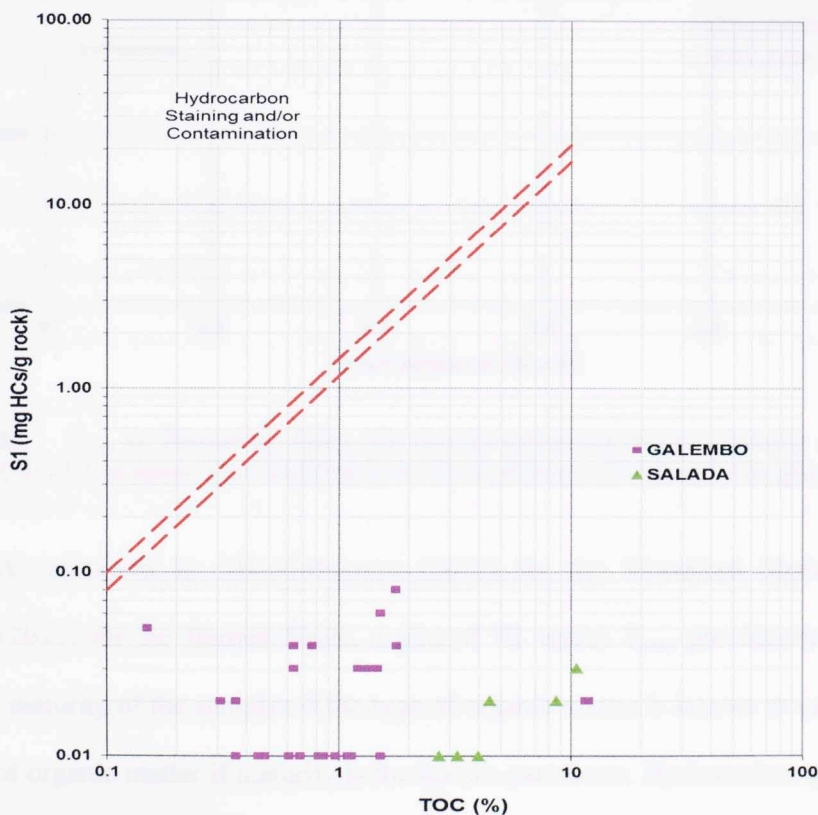
The thermal maturity of the La Luna Formation was assessed through measured and calculated vitrinite reflectance ( $\%R_o$ ) values and Rock Eval pyrolysis. According to Miceli-Romero (2010), Slatt et al. (2011a) and Dahl et al. (2012), in a shale gas/shale oil exploration framework,  $\%R_o$  values besides being useful for determining source rock maturity, have also been used to help estimate and predict gas flow rates. Jarvie et al. (2007) and Dahl et al. (2012) suggested  $\%R_o$  as a geochemical parameter for locating high gas flow rates in the Barnett Shale and Woodford Shale. These authors indicated that areas of low  $\%R_o$  (low maturity) usually exhibit low gas flow rates probably due to low volumes of gas generated and/or because pores are obstructed by residual liquid hydrocarbons. The areas of high  $\%R_o$  commonly show high gas flow rates due to larger amounts of gas generated from cracking of kerogen and bitumen in high-maturity source rocks. It is important to correlate  $\%R_o$  values with other maturity parameters such as  $T_{max}$  and transformation ratios in order to make a more accurate estimation of organic matter conversion.

According to Peters and Cassa (1994) and Peters et al. (2005) since  $T_{max}$  and production index (PI) are dependent on organic matter type, they are used to make rough estimates of thermal maturity and need to be correlated with more reliable maturity parameters. In general, it is expected to observe an increase in PI with  $T_{max}$  where PI constitutes a measure for hydrocarbon retention (Peters, 1986; Cornford et al., 1998, Peters et al. 2005). The La Luna OUTCROP A samples show PI values ranging

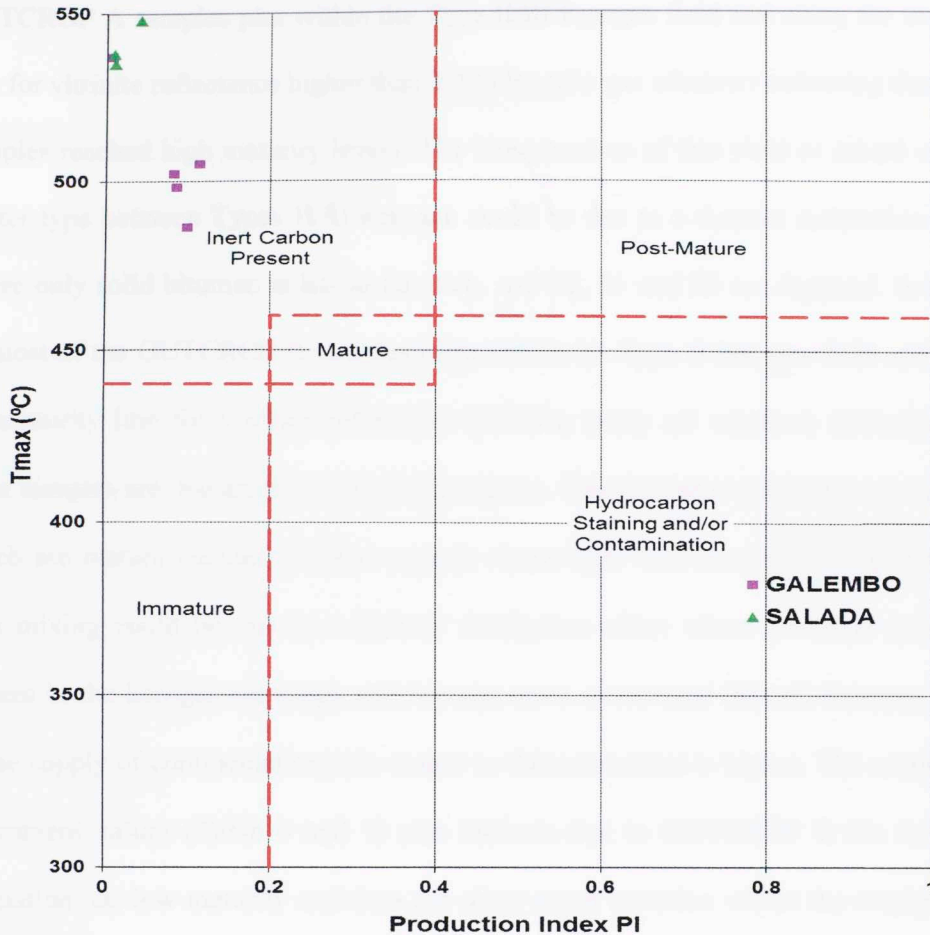


from 0.01 to 0.71 and  $T_{max}$  values beyond 500°C indicating high maturity organic matter beyond the dry gas window.

In a different scenario, the La Luna OUTCROP B samples show PI values ranging from 0.05 to 0.23 and  $T_{max}$  values between 418°C to 440°C indicating low maturity organic matter entering the gas window. The S1 vs TOC plot was useful to determine that the samples analyzed in this study were not contaminated or stained with non-indigenous hydrocarbons (Figure 31 and 32 for OUTCROP A; Figure 35 and Figure 36 for OUTCROP B).



**Figure 31.** S1 vs. TOC plot for identifying the hydrocarbon staining and/or contamination of La Luna OUTCROP A samples. Plot modified from Miceli-Romero (2010) and Albaghdady (2013).



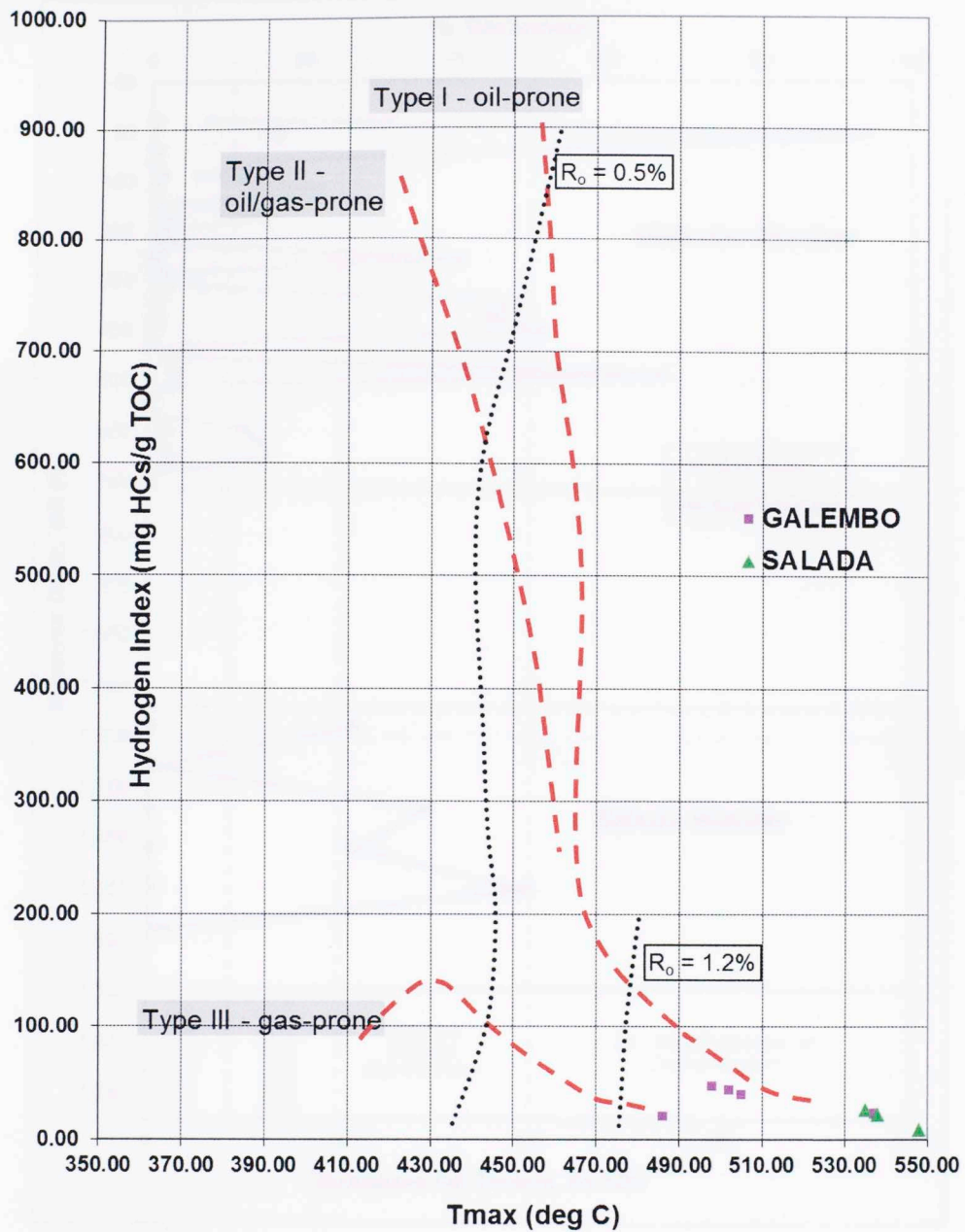
**Figure 32.**  $T_{\max}$  vs. Production Index (PI) plot for estimating thermal maturity of La Luna OUTCROP A samples. Plot modified from Miceli-Romero (2010) and Albaghdady (2013).

As proposed by Miceli-Romero (2010) for the Woodford Shale, and Lo Monaco (2012) for the Barnett Shale, a plot of HI versus  $T_{\max}$  provides information about the maturity of the samples if the type of organic matter is known or can indicate the type of organic matter if maturity is the known parameter. Hydrocarbon generation, as a consequence of thermal maturity, results in a decrease of HI, so the trends represented by gray dotted lines in Figures 33 and 37 indicate the remaining hydrocarbon potential of the rock (Cornford et al., 1998). In Figure 33 most of the

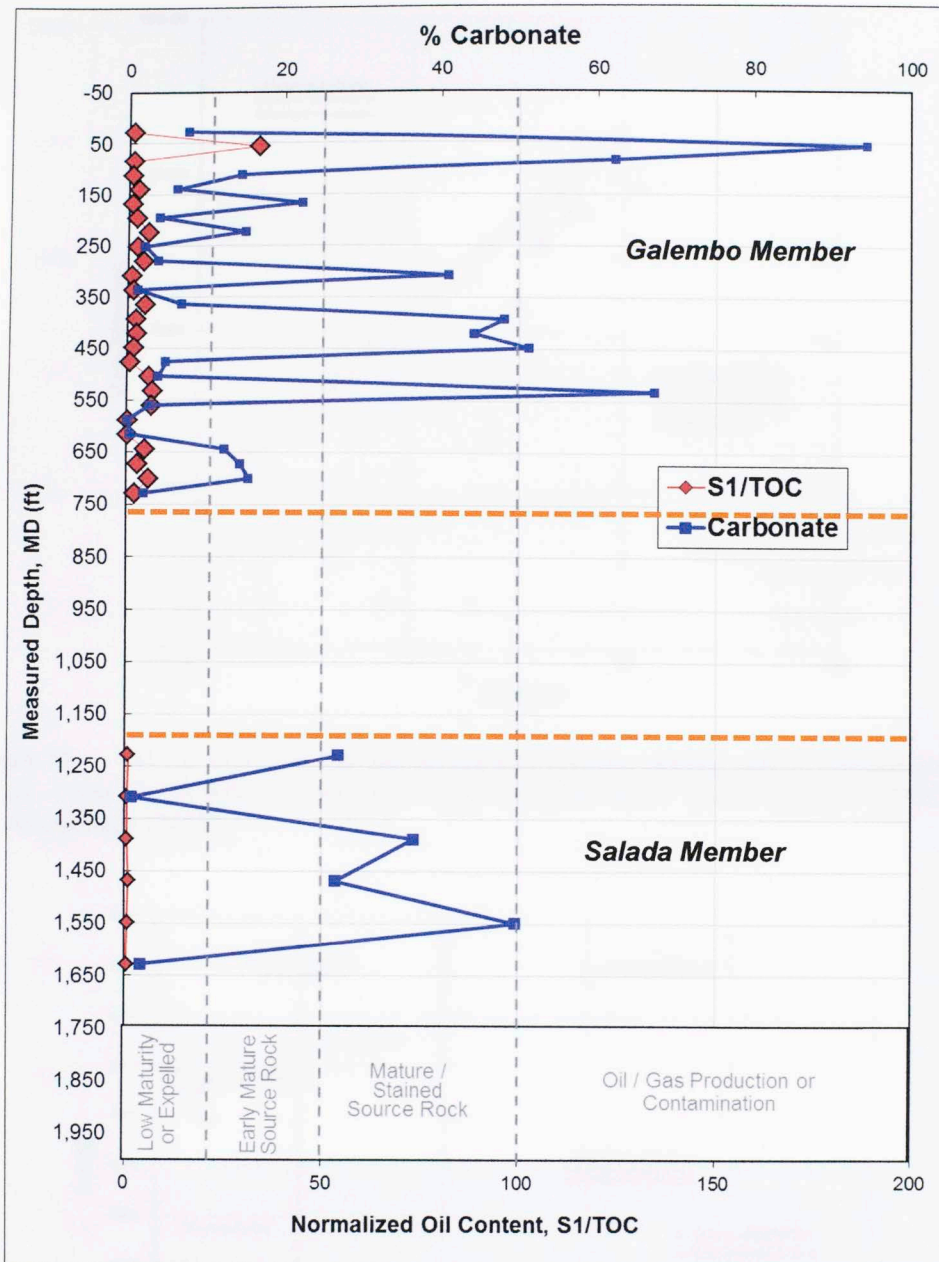
OUTCROP A samples plot within the Type II/III kerogen field and along the maturity line for vitrinite reflectance higher than 2.0 % Ro (dry gas window) indicating that these samples reached high maturity levels. The interpretation of this yield of mixed organic matter type between Types II/III kerogen could be due to a thermal maturation effect where only solid bitumen is left in the rock, and HI, S1 and S2 are depleted. In Figure 37 most of the OUTCROP B samples plots within the Type II kerogen field and along the maturity line for vitrinite reflectance 0.5%Ro (early oil window) indicating that these samples are immature to marginally mature. The Galemba and Pujamana samples which are mature contain a mixed organic matter type between Types II/III kerogen. This mixing could be due to a thermal maturation effect where chemical structures present in the kerogen rearrange and become more aromatized (Miceli-Romero, 2010) or the supply of continental organic matter to these members is higher. The normalized oil content values (Table 6 and 7) also indicate that in OUTCROP B the La Luna Formation has low maturity and does not show much variation within the stratigraphic depths (Figure 40).

Measured and calculated vitrinite reflectance (%R<sub>o</sub>) values for the La Luna Formation OUTCROP A and OUTCROP B samples are presented in Table 6. Jarvie et al. (2005) and Miceli-Romero (2010) proposed a maturity guideline of calculated %R<sub>o</sub> values for the Barnett Shale and Woodford Shale obtained from cores and cuttings that could be applied to similar shale gas plays (Table 7).

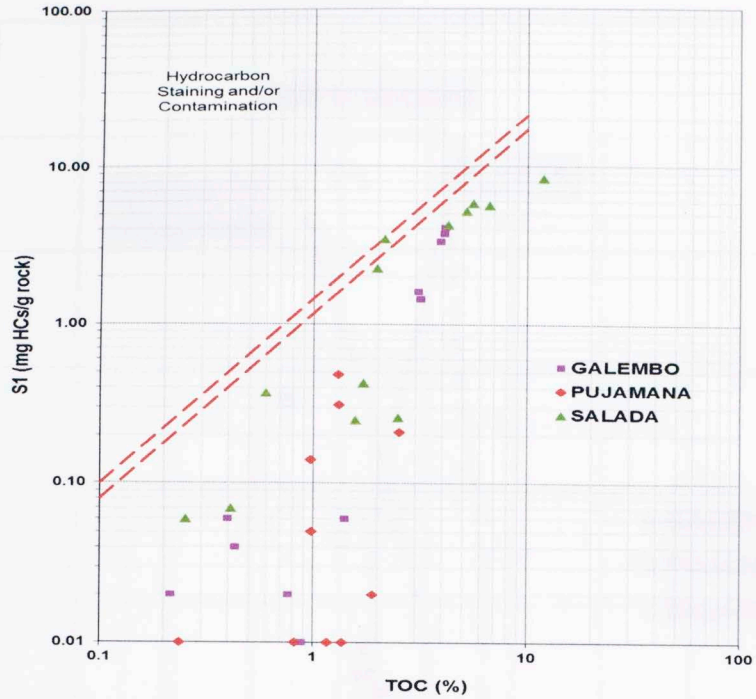




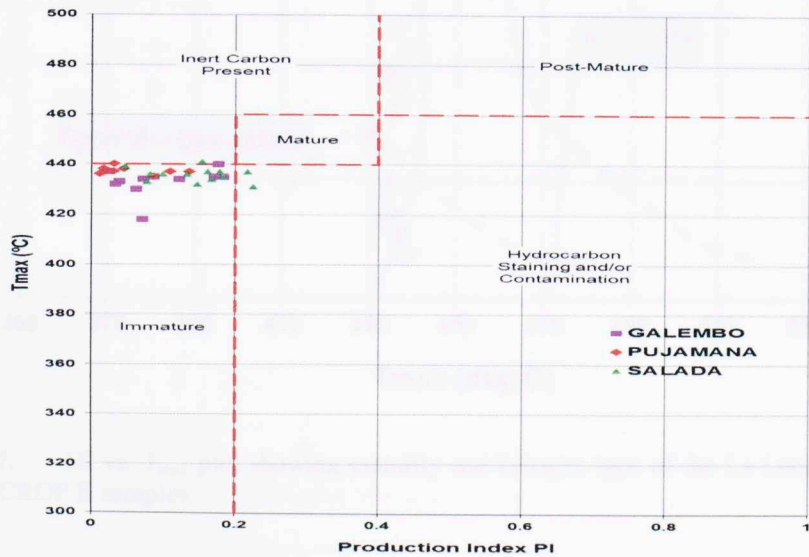
**Figure 33.** HI vs.  $T_{max}$  plot showing maturity and kerogen type of the La Luna Formation OUTCROP A samples.



**Figure 34.** Geochemical log showing normalized oil content for the OUTCROP A section (plot template modified from Humble Geochemical Services).



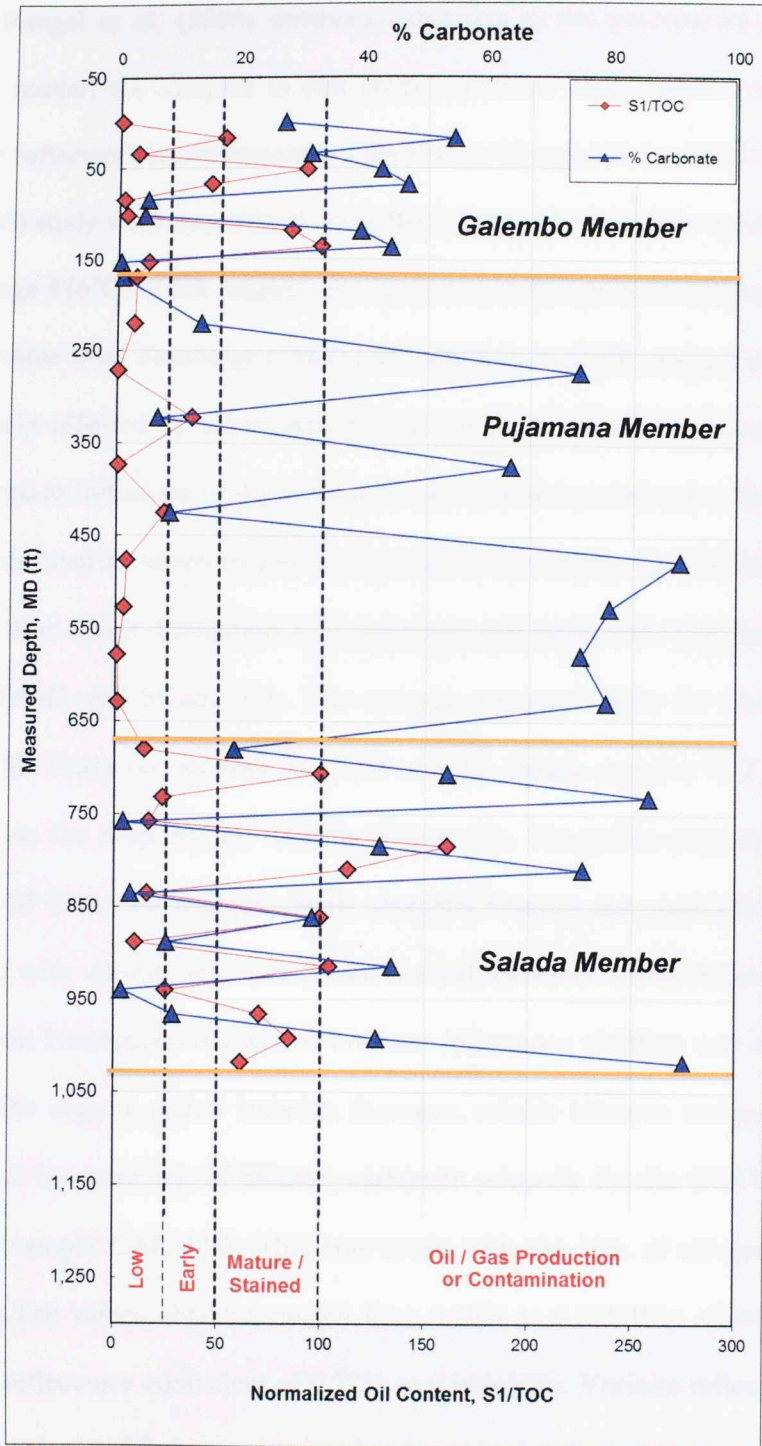
**Figure 35.** S1 vs. TOC plot for identifying hydrocarbon staining and/or contamination of La Luna OUTCROP B samples. Plot modified from Miceli-Romero (2010) and Albaghdady (2013).



**Figure 36.**  $T_{max}$  vs. Production Index (PI) plot for estimating thermal maturity of La Luna OUTCROP B samples.







**Figure 38.** Geochemical log showing normalized oil content for the OUTCROP B section (plot template modified from Humble Geochemical Services).

Rangel et al. (2000) mentioned that due to the predominance of amorphous organic matter, the samples in that study contained little vitrinite, and therefore the vitrinite reflectance measurement are unreliable. The maturation levels in the Rangel et al. (2000) study were determined using Rock Eval pyrolysis with reported Tmax values on average 436°C, which suggests the section is early mature to mature. Average Tmax and S1 value from Zumberge (1984) and Rangel et al. (2000) suggest that the section is not greatly affected by oil migration and that geochemical variations can largely be considered as indicative of depositional conditions and associated variations in the type of organic matter, which is also recognized in this study. For OUTCROP A, a coal sample from Umir Formation was collected and pelletized with the other samples P4M2, P4M3 and Salada Top. The average measured %Ro for Umir Formation is 2.23%, for Galemba member is 2.31% and for Salada member is 2.30%, all values yielding on the deep dry gas window (Figure 39). The pellets prepared from La Luna OUTCROP B section samples contain abundant bitumen and pyrobitumen that might be confused with vitrinite macerals (Brian Cardott, personal communication 2012), so for this reason homogeneous textured bitumen reflectance (%BRo) was measured on the pellets. The organic matter isolation (kerogen, soluble bitumen and pyrobitumen) was conducted by removing of silicate, carbonate minerals for the OUTCROP B Salada member sample CAR M-2. This was made with the idea of recognize the vitrinite macerals. The values obtained ranged from 0.38% to 0.55%BRo allowed calculating a vitrinite reflectance equivalent of 0.72% to 0.96%VRo. Vitrinite reflectance equivalent (VRo) is calculated from an equation developed by Landis and Castano (1995):

$$VRo = (BRo + 0.41)/1.09$$



This equation correlates vitrinite reflectance (%VR<sub>o</sub>) with “homogeneous” solid hydrocarbon (bitumen) reflectance (%SHR<sub>o</sub> or %BR<sub>o</sub>), a maturity indicator for low-content vitrinite and/or mature source rocks (Landis and Castano, 1995). As a result, the corrected %R<sub>o</sub> measurements for the OUTCROP B section have higher maturity levels than the ones that might be interpreted by confusing bitumen and pyrobitumen with vitrinite macerals. In that situation an apparent %R<sub>o</sub> of 0.38% indicates an immature sample, whereas, the corrected value is 0.72% indicating oil window maturity (Figure 40).

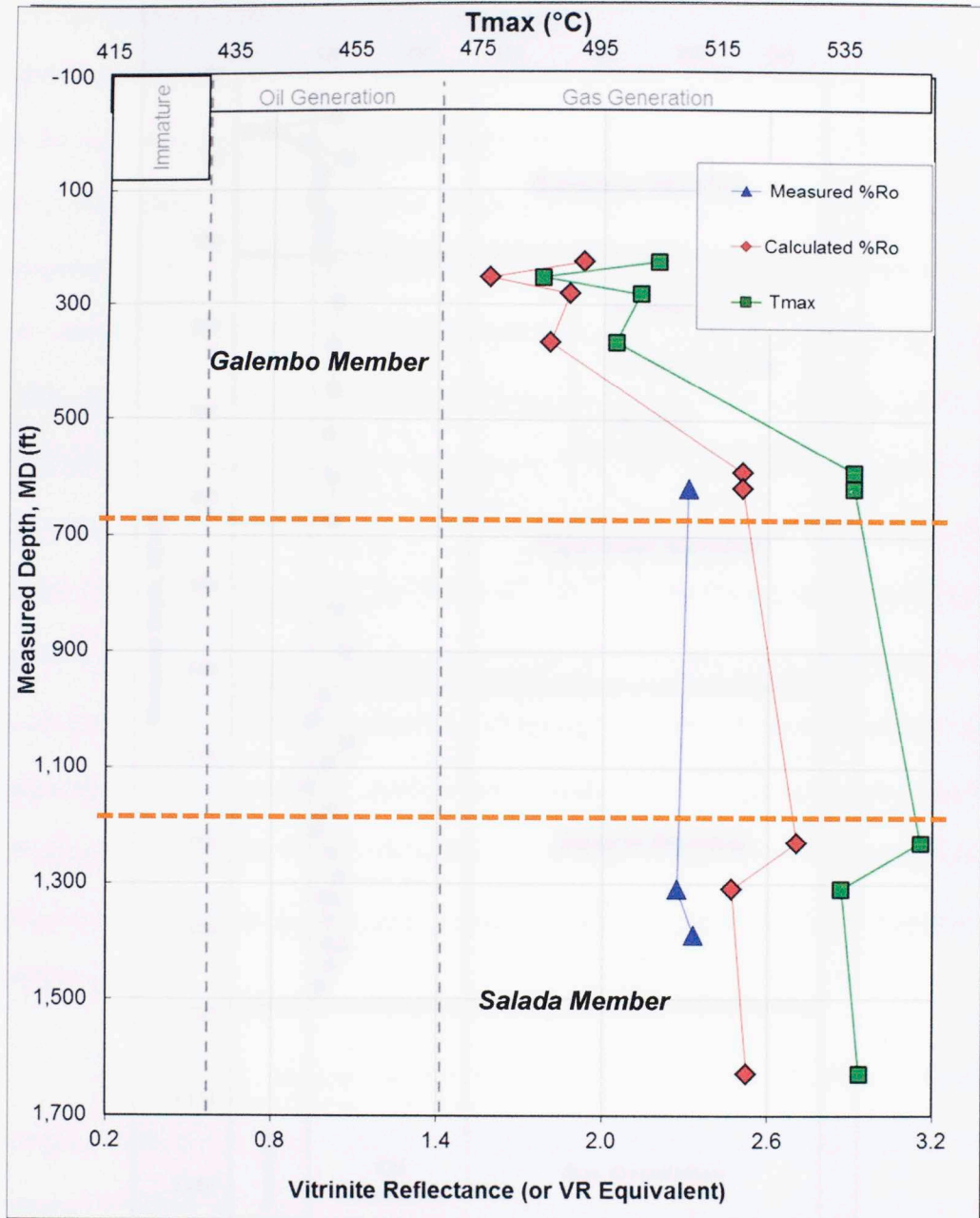
**Table.6.** Measured and calculated vitrinite reflectance (%R<sub>o</sub>) for La Luna samples used in this study.

Sample #	AVG Measured %R <sub>o</sub>	Calculated %R <sub>o</sub>
<b>OUTCROP A</b>		
Salada Top	2.33	N.D.
P4M2	2.27	2.47
P4M3	2.31	2.51
Umir Fm coal A	2.23%	N.D.
OUTCROP B	AVG Measured %BR <sub>o</sub>	Corrected VR <sub>o</sub> %
CAR M-2	0.42	0.76
CAR M-2 ISOLATED	0.64	0.96
UMIR-2	0.38	0.72
QLS M-8	0.44	0.78

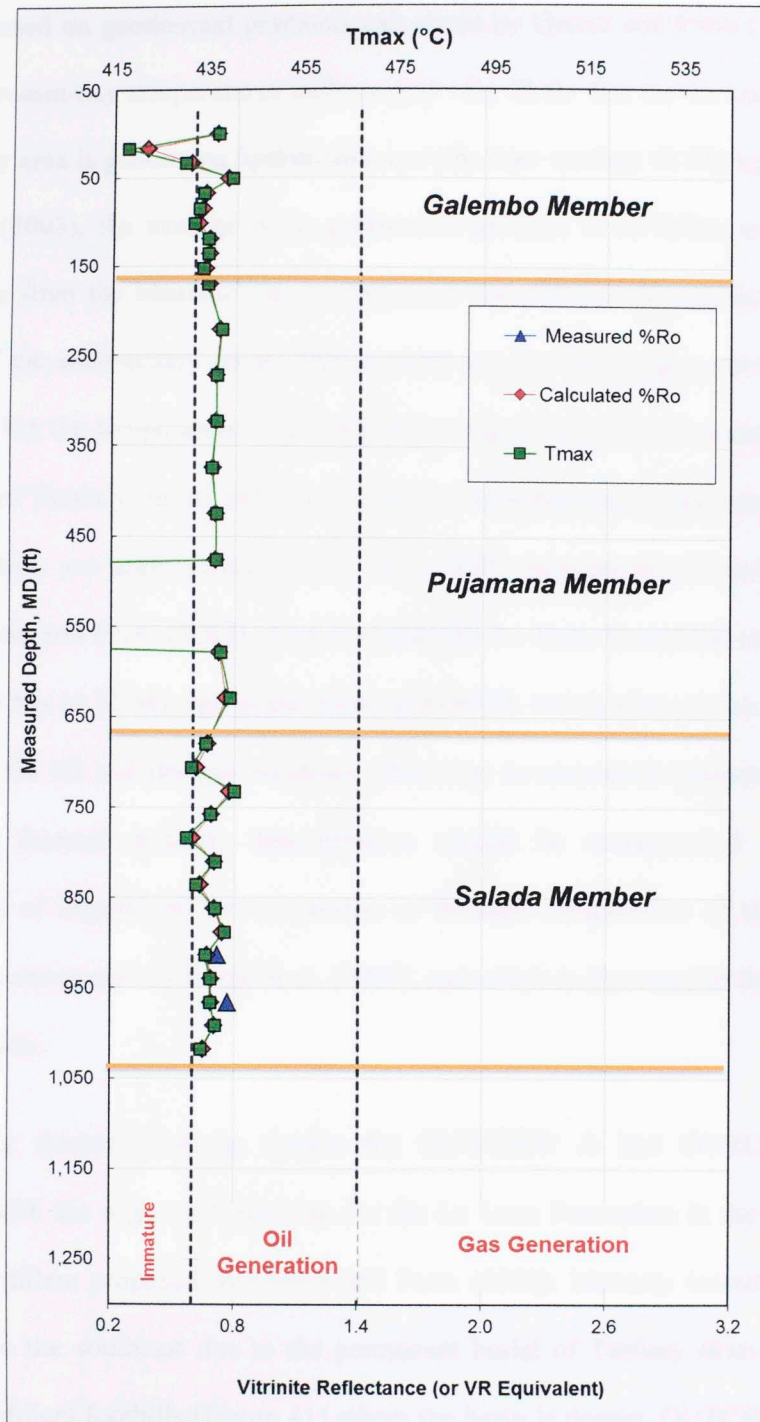
\*Average calculated %R<sub>o</sub> values (see appendix I for complete list).

**Table.7.** Guidelines of calculated vitrinite reflectance values for cuttings and core samples from the Barnett Shale (Jarvie et al., 2005) and Woodford Shale (Miceli-Romero, 2010).

	R <sub>o</sub> Values (%)	Maturity
<b>Cuttings and Cores</b>	<0.55	Immature
	0.55-1.15	Oil window (peak oil at 0.90%R <sub>o</sub> )
	1.15-1.40	Condensate - Wet-gas window
	>1.40	Dry-gas window



**Figure 39.** Geochemical log showing calculated vitrinite reflectance (%R<sub>o</sub>) for OUTCROP A section (plot template modified from Humble Geochemical Services).



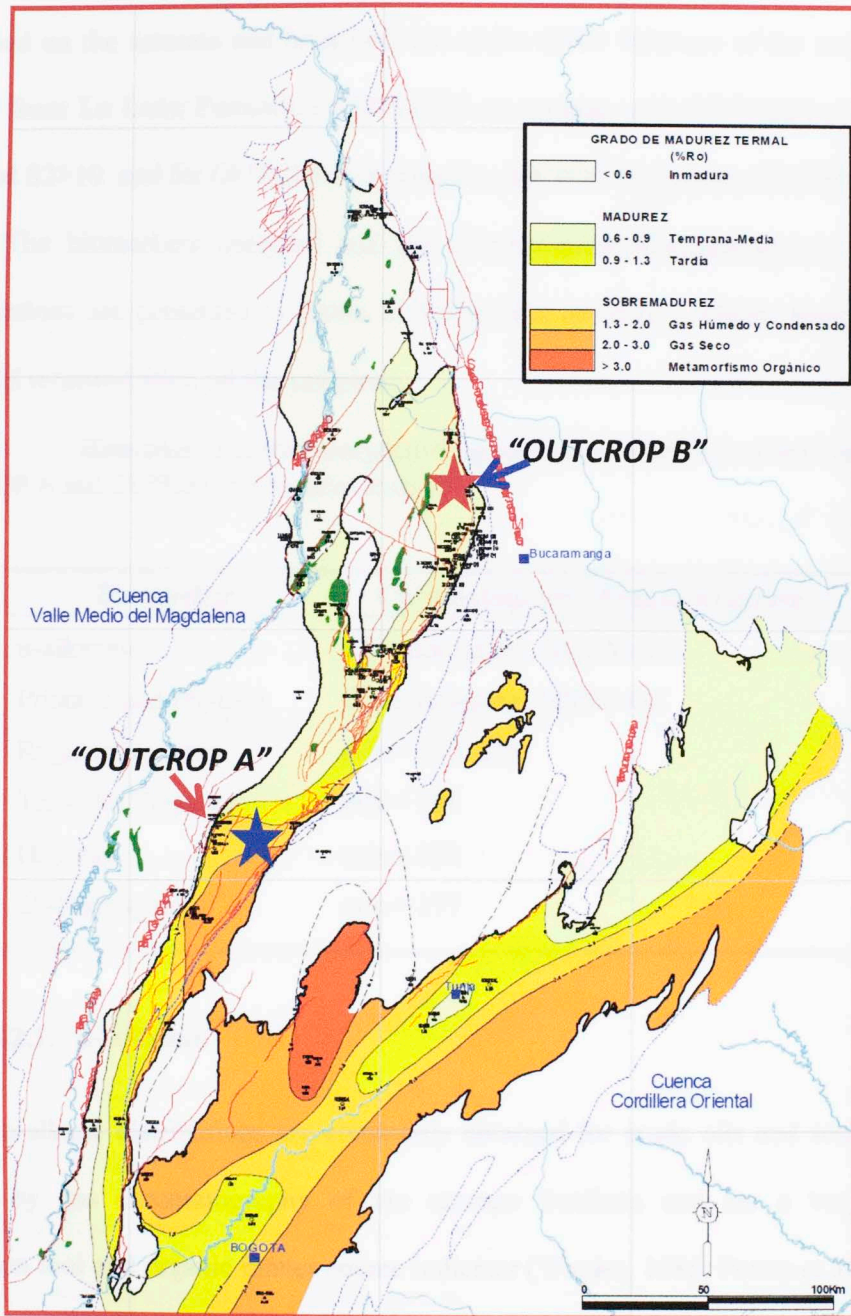
**Figure 40.** Geochemical log showing calculated vitrinite reflectance (%R<sub>o</sub>) for OUTCROP B section (plot template modified from Humble Geochemical Services).



Based on geothermal gradients calculated by Garcia and Parra (2003) for the MMVB, present-day temperatures indicate it is very likely that the La Luna Formation in the study area is generating hydrocarbons at this time starting 40 My ago. According to Acosta (2003), the average basin geothermal gradient is 29°C/Km and the paleo-temperature from the Maastrichtian to Paleocene was 20°C in the surface and 50°C at the base of the sedimentary cover. These values are low for kerogen conversion to oil and/or gas but the temperatures increased following burial of the Cretaceous rocks by deposition of Tertiary fluvial and alluvial strata. The temperatures necessary for oil and gas generation are approximately 50°C and 150°C respectively (Tissot and Welte, 1978). Garcia and Parra (2003) mentioned that the La Luna Formation reached 260°C between 50 My to 16 My ago in the south of MMVB, which allowed this formation to reach both the oil and dry gas windows. However, to accurately evaluate oil and gas generation, thermal maturity determination should be accompanied with kinetic calculations of organic matter conversion or through computation of transformation ratios as recommended by Jarvie et al. (2005), and which is discussed in the Appendix I MSSV section.

The thermal maturity results for OUTCROP A and OUTCROP B are compared with the regional %Ro map for the La Luna Formation in the MMVB and eastern Cordillera proposed by Garcia and Parra (2003). Maturity increased from the northwest to the southeast due to the permanent burial of Tertiary strata towards the eastern Cordillera foothills (Figure 41) where the basin is deeper. OUTCROP A values are 1.3-2.0 %Ro on the map (wet gas window) indicating that this section is in the dry

gas window. With values higher than 2.2%. OUTCROP B is in the early to middle oil generation window, which agrees with the corrected values of 0.72 VRo%.



**Figure 41.** Measured vitrinite reflectance (%R<sub>o</sub>) map for La Luna formation in MMVB (Garcia and Parra, 2003).

### 3.2. Biomarker Analysis

Biomarker analysis was completed through the use of GC and GC-MS performed on the saturate and branched and cyclic (B/C) fractions of the source rock extracts from La Luna Formation OUTCROP A samples with TOC higher than 2%, HI>2 and S<sub>2</sub>>10 and for OUTCROP B samples with TOC higher than 2%, HI>400 and S<sub>2</sub>>10. The biomarkers analyzed and the chromatograms/fragmentograms used for interpretations are presented in Table 8. Sulfur was detected (~1%wt; Rangel et al., 2000) and removed from all the samples.

**Table.8.** Biomarkers and chromatograms/fragmentograms used for La Luna Formation OUTCROP A and OUTCROP B samples analysis.

<b>Biomarker</b>	<b>Chromatogram / Fragmentogram</b>
n-alkanes	Chromatogram , MSSV-GC
Pristane and Phytane	Chromatogram, MSSV-GC
Regular Steranes	m/z = 217, 218
Tricyclic Terpanes	m/z = 191
Hopanes	m/z = 191
25-Norhopanes	m/z = 177

#### 3.2.1. n-Alkanes

The n-alkane distributions are commonly obtained for crude oils and source rock extracts by gas chromatography of the saturate fractions and are a very useful correlation tool and organic matter source indicator (Waples, 1985; Peters et al., 2005). Gas chromatography fingerprints for the saturate fractions of the La Luna Formation OUTCROP A and OUTCROP B samples (Figures 44 to 47) do not show great presence



of n-alkanes, indicating weathering and consequent depletion. The OUTCROP A and OUTCROP B samples that were analyzed for biomarker distribution are shown in Table 9.

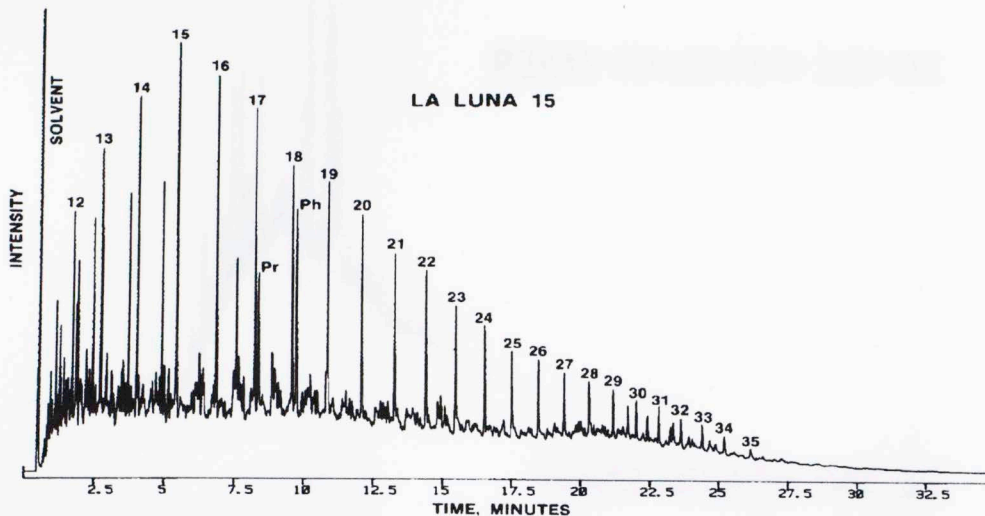
Zumberge (1984) published data for the Salada member in the same location as the OUTCROP B section, and showed phytane typically is more abundant than pristane ( $Pr/Ph = 0.70$ ). The n-alkane distribution indicates only a slight preference of odd over even-numbered alkanes in the  $C_{28+}$  region (average odd-even predominance, OEP = 1.09). Zumberge (1984) reported for the Salada member an even carbon preference in the n- $C_{20}$  to  $C_{28}$  range (average OEP = 0.956). According to his conclusions, most of the aliphatic fraction consists of branched and cyclic alkanes, as evidenced by a large unresolved "hump" under the n-alkane peaks. The interpretation of Zumberge (1984) Salada member chromatogram (Figure 42) suggests that the organic matter is derived from marine plankton and microorganisms deposited in a reducing environment. Phytoplankton, zooplankton and benthic algae are the main organisms contributing to the marine organic matter as typified by the n-alkanes distributions.

The OUTCROP A and OUTCROP B samples do not show variation in the n-alkane distributions along each stratigraphic section (Figures 44 to 47), which is a product of the heavy biodegradation level that is recognized by the removal of n-alkanes and isoprenoids (Wegner et al., 2002). To obtaining the n-alkane and isoprenoid distributions that can be generated from the La Luna Formation, the MSSV-GC experiment was conducted for Salada member sample CAR M-2. Artificial thermal maturation of the present day kerogen, bitumen and pyrobitumen within the rock

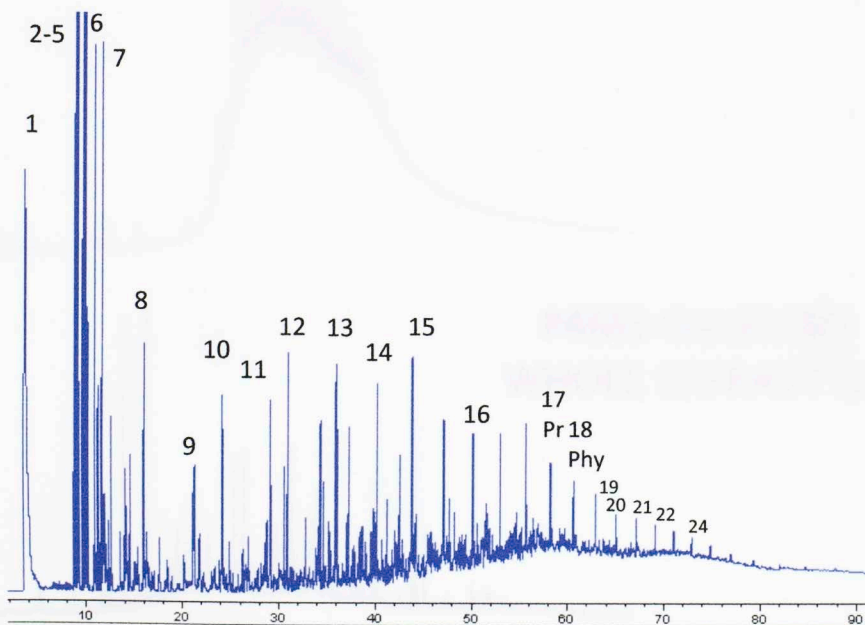
undergo primary and secondary cracking, and simulate generation by aromatization, condensation and isomerization of new n-alkane and isoprenoid peaks (Figure 43 and 47). As observed by Zumberge (1984) phytane is more abundant than pristane.

**Table.9.** Samples for biomarker analysis in OUTCROP A and OUTCROP B.

Sample #	Member	TOC%	HI (mg HC/gTOC)	S2 (mgHC/gRock)
<b>OUTCROP A</b>				
P2M1	Galembo	1.51	44	0.66
P4M3	Galembo	11.90	23	2.65
P4 M2	Salada	10.60	26	2.78
<b>OUTCROP B</b>				
QLS Umir-2	Galembo	3.10	672	20.83
QLS M-3	Galembo	4.09	425	17.39
QLS M-7a	Galembo	3.94	410	16.14
QLS M-8	Galembo	4.12	439	18.10
CAN M-15	Pujamana	2.54	172	4.38
CAN M-8	Pujamana	1.32	189	2.50
CAN M-5	Pujamana	1.90	58	1.11
CAR M-14	Salada	4.27	576	24.61
CAR M-11	Salada	2.15	554	11.91
CAR M-4	Salada	5.58	465	25.92
CAR M-3	Salada	11.90	458	54.54
CAR M-2	Salada	6.68	439	29.31

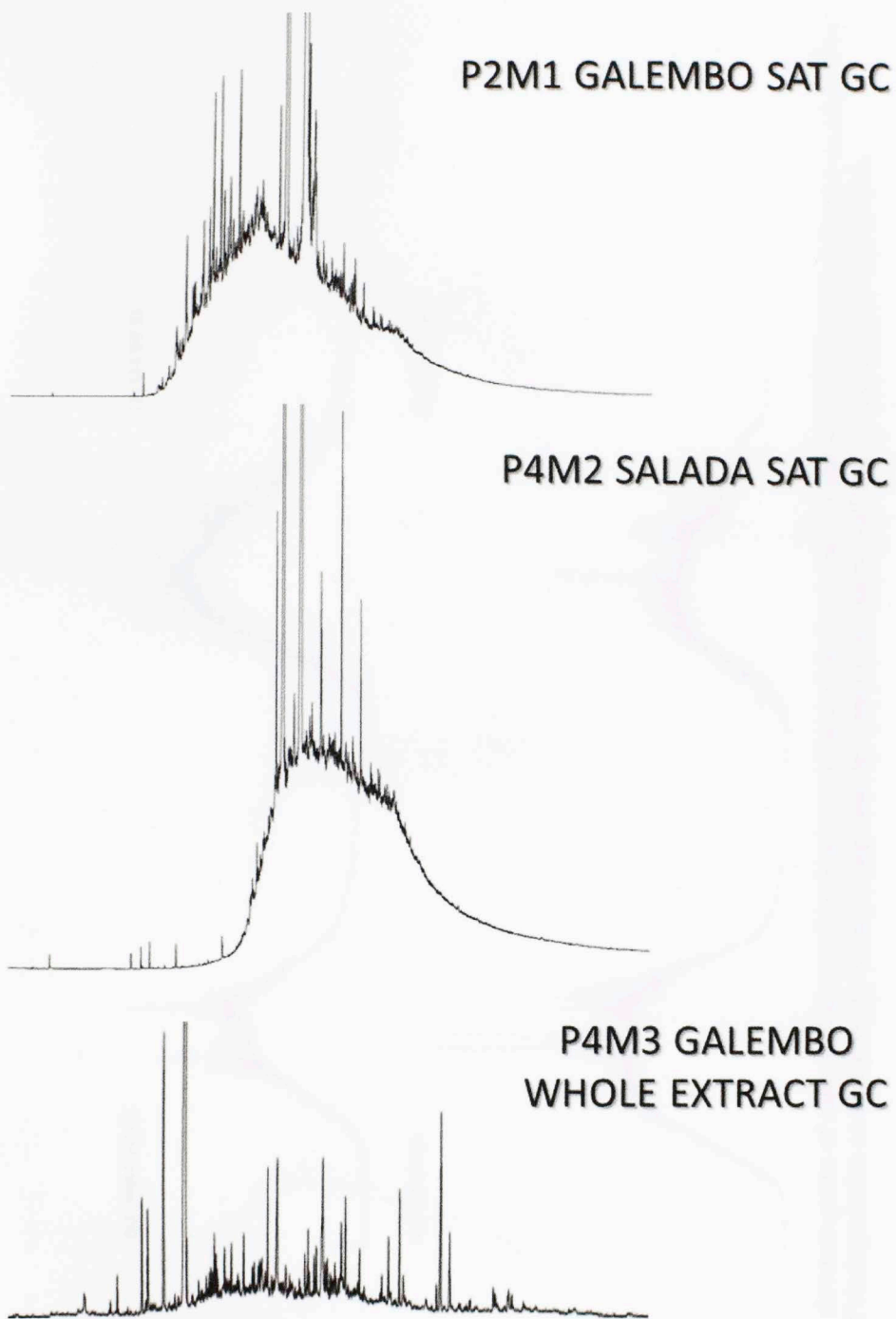


**Figure 42.** Gas chromatogram of Zumberge (1984) showing the aliphatic-hydrocarbon fraction of a Salada member sample from the La Luna Formation nearby OUTCROP B location. Numbered peaks represent n-alkane carbon numbers; Pr and Ph represent pristane and phytane, respectively.



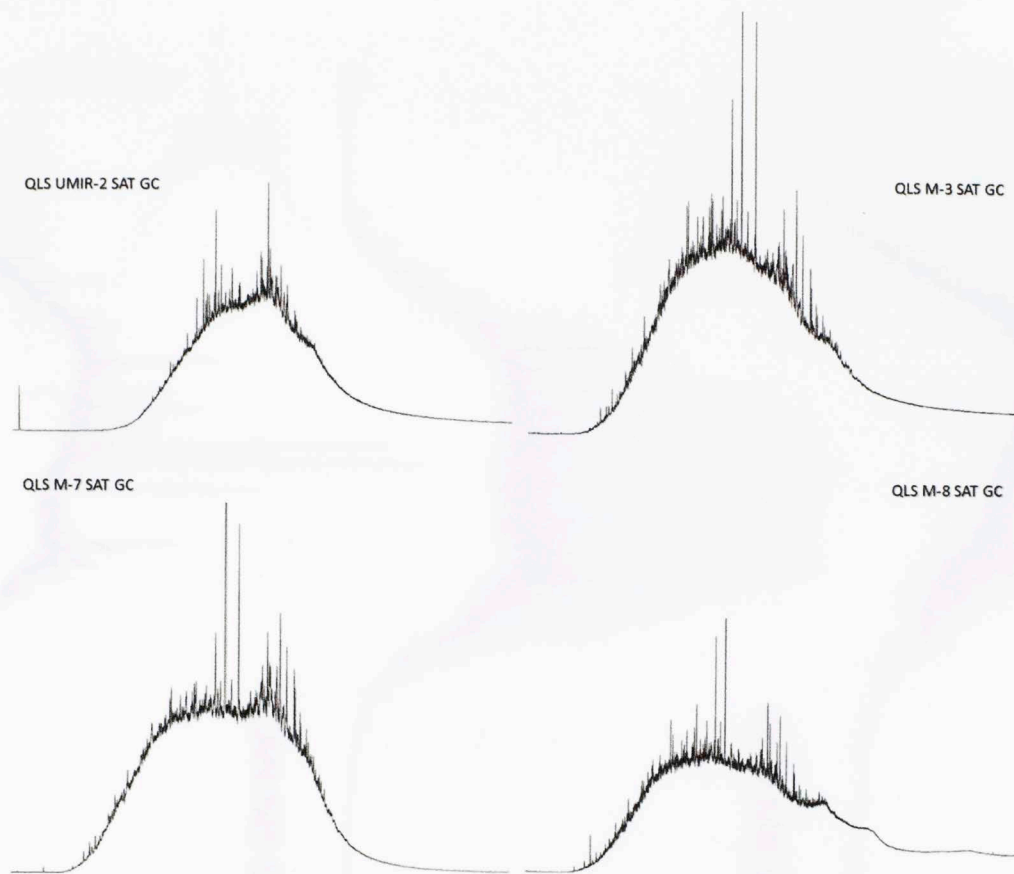
**Figure 43.** Gas chromatogram showing the aliphatic-hydrocarbon fraction of OUTCROP B Salada member sample CAR M-3 after MSSV. Numbered peaks represent n-alkane carbon number; Pr and Ph represent pristane and phytane, respectively.



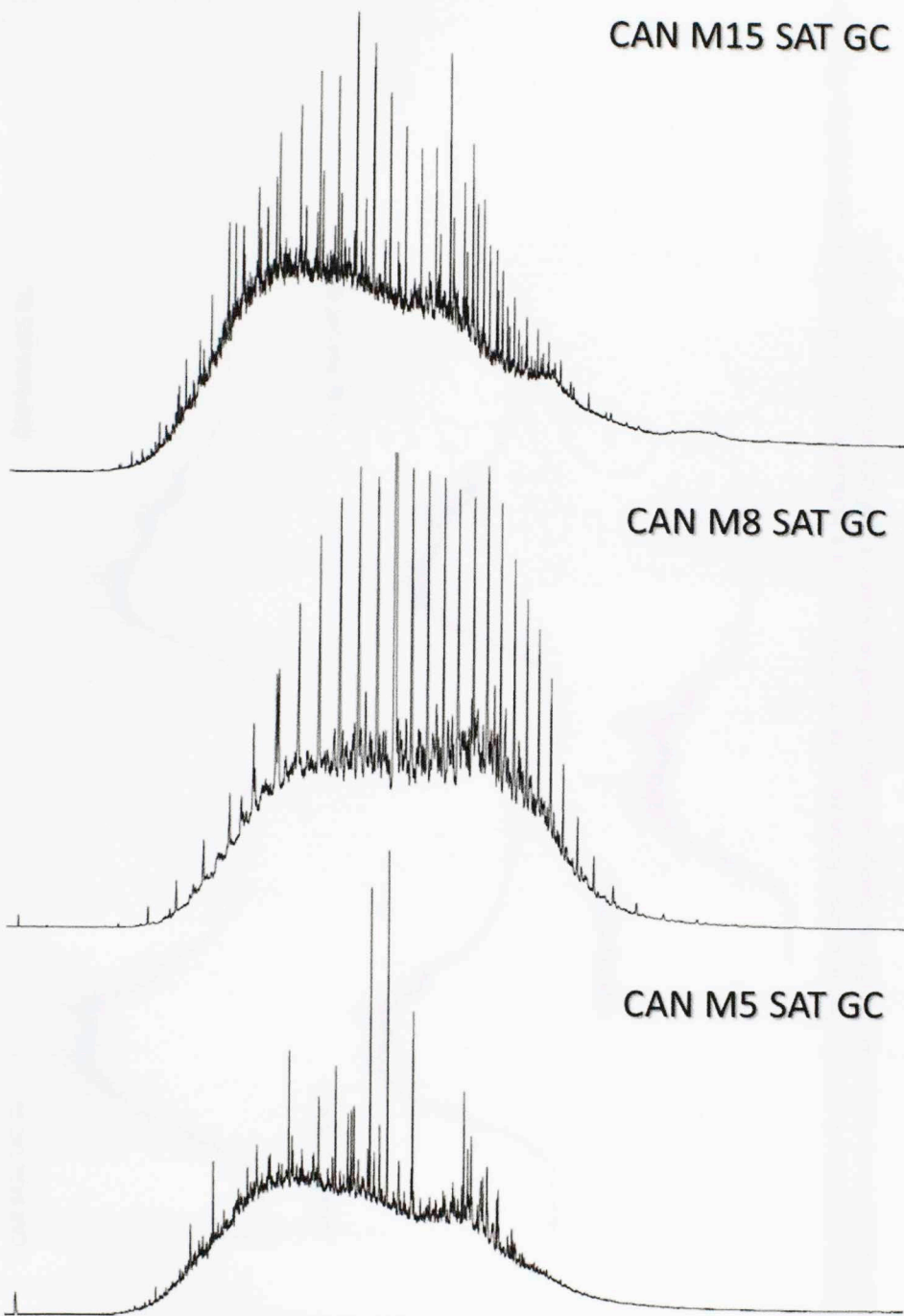


**Figure 44.** Gas chromatograms of saturate fractions from bitumen extracts of the La Luna Formation OUTCROP A Galembó and Salada members. Note the heavy biodegradation level evidenced by big the humps and the removal of n-alkane and depletion of isoprenoids.

Figure 45. Gas chromatograms of saturate fractions from bitumen extracts of the La Luna Formation OUTCROP B Galemba member. Note the high level of biodegradation as evidenced by the big humps and the removal of lighter n-alkane and depletion of isoprenoids.

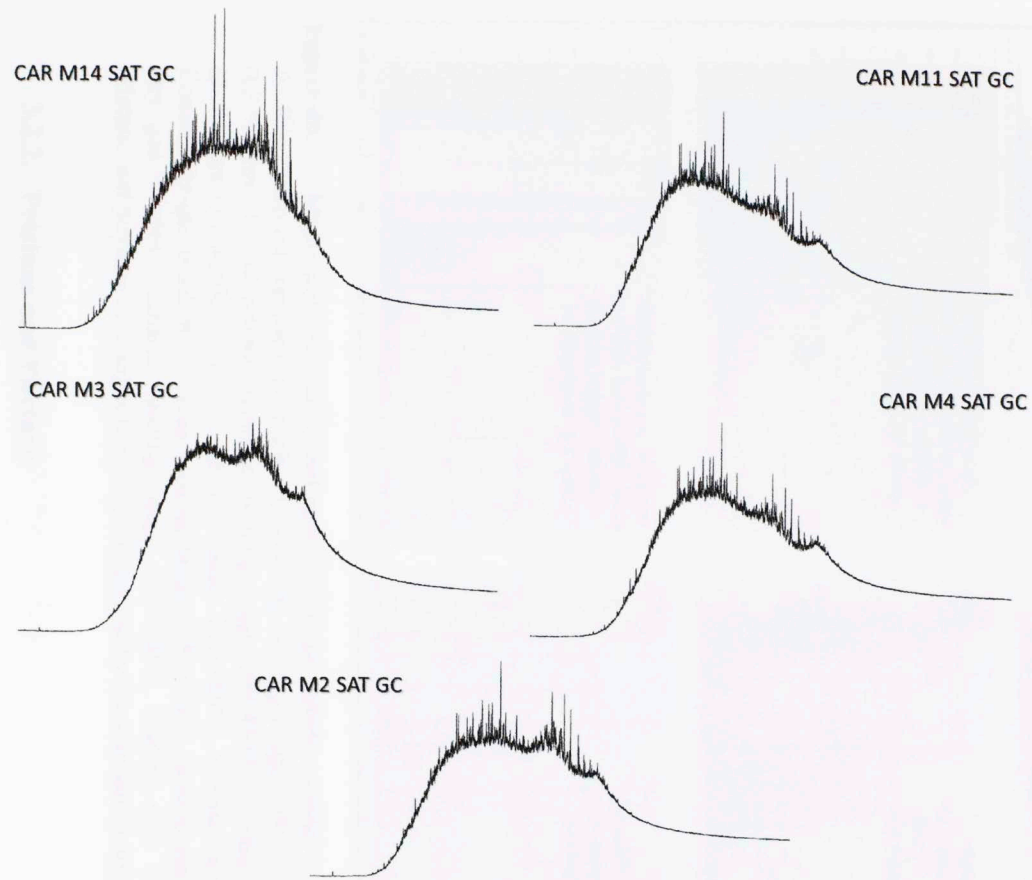


**Figure 45.** Gas chromatograms of saturate fractions from bitumen extracts of the La Luna Formation OUTCROP B Galemba member. Note the high level of biodegradation as evidenced by the big humps and the removal of lighter n-alkane and depletion of isoprenoids.

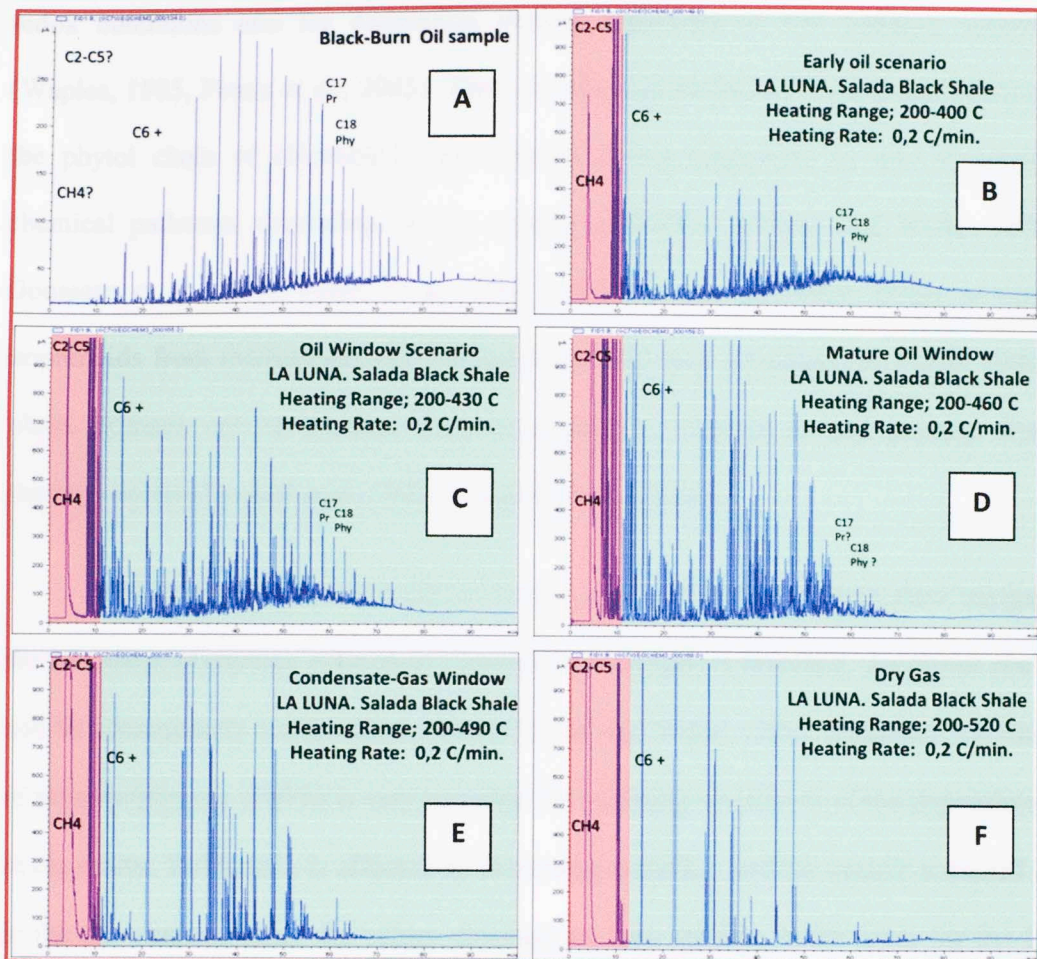


**Figure 46.** Gas chromatograms of saturate fractions from bitumen extracts of the La Luna Formation OUTCROP B Pujamana member. Note the high level of biodegradation as evidenced by the big humps, the removal of lighter n-alkane and depletion of isoprenoids.





**Figure 47.** Gas chromatograms of saturate fractions from bitumen extracts of the La Luna Formation OUTCROP B Salada member. Note the heavy level of biodegradation as evidenced by the big humps and the removal of n-alkane and depletion of isoprenoids.



**Figure 48.** Micro-scale Sealed Vessel analysis for the Salada member CAR M-3 sample. A- Blackburn oil standard; B- Early oil scenario, heating range: 200–400°C, heating rate: 0,2 °C/min; C- Oil window scenario, heating range: 200–430°C, heating rate: 0,2 °C/min; D- Mature Oil window scenario, heating range: 200–460°C, heating rate: 0,2 °C/min; E- Condensate-gas window scenario, heating range: 200–490°C, heating rate: 0,2 °C/min; F- Dry gas window scenario, heating range: 200–520°C, heating rate: 0,2 °C/min. Note pristane and phytane on images B and C, recognized by the standard in image A.

### 3.2.2. Pristane and Phytane

Pristane (Pr) and phytane (Ph) were identified on the gas chromatograms for the whole extract obtained from sample CAR M-2 which was conducted under MSSV analysis. These compounds are two of the most extensively used biomarkers to evaluate

redox conditions and for correlation studies, especially in low maturity samples (Waples, 1985, Peters et al., 2005). These acyclic isoprenoids are mainly derived from the phytol chain of chlorophyll, and formed during diagenesis by one of several chemical pathways depending on the oxygen availability (Tissot and Welte, 1978; Goossens et al., 1984; Peters et al., 2005). However, an alternative origin of these isoprenoids from methanogen-derived lipids has also been proposed (Rowland, 1990), where pristane can be sourced from  $\alpha$ -tocopherols (vitamin E) and phytane from phytanyl ethers (Bechtel et al., 2007; Miceli-Romero, 2010).

When derived from the phytol chain under reducing conditions (low oxygen) the formation of phytane is favored. Conversely, if oxygen is abundant, the phytol chain will be subsequently converted to pristane (Tissot and Welte, 1978). Therefore, the ratio of pristane/phytane (Pr/Ph) is very valuable for assessing conditions of the depositional environment. Pr/Ph ratio is affected by increasing maturity, and the sample analyzed is in the oil window, hence the values obtained are very reliable. Pr/Ph ratios for the La Luna Salada member is  $<1$ , indicating variability in redox conditions of an anoxic environments influenced by input of marine organic matter (Waples, 1985; Peters et al., 2005). Consequently, this parameter can be related to sea-level fluctuations and when combined with n-alkanes  $C_{17}$  and  $C_{18}$  are very useful in evaluating the type of organic matter, depositional environment, maturity, biodegradation and also as a correlation parameter (Waples, 1985). For the other samples without MSSV analysis, neither pristane nor phytane were recognized on the GC traces due to the heavy biodegradation level.



### 3.2.3. Steranes

Sterane distributions for the La Luna Formation samples were determined through analysis of the saturate and B/C fractions by SIM/GCMS using the  $m/z$  217 ion. The resulting fragmentograms (Figures 49 to 54) show the  $C_{27}$ ,  $C_{28}$  and  $C_{29}$  regular steranes (peak identifications are presented in Table 10). This group of biomarkers is mainly derived from sterols whose precursors are eukaryotic organisms, principally algae and higher plants (Peters et al., 2005) but are rare or absent in prokaryotic organisms (Volkman, 1986). Huang and Meinschein (1979) used  $C_{27}$ ,  $C_{28}$  and  $C_{29}$  sterol distributions and plotted them on a ternary diagram to define ecosystems. Moldowan et al., (1985) used this diagram to plot regular sterane distributions from crude oils and source rock extracts in order to assess depositional environments. Other authors (Dzou et al., 1995; Duan et al., 2006; Wang and Philp, 2007; Hodairi, 2012) have applied the same principle to determine organic matter source and for correlation studies.

$C_{27}$  (cholestane) and  $C_{28}$  (ergostane) steranes are derived from sterols that are abundant in plankton and marine invertebrates.  $C_{28}$  steranes can also be derived from terrestrial sources, so they are not a specific indicator for organic matter input (Huang and Meinschein, 1979; Peters et al., 2005).  $C_{29}$  steranes (stigmastane) originate from sterols present in terrigenous organic matter, but also from marine algae (Volkman, 1986). However, Fowler and Douglas, (1987) suggested that some  $C_{29}$  steranes come from cyanobacteria (blue-green algae), and Volkman (1986, 1988) has shown that algae can produce many types of sterols including  $C_{29}$  sterols (Volkman, 1986; Volkman and Maxwell, 1986; Fowler and Douglas, 1987; Volkman, 1988). Generally, oils generated

from kerogens containing organic matter derived from marine phytoplankton display enhanced amounts of C<sub>27</sub> relative to C<sub>29</sub> steranes (Mackenzie et al., 1982; Waples and Machihara, 1991). The presence of C<sub>30</sub> steranes (24-n-propylcholestanes) in oils and extracts is principally related to *pelagophyte* algae, which indicates a contribution from marine and phytoplankton organic matter (Moldowan, 1984; Moldowan et al., 1990; Summons et al., 1992; Peters and Moldowan, 1993; Peters et al., 2005).

From the fragmentograms analyzed for the La Luna formation samples (Figures 49 to 54) it can be seen that C<sub>27</sub> steranes are in relatively higher proportions followed by C<sub>29</sub> and C<sub>28</sub> steranes. According to Volkman (1986), Zumberge (1984) and Rangel et al. (2000) this distribution on a source rock extract indicate a marine organic matter input. The relative proportion of the C<sub>27</sub>, C<sub>28</sub> and C<sub>29</sub> regular steranes was plotted on a ternary diagram (Figure 55) to determine variations resulting from organic matter source and depositional environment. According to the regular sterane ternary diagram developed by Moldowan et al. (1985), most of the La Luna Formation samples are clustered in a wide area of the plot and with the integration with other biomarker parameters and recognized lithofacies, the samples are interpreted as marine shale and marine carbonate source rocks. This interpretation is also associated with the depositional environment of the source rocks of Turonian-Santonian age (92-84 My) in South America.

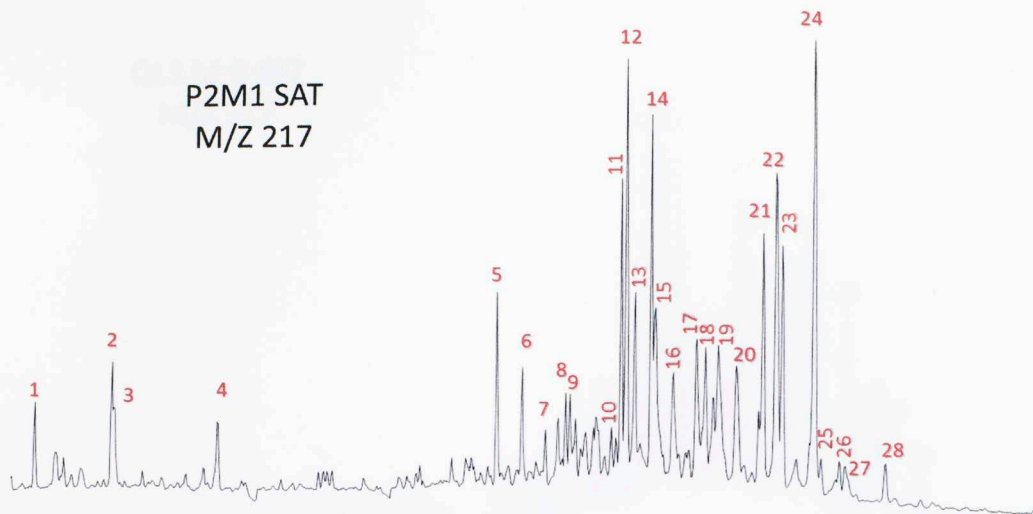
**Table.10.** Identification of steranes in the partial m/z 217 fragmentogram.

Peak #	Compound
1	Diapregthane
2	C <sub>21</sub> 5 $\alpha$ (H), 14 $\alpha$ (H), 17 $\beta$ (H)- Pregnane
3	Diahomopregthane
4	C <sub>22</sub> 5 $\alpha$ (H), 14 $\alpha$ (H), 17 $\beta$ (H)- Homopregthane
5	13 $\beta$ (H), 17 $\alpha$ (H)-Diacholestane (20S)
6	13 $\beta$ (H), 17 $\alpha$ (H)-Diacholestane (20R)
7	13 $\alpha$ (H), 17 $\beta$ (H)-Diacholestane (20S)
8	13 $\alpha$ (H), 17 $\beta$ (H)-Diacholestane (20R)
9	C <sub>28</sub> 24-Methyl-13 $\beta$ (H), 17 $\alpha$ (H)-Diacholestane (20S)
10	C <sub>28</sub> 24-Methyl-13 $\beta$ (H), 17 $\alpha$ (H)-Diacholestane (20S)
11	C <sub>28</sub> 24-Methyl-13 $\alpha$ (H), 17 $\beta$ (H)-Diacholestane (20R) + C <sub>27</sub> 5 $\alpha$ (H), 14 $\alpha$ (H), 17 $\alpha$ (H)-Cholestane (20S)
12	C <sub>28</sub> 24-Ethyl-13 $\beta$ (H), 17 $\alpha$ (H)-Diacholestane (20S) + C <sub>27</sub> 5 $\alpha$ (H), 14 $\beta$ (H), 17 $\beta$ (H)-Cholestane (20R)
13	C <sub>28</sub> 24-Methyl-13 $\alpha$ (H), 17 $\beta$ (H)-Diacholestane (20R) + C <sub>27</sub> 5 $\alpha$ (H), 14 $\beta$ (H), 17 $\beta$ (H)-Cholestane (20S)
14	C <sub>27</sub> 5 $\alpha$ (H), 14 $\alpha$ (H), 17 $\alpha$ (H)-Cholestane (20R)
15	C <sub>28</sub> 24-Ethyl-13 $\beta$ (H), 17 $\alpha$ (H)-Diacholestane (20R)
16	C <sub>28</sub> 24-Ethyl-13 $\alpha$ (H), 17 $\beta$ (H)-Diacholestane (20R)
17	C <sub>28</sub> 24-Methyl- 5 $\alpha$ (H), 14 $\alpha$ (H), 17 $\alpha$ (H)-Cholestane (20S)
18	C <sub>28</sub> 24-Ethyl-13 $\alpha$ (H), 17 $\beta$ (H)-Diacholestane (20S) + C <sub>28</sub> 24-Methyl- 5 $\alpha$ (H), 14 $\beta$ (H), 17 $\beta$ (H)-Cholestane (20R)
19	C <sub>28</sub> 24-Methyl-5 $\alpha$ (H), 14 $\beta$ (H), 17 $\beta$ (H)-Cholestane (20S)
20	C <sub>28</sub> 24-Methyl-5 $\alpha$ (H), 14 $\alpha$ (H), 17 $\alpha$ (H)-Cholestane (20R)
21	C <sub>29</sub> 24-Ethyl-5 $\alpha$ (H), 14 $\alpha$ (H), 17 $\alpha$ (H)-Cholestane (20S)
22	C <sub>29</sub> 24-Ethyl- 5 $\alpha$ (H), 14 $\beta$ (H), 17 $\beta$ (H)-Cholestane (20R)
23	C <sub>29</sub> 24-Ethyl- 5 $\alpha$ (H), 14 $\beta$ (H), 17 $\beta$ (H)-Cholestane (20S)
24	C <sub>29</sub> 24-Ethyl-5 $\alpha$ (H), 14 $\alpha$ (H), 17 $\alpha$ (H)-Cholestane (20R)
25	C <sub>30</sub> 24-Propyl-5 $\alpha$ (H), 14 $\alpha$ (H), 17 $\alpha$ (H) -Cholestane (20S)
26	C <sub>30</sub> 24-Propyl-5 $\alpha$ (H), 14 $\beta$ (H), 17 $\beta$ (H) -Cholestane (20R)
27	C <sub>30</sub> 24-Propyl-5 $\alpha$ (H), 14 $\beta$ (H), 17 $\beta$ (H) -Cholestane (20S)
28	C <sub>30</sub> 24-Propyl-5 $\alpha$ (H), 14 $\alpha$ (H), 17 $\alpha$ (H) -Cholestane (20R)

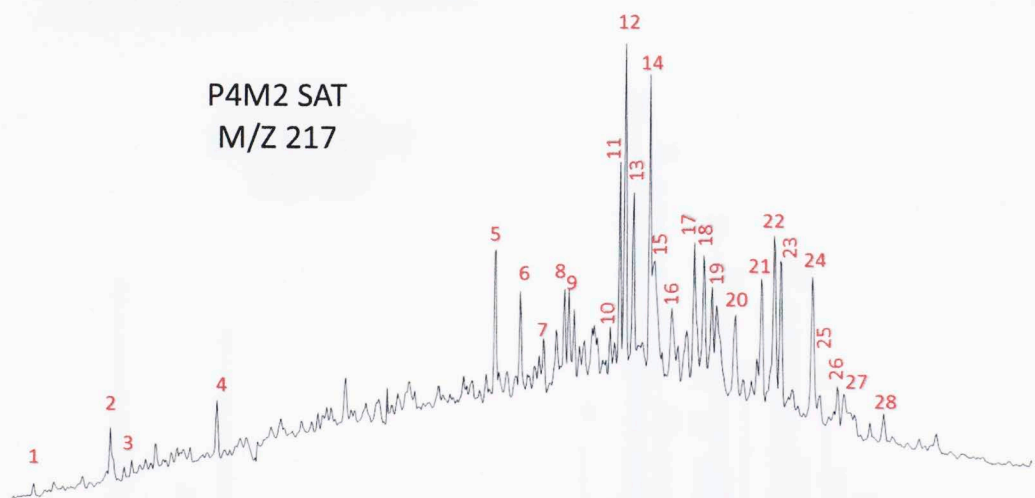


**Table.11.** Steranes data and ratios calculated for the La Luna Formation samples (n.d. = not detected).

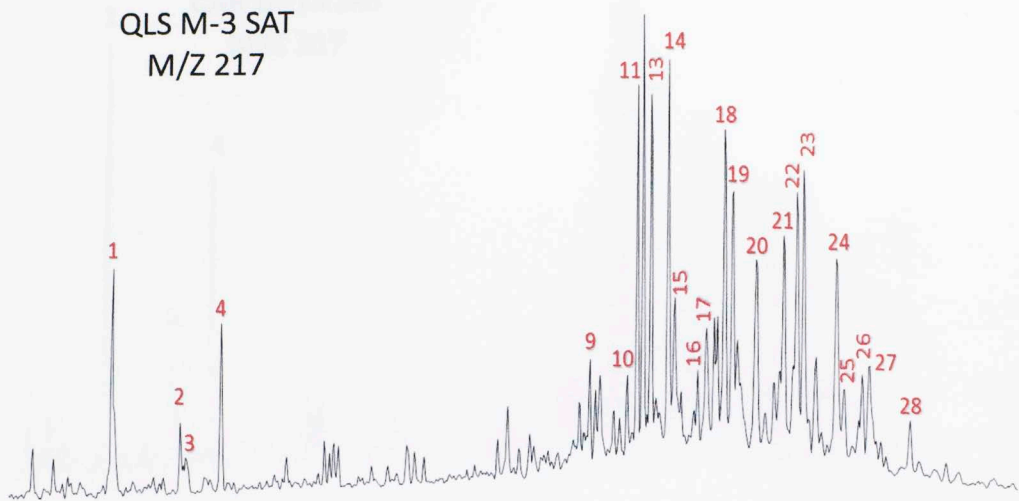
Sample #	Member	C <sub>27</sub> %	C <sub>28</sub> %	C <sub>29</sub> %	C <sub>30</sub> /C <sub>29</sub>	C <sub>30</sub> / C <sub>27</sub> -C <sub>30</sub> %	Diasteranes/ Steranes	Preg/ (Preg+Ster+Diast)
<b>OUTCROP A</b>								
P2M1	Galembo	54.53	17.37	28.10	0.29	4.61	0.54	0.37
P4M3	Galembo	n.d.	n.d.	n.d.	n.d.	n.d.	n.d.	n.d.
P4 M2	Salada	47.45	20.51	32.04	0.21	6.25	0.61	0.21
<b>OUTCROP B</b>								
QLS Umir-2	Galembo	39.94	31.14	28.92	0.40	10.30	0.67	0.59
QLS M-3	Galembo	37.25	30.48	32.27	0.27	7.95	0.25	0.37
QLS M-7a	Galembo	43.96	28.34	27.70	0.28	7.09	0.27	0.56
QLS M-8	Galembo	36.68	30.27	33.05	0.29	8.59	0.31	0.52
CAN M-15	Pujamana	37.71	32.18	30.11	0.39	10.51	0.32	0.59
CAN M-8	Pujamana	48.30	24.18	27.52	0.26	6.70	0.16	0.71
CAN M-5	Pujamana	46.47	24.86	28.67	0.27	7.23	0.91	0.81
CAR M-14	Salada	42.67	28.54	28.79	0.26	6.99	0.33	0.53
CAR M-11	Salada	45.20	23.88	30.91	0.27	7.63	0.35	0.56
CAR M-4	Salada	44.72	22.65	32.63	0.34	9.98	0.43	0.61
CAR M-3	Salada	65.06	8.82	26.12	0.63	14.11	0.57	0.65
CAR M-2	Salada	38.10	31.11	30.79	0.31	8.81	0.44	0.68



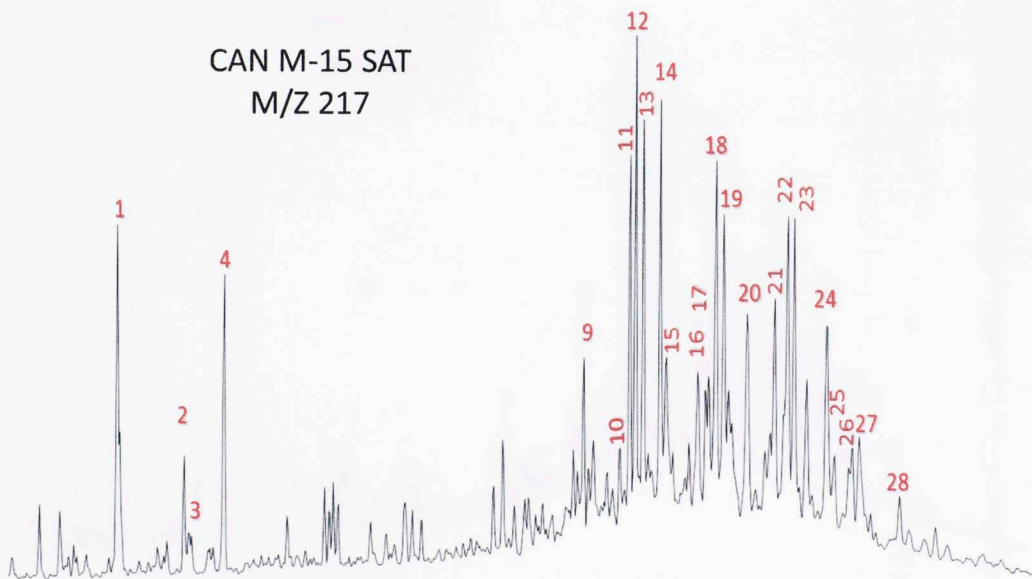
**Figure 49.** Partial fragmentograms of the  $m/z$  217 ion showing steranes distribution in the saturate fractions of the OUTCROP A Galemba member P2M1 sample. Peak identification is presented in Table 10.



**Figure 50.** Partial fragmentograms of the  $m/z$  217 ion showing steranes distribution in the saturate fractions of the OUTCROP A Salada member P4M2 sample. Peak identification is presented in Table 10.

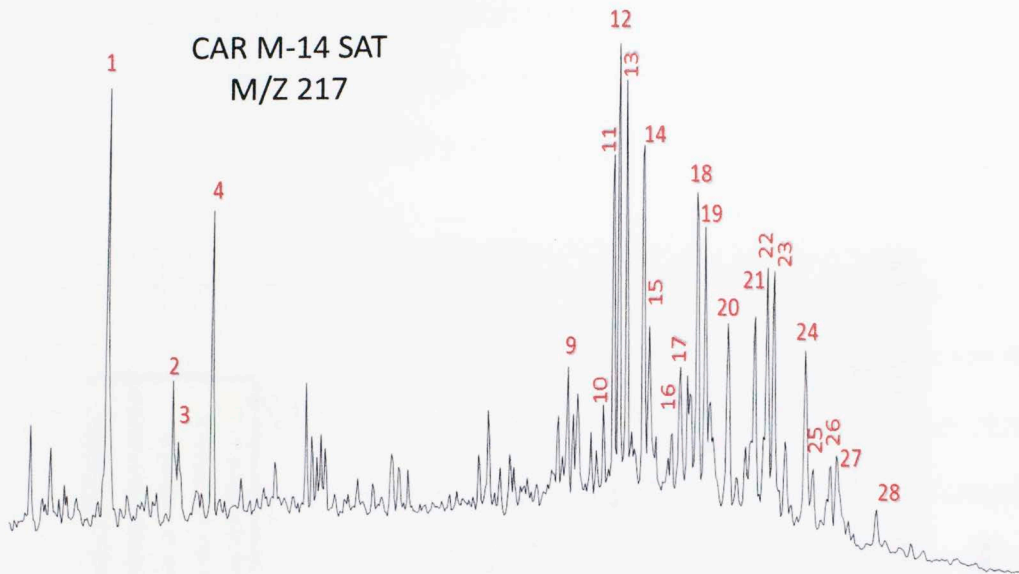


**Figure 51.** Partial fragmentograms of the m/z 217 ion showing steranes distribution in the saturate fractions of the OUTCROP B Galemba member QLS M-3 sample. Peak identification is presented in Table 10.

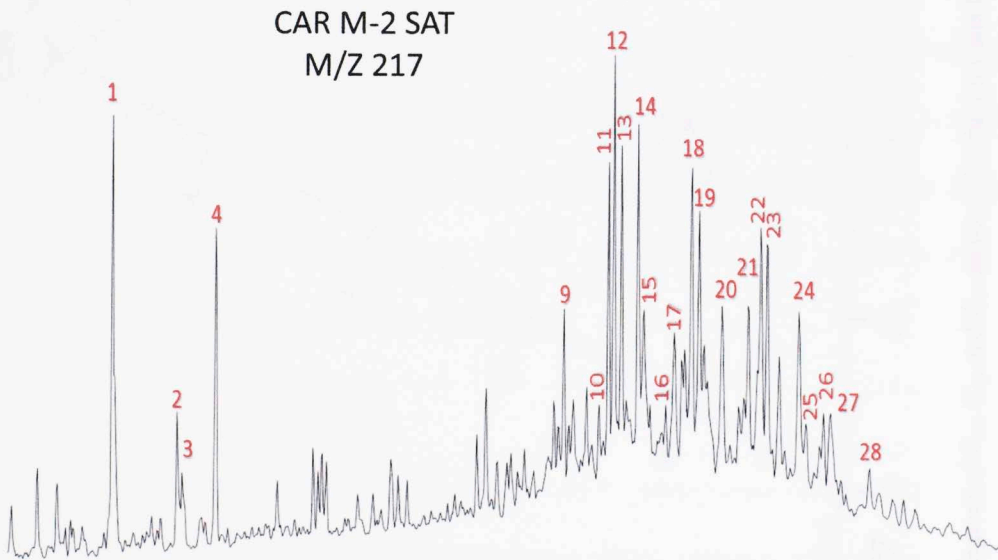


**Figure 52.** Partial fragmentograms of the m/z 217 ion showing steranes distribution in the saturate fractions of the OUTCROP B Pujamana member CAN M-15 sample. Peak identification is presented in Table 10.

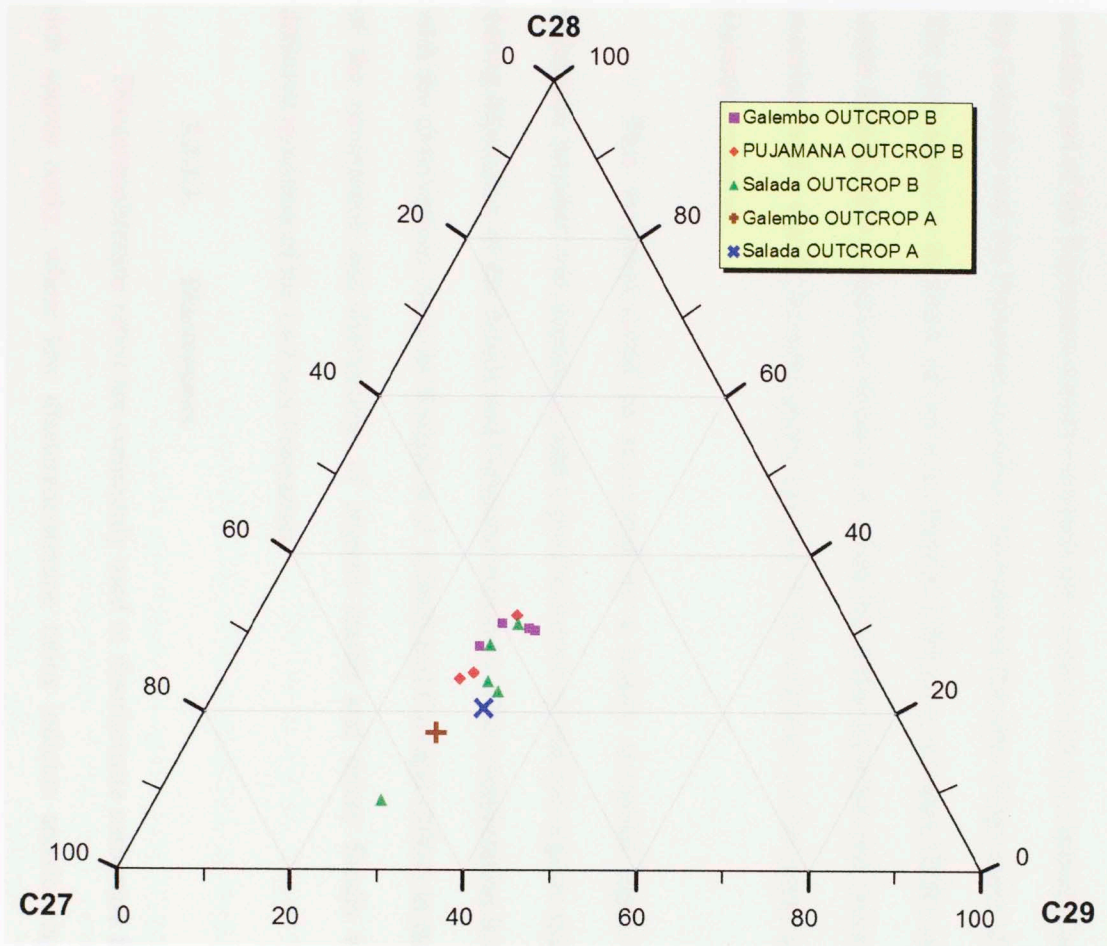




**Figure 53.** Partial fragmentograms of the  $m/z$  217 ion showing steranes distribution in the saturate fractions of the OUTCROP B Salada member CAR M-14 sample. Peak identification is presented in Table 10.



**Figure 54.** Partial fragmentograms of the  $m/z$  217 ion showing steranes distribution in the saturate fractions of the OUTCROP B Salada member CAR M-2 sample. Peak identification is presented in Table 10.



**Figure 55.** Ternary diagram of C<sub>27</sub>, C<sub>28</sub> and C<sub>29</sub> steranes for the La Luna Formation samples.

The biomarker ratio, C<sub>30</sub> steranes (20R)/C<sub>29</sub> steranes (20R) (Table 10 and Figure 56) for the OUTCROP B shows a high value at the Salada member base. This plot also exhibits a change around 900 ft of stratigraphic depth, where the ratio decreases from the Salada member towards the Pujamana member. The ratio increases in the middle part of the Pujamana member towards the contact with the Galembo member. In the Galembo and the Pujamana members' boundaries the ratio drops again (Figure 56). The plot shows a decrease of the C<sub>30</sub> steranes (20R)/C<sub>29</sub> steranes (20R) ratio in the upper Salada, also a decrease along most of the Pujamana member and lower Galembo member, and a steady increase going upward in the sequence to the upper part of the Galembo member.

This variation could be accounted by a higher terrestrial input when the Pujamana member was deposited, and a predominance of marine organic matter input during deposition of the Salada and Galembo members. This interpretation is consistent with the observations made by Rangel et al. (2000) and Carvajal (2004) in the analysis of the occurrence and distribution of organic matter and micro fossils within the different members of the La Luna Formation.

### **3.2.3.1. Diasteranes**

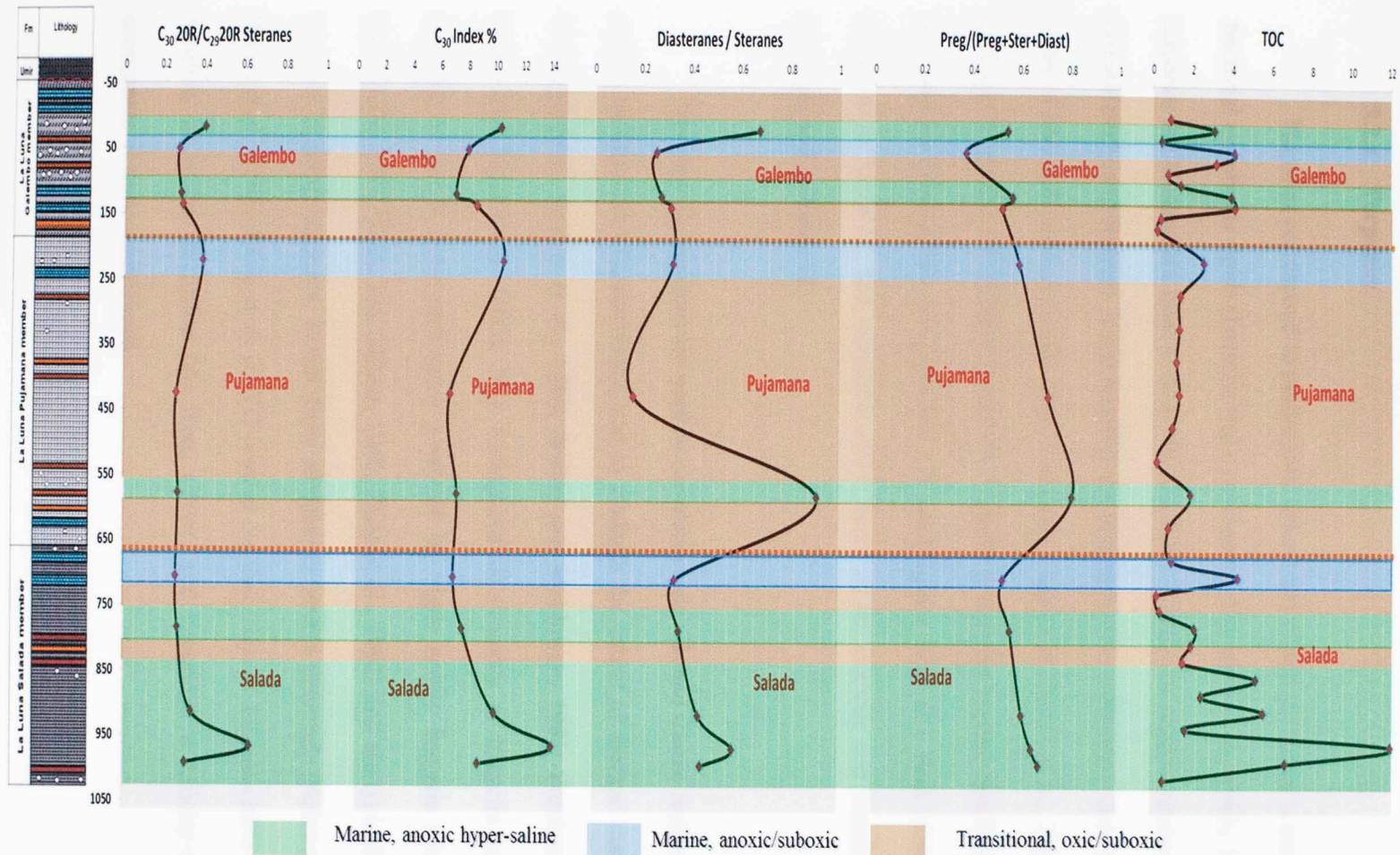
Diasterane/sterane ratios are commonly used to discriminate carbonate from clay-rich source rocks, where low diasterane/sterane ratios indicate anoxic clay-poor or carbonate source rocks (Clark and Philp, 1989), and high ratios are usually a feature of oils, or source rocks, containing abundant clays (Mello et al., 1988). During diagenesis, acidic sites on clays catalyze the conversion of steranes to diasteranes (Grantham and



Wakefield, 1988). It is also proposed that the proportion of diasteranes compared with regular steranes is known to be dependent upon maturity as well, because the original steranes are converted gradually to mixtures of diasteranes and steranes (Hughes et al., 1985; Goodarzi et al., 1989). Seifert and Moldowan (1979) also suggested that high proportions of diasteranes compared with regular steranes in oil are consistent with heavy biodegradation, resulting in elimination of steranes relative to diasteranes. This was observed for the Pujamana base and Galembo top, where the ratio increases drastically that is not consistent with a carbonate matrix for the rocks.

### **3.2.3.2. Pregnane and homopregnane**

The precursors of pregnane ( $C_{21}H_{36}$ ) and homopregnane ( $C_{22}H_{38}$ ) are pregnol and homopregmol which exist in protozoans (Yang, 1991). However, pregnane and homopregnane are also related to hypersaline environments (ten Haven et al., 1985) and could also result from thermal cracking of  $C_{27}$ - $C_{29}$  steranes (Mueller et al., 1995). According to Peters et al. (2005), the pregnane and homopregnane have high resistance to biodegradation comparable to the diasteranes. The difference in susceptibility between steranes with or without extended alkyl side chains at C-17 suggest that attack of the alkyl group is an important step in the microbial degradations of steranes. These compounds were identified for Galembo and Salada member in OUTCROP A and OUTCROP B, and in a relatively lower manner present in Pujamana member. This recognition allowed to estimate intervals of higher salinity relatively with other intervals by the Pregnane/(Pregnane+Sterane+Diasterane) ratio (Figure 56).



**Figure 56.** Proposed geochemical log of sterane biomarker ratios and TOC vs. depth for the La Luna OUTCROP B.



### 3.2.4. Terpanes

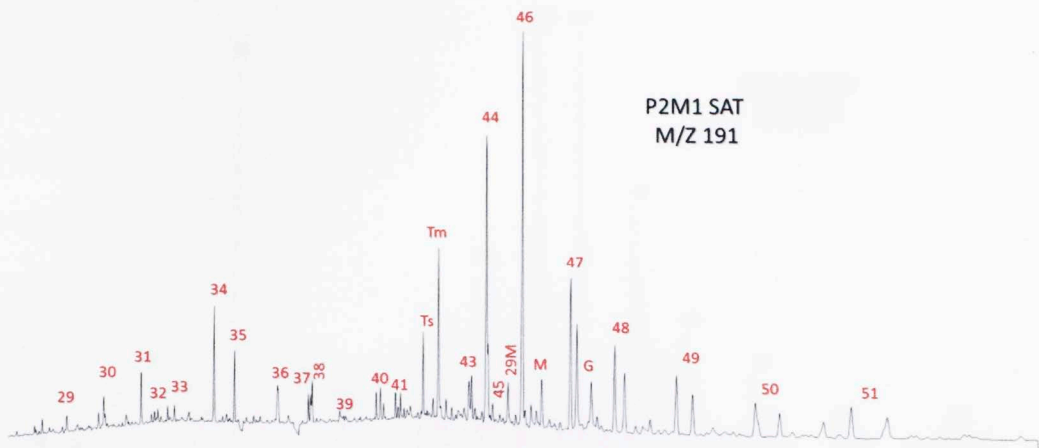
Hopanes correspond to pentacyclic triterpanes whose precursor is derived from bacterial membrane lipids (bacteria and cyanobacteria; Ourisson et al., 1982). In general, terpanes are biomarkers used extensively for determination of organic matter type and depositional environment. Since bacteria are widespread in sediments, theoretically all types of oils and extracts would show a terpane fingerprint (Peters et al., 2005). In the La Luna formation OUTCROP A and OUTCROP B samples hopane distributions were analyzed by SIM/GCMS using the  $m/z$  191 ion (Figures 57 to 62). Peak identifications are given in Table 12, and biomarker ratios based on the tricyclic and hopane terpanes are presented in Table 13.

The tricyclic terpanes are used to correlate crude oils and source rock extracts, to predict source-rock characteristics, and to evaluate the extent of thermal maturity and biodegradation (Seifert et al., 1980; Seifert and Moldowan, 1981; Zumberge, 1984; Peters and Moldowan, 1993). The widespread occurrences of tricyclic terpanes is believed to result from precursors produced by algae and/or bacteria (Seifert and Moldowan, 1979; Philp and Gilbert, 1986; Philp et al., 1992) and are typically absent, or occur in small amounts, in oils from terrigenous source materials (Robinson, 1987; Peters et al., 2005). Philp et al. (1992) pointed out that tricyclic terpanes have also been reported in saline lacustrine oils from China, and suggested a salinity-controlled occurrence of these compounds.

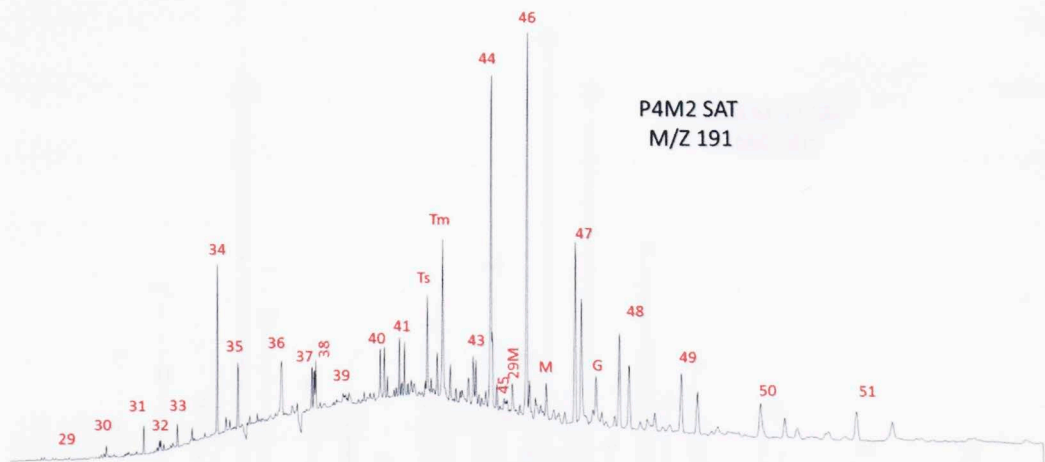


**Table.12.** Identification of terpanes in the partial m/z 191 fragmentograms.

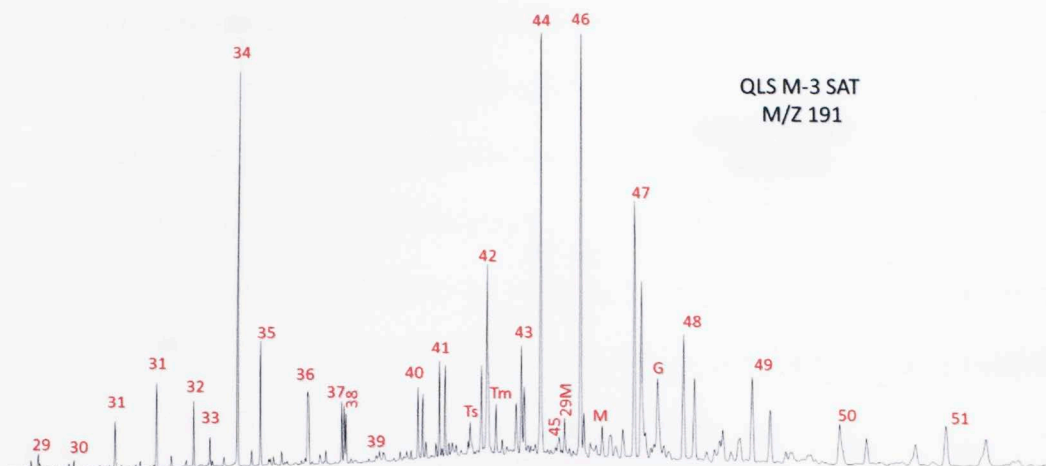
Peak #	Compound
29	C <sub>18</sub> Tricyclic terpane
30	C <sub>19</sub> Tricyclic terpane
31	C <sub>20</sub> Tricyclic terpane
32	C <sub>21</sub> Tricyclic terpane
33	C <sub>22</sub> Tricyclic terpane
34	C <sub>23</sub> Tricyclic terpane
35	C <sub>24</sub> Tricyclic terpane
36	C <sub>25</sub> Tricyclic terpane
37	C <sub>26</sub> Tricyclic terpane (22S + 22R)
38	C <sub>24</sub> Tetracyclic terpane
39	C <sub>27</sub> Tricyclic terpane (22S + 22R)
40	C <sub>28</sub> Tricyclic terpane (22S + 22R)
41	C <sub>29</sub> Tricyclic terpane (22S + 22R)
Ts	17 $\alpha$ Trisnorneohopane (C <sub>27</sub> Ts)
42	C <sub>29</sub> Norhopane
Tm	18 $\alpha$ Trisnorneohopane (C <sub>27</sub> Tm)
43	C <sub>30</sub> Tricyclic terpane
44	C <sub>30</sub> 18 $\alpha$ (H),21 $\beta$ (H)- Norhopane
45	18 $\alpha$ Neonorhopane (C <sub>29</sub> Ts)
29M	C <sub>29</sub> 17 $\beta$ (H),21 $\alpha$ (H)- Normoretane
46	C <sub>30</sub> 17 $\alpha$ (H),21 $\beta$ (H)-Hopane
M	C <sub>30</sub> 17 $\beta$ (H),21 $\alpha$ (H)- Moretane
47	C <sub>31</sub> 17 $\alpha$ (H),21 $\beta$ (H)-Homohopanes (22S & 22R)
G	Gammacerane
48	C <sub>32</sub> 17 $\alpha$ (H),21 $\beta$ (H)-Bishomohopane (22S & 22R)
49	C <sub>33</sub> 17 $\alpha$ (H),21 $\beta$ (H)-Trishomohopane (22S & 22R)
50	C <sub>34</sub> 17 $\alpha$ (H),21 $\beta$ (H)-Tetrakishomohopane (22S & 22R)
51	C <sub>35</sub> 17 $\alpha$ (H),21 $\beta$ (H)-Pentakishomohopane (22S & 22R)



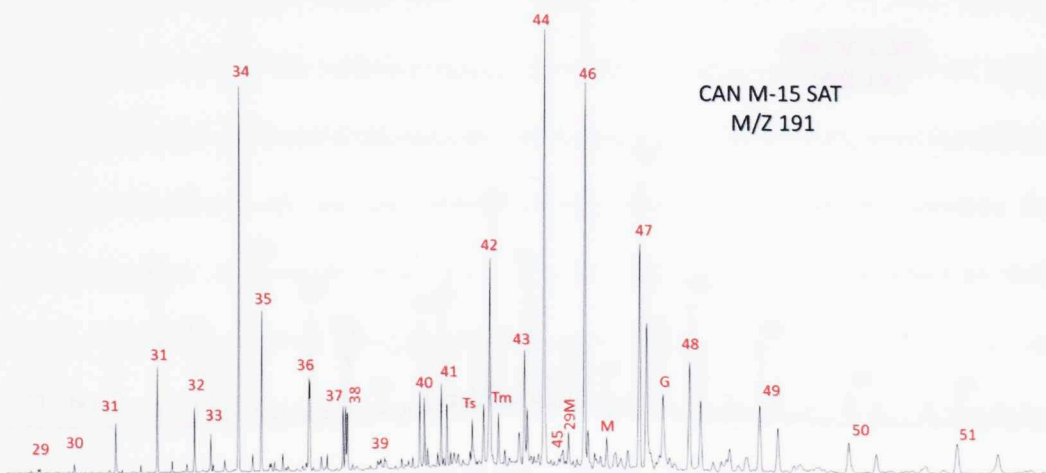
**Figure 57.** m/z 191 fragmentograms showing terpanes distribution in the saturate fractions of the OUTCROP A Galebo member P2M1 sample. Peaks identification is presented in Table 12.



**Figure 58.** m/z 191 fragmentograms showing terpanes distribution in the saturate fractions of the OUTCROP A Salada member P4M2 sample. Peaks identification is presented in Table 12

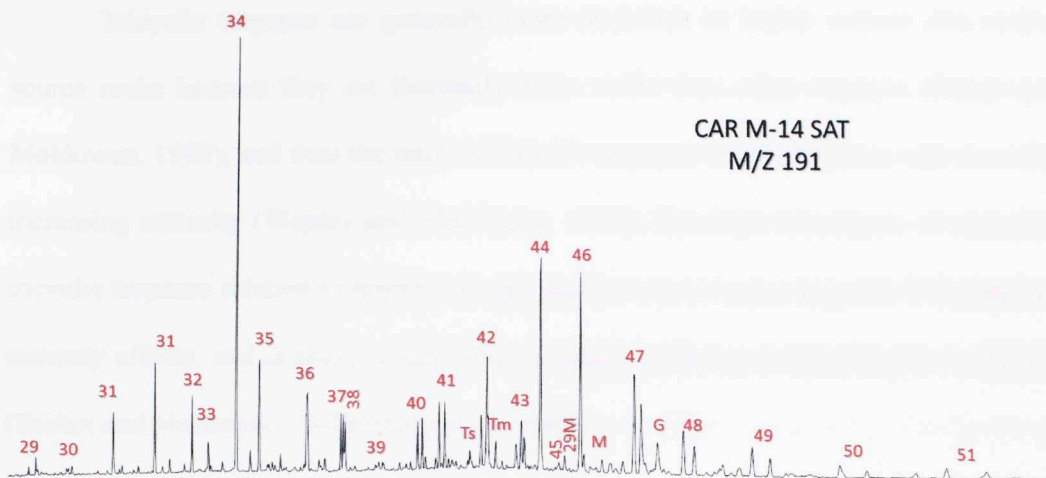


**Figure 59.** m/z 191 fragmentograms showing terpanes distribution in the saturate fractions of the OUTCROP B Galemba member QLS M-3 sample. Peaks identification is presented in Table 12.

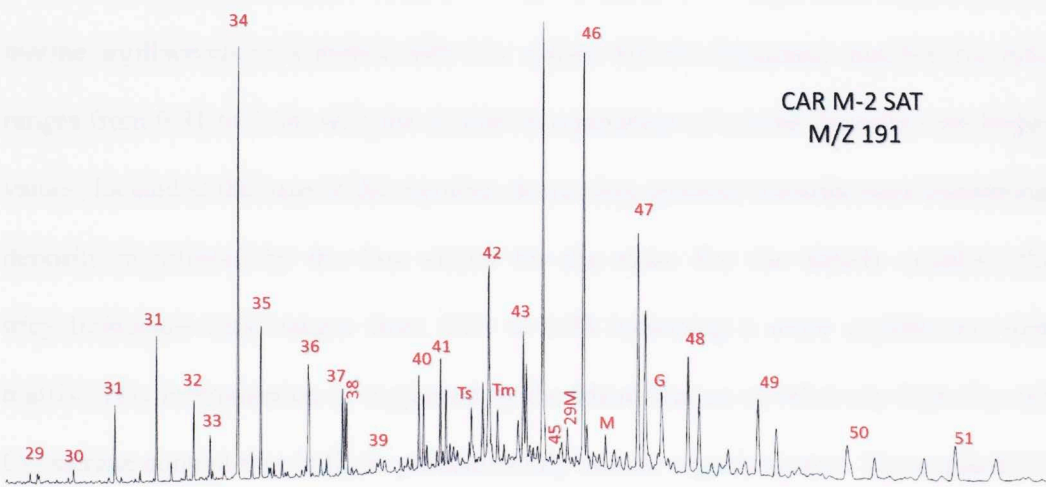


**Figure 60.** m/z 191 fragmentograms showing terpanes distribution in the saturate fractions of the OUTCROP B Pujamana member CAN M-15 sample. Peaks identification is presented in Table 12.





**Figure 61.** m/z 191 fragmentograms showing terpanes distribution in the saturate fractions of the OUTCROP B Salada member CAR M-14 sample. Peaks identification is presented in Table 12.



**Figure 62.** m/z 191 fragmentograms showing terpanes distribution in the saturate fractions of the OUTCROP B Salada member CAR M-2 sample. Peaks identification is presented in Table 12.

Tricyclic terpanes are generally more abundant in highly mature oils and/or source rocks because they are thermally more stable than other terpanes (Peters and Moldowan, 1993), and thus the ratio of tricyclic terpanes to 17 $\alpha$ -hopanes will rise with increasing maturity (Waples and Machihara, 1990). The high abundance of extended tricyclic terpanes relative to hopanes in oils and/or source rocks may also be related to maturity effects, and is also probably due to marine influenced depositional conditions (Seifert and Moldowan, 1979; Philp et al., 1992).

Generally, for OUTCROP A Galembo and Salada members the tricyclic/hopane ratio is 0.17. For the OUTCROP B Galembo member the variation ranges from 0.36 to 1.33, indicating that the rates vary from marine hypersaline deposits for high values to marine argillaceous rock matrix with low values. For the Pujamana member, the ratio ranges from 0.31 to 3.08, with the similar interpretation of marine deposits with higher values, located at the base of the member, decreasing upwards towards more transitional deposits manifested by the low values for the ratio. For the Salada member, the tricyclic/hopane ratio ranges from 0.23 to 0.78 indicating a more argillaceous rock matrix. This interpretation is supported by the identification of relatively high C<sub>27</sub> and C<sub>30</sub> sterane content that indicate predominantly marine organic matter. The explanation of low tricyclic/hopane ratios can be addressed by the predominance of argillaceous black shale deposits over carbonate deposits in the Salada member.

Hopanes are derived primarily from bacteria (Peters et al., 2005) and the C<sub>29</sub> and C<sub>30</sub> 17 $\alpha$  (H)-hopanes are the predominant triterpanes. The C<sub>29</sub>/C<sub>30</sub> hopane ratio is commonly used to distinguish carbonate from clastic lithology (Palacas et al., 1984;

Peters and Moldowan, 1993). Oils sourced from organic rich carbonates and evaporites are generally characterized by high values ( $>1$ ) of  $C_{29}/C_{30}$  hopanes ratios (Zumberge, 1984; Connan et al., 1986; Price et al., 1987; Clark and Philp, 1989), while, low values of  $C_{29}/C_{30}$  hopanes ratios are characteristics of siliceous shaly deposits. For the OUTCROP B samples, the  $C_{29}/C_{30}$  hopane values ranged from 0.86 to 1.61 (Table 13). Association with the identified stratigraphic facies,  $C_{29}/C_{30}$  ratios  $<1.10$  suggests a stronger clastic shaly nature of the source, while the higher values are characteristic of samples with a greater carbonate component.

The contents of tricyclic and tetracyclic terpanes in crude oils are closely related to the nature of their organic matter (Seifert and Moldowan, 1978; Aquino Neto et al., 1983). Connan et al. (1986) and Clark and Philp (1989) reported the occurrence of the  $C_{24}$  tetracyclic terpanes in samples from hypersaline environments. However, according to other authors,  $C_{24}$  tetracyclic terpanes are usually found in relatively high concentrations in oils from evaporite-carbonate sequences and typically dominate the terpane distribution (Palacas et al., 1984; Connan et al., 1986; Clark and Philp, 1989). The high preservation rate of organic matter in evaporitic environments is predominantly due to the decrease in solubility of oxygen with increasing salinity (Sammy, 1985). In addition, tetracyclic terpanes are more resistant to biodegradation than hopanes (Aquino Neto et al., 1983).

The homohopane index (HHI) is used as an indicator of redox potential (Eh) in marine sediments during diagenesis (Moldowan et al., 1991). The homohopanes ( $C_{31}$  to  $C_{34}$ ) are believed to be derived from bacteriopolyhopanol present in prokaryotic cell



membranes (Peters et al., 2005). According to Peters and Moldowan (1993), low ratios of C<sub>35</sub> to C<sub>34</sub> homohopanes (0.38–0.65) suggest prevailing oxic to sub-oxic (high Eh) conditions during deposition and hence low organic matter with low hydrogen index (Dahl et al., 1994). For the OUTCROP B samples the C<sub>35</sub> S/C<sub>34</sub>S ratio is higher than 0.65, indicating a predominantly anoxic depositional environment, hence high preservation and higher TOC values (Figure 63). The intensity of the C<sub>35</sub> homohopane remains relatively high suggesting the existence of reducing marine conditions that allowed accumulation and preservation of the organic matter during La Luna formation sedimentation and diagenesis.

The Ts vs. Tm ratio has been used extensively as an indicator of maturity in samples containing similar source materials (Peters et al., 2005). The ratio is dependent on the depositional environment and the source of organic material (Philp et al., 1992). The ratio is also affected by lithology and oxicity of the depositional environment, where bitumen from many hypersaline source rocks show high Ts/ (Ts+Tm) ratios (Fan Pu et al., 1987; Peters et al., 2005). Moldowan et al. (1986) and Peters et al. (2005) observed that the ratio increases at lower Eh and decreases at higher pH for the depositional environment of a series of Lower Toarcian marine shales from southwestern Germany. It also decreases in an anoxic (low Eh) carbonate section. It has also been observed that oils from carbonate source rocks have unusually low Ts/(Ts+Tm) ratios compared with those from shales (McKirdy et al., 1983; McKirdy et al., 1984; Rullkötter et al., 1985; Price et al., 1987).

The OUTCROP B samples show relatively low  $T_s/T_s+T_m$  values (less than 0.8, Figure 63), and it is interpreted as an indicator of anoxic, low Eh carbonate deposits. The relative changes of this ratio along the stratigraphic column of OUTCRP B section (Figure 63), shows the trends of change of anoxia, where increasing trends are related to more saline deposits and are observed at the middle and base of the Salada member, Middle Pujamana member, and middle to upper Galembo member. The decreasing relative trends are observed at the base of the Galembo member, top of Pujamana member and top of Salada member, indicating transitional deposits and suboxic depositional environments.

The presence of gammacerane (peak G in Figures 57 to 62) in the OUTCROP B samples was determined by SIM/GCMS using the  $m/z$  191 ion. Its presence suggests some interesting variations on the depositional environment. Gammacerane is a C30 triterpane derived from diagenesis of tetrahymanol, a compound biologically related with the freshwater ciliated protozoan *Tetrahymena*. Gammacerane is a very good indicator of water-column stratification during sedimentation in marine and non-marine environments, and is usually associated with hypersaline conditions at depth, especially in alkaline lakes and lagoonal carbonate-evaporite environments; however, it is not restricted to this type of setting (Peters et al., 2005).

**Table.13.** Biomarker ratios for hopanes in the La Luna Formation samples (n.d. = not determined).

Sample #	Member	Ts/Tm	C <sub>23</sub> / C <sub>29</sub> H	C <sub>23</sub> / C <sub>30</sub> H	C <sub>29</sub> H/C <sub>30</sub> H	C <sub>24</sub> Tetra/ C <sub>26</sub>	C <sub>24</sub> Tetra/ C <sub>30</sub>	Gamm. Index	Oleanane Index	C <sub>35</sub> S/ C <sub>34</sub> S	
<b>OUTCROP A</b>											
P2M1	Galembo	0.77	0.24	0.20	0.85	0.98	0.13	0.17	0.11	0.75	
P4M3	Galembo	n.d	n.d	n.d	n.d	n.d	n.d	n.d	n.d	n.d	
P4 M2	Salada	0.75	0.32	0.31	0.99	0.43	0.08	0.15	0.09	0.86	
<b>OUTCROP B</b>											
801	QLS Umir-2	Galembo	0.58	1.86	2.98	1.61	0.42	0.59	0.45	0.17	0.86
	QLS M-3	Galembo	0.45	0.60	0.60	1.00	0.39	0.07	0.25	0.08	0.93
	QLS M-7a	Galembo	0.54	1.12	1.20	1.07	0.61	0.26	0.22	0.08	0.75
	QLS M-8	Galembo	0.45	0.78	0.93	1.20	0.40	0.14	0.38	0.11	0.78
	CAN M-15	Pujamana	0.52	0.63	0.67	1.06	0.41	0.10	0.24	0.08	1.01
	CAN M-8	Pujamana	0.71	1.89	2.16	1.14	1.01	0.56	0.27	0.07	1.12
	CAN M-5	Pujamana	0.63	4.22	8.04	1.90	0.49	0.84	0.52	0.20	0.96
	CAR M-14	Salada	0.55	1.33	1.49	1.12	0.50	0.20	0.23	0.08	0.75
	CAR M-11	Salada	0.63	1.49	1.33	0.89	0.47	0.22	0.22	0.16	1.18
	CAR M-4	Salada	0.65	1.36	1.17	0.86	0.46	0.20	0.22	0.11	1.10
	CAR M-3	Salada	0.28	0.33	0.36	1.10	0.51	0.23	0.52	0.40	1.03
	CAR M-2	Salada	0.54	0.68	0.70	1.02	0.41	0.11	0.24	0.08	0.82

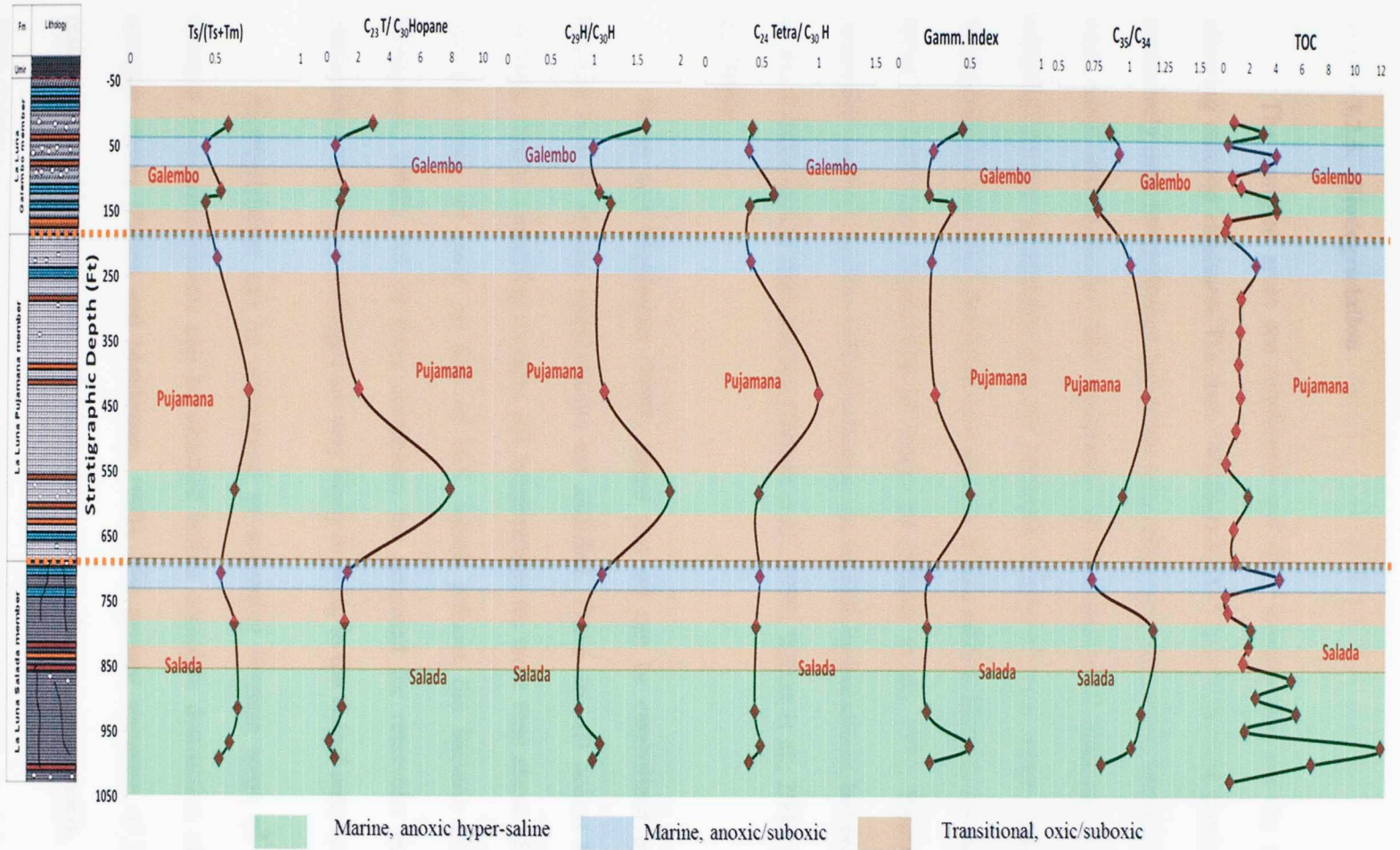


Gammacerane was recognized in all of the analyzed samples, its presence indicates the existence of a stratified water column deposition of strata at OUTCROP B. The geochemical log for the gammacerane index (gammacerane/gammacerane + C<sub>30</sub> hopane) illustrated in Figure 63, shows a higher proportion of gammacerane in the base of the Salada member, the base of the Pujamana member, the base of the Galemba member. This observation suggests that water stratification and salinity played an important role at the transitions of all members, where the transgressive sequences were starting to be deposited. Peters et al. (2005) indicate that a high gammacerane index resulting from water salinity and stratification correlates with a decrease in pristane/phytane ratios due to low oxygen content in bottom waters. This relationship between gammacerane and pristane/phytane ratios could not be estimated due to the high degradation of these isoprenoids.

The most abundant terpane in the majority of the samples is the C<sub>30</sub> hopane (C<sub>30</sub> 17 $\alpha$ (H),21 $\beta$ (H)-Hopane), followed by the C<sub>23</sub> tricyclic terpane (Figures 56 to 62). The C<sub>30</sub> hopane is thought to be derived from diploptene or diplopterol present in bacteria (Ourisson et al., 1982). Dzou et al. (1995) also suggested an origin from bacteriohopanetetrol, a compound present in bacterial membranes. A microbial and/or algal source has been proposed for the tricyclic terpanes although it is thought that their bacterial origin is different from that of the C<sub>30</sub> hopane (Ourisson et al., 1982). The ratio C<sub>23</sub> tricyclic (cheilanthane)/C<sub>30</sub> hopane has been used to determine organic matter input and maturation; however, care must be taken when assessing which parameter has more influence on the samples analyzed, especially for immature samples (Seifert and Moldowan, 1986; Dzou et al., 1995). This ratio has been used to evaluate biomarkers

derived from bacterial or algal sources (tricyclics) against biomarkers derived from prokaryotes (hopanes; Peters et al., 2005). For all three members of the La Luna formation samples this parameter shows significant variations (Figure 56 to 62; Table 13), where the ratio generally decreases with depth on the OUTCROP B section, possibly indicating a higher input of marine algae going up in the sequence.

The presence of the C<sub>23</sub> tricyclic terpane, the predominance of C<sub>27</sub> and C<sub>30</sub> steranes, the strong presence of C<sub>24</sub> tetracyclic, pregnane and homopregnane, all support the input of marine organic matter under a anoxic saline to hypersaline, carbonate dominated environment for samples from OUTCROP A and OUTCROP B



**Figure 63.** Geochemical logs of biomarker ratios from terpanes for the La Luna formation OUTCROP B. Values in table 13.



### 3.2.5. Biodegradation

The sampled areas are rainforests and river streams that cut the rocks and allowing outcrop exposures. The term “biodegradation” has been most commonly and extensively used for reservoirs and crude oils, rather than for soluble bitumen in source rock cores and outcrops. The occurrence of biodegradation affecting outcrops is enhanced by the weathering and the different events of fresh water washing. The biodegradation has been described as a process where aerobic bacteria are the primary factor in subsurface degradation of crude oil (Milner et al., 1977; Palmer, 1984). Anaerobic bacteria, such as sulfate reducers, can oxidize hydrocarbons, but probably do so much more slowly than aerobes (Jobson et al., 1979; Wilkes et al., 2000; Grasby et al., 2009).

Peters and Moldowan (1993) stated that oil can be catabolized by aerobic bacteria only if several requirements are satisfied. These are: (i) access to surface recharge waters containing oxygen; (ii) temperatures no more than about 65 to 80°C; (iii) the crude oil must be free of H<sub>2</sub>S, which poisons the bacteria (Peters and Moldowan, 1993). All of these conditions are proposed for reservoirs but similar characteristics of water recharges are very likely to occur in the visited outcrops.

Biodegradation can be understood as sequential because some of the more resistant compound classes can be attacked before complete destruction of the less resistant classes (Peters and Moldowan, 1993). The general sequence of increasing resistance to biodegradation of biomarkers is: *n*-alkanes, isoprenoids, steranes,

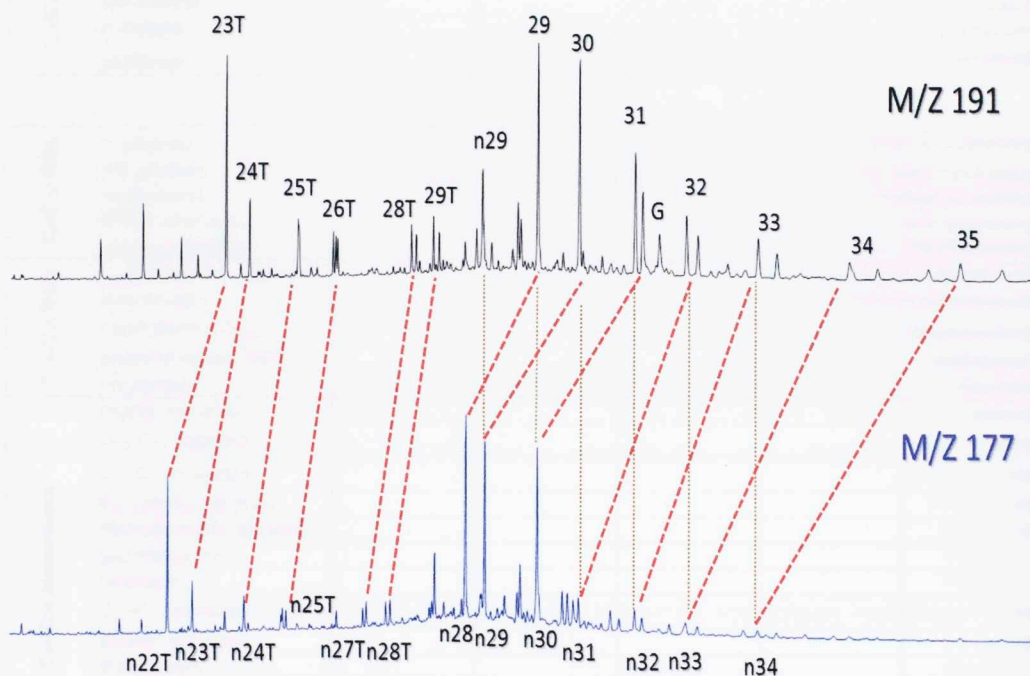
hopanes/diasteranes, aromatic steroids, and porphyrins (Chosson et al., 1992; Moldowan et al., 1992; Wenger et al., 2002).

Because of their differential resistance to biodegradation, comparison of the amounts of biomarker types in crude oils can be used to rank the relative extent of biodegradation; these were applied for recognizing the level of biodegradation for the soluble bitumen extracts of OUTCROP A and OUTCROP B samples. The ranking that was applied to estimate the level of biodegradation was that proposed by Wenger et al. (2002), who developed a scale based on Volkman et al. (1983) and Moldowan et al. (1992) to assess the extent of biodegradation based on the relative abundance of various hydrocarbon classes (Figure 65).

A heavy level of biodegradation was interpreted for all outcrop samples by recognizing the removal of n-alkanes, isoprenoids, and partial depletion of regular steranes and hopanes by recognizing on the m-z ion 177 the presence of 25-norhopane compounds (Figure 64), which according to Peters et al. (2005) are identified as a series of C<sub>26</sub>-C<sub>34</sub> compounds that are structurally equivalent to the regular hopanes, except for the absence of the methyl group at the A/B ring junction.

The separation and identification of the 25-norhopanes was conducted following the same methodology as that for the hopanes. In the m/z 191 ion, the A/B ring fragment of the hopanes shifts to the m/z 177 ion in the 25-norhopane (Dzou, 1999; Peters et al., 2005). The origin of 25-norhopanes is related to microbial activity where these compounds are generated and expelled as petroleum, and these are less abundant

than hopanes. Where biodegradation occurs it removes the hopanes, therefore the 25-norhopanes are unmasked as they become enriched (Peters et al., 2005).



**Figure 64.** m/z 191 and 177 for CAR M-2 sample indicating the occurrence of 25-norhopanes indicated by n-carbon number notation and the degradation of the tricyclic terpanes n-carbon number T notation.



		REMOVAL OF SELECTED COMPOUND GROUPS AT VARIOUS LEVELS OF BIODEGRADATION*				
		Level of Biodegradation				
		very slight	slight	moderate	heavy	severe
C <sub>1</sub> -C <sub>5</sub> gases	methane					
	ethane					
	propane					→
	iso-butane					→
	n-butane					→
	pentanes					→
C <sub>6</sub> -C <sub>15</sub> HCs	n-alkanes					→
	iso-alkanes					→
	isoprenoids					→
	BTEX aromatics					→
	alkylcyclohexanes					→
C <sub>15</sub> -C <sub>35</sub> HCs	n-alkanes, iso-alkanes					→
	isoprenoids					→
	naphthalenes (C <sub>10</sub> +)					→
	phenanthrenes, DBTs					→
C <sub>15</sub> -C <sub>35</sub> biomarkers	chrysenes					→
	regular steranes					→
	C <sub>30</sub> -C <sub>35</sub> hopanes					→
	C <sub>27</sub> -C <sub>29</sub> hopanes					→
	triaromatic steranes					→
	monoaromatic steranes					→
	gammacerane					→
	oleanane					→
	C <sub>21</sub> -C <sub>22</sub> steranes					→
	tricyclic terpanes					→
	diasteranes					→
	diahopanes					→
25-norhopanes**					□□□→	
seco-hopanes**					□□□→	

\*Table represents a generalized sequence of degradation. Different biodegradation pathways (aerobic vs. anaerobic) and different types of bacteria will attack specific molecules and compound ranges. Degradation sequence is based on observation of reservoir oils and seabottom seeps. BTEX refers to benzene, toluene, ethylbenzene, and xylene.

\*\*Appearance, rather than removal of compounds (these compounds believed to be created during biodegradation).

**Figure 65.** Ranking of biodegradation levels proposed by Wenger et al. (2002). This chart represents the extent of biodegradation of mature crude oil based on differing resistance of compound classes to microbial attack. Dashed lines indicate where compound classes are initially altered, the solid gray lines indicate substantial depletion and the black arrows indicate those that are completely

### 3.3. Lithofacies Characterization

#### 3.3.1. Lithofacies Definition, Outcrop and Thin Section

##### descriptions.

The lithofacies definition was conducted in detail for the OUTCROP B section, which has reached a maturity level equivalent to the oil window. This section is the most stratigraphically complete and presents the three La Luna Formation members. Seven major lithofacies association were identified at OUTCROP B based upon outcrop and thin section description. This section presents a general description for each facies including outcrop and petrographic observations. A more detailed thin section analysis can be found in Appendix II. The lithofacies description starts from the base of the OUTCROP B section.

##### 3.3.1.1. Lithofacies and Organic Facies in the Salada member.

- **Lithofacies S-i, Salada base.** This lithofacies corresponds to the samples CAR M-1 to M-4a (Table 5) and consists of crystalline limestone intercalated with poorly laminated wackestones and calcareous black shales. These layers are from 0.5 to 1.5 ft. thick and are parallel-planar stratified. The wackestones consist mainly of planktonic foraminifera with some pyrite traces. The crystalline limestone layers are of greenish-gray color with observed laminae filled with bitumen (Figure 66). This organic facies present the highest TOC, values from 2.50% to 11.90%; HI values around 458 and S2 between 25.92 and 54.54; high C<sub>30</sub> sterane index (8 -14%); high gammacerane index; high

pregnane content (0.61-0.68); all indicating from a Type II organic matter marine anoxic hypersaline environment with a very good potential for hydrocarbon generation.

- **Lithofacies S-ii, upper part of Salada member.** This lithofacies corresponds to samples CAR M-5 to M-14 (Table 5) and is composed of muddy laminated dark gray and thin bedded foraminiferal wackestones and calcareous shales with small nodules of pyrite. Calcite crystals are cemented and the micro fractures are filled with bitumen. The foraminifera *Globigerina* is present. The thickness of this facies varies from 1 to 5 ft. and is located from the middle part to the upper part of the Salada member. This facies contains foraminifera and fecal pellets which are usually oriented parallel to the bedding planes. This facies ranges from predominately a clay rich interval to diluted carbonate intervals. Bitumen saturation is observed in the thin sections of this facies (Figure 67). This organic facies contain TOC values from 0.25% to 5.20%; HI from 130 to 554; S2 peak between 0.33 and 23.72; lower C<sub>30</sub> sterane index than S-A facies (6 -8%); low gammacerane index; less pregnane content (0.53-0.56); all indicating from a Type II organic matter marine suboxic to anoxic saline environment with a good potential for hydrocarbon generation.

#### 3.3.1.2. Lithofacies and Organic Facies in the Pujamana member.

- **Lithofacies P-iii. Observed at the base of the Pujamana member.** This lithofacies corresponds to samples CAN M1 to M-5 (Table 5). It is



composed of calcareous shales, micritic mudstones and laminated siliceous mudstones and siltstones filled with bitumen. The laminations are alternations of foraminifera (*Globigerina*) organic matter, clay minerals and layers filled with bitumen (Figure 68). This organic facies have TOC values ranging from 0.25% to 5.20%; HI from 36 to 152; S2 peak between 0.30 and 1.48; relatively high C<sub>30</sub> sterane index compared with Salada facies (7.23%); high gammacerane index and highest pregnane content (0.81); all indicating that this facies has layers that are source intervals with the predominance of transitional environment deposits, from a Type II/III organic matter mixed marine and terrigenous oxic to suboxic environment.

- **Lithofacies P-iv. Observed in the middle part of the Pujamana member.**

This lithofacies corresponds to samples CAN M6 to M8 (Table 5) of the middle Pujamana member (Figures 16 and 68). It is composed of intercalations of bentonites (possible deposits from weathering of volcanic ashes) that are less than 5 inches thick, cherts, phosphate layers, siliceous mudstones and claystones that are yellowish to gray color, planar laminated and also fewer foraminifera (*Globigerina*). Some layers are filled with bitumen as are the foraminifera shells. These layers correspond to the compacted mudstones. This organic facies TOC ranges from 0.24%-1.32%; HI from 30 to 189; the S2 peak between 0.01 and 0.31; from the extracts relatively high C<sub>30</sub> sterane index compared with the Salada facies, but less than the Pujamana *P-iii* facies (6.7%); lower gammacerane index and high

pregnane content (0.71); all indicating that this facies has layers that are source intervals with the predominance of transitional environment deposits, from a Type II/III organic matter mixed marine and terrigenous oxic to suboxic environment.

- **Lithofacies P-v. Observed at the upper part of the Pujamana member.**

This lithofacies corresponds to samples CAN M10 to M-8 (Table 5) of the middle Pujamana member (Figure 68). It is composed of muddy laminated wackestones and calcareous dark gray shales that are thin bedded, planar laminated with foraminifera (*Globigerina*) that are sometimes filled with bitumen. Phosphatic layers occur at the base of this facies. This organic facies has the highest TOC of the Pujamana member with values ranging from 1.17% to 2.54%; HI from 34 to 231; the S2 peak between 0.47 and 4.38; from the extracts relatively high C<sub>30</sub> sterane index compared with the Salada and other Pujamana facies (10.51%); the lowest gammacerane index, high pregnane content (0.59) but decreasing from Pujamana *P-iv* facies; all indicating that the organic rich rocks of this facies correspond to a source rock of Type II/III shallow marine suboxic organic matter.

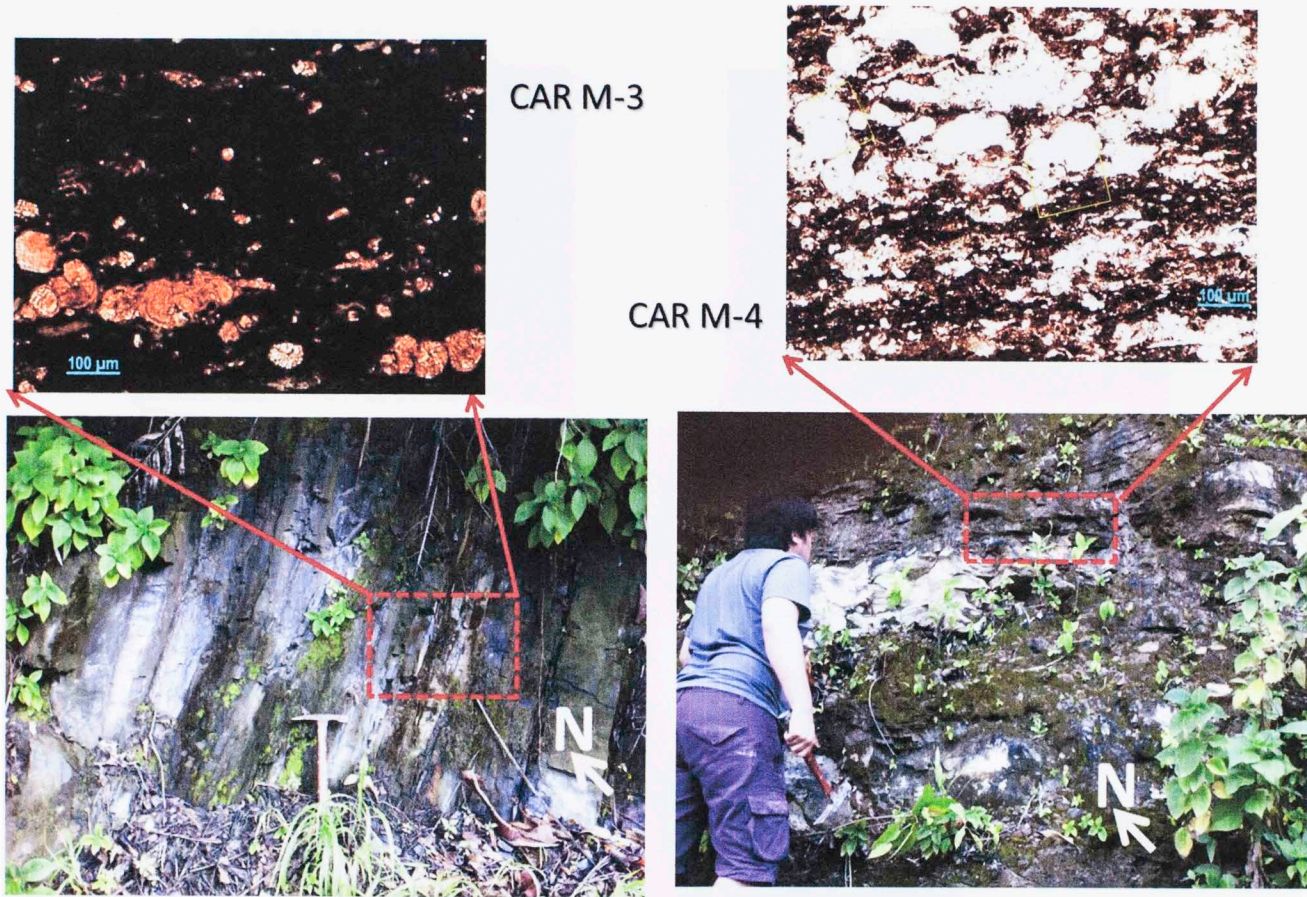
**Table 5.** Total Organic Carbon (TOC) and Rock Eval data from La Luna central MMVB section, OUTCROP B samples used in this study.

Sample Name	TOC	S1	S2	S3	Tmax	HI	OI	S2/S3	S1/TOC	PI
QLS Umir	0.89	0.01	0.45	0.48	437	51	54	1	1	0.02
QLS Umir-2	3.10	1.60	20.83	0.53	418	672	17	39	52	0.07
QLS M-1	0.43	0.04	0.61	0.23	430	141	53	3	9	0.06
QLS M-3	4.09	3.74	17.39	0.28	440	425	7	62	91	0.18
QLS M3-5	3.18	1.44	10.32	0.49	434	325	15	21	45	0.18
QLS M-6	0.77	0.02	0.50	0.46	433	65	60	1	3	0.04
QLS M-7	1.41	0.06	1.77	0.53	432	126	38	3	4	0.03
QLS M-7a	3.94	3.32	16.14	0.37	435	410	9	44	84	0.17
QLS M-8	4.12	4.07	18.10	0.25	435	439	6	72	99	0.18
QLS M-10	0.40	0.06	0.77	0.08	434	193	20	10	15	0.07
QLS CHERT-BIT	0.22	0.02	0.21	0.05	435	97	23	4	9	0.09
CAN M-15	2.54	0.21	4.38	0.57	438	172	22	8	8	0.05
CAN M-13	1.37	0.01	0.47	0.60	437	34	44	1	1	0.02
CAN M-11	1.31	0.48	3.03	0.23	437	231	18	13	37	0.14
CAN M-10	1.17	0.01	0.84	0.77	436	72	66	1	1	0.01
CAN M-8	1.32	0.31	2.50	0.31	437	189	23	8	23	0.11
CAN M-7	0.98	0.05	1.60	0.26	437	163	26	6	5	0.03
CAN M-6	0.24	0.01	0.07	0.14	N.D.	30	59	1	4	0.13
CAN M-5	1.90	0.02	1.11	1.23	438	58	65	1	1	0.02



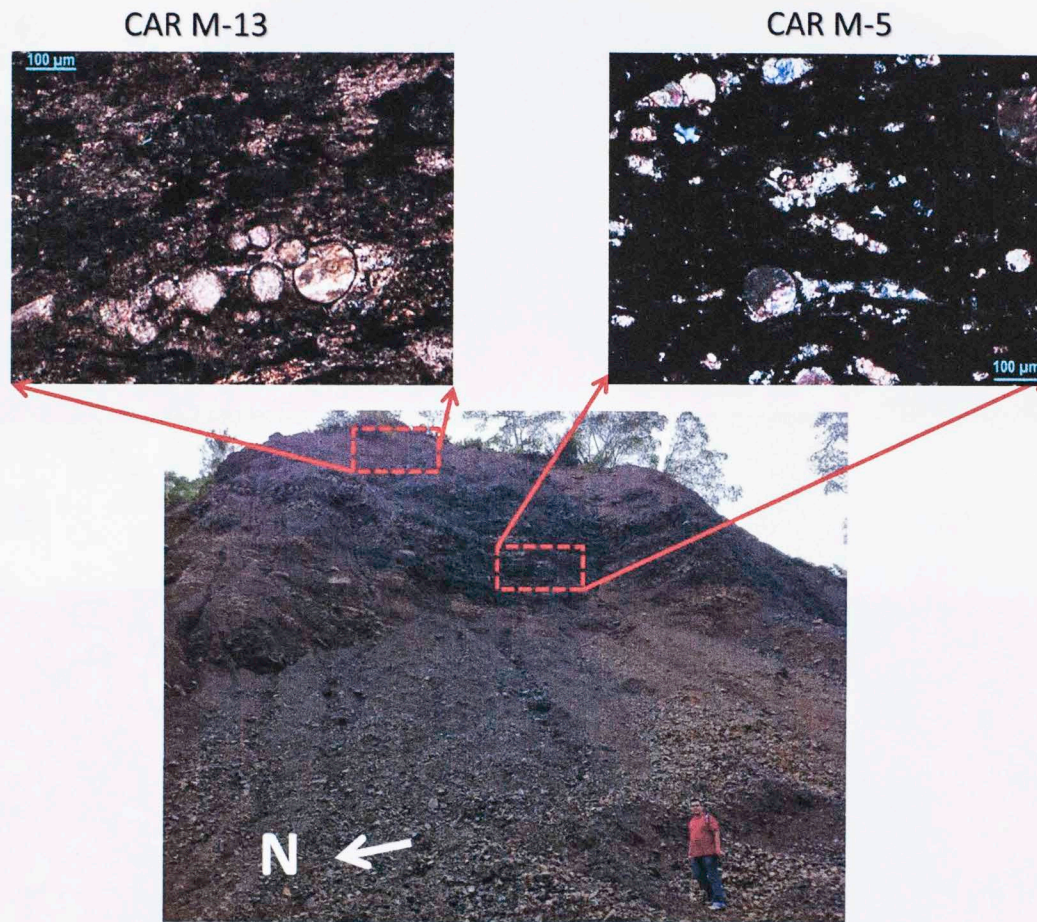
**Table 5.** Total Organic Carbon (TOC) and Rock Eval data from La Luna central MMVB section, OUTCROP B samples used in this study (cont.).

<b>Sample Name</b>	<b>TOC</b>	<b>S1</b>	<b>S2</b>	<b>S3</b>	<b>Tmax</b>	<b>HI</b>	<b>OI</b>	<b>S2/S3</b>	<b>S1/TOC</b>	<b>PI</b>
<b>CAN M-1</b>	0.83	0.01	0.30	0.41	440	36	50	1	1	0.03
<b>CAN M-1N</b>	0.97	0.14	1.48	0.27	435	152	28	5	14	0.09
<b>CAR M-14</b>	4.27	4.26	24.61	0.30	432	576	7	79	100	0.15
<b>CAR M-13</b>	0.25	0.06	0.33	0.10	441	130	39	3	24	0.15
<b>CAR M-12</b>	0.41	0.07	0.78	0.09	436	188	22	9	17	0.08
<b>CAR M-11</b>	2.15	3.46	11.91	0.26	431	554	12	46	161	0.23
<b>CAR M-9</b>	1.98	2.24	8.03	0.21	437	406	11	38	113	0.22
<b>CAR M-8</b>	1.57	0.25	2.97	0.28	433	189	18	11	16	0.08
<b>CAR M-5</b>	5.20	5.18	23.72	0.26	437	456	5	91	100	0.18
<b>CAR M-4a</b>	2.50	0.26	5.25	0.49	439	210	20	11	10	0.05
<b>CAR M-4</b>	5.58	5.81	25.92	0.23	435	465	4	113	104	0.18
<b>CAR M-3N</b>	1.72	0.43	3.90	0.20	436	227	12	20	25	0.10
<b>CAR M-3</b>	11.90	8.36	54.54	0.24	436	458	2	227	70	0.13
<b>CAR M-2</b>	6.68	5.65	29.31	0.24	437	439	4	122	85	0.16
<b>CAR M-1</b>	0.60	0.37	1.83	0.17	434	304	28	11	62	0.17



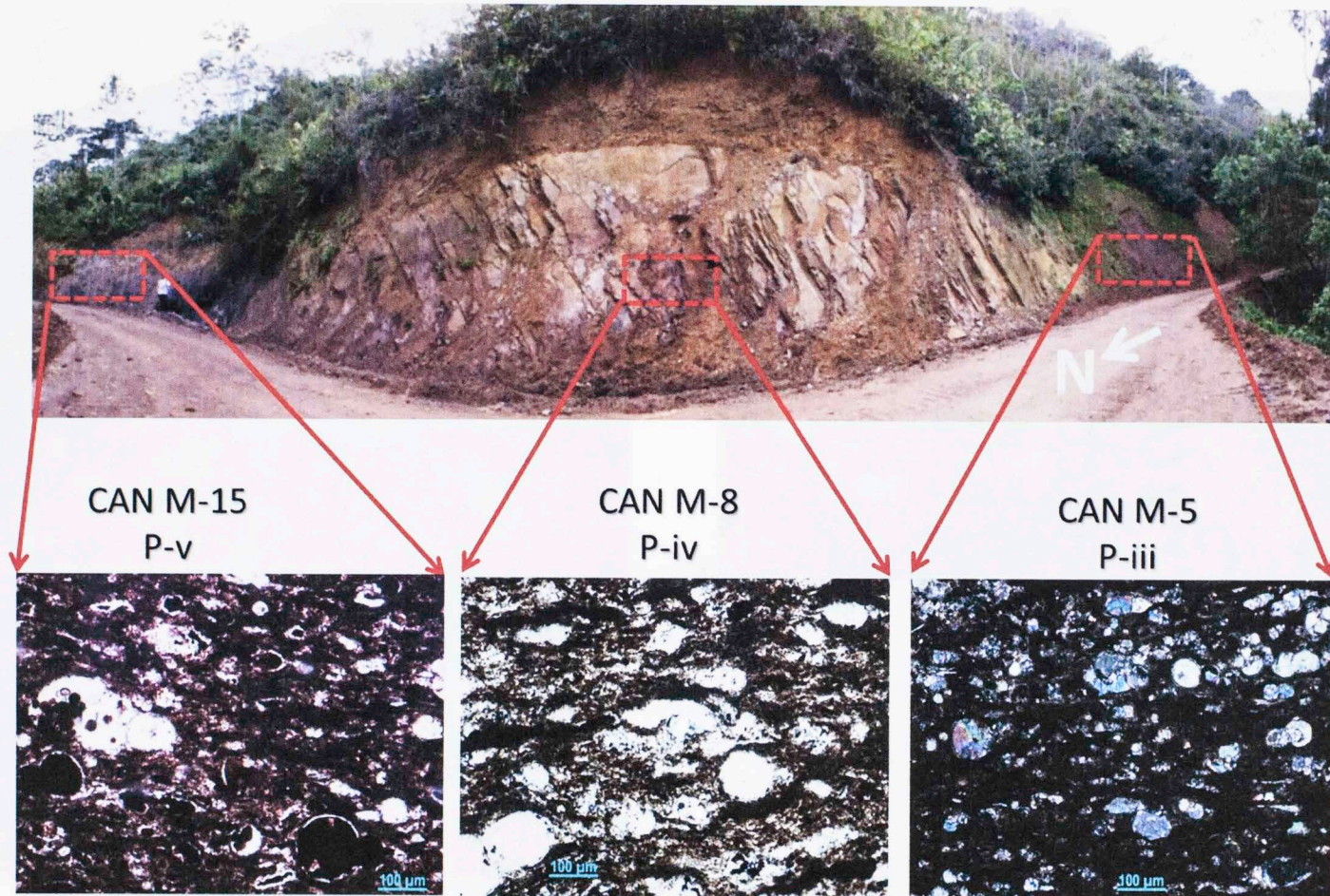
**Figure 66.** Lithological facies Salada-i. Outcrop sample and thin section in parallel nichols (parallel polarized light).





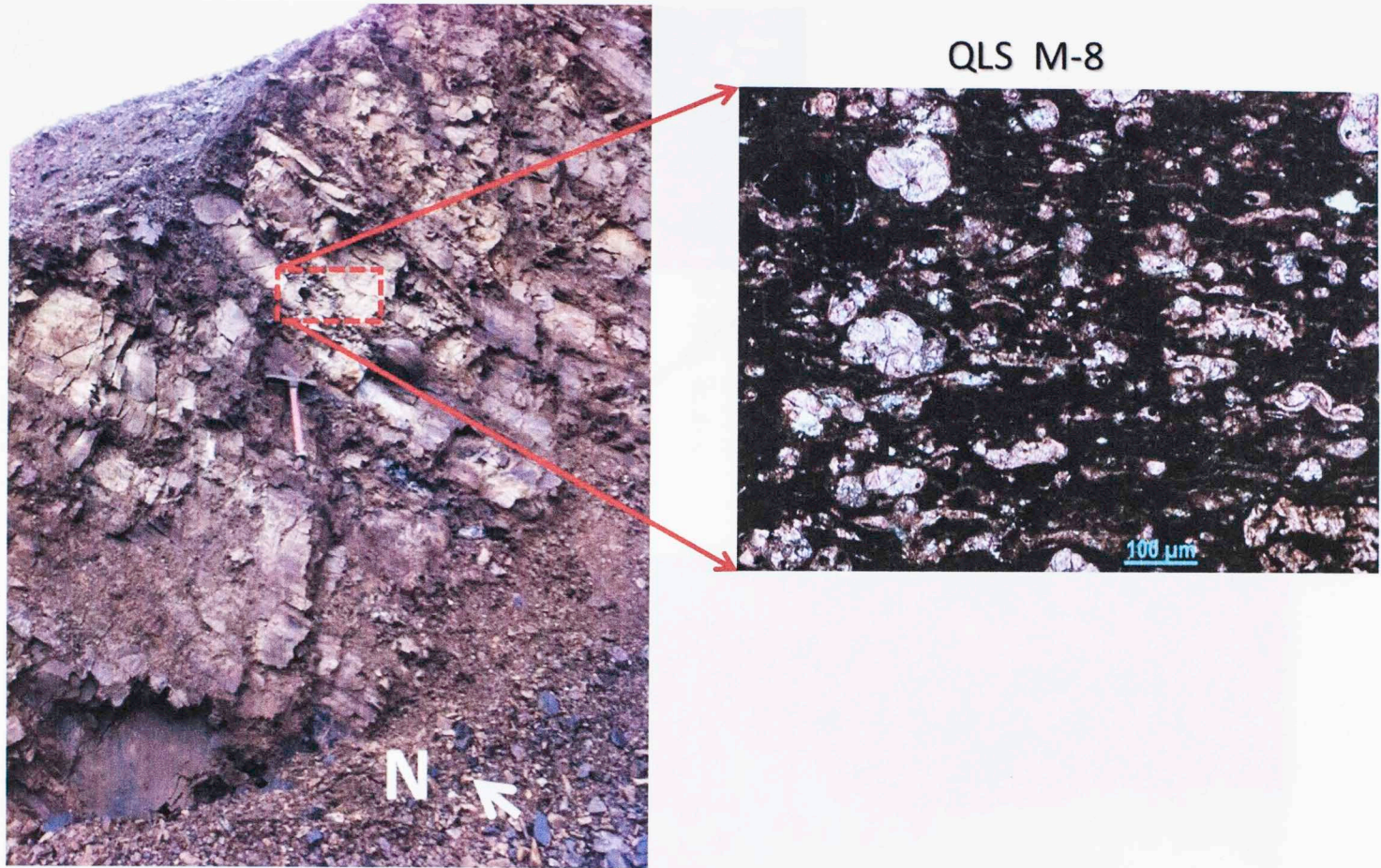
**Figure 67.** Lithological facies Salada-ii. Outcrop sample and thin section in parallel nichols (parallel polarized light).





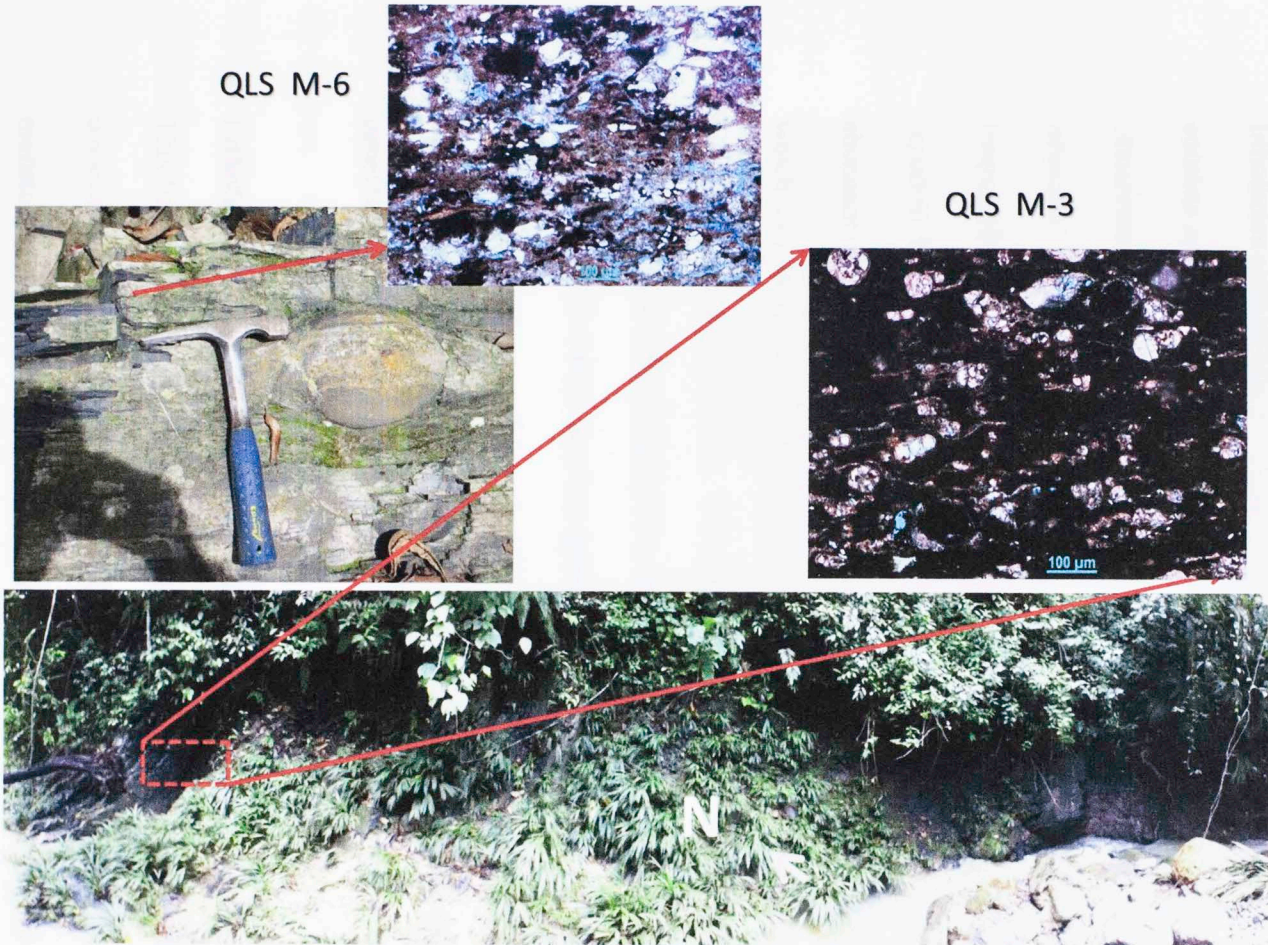
**Figure 68.** Lithological facies Pujamana iii, iv and v. Outcrop sample and thin section in parallel nichols (parallel polarized light).





**Figure 69.** Lithological facies Galembo vi. Outcrop sample and thin section in parallel nichols (parallel polarized light).





**Figure 70.** Lithological facies Galembó vii. Outcrop sample and thin section in parallel nichols (parallel polarized light).



### 3.3.1.3. Lithofacies and Organic Facies in the Galembo member.

- **Lithofacies G-vi, observed at the lower part of the Galembo member.** This lithofacies corresponds to samples QLS CHERT-BIT to QLS M-7 (Table 5). It consists of crystalline limestone intercalated with laminated packstones and calcareous black shales. These layers are from 0.5 ft. to 1 ft. thick with wavy lenticular lamination. The crystalline limestones are greenish-gray with foraminifera (Figure 69). The packstone contain some phosphorites that were reported by Zumberge (1984) and Rangel et al., (2000). There are also abundant calcite and phosphate concretions associated with upwelling effects, which can be up to 0.5 ft. in diameter. The carbonates are enriched with *Globigerina* and fecal pellets. The organic facies contains very variable TOC from 0.22% to 4.12%; HI from 97 to 439 and S2 from 0.21 to 18.10; high C<sub>30</sub> sterane index (8 -14%); very low gammacerane index, high pregnane content (0.61-0.68). These organic geochemistry parameters indicate a Type II marine anoxic, hypersaline organic matter with a very good potential for hydrocarbon generation.
- **Lithofacies G-vii, observed ath the upper part of the Galembo member.** This lithofacies corresponds to samples QLS M-6 to QLS Umir (Table 5) and consists of slightly phosphatic calcareous shales, asphaltites, finely laminated mudstones, packstones and wackestones, with foraminifera (Figure 70). The packstone contain some phosphorites that were reported by Zumberge (1984)

and Rangel et al. (2000). There are abundant calcite and phosphate concretions associated with upwelling effects, which can be up to 2 ft. in diameter. Fecal pellets and macro fossil shells, oolites and benthonic fossils are abundant. The organic facies contains variable TOC from 0.43% to 4.09%; HI from 51 to 672 and S2 from 0.45 to 20.83; high C<sub>30</sub> sterane index towards the top (10.3%), very low gammacerane index; high pregnane content towards the top (0.54). These organic geochemistry parameters indicate a Type II marine anoxic, hypersaline organic matter with a very good potential for hydrocarbon generation. The importance of fecal pellets in hydrocarbon resource shales can be found in the Appendix III.

To summarize, facies identification in the field and based on thin section analysis, provided some distinguishing characteristics. Laminations are mainly planar parallel, indicating sporadic or cyclic deposition. According to Kirkland et al. (1992) the presence of laminae in source rocks represents subtle changes in temperature, precipitation, humidity or wind intensity, reflected in the thickness and composition of the laminae. The importance of the laminae is that they record seasonal climatic changes during the extremely quiet restricted environment in which the La Luna Formation was deposited, which allowed deposition, accumulation and preservation of the organic matter. The majority of the analyzed La Luna samples in the OUTCROP B thin sections are rich in calcite.

Phosphate deposits occur in Salada and Galembo member limestones, along with coarser and more abundant calcite concretions in the Galembo member than in the Salada member. Föllmi et al. (1992) presented three possible origins for the La Luna phosphorites: 1) as pristine beds, formed due to microbial mediation mechanisms; 2) as condensed beds, composed of phosphatized fossil debris and lithoclasts and formed by winnowing of shelf units over long periods of time; 3) as allochthonous beds, composed of phosphatized and non-phosphatized particles transported as gravity flows or as admixtures within winnowed units. Föllmi et al. (1992) associated allochthonous and condensed beds with transgressive systems tracts (TST) and the basal parts of high-stand systems tracts (HST) in MMVB, where they may represent erosional lag deposits of inner to outer shelf depositional environments. The macro scale calcite and phosphate nodules appear to be allochthonous, according to the criteria of Föllmi et al. (1992) and Föllmi (1996). The phosphorite layers in the Salada and Galembo members show characteristics of being condensed types as they are micro laminated and thus possibly related to TST.

### **3.3.2. XRD Results**

The X-Ray diffraction, organic free analysis was conducted for the OUTCROP B section, which is the section that is in the oil window in terms of maturity and hence, the best for biomarker and lithofacies analysis. This stratigraphic section presents all three La Luna Formation members and according to XRD analysis results, the majority of the samples are composed mainly of calcite (>40%), and contain quartz and clay minerals. Neither dolomite nor feldspars were detected in the samples (Table 14).



**Table.14.** Semi-Quantitative mineral content from XRD analysis, La Luna formation OUTCROP B.

Sample #	Member	Depth ft.	Quartz%	Calcite%	Siderite%	Pyrite%	Illite/Mica %	Kaolinite%	Grain Density
<b>OUTCROP B</b>									
QLS M-3	Galembo	51	98	2	0	0	0	0	2.65
QLS M-6	Galembo	85	47	46	0	1	7	0	2.70
QLS M-7	Galembo	102	46	46	0	1	8	0	2.70
CAN M-15	Pujamana	221	93	7	0	0	0	0	2.65
CAN M-8	Pujamana	425	63	0	1	1	32	3	2.70
CAN M-5	Pujamana	578	16	82	0	0	2	0	2.70
CAR M-13	Salada	732	10	90	0	0	0	0	2.70
CAR M-5	Salada	862	55	42	0	1	3	0	2.69
CAR M-4	Salada	914	48	41	0	1	10	0	2.72
CAR M-3	Salada	966	64	19	0	1	17	0	2.72

The XRD results are the first to be published for the La Luna Formation and indicate possible accumulations of detrital silica and calcite deposition related with possible coastal upwelling or thermal water column stratification (planktonic forams, high gammacerane index and high pregnane content from biomarkers).

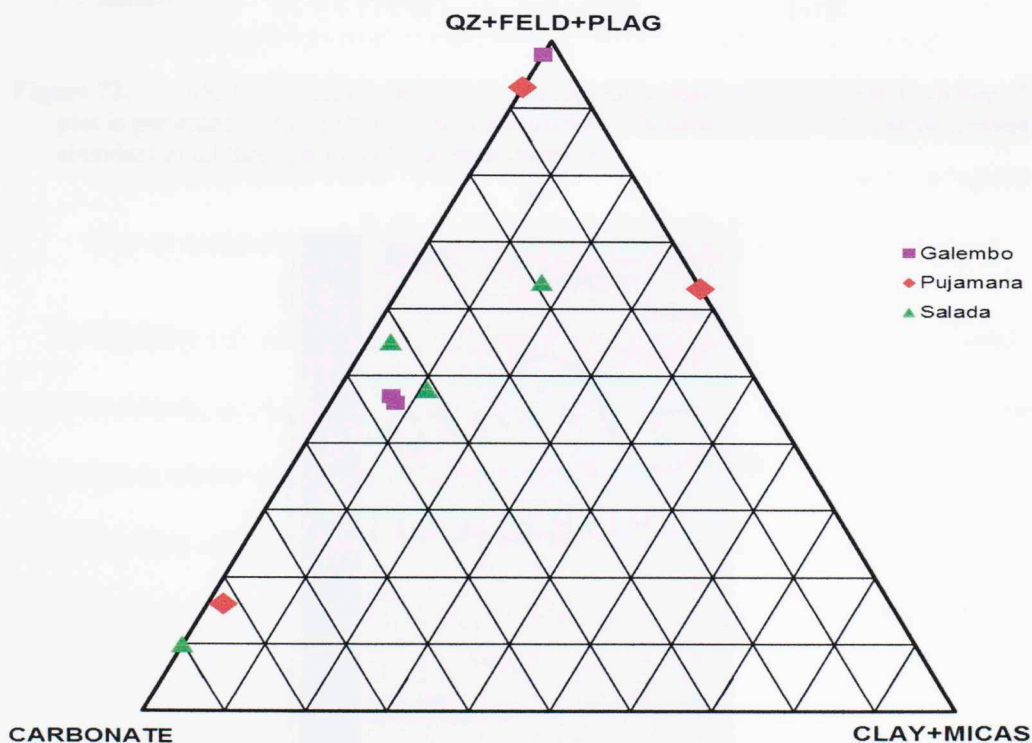
Four of the La Luna samples contain high percentages of quartz: (i) the Galembó top sample QLS-M-3 corresponds to a black shale (98% Qtz); (ii) the CAN M-15 (93% Qtz) corresponds to a Pujamana black shale; (iii) the CAN M-8 Pujamana siliceous mudstone with bentonites (63% Qtz); and (iv) the CAR M-3 Salada Black calcareous shale (64% Qtz). Figure 71 shows a ternary plot from the XRD analyses. Figure 72 shows mineralogy variation with stratigraphic depth of the OUTCROP B section. As can be observed, the majority of the samples are rich in calcite and a few are rich in quartz.

The clay minerals content in the La Luna samples is higher for the argillaceous rocks in the Salada and Pujamana members, suggesting that some detrital components were not abundant during most of the La Luna deposition. These results agree with the interpretations of Zumberge (1984), Rangel et al. (2000) and Carvajal (2004), which suggest a minimum terrestrial clastic sediment input during La Luna deposition, and are also corroborated by the biomarker analyses section of this study.

According to Jarvie et al. (2007), the Brittleness Index (BI), is one of the important parameters for screening shale-gas systems, as a function of mineral composition and

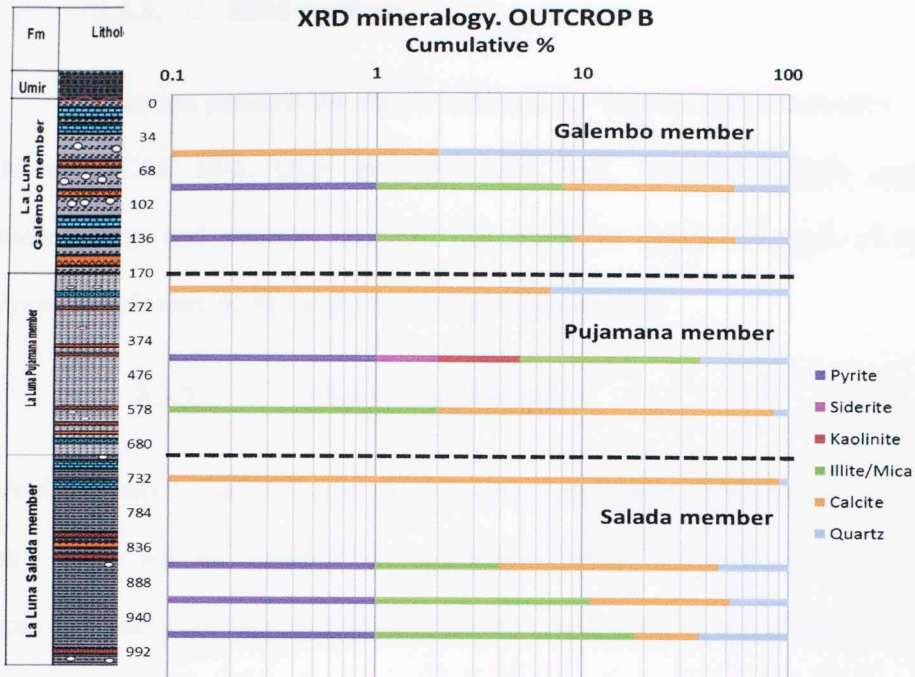
diagenesis. According to Wang and Gale (2009), in addition to mineral composition, brittleness is a function of diagenesis caused by changes in temperature and fluid composition related to tectonic setting and burial history, %Ro, etc. For shale-gas systems, %Ro, reflecting maximum paleo-temperature, is one of the commonly available data related to diagenesis. In order to identify the brittle-ductile couples of the La Luna Formation OUTCROP B, the Brittleness Index is calculated using Jarvie et al. (2007) equation, and the results are shown in figure 73:

$$BI = \frac{Quartz}{Quartz+Calcite+Clay+TOC} \quad \text{Jarvie et al. (2007)}$$

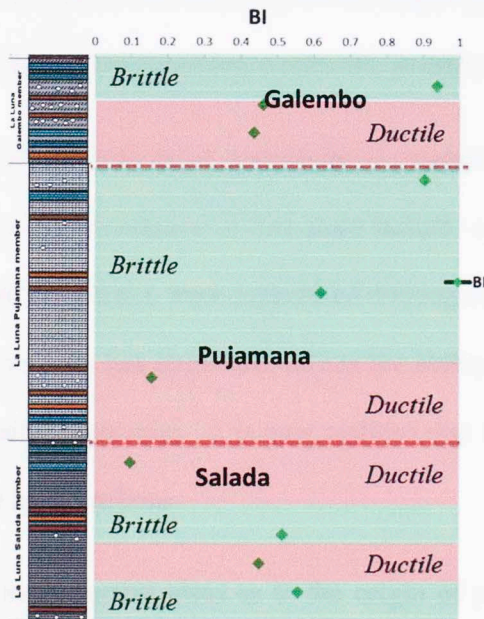


**Figure 71.** Ternary plot from XRD analysis of La Luna Formation OUTCROP B samples.





**Figure 72.** XRD mineralogy variation vs. stratigraphic depth of OUTCROP B section. The plot is presented in logarithmic scale for cumulative mineral content. The calcite content is abundant in all three La Luna Formation members.



**Figure 73.** Brittleness Index (BI) for OUTCROP B section.

### **3.3.3. SEM Analysis.**

This section presents the results obtained for four La Luna Formation samples, CAR M-3, CAR M-5, QLS M-8 and QLS M-3. Analyses include microfabric characterization and porosity analysis. The complete results for each of the SEM analyzed samples are in Appendix II SEM porosity section.

#### **3.3.3.1. Pore Classification**







A pore is any volume of open space within a rock into which gases and liquids can occur. Pores are the result of the sedimentary fabric not fitting perfectly together (Figure 74). There are two main types of porosity, true porosity and effective porosity.

- True porosity is the total volume of pore space contained within a rock.
- Effective porosity is the total volume of space contained within a rock which is connected to other pores, thus allowing for the transmission of gases or liquids (i.e. an isolated pore is not considered effective porosity).








As thinking has shifted from what constitutes a reservoir rock (conventional vs unconventional), so has the importance of fine scale (micro- and nano-meter) porosity. In years past, shales and carbonates were considered nothing more than potential source rocks; however, as technology has improved, so has the ability to extract hydrocarbons from these “poor porosity” reservoirs. It is now realized that fine scale pores in shales can contain extractable hydrocarbons.

There are two main current ideas as to the origin of porosity within shales: 1) that the only porosity contained within shales is “organoporosity”, which is porosity

found within organic matter contained in the shale (Jarvie et al., 2007); and 2) that along with “organoporosity” there exists microfabric porosity which is generated from the flocculation of clays, fossil fragments, intraparticle pores, interparticle pores, microchannels and micro-fractures (O’Brien and Slatt, 1990; Slatt and O’Brien, 2011) (Figure 74).

Pore Type	Image	Distinctive Features
Porous floccules		Clumps of electrostatically charged clay flakes arranged in edge-face or edge-to-edge cardhouse structure. Pores up to tens of micrometers in diameter. Pores may be connected.
Organopores		Pores in smooth surfaces of organic flakes or kerogen. Pore diameters are at nanometer scale. Pores are generally isolated. Porous organic coatings can also be adsorbed on clays.
Fecal pellets		Spheres and ellipsoids with randomly oriented internal particles, giving rise to intrapellet pores. Pellets are sand size and may be aligned into laminae.
Fossil fragments		Porous fossil particles, including sponge spicules, radiolaria, and spores ( <i>Tasmanites?</i> ). Interior chamber may be open or filled with detrital or authigenic minerals.
Intraparticle grains/pores		Porous grains, such as pyrite framboids that have internal pores between microcrystals. Grains are of secondary origin and are usually dispersed within the shale matrix.
Microchannels and microfractures		Linear nanometer to micrometer size openings that often crosscut bedding planes. Occur at nanometer and larger scales.

**Symbols used:**

 Clay flake	 Organic particle	 Silt grain
 Fossil fragment	 Gas	 Gas migration
 Microchannel/microfracture		

**Figure 74.** Pore classification for shales recognized under SEM analysis. Slatt and O’Brien (2011).



### 3.3.3.2. SEM microfabric and porosity characterization

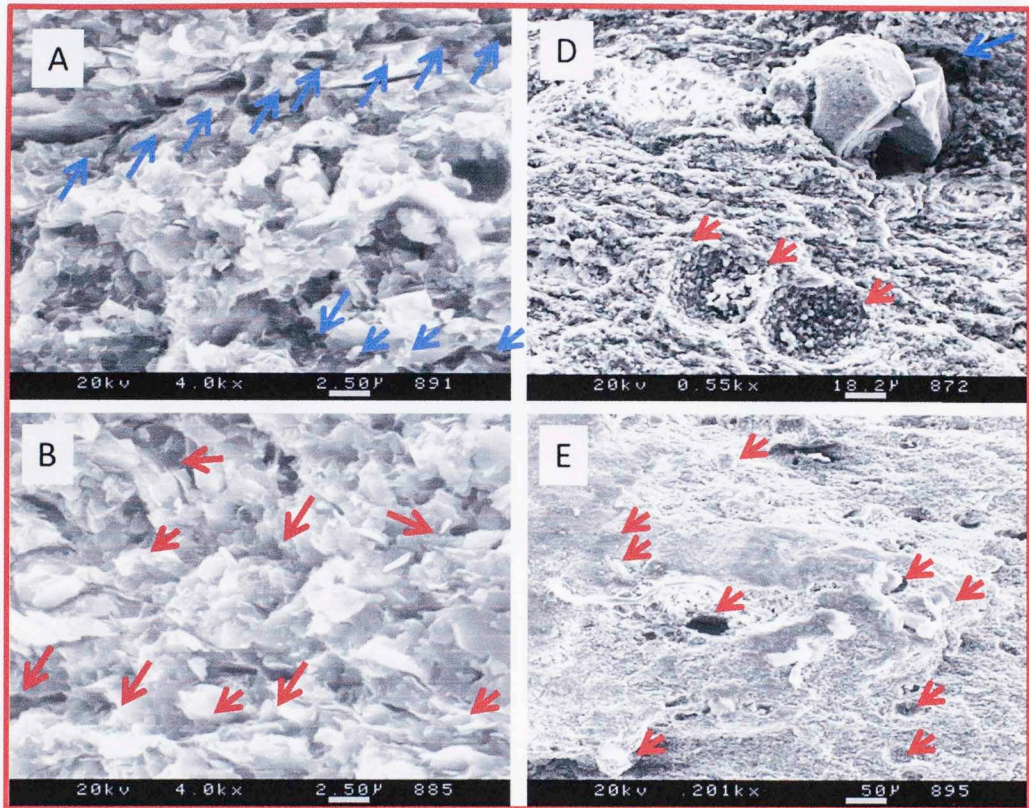
#### Salada Member, OUTCROP B.

Within the lower La Luna interval, two samples were analyzed using the SEM technique. Two lithofacies represented in this set are: *S-i Salada base*, and *S-ii Salada middle and top*. The Salada unit is a calcite-rich interval with abundant planktonic foraminifera (*Globigerina*) and clay floccules. Some of the samples show abundant pore types in different forms such as porous floccules, intraparticle porosity and microchannels. Figure 75 shows the SEM images of Sample CAR M-3 and Figure 77 corresponds to CAR M-5. For each sample 10 images were obtained for each sample top, front and side. The 10 images per sample face were obtained in order to get a representative analysis of the microfabric type.

Based on SEM observation, two microfabric types were identified within the samples: 1) *organic hash*: composed dominantly of organic particles preferentially oriented with platy minerals and with diffuse particle edges (O'Brien and Slatt, 1990; Figures 75 and 76); and 2) *organic clayey*: composed dominantly of well defined minerals shapes, more visible, with abundant calcite minerals and minor quartz grains (O'Brien and Slatt, 1990; Figures 78 and 79).

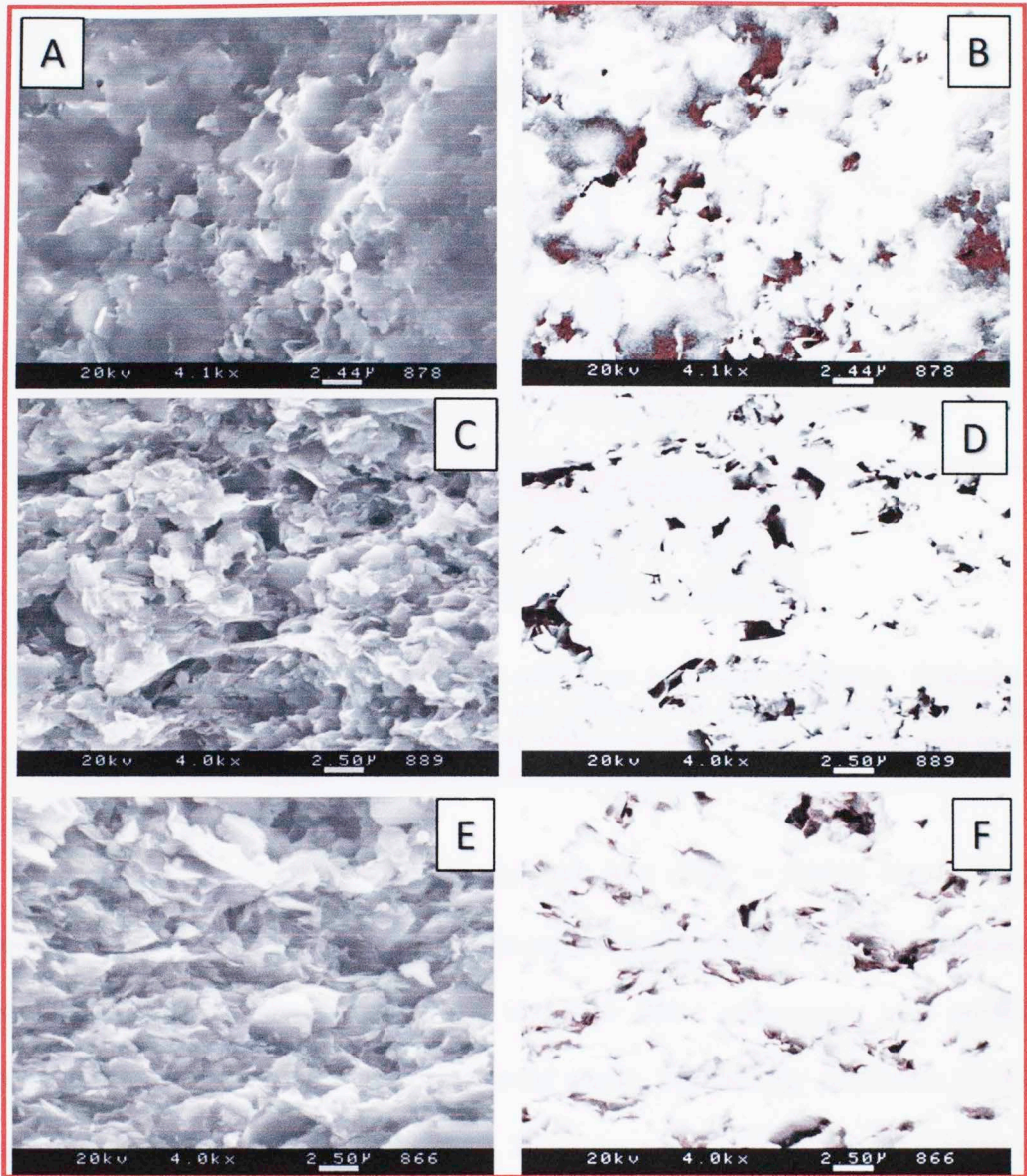
The associated porosity for CAR M-3 (TOC = 11.90%; Figures 75 and 76) sample is mainly clay-floccule porosity and microchannel porosity. Clay flakes appear to have been deposited as hemipelagic rain (flat stacking of clay flakes) or clay floccules which were compressed after deposition. Clay floccules and micro-channels represent the majority of pore space. The porosity calculation is illustrated on Figures

76 and 77. The average total porosity for the top of the sample is 2.53%; for the side of the sample is 2.75%; for the front part of the sample is 4.99%. 70.85% of the average nanopores length are less than  $1 \mu\text{m}^2$  and 29.45% are higher than  $1 \mu\text{m}^2$  (Figure 77).



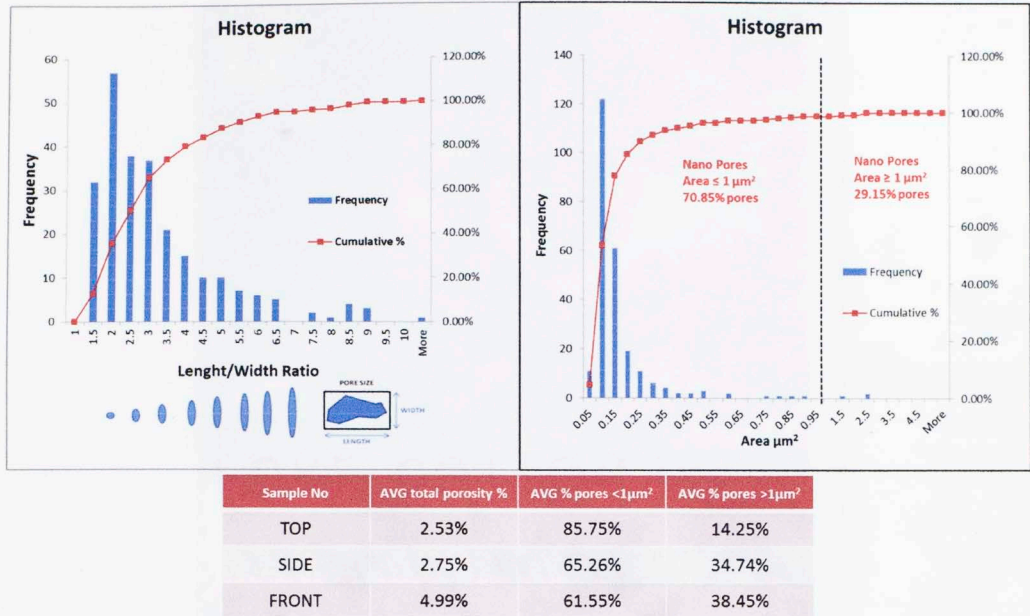
**Figure 75.** SEM analysis of sample CAR M-3 corresponding to lithofacies S-i. Image A (4,000X) presents clay floccules and micro channel porosity indicated by blue arrow. Image B (4,000X) shows clay floccules with clay floccule porosity indicated by the red arrows. Image D (550X) show calcite interparticle porosity indicated by red arrows and *Globigerina* replacement with calcite indicated by blue arrow. Image E (200X) presents abundant fecal pellets (red arrows). Clay flakes show more of a flocculated fabric; clay floccules contain the dominate pore type. TOC% = 11.90.





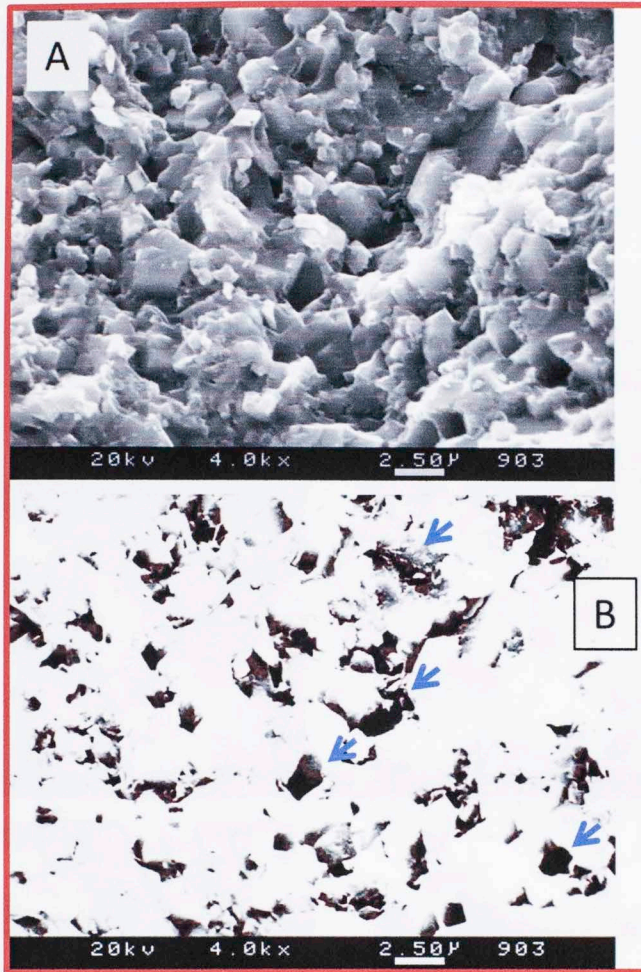
**Figure 76.** Calculation of total porosity for sample CAR M-3, all images are at 4,000X magnification. Images correspond to: A- Top of the sample; B- Top pore distribution; C- Side part of the sample; D- Side pore distribution; E- Front part of the sample; F-Front pore distribution.





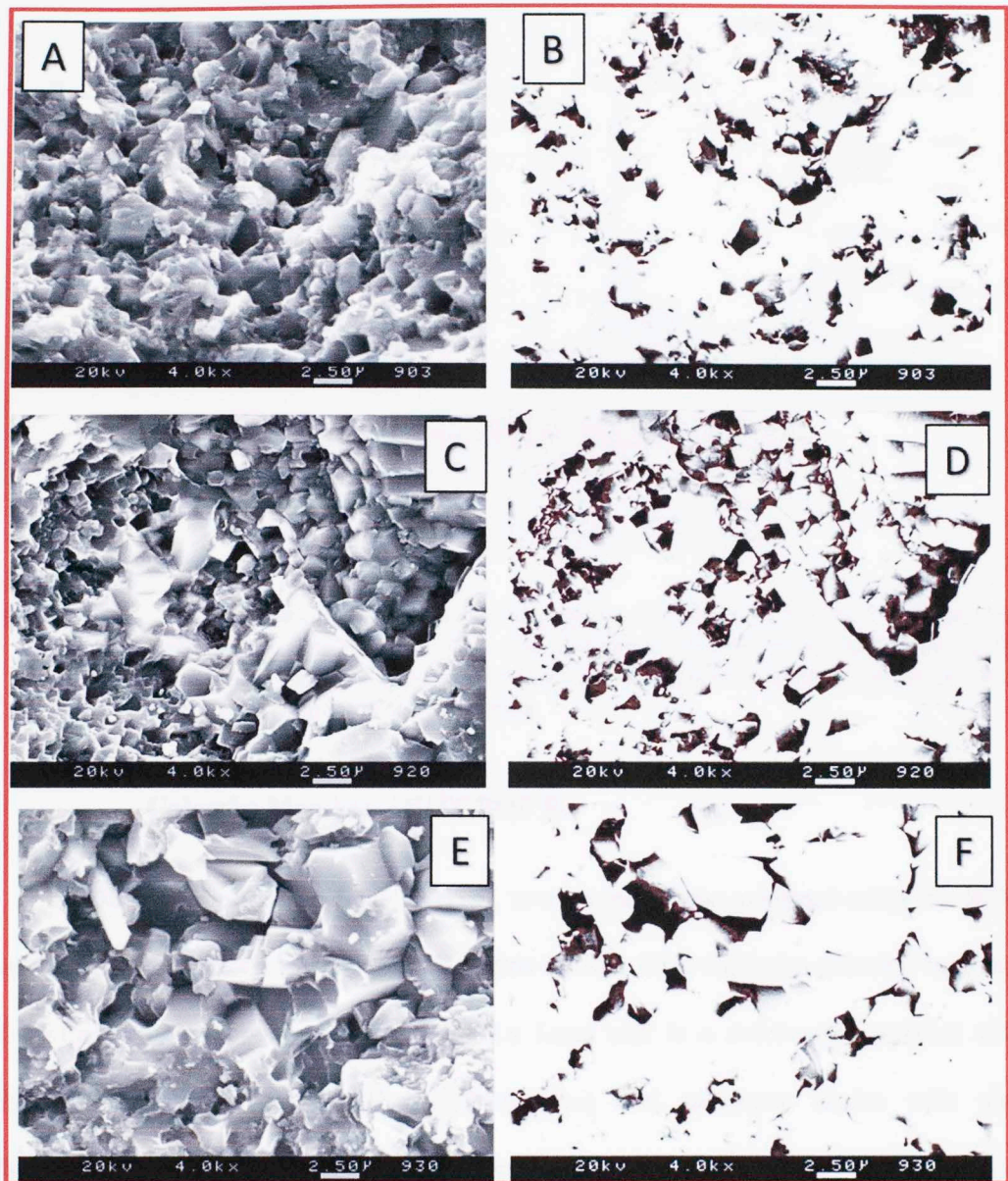
**Figure 77.** Total porosity calculation and histograms for sample CAR M-3. Histograms provide average pore length/width ratio and histogram of pore area distribution in the microbric are given. Table of average total porosity of the top, side and front parts of the sample with their respective average pore area distributions.

The associated porosity for sample CAR M-5 (TOC = 5.90%; Figure 78) is mainly interparticle porosity with abundant calcite content. Clay flakes are not present or are very low in abundance, so the identified fabric corresponds to a micritic Packstone. The quartz in the matrix is detrital quartz. The porosity calculation for this sample is illustrated on Figures 79 and 80. The average total porosity for the top part of the sample is 8.11%; for the side part of the sample is 12.30%; for the front part of the sample is 6.92%. 53.11% of the average nanopores length are less than  $1 \mu\text{m}^2$  and 46.89% are higher than  $1 \mu\text{m}^2$  (Figure 80).



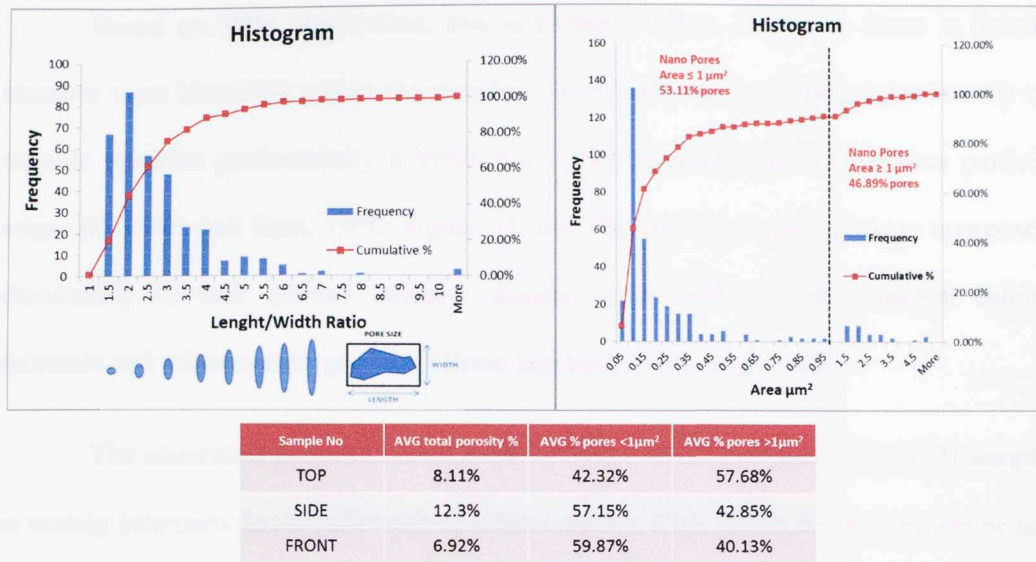
**Figure 78.** SEM analysis of sample CAR M-5 corresponding to lithofacies S-ii. Image A (4,000X) shows abundant calcite. The prominent porosity is interparticle porosity. Image B (4,000X) shows the calculation of the interparticle porosity by highlighting the pore areas (blue arrow). Average porosity 8.11%; the average number of measured pores is 658; the average pore area is  $0.083 \mu\text{m}^2$ ; TOC = 5.90%.





**Figure 79.** Calculation of total porosity for sample CAR M-5, all images are at 4,000X magnification. Images correspond to: A- Top of the sample; B- Top pore distribution; C- Side part of the sample; D- Side pore distribution; E- Front part of the sample; F-Front pore distribution.





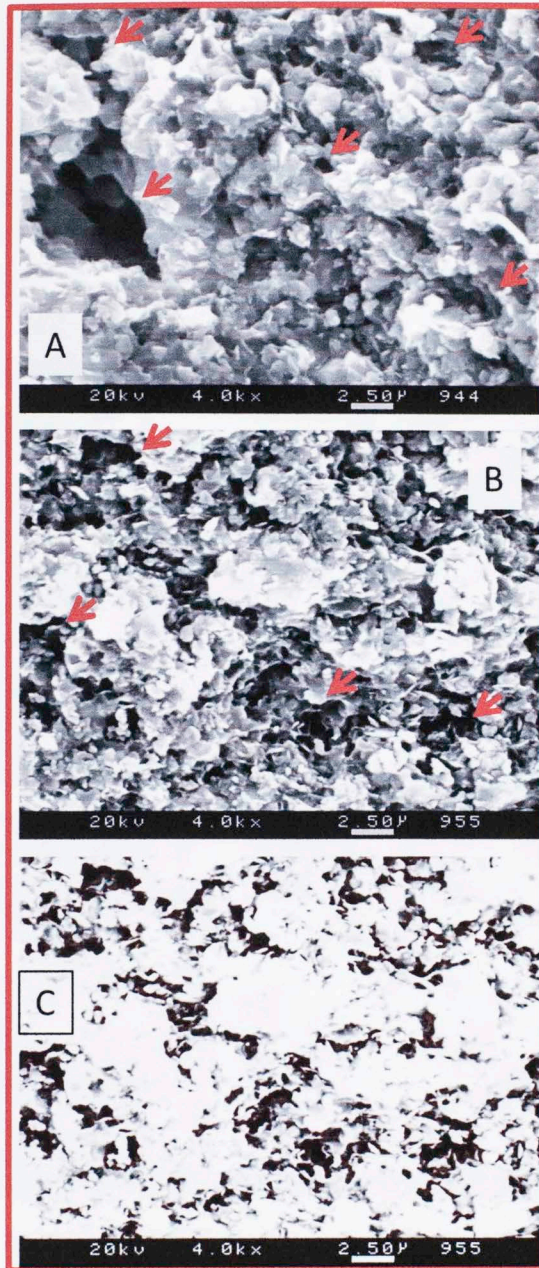
**Figure 80.** Total porosity calculation and histograms for sample CAR M-5. Histograms provide average pore length/width ratio and histogram of pore area distribution in the microbric. Table of average total porosity of the top, side and front parts of the sample with their respective average pore area distribution.

### Galemba Member, OUTCROP B.

Within the upper La Luna interval, two samples were analyzed using the SEM technique. Two lithofacies represented in this set are: *G-vi* Galemba member base and *S-vii* Galemba member top. The upper La Luna unit is a calcite-rich interval with abundant planktonic foraminifera (*Globigerina*) and carbonate shales with clay floccules. Some of the samples show abundant pore types in different forms such as porous floccules, calcite framboids, intraparticle porosity and micro-channels. Figure 77 shows the SEM of sample QLS M-8 and Figure 78 corresponds to QLS M-3. For each sample 10 images were obtained for the top, front and side of the sample. The 10 images per sample face were obtained in order to get a representative analysis of the microfabric type.

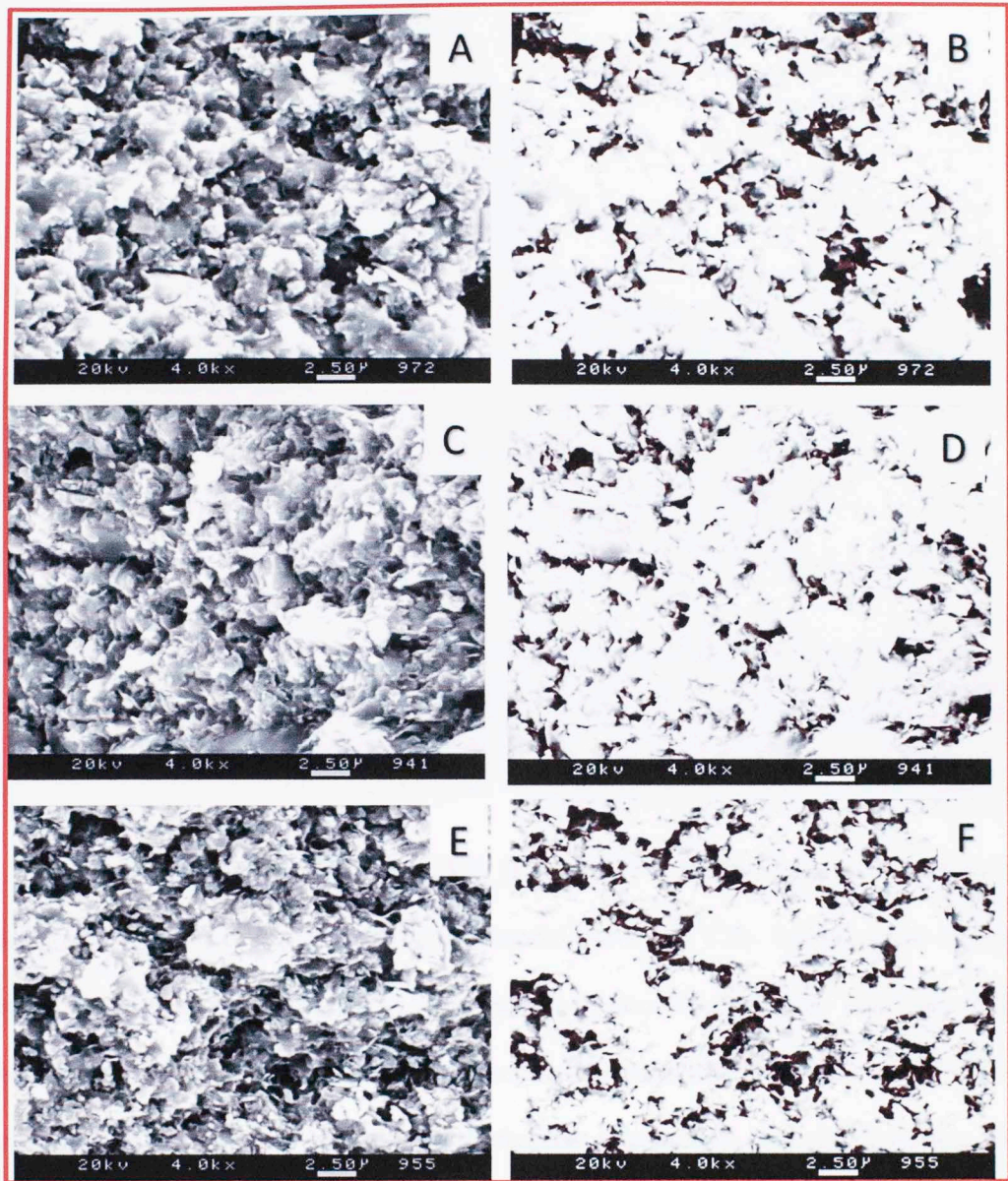
Based on SEM observation, two microfabric types, similar to those in Salada member were identified within the samples: 1) *organic hash*: composed dominantly of organic particles preferentially oriented with platy minerals and with diffuse particle edges (O'Brien and Slatt, 1990; Figure 81 and 82); and 2) *organic clayey*: composed dominantly of well defined minerals shapes, more visible, with abundant calcite minerals and minor quartz grains (O'Brien and Slatt, 1990; Figure 84).

The associated porosity for QLS M-8 (TOC = 4.12%; Figure 81 and 82) sample is mainly interparticle porosity with abundant calcite. Clay flakes are not present or are rare. The identified fabric corresponds to a micritic packstone. The porosity calculation is illustrated on Figures 82 and 83. The average total porosity for the top part of the sample is 6.74%; for the side part of the sample is 6.02%; for the front part of the sample is 8.49%. 62.60% of the average nanopores lengths are less than 1  $\mu\text{m}$  and 38.40% are higher than 1  $\mu\text{m}$  (Figure 83).

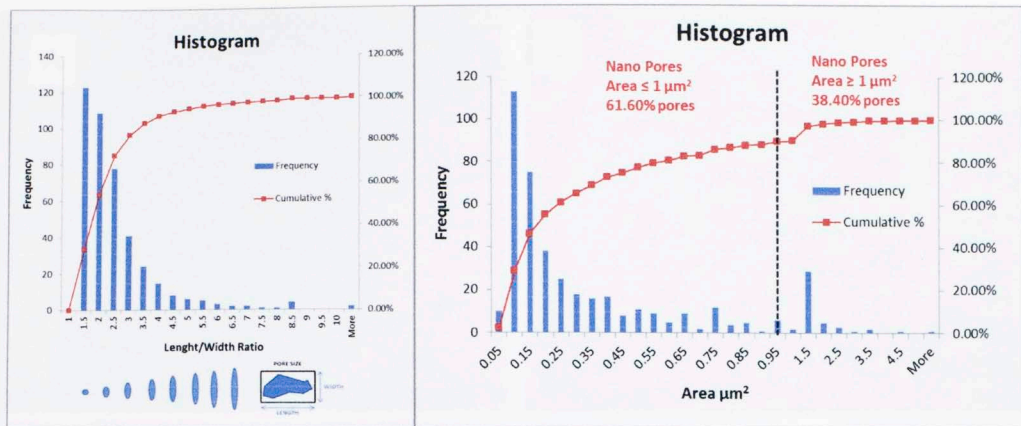


**Figure 81.** SEM analysis of sample QLS M-8 corresponding to lithofacies G-vi. Image A and B (4,000X) show abundant calcite content. The principal porosity is interparticle porosity (red arrows). Image C (4,000X) shows the image of the rendered pores. The average total porosity is 8.49%; number of counted pores 580; the average pore area is  $0.099 \mu\text{m}^2$ . TOC = 4.12 %.





**Figure 82.** Calculations of total porosity for sample QLS M-8, all images are at 4,000X magnification. Images correspond to: A- Top of the sample; B- Top pore distribution; C- Side part of the sample; D- Side pore distribution; E- Front part of the sample; F-Front pore distribution.

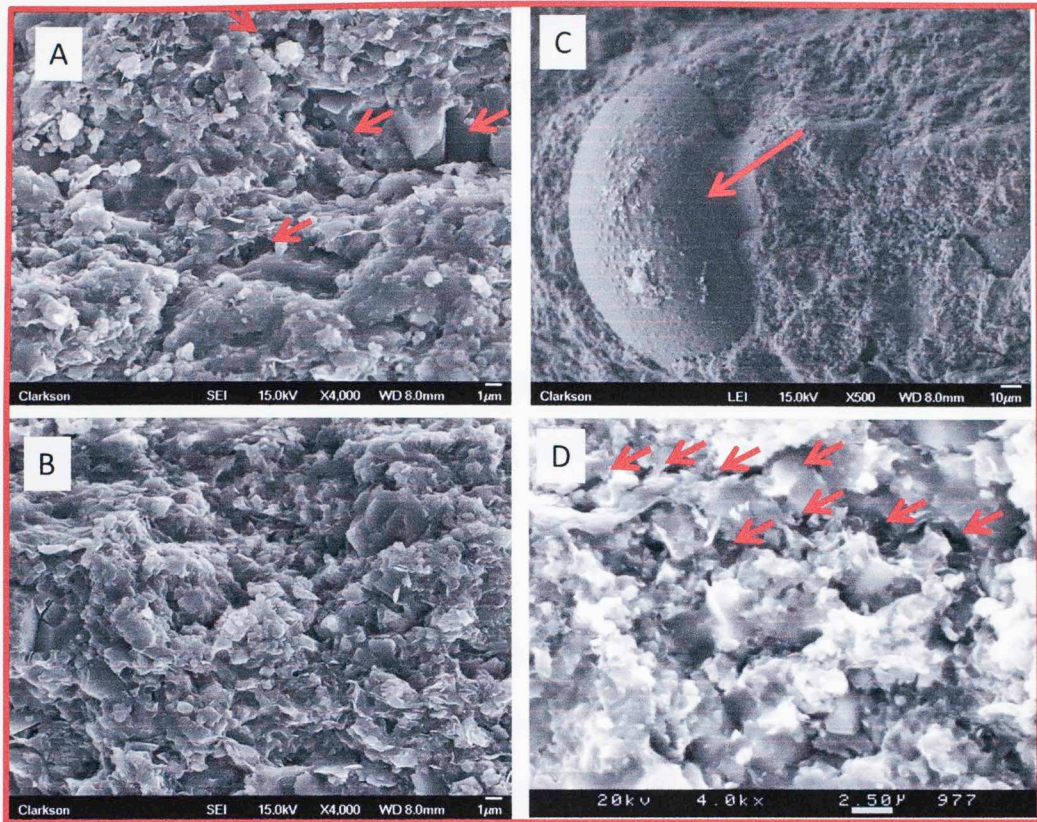


Sample No	AVG total porosity %	AVG % pores <1μm <sup>2</sup>	AVG % pores >1μm <sup>2</sup>
TOP	6.74%	57.98%	42.02%
SIDE	6.02%	65.26%	34.74%
FRONT	8.49%	61.55%	38.45%

**Figure 83.** Total porosity calculation and histograms for sample QLS M-8. Histograms of average pore length/with ratio and histogram of pore area distribution in the microbric. Table of average total porosity of the top, side and front parts of the sample with their respective average pore area distribution.

The associated porosity for QLS M-3 (TOC = 4.09%; Figure 84) sample is mainly clay-floccule porosity and microchannel porosity. Clay flakes appear to have been deposited as hemipelagic rain (flat stacking of clay flakes) or clay floccules which were compressed after deposition. The moderately preferred orientation of clay flakes contains a mixture of clay and silt; micro-channel, interparticle, and clay floccules. The quartz in the matrix is detrital quartz.





**Figure 84.** SEM analysis of sample QLS M-3 corresponding to lithofacies G-vii. Image A (4,000X) presents clay floccules and interparticle porosity indicated by the red arrow. Image B (4,000X) shows clay floccules with open microchannel pores. Image C (550X) show *Globigerina* shell replacement with calcite indicated by red arrow. Image D (4,000X) presents clay floccule and open microchannel pores indicated by the red arrows. Clay flakes show more of a flocculated fabric; clay floccules are the dominate pore type. TOC% = 4.09.

### Salada Member, OUTCROP A.

Within the Salada member of Outcrop A, two samples were analyzed using the SEM technique, porosity types were identified but not quantified as it was on OUTCROP B. The two lithofacies represented in this set are: calcite-rich shales and micritic mudstones (limestones). Some of the samples show abundant pore types in



different forms such as porous floccules, intraparticle porosity and weakly oriented microchannels. Figure 85 shows the SEM of sample P4M2 and Figure 86 corresponds to Salada-1. Based on SEM observations, the principal microfabric type identified within the samples is organic clayey, with well defined mineral edges and abundant calcite grains.

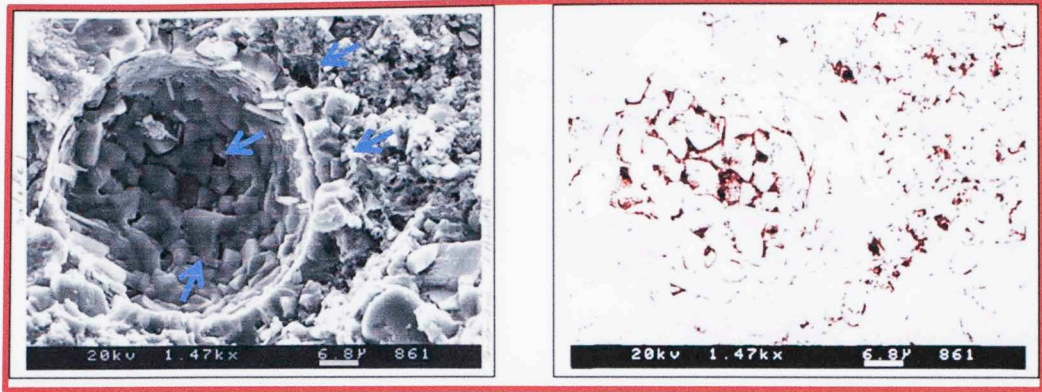
The associated porosity for Salada-1 (TOC = 3.25%; Figure 86) sample is mainly clay-floccule porosity and not very well oriented microchannel porosity. Also porosity is associated with the presence of fecal pellets. Clay flakes appear to have been deposited as hemipelagic rain (flat stacking of clay flakes) or clay floccules which were compressed after deposition. Interparticle pores and micro-channels represent the majority of pore space. The associated porosity for P4M2 (TOC = 10.60%; Figure 85) sample is mainly interparticle porosity with abundant calcite. Clay flakes are also present. The identified fabric corresponds to a micritic mudstone. The quartz content in the matrix corresponds to detrital quartz. The maturity values are beyond the gas generation window for both samples.

#### **Galembo Member. OUTCROP A.**

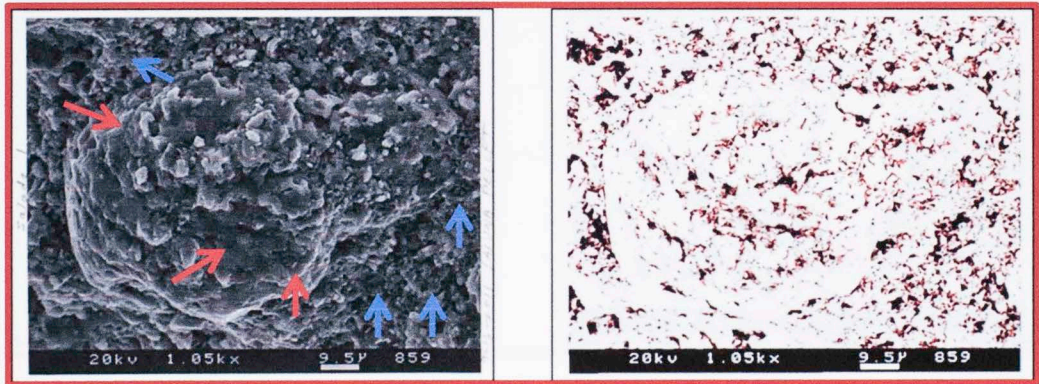
For the Galembo member of OUTCROP A, two samples were analyzed using the SEM technique. Porosity types were identified but not quantified as was the case on OUTCROP B. Two lithofacies represented in this set are: calcite-rich shales and micritic packstones. There are no observed planktonic foraminifera (*Globigerina*) as is the case with OUTCROP B Galembo samples. But there are abundant clay floccules in the shale sample. As with the Salada member, there are abundant pore types in different

forms such as porous floccules, interparticle porosity, intra and inter pellet porosity, and weakly oriented microchannels. Figure 87 shows the SEM of Sample P2M1 and Figure 88 corresponds to P4M3. Based on SEM observation, the principal microfabric types identified within the samples is organic clayey, with well defined mineral edges and abundant calcite grains.

The associated porosity for P4M3 (TOC = 11.90%; Figure 88) sample is mainly clay-floccule porosity and microchannel porosity. Clay flakes appear to have been deposited as hemipelagic rain (flat stacking of clay flakes) or clay floccules which were compressed after deposition. There is also detrital quartz within the microfabric of allochthonous grains. Interparticle pores and weakly oriented micro-channels represent the majority of pore space (blue arrow). The associated porosity for P2M1 (TOC = 1.51%; Figure 87) is mainly interparticle porosity with abundant calcite grains. Clay flakes are also present with floccule porosity (red arrows in Figure 87). The identified lithofacies corresponds to a micritic packstone. The quartz in the matrix is detrital. The maturity values are beyond the gas generation window for both samples.



**Figure 85.** SEM analysis of sample P4M2 corresponding to micritic mudstone. Image at 1,470X shows interparticle porosity indicated by blue arrow. The left image shows the organic clayey microfabric with interparticle porosity and the right image shows the total associated porosity by highlighting the pore spaces. TOC% = 10.60%.

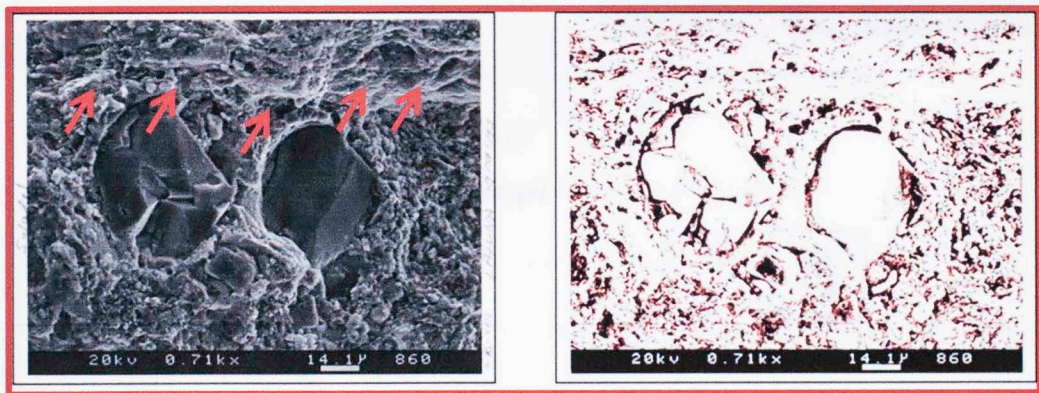


**Figure 86.** SEM analysis of sample Salada-1 corresponding to a carbonate shale. Image on the left has 1,050X of magnification and shows clay floccule porosity indicated by blue arrow, the red arrow indicates a fecal pellet and some associated intra and inter pellet porosity. The right image shows the total associated porosity by highlighting the pore spaces. TOC% = 3.25%.





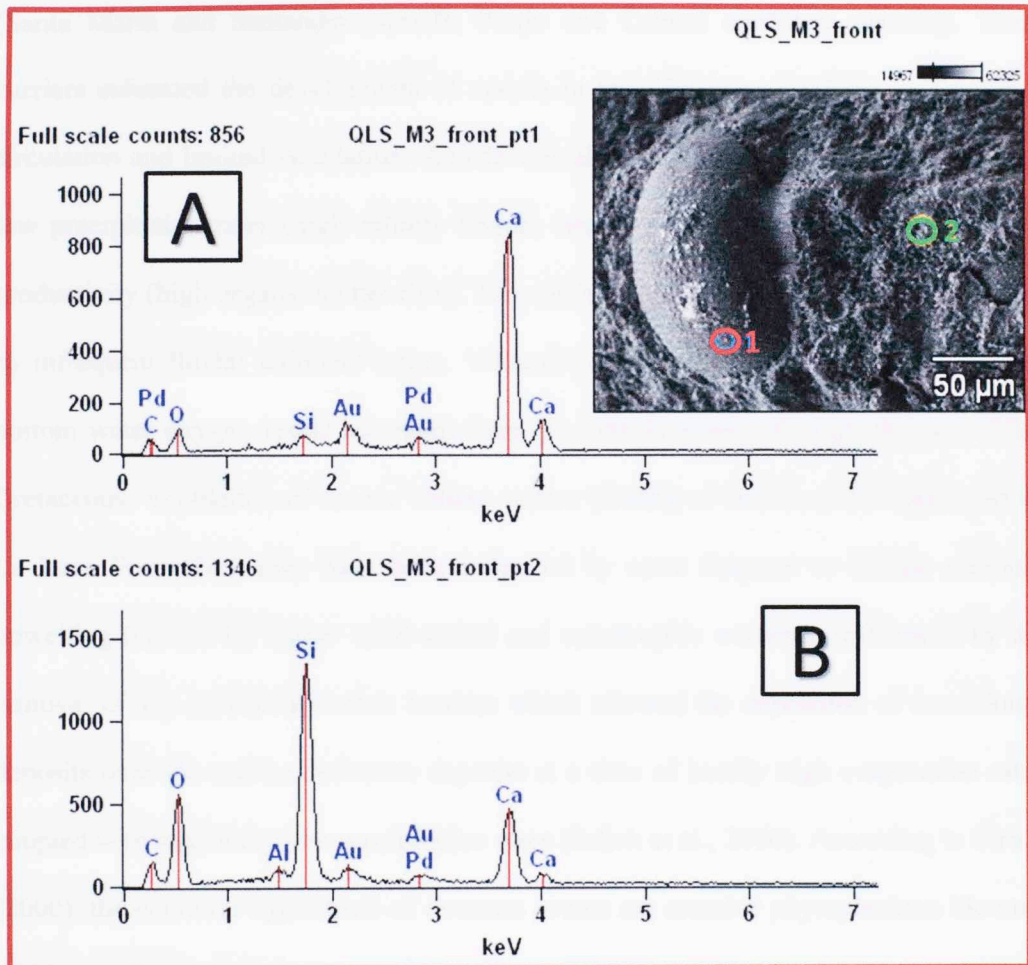
**Figure 87.** SEM analysis of sample P2M1 corresponding to micritic Packstone. Image on the right is at 4,100X of magnification and shows interparticle porosity indicated by red arrows. The image on the right shows the total associated porosity by highlighting the pore spaces. TOC% = 1.51%.



**Figure 88.** SEM analysis of sample P4M3 corresponding to carbonate shale. Image on the left has 710X of magnification and shows clay floccule porosity and weakly oriented micro channel porosity indicated by red arrow. Quartz clasts are abundant. Image on the right shows the total associated porosity by highlighting the pore spaces. TOC% = 11.90%.

In order to identify the details of mineral components for the microfabric features, an additional Energy-Dispersive X-Ray analysis (EDX) was made for OUTCROP B sample QLSM-3 with the help of Dr. Neil O'Brien at the State University of New York, Potsdam. The results determined that the composition of the analyzed microfabric features correspond to quartz and calcite (Figure 89). A possible interpretation for the

Galebo member is that foraminifer's shells (*Globigerina*) were deposited in a quiet environment and were replaced by calcite. As shown in Figure 83b, the quartz content is also present as the component of the microfabric.



**Figure 89.** EDX results of OUTCROP B QLS M-3 sample, showing the calcite composition of the foraminifera structures (83a) in the circle 1, and calcite and quartz composition of the microfabric (83b) in the circle 2 of the image.



### **3.4. Paleoenvironmental Interpretation**

The deposition of organic carbon rich intervals of the La Luna Formation members in MMVB was governed by the development of key paleobathymetric barriers (Santa Marta and Santander massifs, Perija and Central cordillera massifs). These barriers enhanced the development of anoxia in the "La Luna Sea" by causing poor circulation and limited ventilation. Anoxia was also promoted by high evaporation and low precipitation rates (high salinity bottom water), and high levels of marine algal productivity (high organic matter flux). The nutrient supply could have been augmented by infrequent fluvial sediment influx. Villamil (1999) and Elrich (2000) reported that bottom water oxygen levels increased from the Late Santonian through the end of the Cretaceous. Ventilation of anoxic bottom waters (ending of anoxia at the upper part of La Luna Formation) may have been enhanced by more frequent or intense seasonal upwelling (caused by higher wind stress) and catastrophic overturn, influenced by the removal of key paleobathymetric barriers which allowed the deposition of transitional deposits over the marine carbonate deposits at a time of locally high evaporation rates coupled with regionally low precipitation rates (Elrich et al., 2000). According to Elrich (2000), the common byproducts of overturn events are massive phytoplankton blooms, which produce "red tides". During upper Cretaceous time, increasing ventilation, combined with siliciclastic dilution, ultimately produced sediments with lower TOC content.

The current stratigraphic framework of the La Luna Formation extends from upper Cenomanian to upper Campanian with duration of about 20 million years. The La



Luna Formation was deposited in mid-shelf to upper-slope environments on the Late Cretaceous passive continental margin of northern South America (Macellari and De Vries, 1987; Erlich et al., 2000). Laminated organic carbon rich intervals in the La Luna Formation suggest deposition in highly dysoxic or anoxic environments. The Pujamana member of the formation was probably deposited in persistent upwelling conditions on the basis of common chert and phosphorite (Macellari and De Vries, 1987). The remainder of the La Luna Formation was likely deposited under more normal conditions, except during global anoxic events at the Cenomanian/Turonian boundary and in the Coniacian–Santonian.

Variations related to depositional environments and type of organic matter within the different La Luna Formation members are also summarized with the biomarker ratios presented in Figure 56 and 63.  $C_{30}$  sterane/ $C_{29}$  sterane, hopane/sterane,  $C_{23}$  tricyclic/ $C_{30}$  hopane ratios indicate that the La Luna Formation members are characterized by a mix of terrestrial and marine organic matter, where the lower and upper members show the greatest marine input. Based on biomarker ratios and facies association, the upper member is characterized by anoxic/suboxic conditions. The lower Salada member shows a predominance of euxinic/anoxic conditions, the middle Pujamana member is more suboxic with terrestrial input. The presence of gammacerane and pregnanes indicate that high water salinity and water density stratification prevailed during most of La Luna Formation deposition, especially for the lower and upper members which show higher gammacerane index values and higher pregnane presence. These observations suggest that deposition of the lower Salada member was

characterized by higher organic productivity and preservation, where the chemocline was located at shallower depths into the photic zone, within an inner shelf-slope depositional environment. On the contrary, during deposition of the middle Pujamana and upper Galembo members, sea-level fluctuations produced an intermittent depth-change of the chemocline resulting in a probable episodic euxinia, where oxidative periods degraded part of the organic matter. It is clear that the La Luna Formation deposition was influenced by sea-level changes, which in turn affected redox conditions and the extent of anoxia. These variations had a direct effect on the type and amount of organic matter that accumulated and was preserved within the sediments to give the present day organic richness of the La Luna Formation members in MMVB. A method that could significantly contribute to a complete and further understanding of these paleogeographic interpretations is a more detailed integration and correlation within a sequence stratigraphic framework, an approach that has succeeded in other shale gas plays (Singh, 2008; Slatt et al., 2011a).

### **3.5. Sequence Stratigraphy Interpretation**

An attempt has been made to establish sea-level changes during La Luna deposition based on a geochemical parameter called Relative Hydrocarbon Potential (RHP; Fang et al., 1993). These observations are also correlated with lithostratigraphic, regressive-transgressive cycles and the sequence stratigraphic framework of the La Luna Formation defined by previous authors (Garner, 1926; Hubach, 1957; Morales, 1958; Zumberge, 1984; Rangel et al., 2000). RHP is a geochemical parameter derived from Rock Eval pyrolysis data ( $(S_1+S_2)/TOC$ ) to characterize depositional environments

and their temporal variations (Fang et al., 1993; Singh, 2008; Miceli-Romero, 2010; Slatt et al., 2010). Fang et al. (1993) were the first to use this parameter to define vertical organic facies changes called Vertical Organic Facies Sequence (VOFS). Based on RHP they established two main VOFS, rising-upward and falling-upward VOFS. Rising-upward VOFS represents a vertically upward change in organic facies from hydrogen-poor to hydrogen-rich going up the stratigraphic sequence; it indicates a change from oxic to anoxic conditions (relative sea-level rise) where more of the organic matter is preserved. On the contrary, a falling-upward VOFS represents a vertical change in organic facies from hydrogen-rich to hydrogen-poor, thus this VOFS indicates a change from anoxic to oxic conditions (relative sea-level fall) where less organic matter is preserved. From this, definitions of regressive-transgressive cycles can be applied to sequence stratigraphy.

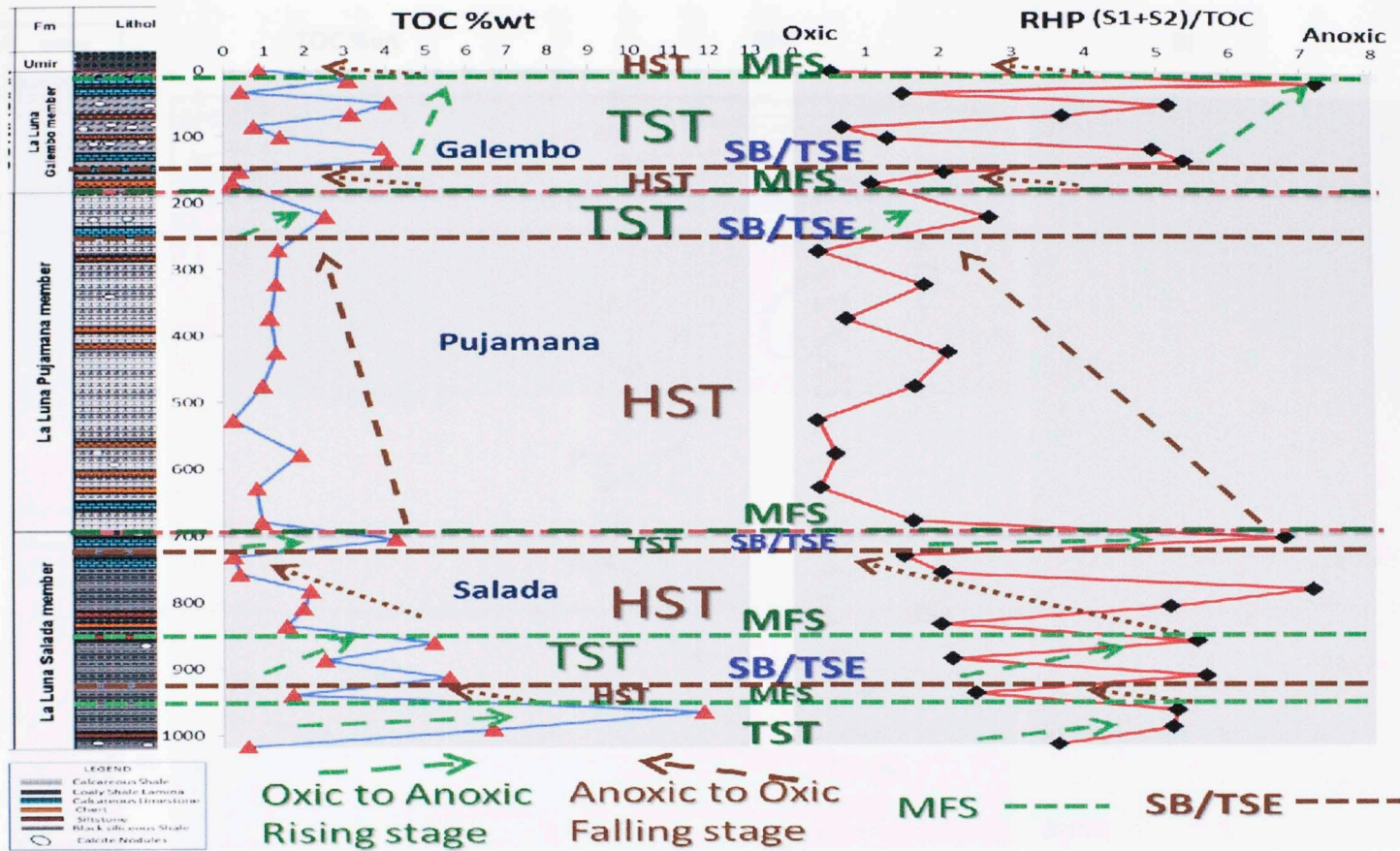
RHP analysis in the OUTCROP B section revealed four major third order stratigraphic cycles (from 1 to 10 My in duration) in the La Luna Formation (Figure 90). Based upon the sampled stratigraphic intervals, these variations in the RHP curve indicate several cycles of transgression and regression that positively correlate with the proposed transgressive-regressive cycles from the TOC curve (Figure 90).

The base of the lower Salada member is characterized by a major transgression and deposition of Transgressive System Tract (TST) and the first Maximum Flooding Surface (MFS). This TST is followed by small regression-transgression fluctuation which is part of a Highstand System Tract (HST) also occurring in the lower part of the Salada member, which ended with a sequence boundary and a possible transgressive



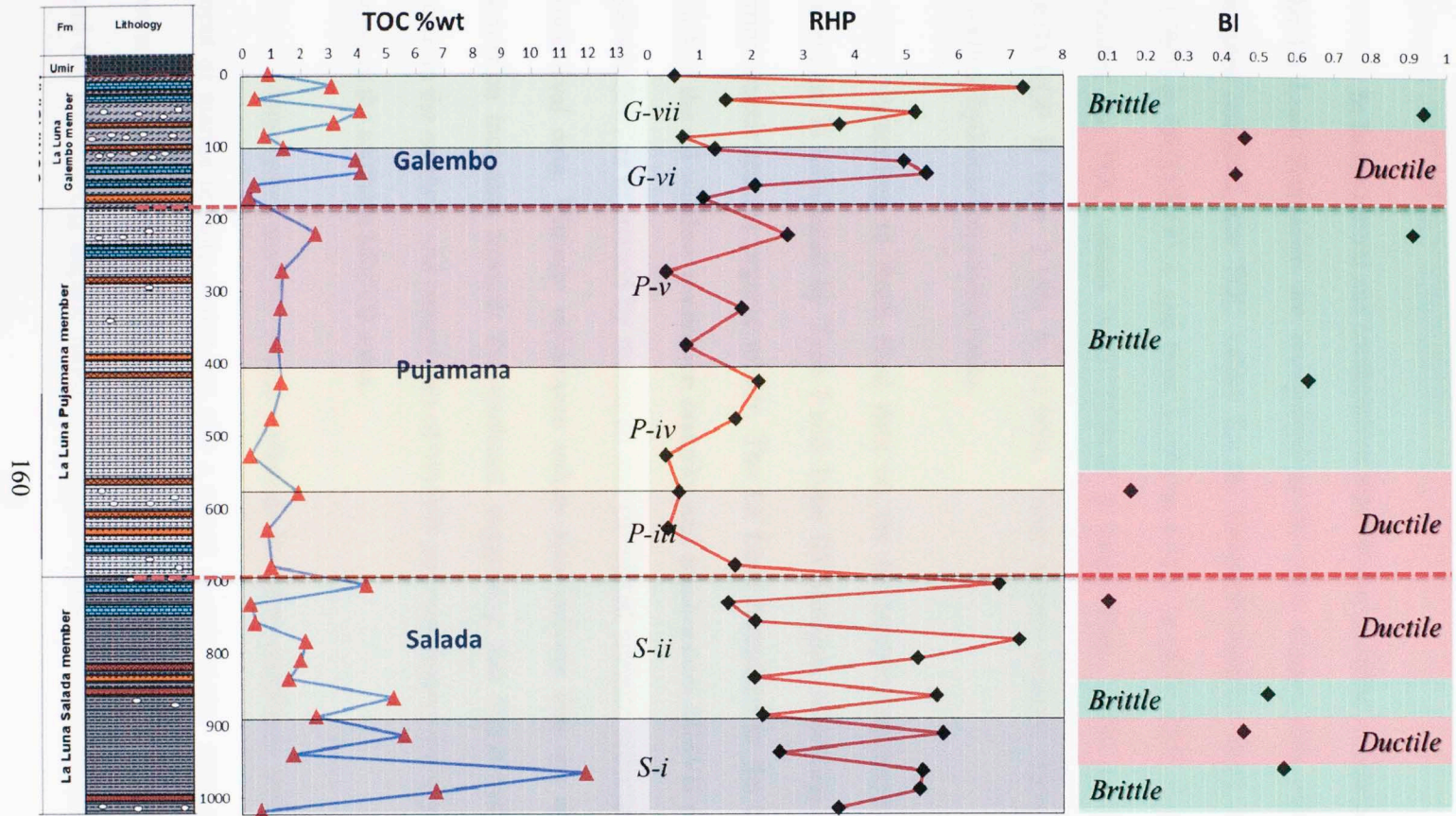
surface of erosion (TSE). The middle part of the Salada member is a TST deposit with a second MFS. The upper part is a HST, above which is a second sequence boundary and TSE. The top of the Salada member is a TST and third MFS (Figure 90). Coinciding with the sequence stratigraphic framework proposed by Rangel et al. (2000), the Salada-Pujamana contact is a MFS. A major regression (HST) is proposed for much of the Pujamana member as observed on the RHP graph (Figure 90). The upper part of the Pujamana member is a TST-HST deposit capped by a third sequence boundary and possible TSE. The Pujamana – Galembo member boundary corresponds a fourth MFS which is overlain by a thin HST, which marks the basal part of the Galembo member. A fourth sequence boundary then is present which is overlain by a TST and fifth MFS in the upper part of the Galembo member. This Galembo member TST is possibly followed by deposition of a minor HST in the top of the Galembo member. This minor HST at the top of the La Luna Formation is proposed as the Upper Cretaceous onset of progradational deposits, which consequently led to the deposition of the Umir Formation transitional aerobic deposits (fine sandstone and coaly shales) that created an erosional unconformity above the La Luna Formation. Hence, it is expected to find that the redox conditions were suboxic/anoxic during sediment deposition of the Galembo member, whereas the end of anoxia and salinity stratification starting at the La Luna Formation top was very likely caused primarily by changes in local/regional wind and rainfall patterns due to changes in paleotopography and paleoclimate and by the loss of key paleobathymetric barriers (erosion and/or uplifts), where cooler, fresher and oxygenated waters filled the basin and formed the progradational strata.

The association of RHP curve, lithofacies and Brittleness Index ( $BI = \frac{Qz}{Qz+Clays+Calcite+TOC}$ ; Jarvie et al., 2007) is illustrated in Figure 91. For the Salada member, the brittle intervals are associated with the carbonate layers, and the ductile intervals to the calcareous shales; for the Pujamana member the brittleness is associated with the siliceous deposits, cherts, siliceous shales, phosphates, bentonites and claystones, The ductile intervals are associated with the calcareous and clay rich shales. For the Galembo member the brittle intervals are associated with the micritic limestone layers, and the ductile intervals to the calcareous shales.



**Figure 90.** Sequence stratigraphy cycles of the La Luna Formation based on TOC and relative hydrocarbon potential (RHP) vs depth for OUTCROP B section (HST, highstand systems tract; TST, transgressive systems tract, oxic to anoxic deposition; MFS, maximum flooding surface; SB/TSE, Sequence boundary and transgressive surface of erosion).





**Figure 91.** TOC, relative hydrocarbon potential (RHP) and Brittleness Index (BI) variation with depth for OUTCROP B section, showing the facies association with the regressive-transgressive cycles and brittle-ductile couplets. BI=  $Qz/Qz+Clays+Calcite+TOC$  (Jarvie et al., 2007).

## CONCLUSIONS. UNCONVENTIONAL ASSESMENT.

In In the central and southeastern MMVB the Galemba and Salada members of the La Luna Formation are recognized as the most organic-rich units. For the 66 samples analyzed, the TOC values for the Galemba member range from 1.09% to 11.90% in OUTCROP A and from 3.10% to 4.12% in OUTCROP B. For the Salada member the TOC values in OUTCROP A range from 2.70% to 10.60% and in OUTCROP B from 2.15% to 11.90%. These values indicate these members are excellent hydrocarbon source rocks.

According to Rock Eval data on the 66 samples analyzed, the La Luna Formation is dominated by Type I and Type IIS kerogen, indicating an oil and gas prone anoxic marine organic matter. The La Luna formation in the central MMVB reached the oil window generation maturity and southeastern MMVB reached the dry gas window, as expressed by measured and calculated vitrinite reflectance values and Rock Eval data. Vitrinite reflectance values also indicate that the maturity of this formation increases towards the southeast, suggesting that liquid hydrocarbons will occur in the northern and central part of MMVB and condensates and dry/wet gases will occur in the southern MMVB areas.

Biomarker analyses reveal variations in redox conditions and a predominant input of marine organic matter, but also a mixed organic matter input was recognized towards the contact with the Pujamana member.  $C_{30}$  sterane/ $C_{29}$  sterane, hopane/sterane, and  $C_{23}$  tricyclic/ $C_{30}$  hopane ratios, all suggest a predominance of anoxic conditions



during deposition of the Galembó and Salada members. The presence of pregnanes and gammacerane indicate higher salinity on the organic matter input along the MMVB areas. Biodegradation was recognized by the removal of n-alkanes and isoprenoids, affecting also the tricyclic and hopane terpanes, but not affecting the steranes. This alteration is very likely to be caused by the weathering of fresh water washings in the surface outcrop samples.

Integration and correlation of biomarker ratios, lithofacies and relative hydrocarbon potential (RHP) indicate that the La Luna Formation was deposited under dysoxic/anoxic conditions and episodic periods of photic zone anoxia (PZA) during major transgressive-regressive cycles. The Salada member was deposited under anoxic hypersaline conditions and persistent PZA during two major transgressions (sea-level rise); The middle Pujamana member was deposited under transition of sea level falls, with more suboxic characteristics. The upper Galembó member was deposited mainly under suboxic/anoxic conditions and episodic PZA during a general TST towards the La Luna top.

High salinity conditions and water density stratification also prevailed during deposition of the Salada and Galembó members. The chemocline was located at shallower depths during Salada deposition and fluctuated within different depths during deposition of the Pujamana (more transitional, regressive) and Galembó members.

The Reservoir characterization allowed the identification of carbonates and shaly lithofacies for the Galembó and the Salada members, and transitional lithofacies for the Pujamana member. The mineral content in the Salada member corresponds to a



mix of quartz and calcite, the Galembo is more carbonate rich, and the Pujamana is richer in silicates, clays and micas. The organic rich deposits in the Salada member are related to shales rich in calcite intercalated with layers of dark limestones. This may indicate a possible brittleness associated with the layering where brittle-ductile couplets might be associated. The Galembo member is a richer carbonate lithofacies, which might be related to more brittle intervals.

The SEM analysis permitted the identification of two major microfabric types in the Salada and Galembo member according to the O'Brien and Slatt (1990) classification: 1) *organic hash*: composed dominantly of organic particles preferentially oriented with platy minerals and with diffuse particle edges; and 2) *organic clayey*: composed dominantly of well defined calcite mineral shapes, which are more visible, where quartz grains are a minor component. The porosity types associated with the Salada and Galembo members are porous floccules, interparticle porosity, fecal pellet inter and intra particle porosity, and microchannels. The Galembo member analyzed samples present an average total porosity of 8.5% with average pore area of  $0.099 \mu\text{m}^2$ , and the Salada member averages SEM total porosity of 8.11% with average pore area of  $0.083 \mu\text{m}^2$ .

The RHP parameter constitutes a valuable parameter for evaluating sea-level changes that can be linked to regressive-transgressive cycles and consequently to temporal variations in depositional environments. Correlation of this parameter to biomarker parameters and geological data was effective for establishing four major third order stratigraphic cycles in the OUTCROP B section corresponding to the three

La Luna Formation members deposition events. The base of the lower Salada member is characterized by a major transgression and the deposition of the first MFS, followed by a HST with regression-transgression fluctuations at the middle part of the Salada member, which ended with the first sequence boundary and first Transgressive Surface of Erosion (TSE). This sequence boundary is followed by another TST and second MFS at the Salada member middle part. A second HST and second sequence boundary TSE occurs in the upper part of the Salada member which top corresponds to a TST. The Salada - Pujamana member boundary is interpreted as a third MFS. The Pujamana member deposition was interpreted in the lower middle part of this member as a HST and towards Pujamana member upper part it has been proposed as a TST (third sequence boundary and subsequent third TSE). The observed Pujamana – Galembo boundary corresponds to a fourth MFS and the deposition of the Galembo member starts with a HST and is followed by general transgression with some fluctuations, which indicates that deposition of the Galembo member occurred during a TST phase. A fifth MFS is proposed at the top of The La Luna Formation.

As described before, the biomarker analysis and reservoir characterization for the La Luna Formation in MMVB permitted identification of the Salada and Galembo members as good candidates for an unconventional shale gas play. Both members were deposited and buried under favorable conditions for hydrocarbon generation and storage, therefore these can be considered as separate operational units, with thicknesses in outcrop from 180 ft. to 720 ft. for the Galembo member and thickness from 300 ft. to 400 ft for the Salada member. The transitional Pujamana member (~500ft. thickness) may be a lithological barrier.

## RECOMMENDED FUTURE WORK

1. Perform additional geochemical and reservoir properties analysis on a larger suite of samples in MMVB, particularly to core samples in order to have a larger dataset with neither weathering nor biodegradation effects.
2. Correlate the different identified organic facies of the La Luna Formation with subsurface data, which can be mapped and utilized for defining areas of economic potential.
3. Evaluate the distribution of the different La Luna members across MMVB based on additional log measurements from wells and outcrops to understand their extent and thickness variations, which was not addressed in this study due to the lack of subsurface information.
4. Assess the organic matter variations (terrestrial versus marine) and lithofacies variations within the individual La Luna Formation members in order to determine lateral changes across the MMVB.
5. Develop a sequence stratigraphic framework for the La Luna Formation in MMVB through the integration of outcrop and subsurface geological and geochemical data as has been performed with similar shale-gas plays elsewhere.
6. Expand the use of the relative hydrocarbon potential (RHP) and different biomarker parameters as geochemical tools for paleo-environmental studies that allow defining TST, HST and LST of shale gas/ shale oil systems.



## BIBLIOGRAPHY

- A Acosta, J., Graham, R.H., 2003. Structural interpretation and source rock maturation modeling along two distinct transects in the Upper/Middle Magdalena basin, Colombia. *Memorias del VIII Simposio Bolivariano de Exploración en Cuencas Subandinas*, pp 135.
- Agencia Nacional de Hidrocarburos, ANH., 2008. Colombian Sedimentary Basins: Nomenclature, boundaries and petroleum geology, a new proposal. pp. 92.
- Albaghdady, A., 2013. Organic geochemical characterization of source rocks (Sirt Shale) and crude oils from central Sirt basin, Lybia. Ph.D. Thesis, The University of Oklahoma, pp. 259.
- Aquino-Neto, F.R., Trendel, J.M., Restle, A., Albrecht, P., Connan, J., 1983. Occurrence and formation of tricyclic and tetracyclic terpanes in sediments and petroleum. In *Advances in Organic Geochemistry 1981* Bjoroy M. et al. ed, Wiley, Chichester, p. 659-667.
- Bayona, G., Garcia, D., Mora, G., 1994. La formación Saldaña: Producto de la actividad de estratovolcanes continentales en un dominio de retroarco *Estudios Geológicos del Valle superior del Magdalena, Capitulo 1*. Universidad Nacional de Colombia – Ecopetrol S.A. Bogotá, pp. 21.
- Carvajal, H., 2004. Nuevas consideraciones acerca del estado de madurez termal de la Formación La Luna en el Valle Medio del Magdalena, Colombia. B.Sc. Tesis, Universidad Industrial de Santander, Colombia, p. 106.

- Cediel F. (1968): El Grupo Girón: una molasa mesozoica de la Cordillera Oriental. Servicio Geológico Nacional (Colombia). Boletín Geológico. v. XVI, p. 5-96.
- Chosson, P., Connan, J., Dessort, D., Lanau, C., 1992. In vitro biodegradation of steranes and terpanes: a clue to understanding geological situations. In: Moldowan, J.M., Albrecht, P., Philp, R.P. (Eds.), *Biological Markers in Sediments and Petroleum*. Prentice Hall, p. 320-349.
- Clark, J.P., Philp, R.P., 1989. Geochemical characterization of evaporate and carbonate depositional environments and correlation of associated crude oils in the black Creek Basin, Alberta. *Bulletin of Canadian Petroleum Geology* 37, p. 401-416.
- Comer J. B., 2009. The forms of quartz and dolomite in Woodford Shale of the southern Midcontinent, USA: indicators of paleoclimate, paleogeography, paleoceanography, and depositional processes. American Association of Petroleum Geologists AAPG Mid-Continent Meeting, Tulsa, Oklahoma. Book of Abstracts, pp. 154.
- Connan, J., Bouroullec, J., Dessort, D., Albrecht, P., 1986. The microbial input in carbonate-anhydrite facies of sabkha paleoenvironment from Guatemala: A molecular approach. In: Leythausen, D. & Rulkötter, J. (eds) *Advances in Organic Geochemistry*. *Organic Geochemistry* 10, p. 29-50.
- Cooper, M.A., Addison, F.T., Alvarez, R., Coral, M., Graham, R.H., Hayward, A.B., Howe, S., Martinez, J., Naar, J., Peñas, R., Pulham, A.J. and Taborda, A., 1995. Basin Development and tectonic history of the Llanos Basin, Eastern Cordillera

- and Middle Magdalena Valley, Colombia. American Association of Petroleum Geologists AAPG Bulletin, Vol. 79 (10), p. 1421-1443.
- Cornford C., Gardner P. and Burgess C., 1998. Geochemical truths in large data sets. I: Geochemical screening data. Organic Geochemistry 29(1-3), p. 519-530.
- Curtis J. B., 2002. Fractured shale-gas systems. American Association of Petroleum Geologists AAPG Bulletin, Vol. 86(11), p. 1921-1938.
- Dahl, J., Moldowan, J.M., Walls, J., Amos, N., and DeVito, J. Creation of porosity in tight shales during organic matter maturation. 2012. AAPG Annual Convention and Exhibition, Long Beach, California, USA, April 22-25, 2012 AAPG Search and Discovery Article #40979.
- Dahl, J.E., Moldowan, J.M., Teerman, S.C., McCaffrey, M.A., P., S., Pena, M., Stelting, C.E., 1994. Source rock quality determination from oil biomarkers I. – An example from the Aspen Shale, Scully's Gap, Wyoming. American Association of Petroleum Geologists AAPG Bulletin, Vol. 78, p. 1507-1526.
- Dengo, C., and Covey, M., 1993. Structure of the Eastern Cordillera of Colombia: Implications for trap styles and regional tectonics. American Association of Petroleum Geologists AAPG Bulletin, Vol. 77, p. 1315-1337.
- Duan Y., Zheng C., Wang Z., Wu B., Wang C., Zhang H., Qian Y. and Zheng G., 2006. Biomarker geochemistry of crude oils from the Qaidam Basin, NW China. Journal of Petroleum Geology 29(2), p. 175-188.



Dzou L. I. P., Noble R. A. and Senftle J. T., 1995. Maturation effects on absolute biomarker concentration in a suite of coals and associated vitrinite concentrates. *Organic Geochemistry* 23(7), p. 681-697.

Energy Information Administration, 2012. U.S. Lower 48 states Shale plays map. <http://www.eia.gov/analysis/studies/usshalegas/images/shalemap-sm.png>

Erdmann, M., and B., Horsfield, 2006, Enhanced late gas generation potential of petroleum source rocks via recombination reactions: Evidence from the Norwegian North Sea: *Geochimica et Cosmochimica Acta*, v.70, no. 1-5, p. 3943-3956.

Erlich, R.N., MacSotay, O., Nederbragt, A.J., and Lorente, M.A., 2000, Birth and death of the Late Cretaceous "La Luna Sea", and origin of the Tres Esquinas phosphorites: *Journal of South American Earth Sciences*, v. 13, p. 21-45.

Etayo-Serna, F., D. Barrero, H. Lozano, A. Espinosa, G. González, A. Orrego, A, Zambrano, H. Duque, R. Vargas, A. Nuñez, J. Alvarez, C. Ropain, I. Ballesteros, E. Cardozo, H. Forero, N. Galvis, C. Ramirez, and L. Sarmiento, 1983, Mapa de terrenos geológicos de Colombia: Publicaciones Geológicas Especiales del INGEOMINAS, No. 14, pp. 235.

Fabre, A. 1981. Estratigrafía de la Sierra Nevada del Cocuy, Boyaca y Arauca, Cordillera Oriental (Colombia). *Geología Norandina*, V4, Bogotá, p. 3-12.

- Fabre, A. 1983. La subsidencia de la Cuenca del Cocuy (Cordillera oriental de Colombia) durante el Cretácico y Terciario inferior. *Geología Norandina*, V8. Bogotá, p. 21-27 y 49-61.
- Fabre, A., 1985, Dinámica de la sedimentación Cretácica en la región Sierra Nevada del Cocuy (Cordillera Oriental de Colombia) In F.Etayo-Serna and F. Laverde, eds., Proyecto Cretácico, contribuciones: Publicaciones Geológicas Especiales de INGEOMINAS, n. 16, Chapter XIX, p.1-20.
- Fan Pu, King, J.D., Claypool, G.E., 1987. Characteristics of biomarker compounds in Chinese crude oils. In: R. K. Kumar, P. Dwivedi, V. Banerjee, and V. Gupta (Eds.) *Petroleum Geochemistry and Exploration in the Afro-Asian Region*, Dehradun, 25-27 November 1985, Rotterdam, Balkema, p. 197-202.
- Fang H., Jianyu C., Yongchuan S. and Yaozong L., 1993. Application of organic facies studies to sedimentary basin analysis: a case study from the Yitong Graben, China. *Organic Geochemistry* 20 (1), p. 27-42.
- Föllmi , K.B., Garrison, R.E., Ramirez, P.C., Zambrano-Ortiz, F., Kennedy, W.J., Lehner, B.L., 1992. Cyclic phosphate-rich successions in the Upper Cretaceous of Colombia. *Palaeogeography, Palaeoclimatology, Palaeoecology* 93, p. 151-182.
- Föllmi, K.B., 1996. The phosphorus cycle, phosphogenesis and marine phosphate-rich deposits. *Earth-Science Reviews* 40, p. 55-124.

- Fowler, M.G., Douglas, A.G., 1987. Saturated hydrocarbon biomarkers in oils of late Precambrian age from eastern Siberia. *Organic Geochemistry* 11, p. 201-213.
- García, D.F., and Parra, P., 2003. Áreas con mayor potencial de carga de petróleo: Cuenca Valle Medio del Magdalena (VMM) y occidente de la Cordillera oriente, Colombia. *Memorias del VIII Simposio Bolivariano de Exploración en cuencas subandinas*, pp. 135.
- Garner, A. H., 1926. Suggested nomenclature and correlation of the geological formations in Venezuela, *Am. Inst. Min. Metall. Eng., Tr.*, p. 677-684
- Gomez, E. 2001. Tectonic controls on the Late Cretaceous to Cenozoic sedimentary fill of the Middle Magdalena Valley Basin, Eastern Cordillera and Llanos Basin, Colombia. Ph.D. Dissertation, Graduate School of Cornell University. V(1-3), pp. 325.
- Goodarzi, F., Brooks, P.W., Embry, P.F., 1989. Regional maturity as determined by organic petrology and geochemistry of the Schei Point Group (Triassic) in Western Sverdrup Basin, Canadian Archipelago. *Marine and Petroleum Geology* 6, p. 290-302.
- Goossens H., de Leeuw J. W., Schenck P. A. and Brassell S. C., 1984. Tocopherols as likely precursors of pristane in ancient sediments and crude oils. *Nature* 312, p. 440-442.



- Grantham, P.J., Wakefield, L.L., 1988. Variations in the sterane carbon number distributions of marine source rock derived crude oils through geological time. *Organic Geochemistry* 12, p. 61-73.
- Grasby, S.E., Chen, Z., Issler, D., Stasiuk, L., 2009. Evidence for deep anaerobic biodegradation associated with rapid sedimentation and burial in the Beaufort-Mackenzie basin, Canada. *Applied Geochemistry* 24, p. 536-542.
- Hedberg, H.D., and Sass, L.C., 1937, Synopsis de las formaciones geológicas de la parte occidental de la Cuenca de Maracaibo, Venezuela: Boletín de Geología y Mineralogía (Venezuela), Servicio Técnico de Geología y Minería, Caracas, v. 2-4, p. 83-84.
- Hérbard, F., 1985. Les foothills de la Cordillère Oriental de Colombie entre les Ríos Casanare et Cusiana. Evolution geodinamique depuis du Cretacé. Ph.D. These. Univ. Pierre et Marie Curie, Paris, pp. 62.
- Hill R. J., Jarvie D. M., Zumberge J., Henry M. and Pollastro R. M., 2007a. Oil and gas geochemistry and petroleum systems of the Fort Worth Basin. *American Association of Petroleum Geologists AAPG Bulletin*, Vol. 91(4), p. 445-473.
- Hill R. J., Zhang E., Katz B. J. and Yongchun T., 2007b. Modeling of gas generation from the Barnett Shale, Fort Worth Basin, Texas. *American Association of Petroleum Geologists AAPG Bulletin*, Vol. 91(4), p. 501-521.

- Horsfield, B., U., Disko, F., Leistner, 1989, The microscale simulation of maturation: Outline of a new technique and its potential applications: *Geologische Rundschau*, v. 78, p.361-374.
- Huang W. Y. and W. G. Meinschein, 1979. Sterols as ecological indicators. *Geochimica et Cosmochimica Acta* 43, p. 739-745.
- Hubach, E., 1957. Estratigrafía de la Sabana de Bogotá y alrededores. *Boletín Geológico*, Instituto Geológico Nacional, vol. 5, nº 2, p. 93-112.
- Hughes, W.B., Holba, A.G., Miller, D.E., Richardson, J.S., 1985. Geochemistry of greater Ekofisk crude oils. In: Thomas, B. M., Dore', A.G., Eggen, S.S., Home, P.C. & Larsen, R.M. (Eds.) *Petroleum Geochemistry in Exploration of the Norwegian Shelf*. Graham and Trotman, London, p. 75-92.
- Jarvie D. M., Hill R. J. and Pollastro R. M., 2005. Assessment of the gas potential and yields from shales: The Barnett Shale model. *Oklahoma Geological Survey Circular* 110, p. 37-50.
- Jarvie D. M., Hill R. J., Ruble T. E. and Pollastro R. M., 2007. Unconventional shale-gas systems: The Mississippian Barnett Shale of north-central Texas as one model for thermogenic shale-gas assessment. *American Association of Petroleum Geologists AAPG Bulletin*, Vol. 91(4), p. 475-499.
- Jobson, A.M., Cook, F.D., Westlake, D.W.S., 1979. Interaction of aerobic and anaerobic bacteria in petroleum biodegradation. *Chemical Geology* 24, p. 355-365.

Julivert, M., 1968. Lexico Estratigrafico de Colombia, Primera Parte. Précambrien, Paléozoïque, Mésozoïque, et intrusions d'âge mésozoïque – tertiaire. Centre National de la Recherche Scientifique 15, quai Anatole-France, Paris – VII, p. 572.

Julivert, M., 1970. Cover and basement tectonics in the Cordillera Oriental de Colombia, and comparison with other faulted chains. Geological Society of America Bulletin vol. 81, p. 3623-3646.

Kingston, D., C. Dishroon, and P. Williams, 1983, Global basin classification system. American Association of Petroleum Geologists AAPG Bulletin, Vol. 67, p. 2175-2213.

Kinley T. J., Cook L. W., Breyer J. A., Jarvie D. M. and Busbey A. B., 2008. Hydrocarbon potential of the Barnett Shale (Mississippian), Delaware Basin, west Texas and southeastern New Mexico. American Association of Petroleum Geologists AAPG Bulletin, Vol. 92(8), p. 967-991.

Kirkland D, W., Denison, R, E., Summers, D, M., and Gormly, J, R., 1992. Geology and organic geochemistry of the Woodford Shale in the Criner Hills and western Arbuckle Mountains, Oklahoma, Oklahoma Geological Survey, Circular 93, p. 38-69.

Landis C. R. and Castano J. R., 1995. Maturation and bulk chemical properties of a suite of solid hydrocarbons. Organic Geochemistry 22(1), p. 137-149.



- Law B. E. and Curtis J. B., 2002. Introduction to unconventional petroleum systems. American Association of Petroleum Geologists AAPG Bulletin, Vol. 86(11), p. 1851-1852.
- Lo Monaco, G.A., 2012. Characterization of the Mississippian Barnett Shale Formation well, using organic geochemistry parameters and their relationship with different lithofacies, Fort Worth Basin, Texas. M.Sc. Thesis manuscript, The University of Oklahoma, pp. 106.
- Macellari, C., 1988. Cretaceous Paleogeography and depositional cycles of Western South America. *Journal of South America Earth Science*. V1, p. 373-418.
- Maceralli, C.E., and De Vries, T.J., 1987, Late Cretaceous upwelling and anoxic sedimentation in northwestern South America: *Palaeogeography, Palaeoclimatology, Palaeoecology*, v. 59, p. 279–292.
- Mackenzie, A.S., Brassell, S.C., Eglinton, G., R., M.J., 1982. Steroid hydrocarbons and the thermal history of sediments *Nature*, London 295, p. 223-226.
- Mann, U., and Stein, R., 1997, Organic facies variations, source rock potential, and sea level changes in Cretaceous black shales of the Quebrada Ocal, Upper Magdalena Valley, Colombia: American Association of Petroleum Geologists AAPG Bulletin, Vol. 81, p. 556–576.
- McKirdy, D.M., Aldridge, A.K., Ypma, P.J.M., 1983. A geochemical comparison of some crude oils from pre-Ordovician carbonate rocks. In M. Bjoroy et al. (Ed.)

- Advances in Organic Geochemistry 1981. Organic Geochemistry, London: Wiley, p. 99-107.
- McKirdy, D.M., Kantsler, A.J., Emmett, J.K., Aldridge, A.K., 1984. Hydrocarbon genesis in Cambrian carbonates of the eastern Officer Basin, South Australia. In: Palacas, J.G. (Ed.) Petroleum Geochemistry and Source Rock Potential of Carbonate Rocks, American Association of Petroleum Geologists AAPG Studies in Geology 18, p. 13-31.
- Mello, M.R., Telnaes, N., P.C., G., Chicarelli, M.I., Brassell, S.C., Maxwell, J.R., 1988b. Organic geochemical characterization of depositional environment in Brazilian marginal basins. Organic Geochemistry 13, p. 31-46.
- Miceli-Romero, A., 2010. Geochemical characterization of the Woodford Shale, central and southeastern Oklahoma. M.Sc. Thesis manuscript, The University of Oklahoma, pp. 149.
- Milner, C.W.D., Rogers, M.A., Evans, C.R., 1977. Petroleum transformations in reservoirs. Journal of Geochemical Exploration 7, p. 101-153.
- Moldowan, J.M., 1984. C30-steranes, novel markers for marine petroleum and sedimentary rocks. Geochimica et Cosmochimica Acta 48, p. 2767-2768.
- Moldowan, J.M., Fago, F.J., Lee, C.Y., Jacobson, S.R., Watt, D.S., Slougui, N.E., Jeganathan, A., Young, D.C., 1990. Sedimentary 24-n-propylcholestanes, molecular fossils diagnostic of marine algae. Science 247, p. 309-312.

- Moldowan, J.M., Seifert, W.K., Gallegos, E.J., 1985. Relationship between petroleum composition and depositional environment of petroleum source rocks. American Association of Petroleum Geologists AAPG Bulletin, Vol. 69, p. 1255-1268.
- Morales, L.G., 1958. General Geology and oil occurrences of Middle Magdalena Valley, Colombia. Habitat of Oil Symposium, American Association of Petroleum Geologists AAPG, p. 641-695.
- Mueller, E., Philp, R.P., Allen, J., 1995. Geochemical characterization and relationship of oils and solid bitumens from S.E. Turkey. Journal of Petroleum Geology 18, p. 289-308.
- O'Brien, N., and Slatt, R. M., 1990. Argillaceous Rock Atlas. New York, Springer-Verlag, pp. 156.
- Ourisson G., Albrecht P. and Rohmer M. (1982) Predictive microbial biochemistry – from molecular fossils to prokaryotic membranes. Trends in biochemical sciences 7(7), p. 236-239.
- Palacas, J.G., Anders, D.E., King, J.D., 1984. South Florida basin-a prime example of carbonate source of Petroleum Geochemistry and source rock potential of carbonate rocks. AAPG Studies in Geology, Palacas J. G. ed. American Association of Petroleum Geologists AAPG, p. 71-96.
- Palmer, S., 1984. Effect of water washing on C15+hydrocarbon fraction of crude oils from Northwest Palawan, Philippines. American Association of Petroleum Geologists AAPG Bulletin, Vol. 68, p. 137-149.



- Perez-Infante, J., Farramond, P., and Furrer, M., 1996, Global and local controls influencing the deposition of the La Luna Formation (Cenomanian–Campanian), western Venezuela: *Chemical Geology*, v. 130, p. 271–288.
- Peters K. E. and Cassa M. R., 1994. Applied source rock geochemistry. In Magoon L. B. and Dow W. G. (eds.) *The petroleum system – from source to trap*. American Association of Petroleum Geologists AAPG, Memoir 60, p. 93-120.
- Peters K. E., 1986. Guidelines for evaluating petroleum source rock using programmed pyrolysis. *American Association of Petroleum Geologists AAPG Bulletin*, Vol. 70 (3), p. 318-329.
- Peters, K.E., Moldowan, J.M., 1993. *The Biomarker Guide: Interpreting Molecular Fossils in Petroleum and Ancient Sediments*. Prentice Hall, Englewood Cliffs, N.J., pp. 363.
- Peters, K.E., Walters, C.C., Moldowan, J.M., 2005. *The Biomarker Guide: Biomarkers and Isotopes in Petroleum Exploration and Earth History*, Sec. Edition. ed. Cambridge University Press UK, v. 2, pp. 1155.
- Philp R. P., 2007. The role of geochemistry in characterization of gas shales and produced gas. In *Geological Society of America Annual Meeting and Exposition – Abstracts with programs*, pp. 356.
- Philp, R.P., 1982. Correlation of crude oils from the San Jorge Basin, Argentina. *Geochimica et Cosmochimica Acta* 47, p. 267-275.

- Philp, R.P., 1985. Fossil Fuel Biomarker. Elsevier Science Publishers New York, p. 294.
- Philp, R.P., 2003. Formation and Geochemistry of Oil and Gas in Treatise on Geochemistry. Elsevier Ltd., p. 223-256.
- Philp, R.P., Chen, J.H., Fu, J.M., Sheng, G.Y., 1992. A geochemical investigation of crude oils and source rocks from Biyang Basin, China. *Organic Geochemistry* 18, p. 933-945.
- Philp, R.P., Gilbert, T.D., 1986. Biomarker distributions in Australian oils predominantly derived from terrigenous source material. In Leythausen D. and Rullkötter J. Advances (Eds.) *Organic Geochemistry 1985*. Pergamon Press, Oxford, p. 73-84.
- Philp, R.P., Li Jingui, Lewis, C.A., 1989. An organic geochemical investigation of crude oils from Shanganing, Jianghan, Chaidamu and Zhungeer Basins, People's Republic of China. *Organic Geochemistry* 14, p. 447-460.
- Pindell, J. 1993. Regional synopsis of Gulf of Mexico and Caribbean evolution. *Transactions of GCSSEPM 13<sup>th</sup> Annual research conference*, p. 251-254.
- Pindell, J. and Dewey, J., 1982. Permo-Triassic reconstruction of western Pangea and the evolution of the Gulf of Mexico-Caribbean region, *Tectonics* 1: p. 179-211.

Pindell, J., and Barret, S., 1990. Geological evolution of the Caribbean region: A plate tectonic perspective: The Caribbean Region, Vol. H. The geology of North America. Geological Society of America, p. 405-432.

Pindell, J., and Erikson, 1993. The Mesozoic passive margin of northern South America, in J.A. Salfity, ed., Cretaceous Tectonics of the Andes: Braunschweig/Weisbaden, Earth Evolution Sciences, Vieweg Publishing, p. 1-60.

Pollastro R. M., 2007. Total petroleum system assessment of undiscovered resources in the giant Barnett Shale continuous (unconventional) gas accumulation, Fort Worth Basin, Texas. American Association of Petroleum Geologists AAPG Bulletin, Vol.91(4), p. 551-578.

Pollastro R. M., Jarvie D. M.; Hill R. J. and Adams C. W., 2007. Geological framework of the Mississippian Barnett Sahel, Barnett-Paleozoic total petroleum system, Bend arch-Fort Worth Basin, Texas. American Association of Petroleum Geologists AAPG Bulletin, Vol. 91(4), p. 405-436.

Price, P.L., O'Sullivan, T., Alexander, R., 1987. The nature and occurrence of oil in Seram, Indonesia. In: Proceedings of the Indonesian Petroleum Association, 16th Annual Convention. Indonesian Petroleum Association, Jakarta 1, p. 141-173.

Rangel, A., Giraldo, B., Magoon, L., Sarmiento, L., Bartels, H., Mora, C., Cordoba, F., Luna, O., Reyes, J., 1996. Oil potential of the cretacic megasequence and



- associated oil families in the Middle Magdalena Valley-Colombia. In: Memorias del V Congreso Latinoamericano de Geoquímica Orgánica, Cancun, Mexico, pp. 105.
- Rangel, A., Parra, P., Niño, C. 2000. The La Luna formation: chemostratigraphy and organic facies in the Middle Magdalena Basin. *Organic Geochemistry* (31), p. 1267-1284.
- Renz, O., 1959, Estratigrafía del Cretáceo en Venezuela occidental: *Boletín Geológico*, v. 5,10, p. 3-48.
- Restrepo-Pace, P.A., 1999, Late Precambrian to early Mesozoic tectonic evolution of the Colombian Andes, based on new geochronological, geochemical and isotopic data (Ph.D. thesis): Tucson, University of Arizona, pp. 189.
- Rullkötter, J., Spiro, B., Nissenbaum, A., 1985. Biological marker characteristics of oils and asphalts from carbonate source rocks in a rapidly subsiding graben, Dead Sea. *Geochimica et Cosmochimica Acta* 49, p. 1357-1370.
- Sammy, N., 1985. Biologsarmiento  
ical systems in northern Australia solar salt and fields. In: B.C. Schreiber and L. Harner (Eds.) 6th International Symposium on Salt. Salt Institute, Alexandria, Virginia 1, p. 207-215.

- Sarmiento, L. 2001. Mesozoic Rifting and Cenozoic basin inversión history of the Eastern Cordillera, Colombian Andes. Inferences from tectonic models. Bogota, pp. 295.
- Schamel, S., 1991, Middle and Upper Magdalena Basins, Colombia, in Biddle, K. T., ed., Active Margin Basins: American Association of Petroleum Geologists AAPG Memoir 52, p. 283-301.
- Schenk C. J., 2005. Geologic Definition of Conventional and Continuous Accumulations in Select U.S. Basins – The 2001 Approach. In 2005 American Association of Petroleum Geologists AAPG Hedberg Conference: Understanding, Exploring and Developing Tight Gas Sands. AAPG Search and Discovery, article #90042; accessed September 16, 2009.
- Schenk, H.J., and V., Dieckmann, 2004, Prediction of petroleum formation: the influence of laboratory heating rates on kinetic parameters and geological extrapolations: Marine and Petroleum Geology, v. 21, no. 1, p. 79-95.
- Schmoker J. W., 2002. Resource-assessment perspectives for unconventional gas systems American Association of Petroleum Geologists AAPG Bulletin, Vol. 86(11), p. 1993-1999.
- Schmoker J. W., Fouch T. D. and Charpentier R. R., 1996. Gas in the Uinta Basin, Utah. Resources in continuous accumulations. The Mountain Geologist 33(4), p. 95-104.

- Seifert, W.K., Moldowan, J.M., 1979. The effect of biodegradation on steranes and terpanes in crude oils. *Geochimica et Cosmochimica Acta* 43, p. 111-126.
- Seifert, W.K., Moldowan, J.M., Jones, R.W., 1980. Application of biological marker chemistry to petroleum exploration. In *Proc. Tenth World Petroleum Congress*, Bucharest, Romania. September 1979. Paper SP8, p. 425-440.
- Singh P., 2008. Lithofacies and sequence stratigraphic framework of the Barnett Shale, Northeast Texas. Ph.D. Thesis manuscript, The University of Oklahoma, pp. 181.
- Singh P., 2008. Lithofacies and sequence stratigraphic framework of the Barnett Shale, Northeast Texas. Ph.D. Dissertation, The University of Oklahoma, pp. 181.
- Slatt R. M., Singh P., Philp R. P., Marfurt K. J., Abousleiman Y. and O'Brien N. R., 2010. Workflow for stratigraphic characterization of unconventional gas shales. 2008 Society of Petroleum Engineers Shale Gas Production Conference, Fort Worth, Texas, p. 699-710.
- Slatt, R. M., N. Buckner, Y. Abousleiman, R. Sierra, P. Philp, A. Miceli-Romero, R. Portas, N. O'Brien, M. Tran, R. Davis, and T. Wawrzyniec, 2011a. Outcrop/behind outcrop (quarry), multiscale characterization of the Woodford Gas Shale, Oklahoma, in J. Breyer, ed., *Shale reservoirs—Giant resources for the 21st century: American Association of Petroleum Geologists AAPG Memoir 97*, p. 1–21.



- Slatt, R. M., Rodriguez, N.D., 2012. Comparative sequence stratigraphy and organic geochemistry of gas shales: Commonality or coincidence? *Journal of Natural Gas Science and Engineering*, volume 8, p. 68-84.
- Slatt, R., and O'Brien, N., 2011. Pore Types in the Barnett and Woodford Gas Shales: Contribution to Understanding Gas Storage and Migration. *American Association of Petroleum Geologists AAPG Bulletin*, Vol. 95, No 12. December 2011. p. 2017-2030.
- Summons, R.E., Thomas, J., Maxwell, J.R., Boreham, C.J., 1992. Secular and environmental constraints on the occurrence of dinosterane in sediments. *Geochimica et Cosmochimica Acta* 56, p. 2437–2444.
- Talukdar, S., Gallango, O., and Ruggiero, A., 1985, Formaciones La Luna y Querecual: rocas madres de petróleo: in Espejo, A., Ríos, J.H., de Bellizzia, N.P., and de Pardo, A.S., eds., *Memoria: VI Congreso Geológico Venezolano, Memorias. Sociedad Venezolana de Geólogos, Caracas*, p. 3606–3642.
- ten Haven, H.L., de Leeuw, J.W., Peakman, T.M., Maxwell, J.R., 1986. Anomalies in steroid and hopanoid maturity indices. *Geochimica et Cosmochimica Acta* 50, p. 853-855.
- Tissot B. P. and Welte D. H., 1978. *Petroleum formation and occurrence*. Springer-Verlag Berlin Heidelberg, Germany, pp. 538.

- Tissot B., Durand B., Espitalie J. and Combaz A., 1974. Influence of nature and diagenesis of organic matter in formation of petroleum. American Association of Petroleum Geologists AAPG Bulletin, Vol. 58(3), p. 499-506.
- Tussaint J. and Restrepo J., 1985. Hipotesis del marco geodinamico de Colombia durante el Mesozoico temprano, contribucion a IGCP 322 Jurassic Events in South America. Geología Colombiana., Bogotá, 20: p. 150-155.
- Villamil, T., 1998. Chronology, relative sea level history and new sequence stratigraphic model for basinal Cretaceous facies of Colombia. Paleogeographic evolution and non-glacial eustacy. Northern South America. SEPM. Special Publication No 58.
- Villamil, T., Aarango, C., and Hay, W.W., 1999. Plate tectonic paleoceanographic hypothesis for Cretaceous source rocks and cherts of northern South America: in Barrera, E., and Johnson, C.C., eds., Evolution of the Cretaceous Ocean-Climate System: Geological Society of America Special Paper 332, Geological Society of America, p. 191-202.
- Volkman J. K., 1986. A review of sterol markers for marine and terrigenous organic matter. Organic Geochemistry 9(2), p. 83-99.
- Volkman, J.K., 1988. Biological marker compounds as indicators of the depositional environments of petroleum source rocks. In Fleet, A.J., Kelts, K., and Talbot, M.R. (Eds.), Lacustrine Petroleum Source Rocks. Geological Society, London, Special Publications 40, p. 103-122.

- Volkman, J.K., Maxwell, J.R., 1986. Acyclic isoprenoids as biological markers In: R.B. Johns (Ed.) *Biological Markers in the sedimentary Record* Elsevier, New York, p. 1-42.
- Wang D. H. and Philp R. P., 2007. Geochemical study of potential source rocks and crude oils in the Anadarko Basin, Oklahoma. *American Association of Petroleum Geologists AAPG Bulletin*, Vol. 81(2), p. 249-275.
- Wang, F. P., and J. F. W. Gale, 2009, Screening criteria for shale-gas systems: Gulf Coast Association of Geological Societies Transactions, v. 59, p. 779-793.
- Waples D. W., 1985. *Geochemistry in petroleum exploration*. International Human Resources Development Corporation. USA, pp. 178.
- Waples, D.W., Machihara, T., 1991. Biomarkers for geologists. *AAPG Methods in Exploration Series 9*, pp. 91.
- Warren, A., Allen, J.D., and Philp, R.P., 2012. Gas generation from the Woodford Shale and the Caney Shale 1 in the Arkoma Basin, Oklahoma: Insights from GC-IRMS and MSSV-PY-GC-IMRS. *In-press*, *American Association of Petroleum Geologists AAPG Bulletin*, pp. 49.
- Wenger, L.M., Davis, C.L., Isaksen, G.H., 2002. Multiple controls on petroleum biodegradation and impact on oil quality. *Society of Petroleum Engineering (SPE) Reservoir Evaluation and Engineering 5*, p. 375-383.



- Wilkes, H., Boreham, C., Harms, G., Zengler, K., Rabus, R., 2000. Anaerobic degradation and carbon isotopic fractionation of alkylbenzenes in crude oil by sulphate-reducing bacteria. *Organic Geochemistry* 31, p. 101-115.
- Yang, B., 1991. Geochemical characteristics of oil from well Shacan-2 in the Tarim Basin. *Journal of Southeast Asian Earth Sciences* 5, p. 401-406.
- Zhao H., Givens N. B. and Curtis B., 2007. Thermal maturity of the Barnett Shale determined from well-log analysis. *American Association of Petroleum Geologists AAPG Bulletin*, Vol. 91(4), p. 535-549.
- Zumberge, J., 1984. Source Rocks of the La Luna Formation (Upper Cretaceous) in the Middle Magdalena Valley, Colombia. In Palacas J. (Ed.). *Petroleum Geochemistry and Source Rock Potential of Carbonate Rocks*. American Association of Petroleum Geologists AAPG Studies in Geology No.18, p. 127-133.

## APPENDICES

### APPENDIX I. Organic Geochemistry

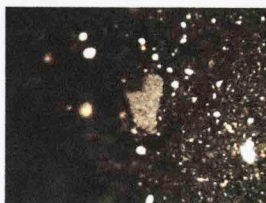
#### Appendix I-A. Vitrinite Reflectance. OUTCROP B samples.

##### QLS M-8. Granular Bitumen 0.55% BRo

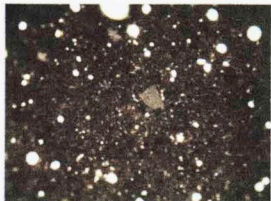


##### CAR M-2, kerogen isolated sample. Granular Bitumen 0.44% Bro.

CAR M-2. Bitumen granular 0.43% BRo CAR M-2. Bitumen granular 0.46% BRo

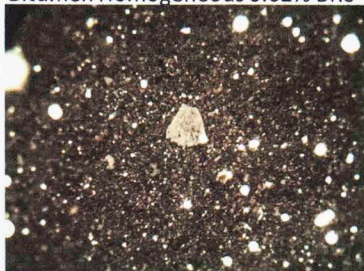


CAR M-2. Bitumen granular 0.45% BRo CAR M-2. Bitumen granular 0.43% BRo



##### CAR M-2, kerogen isolated sample. Granular Bitumen 0.64%BRo

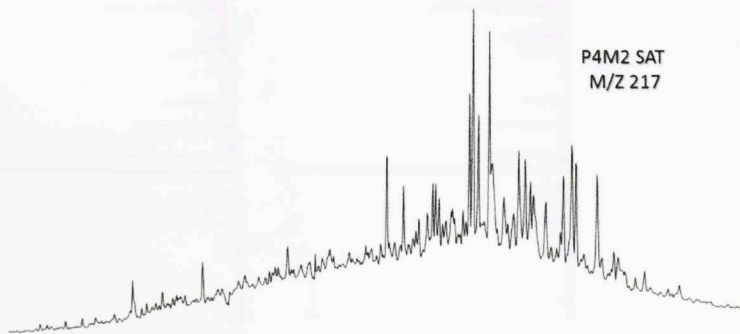
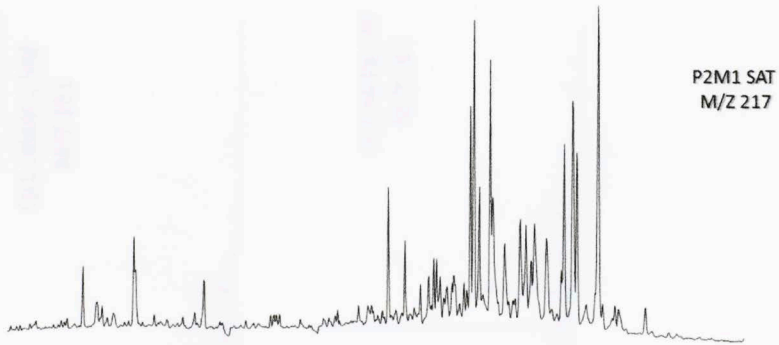
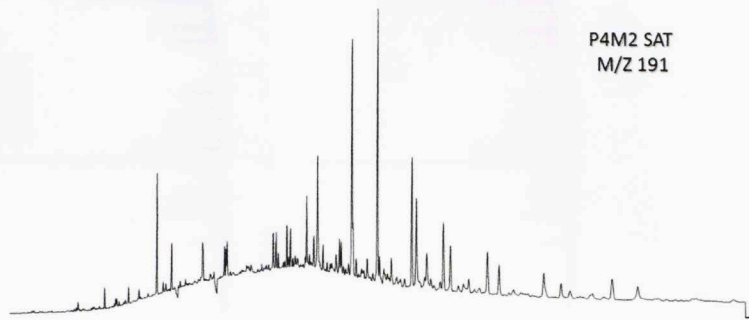
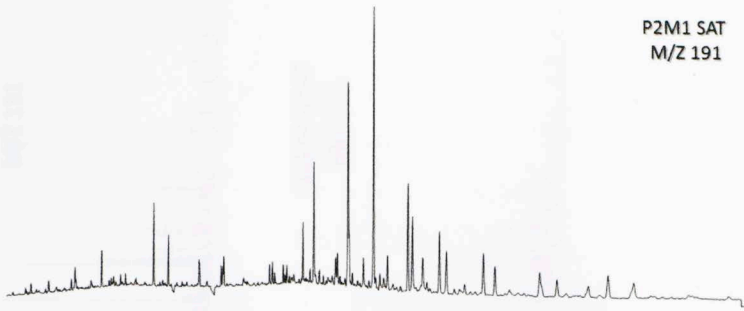
Bitumen Homogeneous 0.62% BRo



Bitumen Homogeneous 0.65% BRo



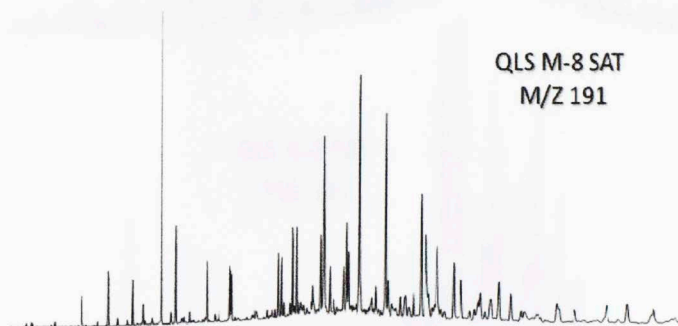
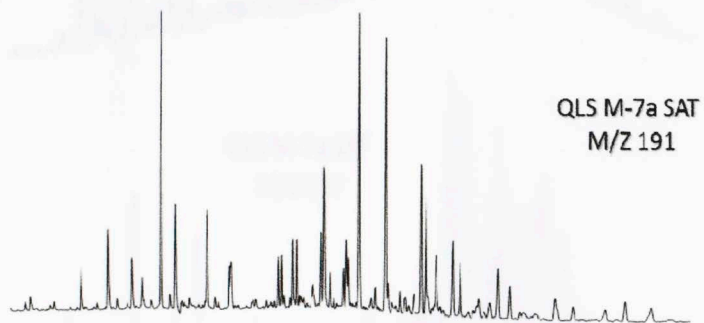
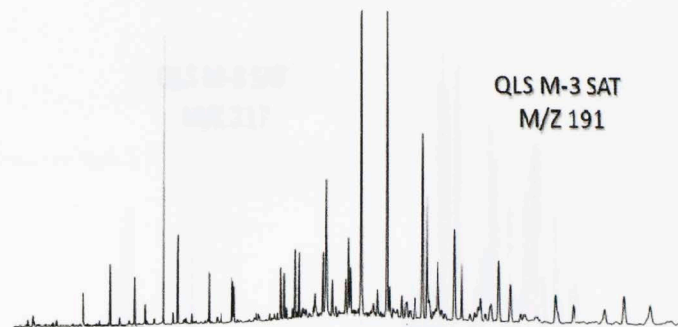
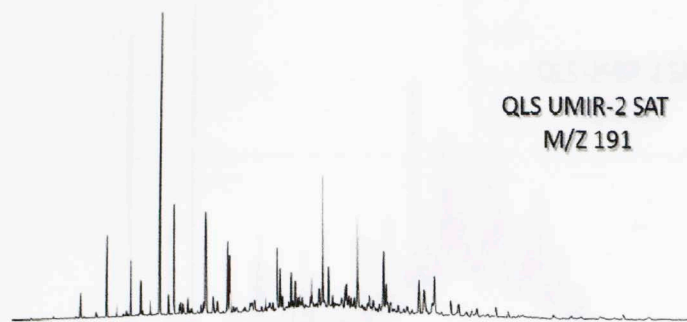
**Appendix I-B. Biomarker GC-MS Fragmentograms. OUTCROP A.**





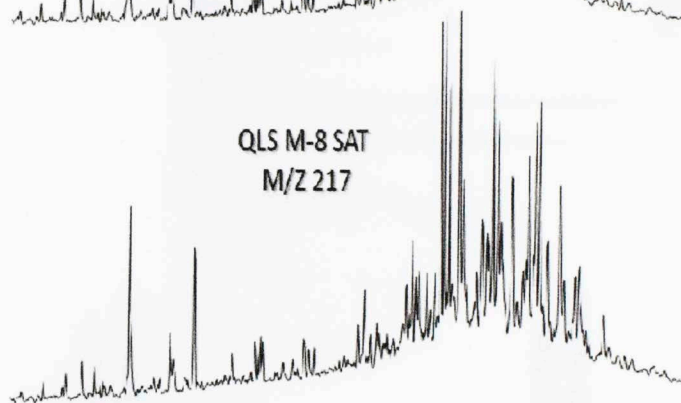
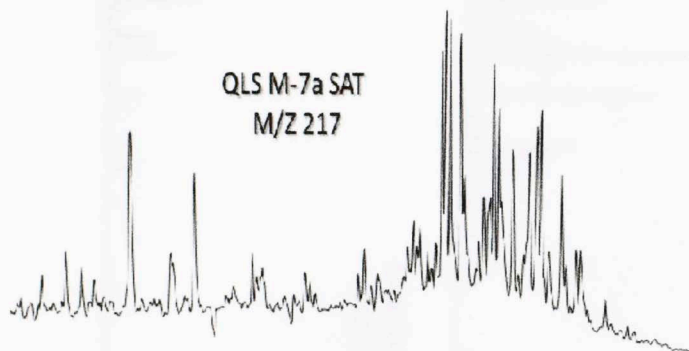
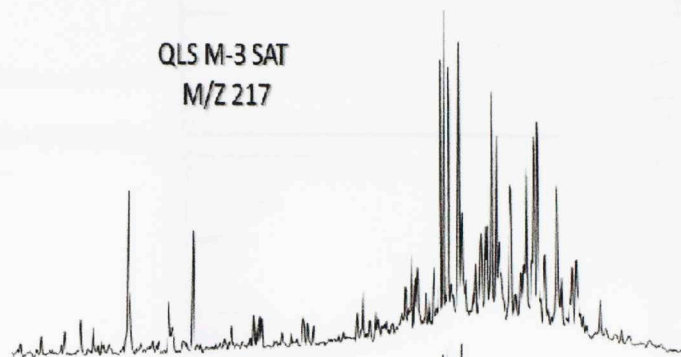
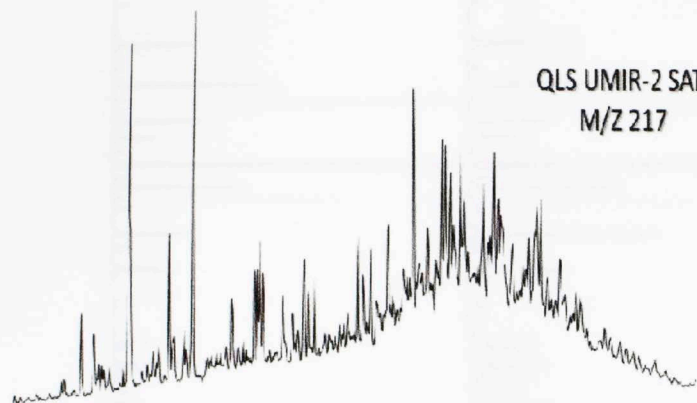
Appendix I-C. Biomarker GC-MS Fragmentograms. OUTCROP B. GALEMBO M/Z 191.

190



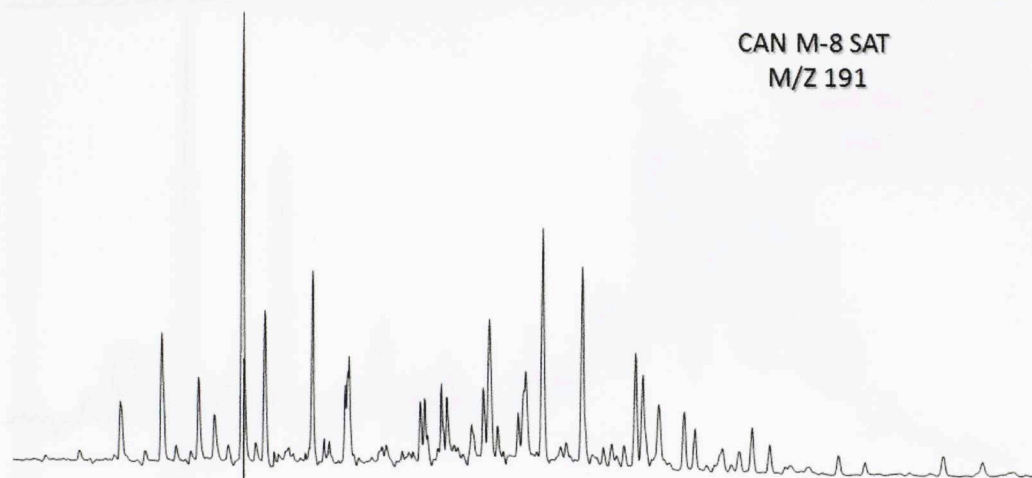
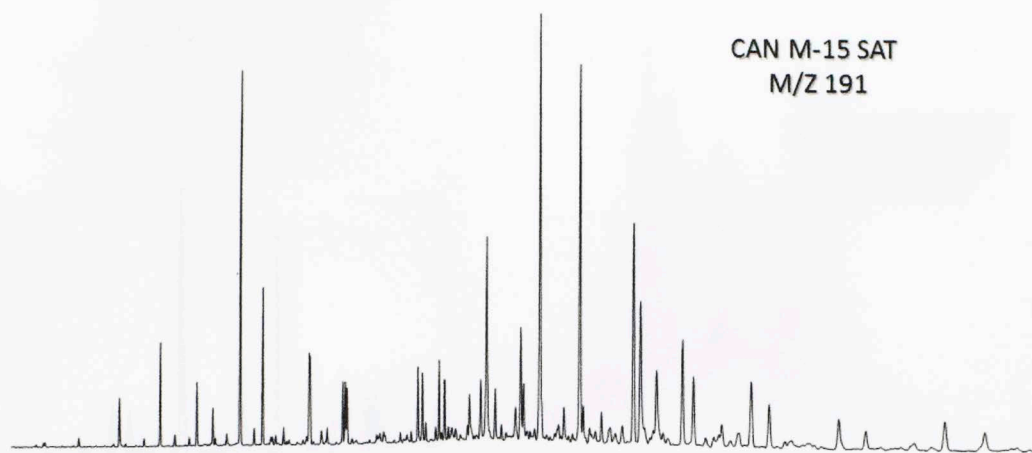
Appendix I-D. Biomarker GC-MS Fragmentograms. OUTCROP B. GALEMBO M/Z 217.

161



**Appendix I-E. Biomarker GC-MS Fragmentograms. OUTCROP B. PUJAMANA**

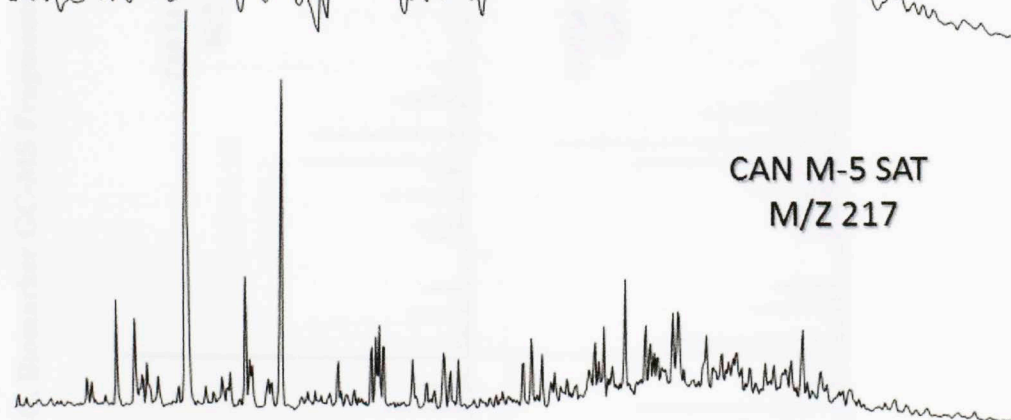
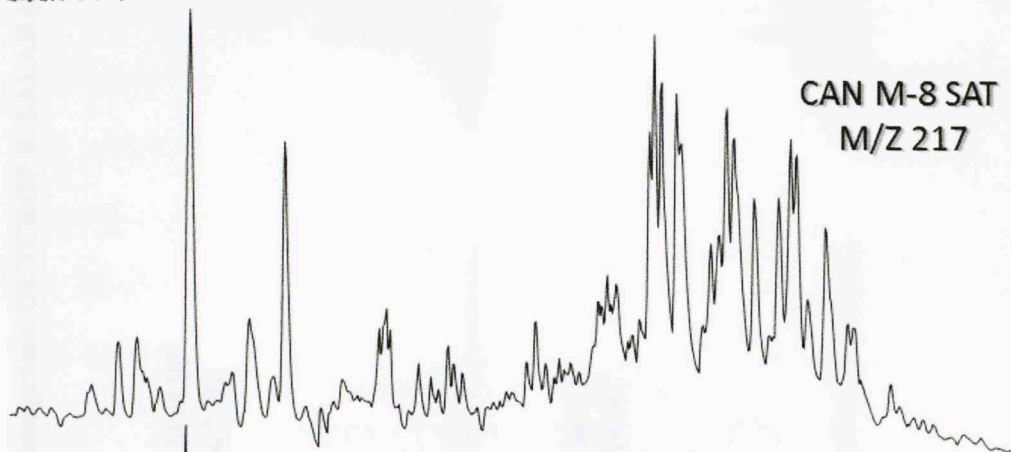
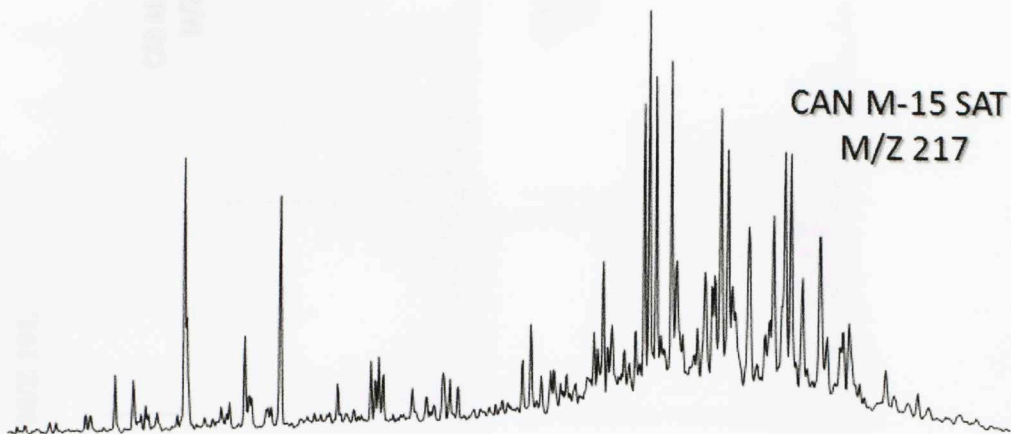
**M/Z 191.**



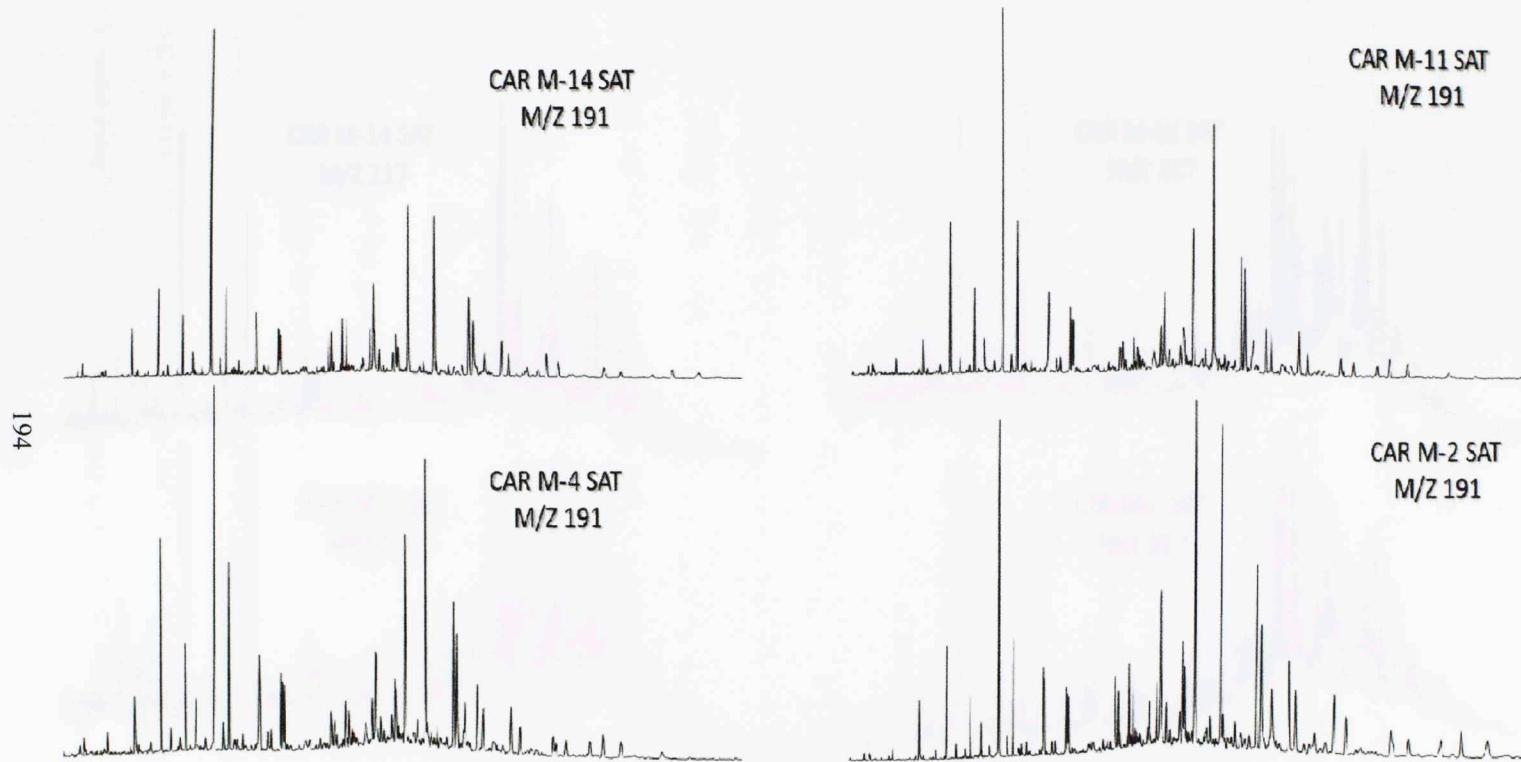


**Appendix I-F. Biomarker GC-MS Fragmentograms.**

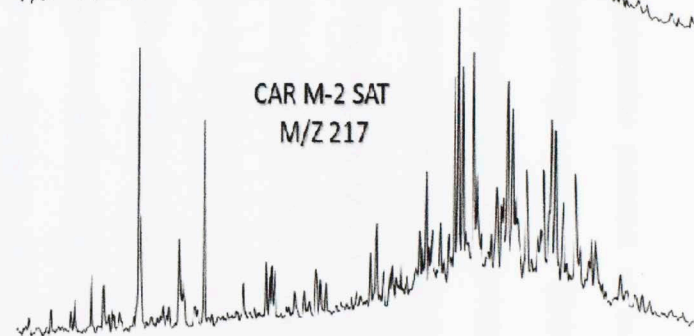
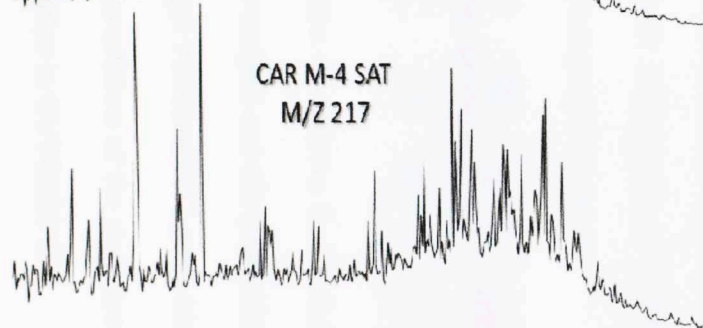
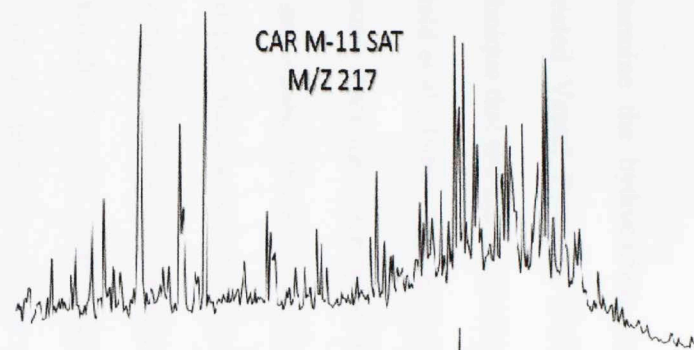
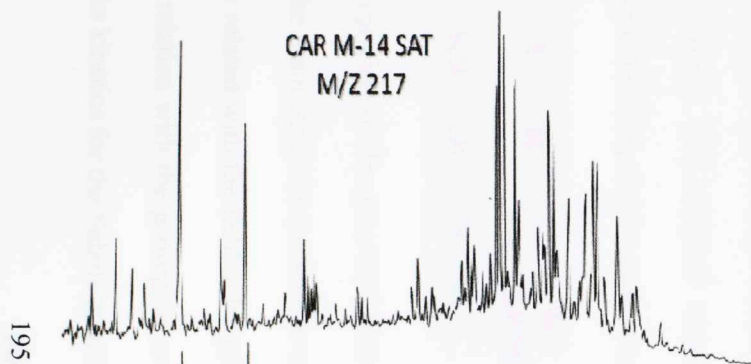
**OUTCROP B. PUJAMANA M/Z 217.**



**Appendix I-G. Biomarker GC-MS Fragmentograms. OUTCROP B. SALADA M/Z 191.**



Appendix I-H. Biomarker GC-MS Fragmentograms. OUTCROP B. SALADA M/Z 217.





## Appendix I-I. Microscale Sealed Vessel

To determine the hydrocarbon generation potential of La Luna formation, MicroScale Sealed Vessel Pyrolysis (MSSV-Py) was used- MSSV is an artificial maturation technique that simulates petroleum generation from a source rock in a closed system (Horsfield et al., 1989). This method allows the generation of gas and “oil-like” pyrolysates issued from the cracking of the kerogen (primary cracking) and of the generation of gas issued from the cracking of oil and bitumen (secondary cracking). Furthermore, as the source rock is matured in a closed cell, primary products may be recombined by aromatization/condensation reactions into a gas-prone residue called pyrobitumen (Horsfield et al., 1989; Erdmann and Horsfield, 2006). The cracking at high maturity of pyrobitumen extends gas generation beyond the conventional secondary cracking window and provides significant quantities of methane (Erdmann and Horsfield, 2006). The analyzed sample corresponds to OUTCROP B Salada member, sample CAR M-3, and its source rock properties are:

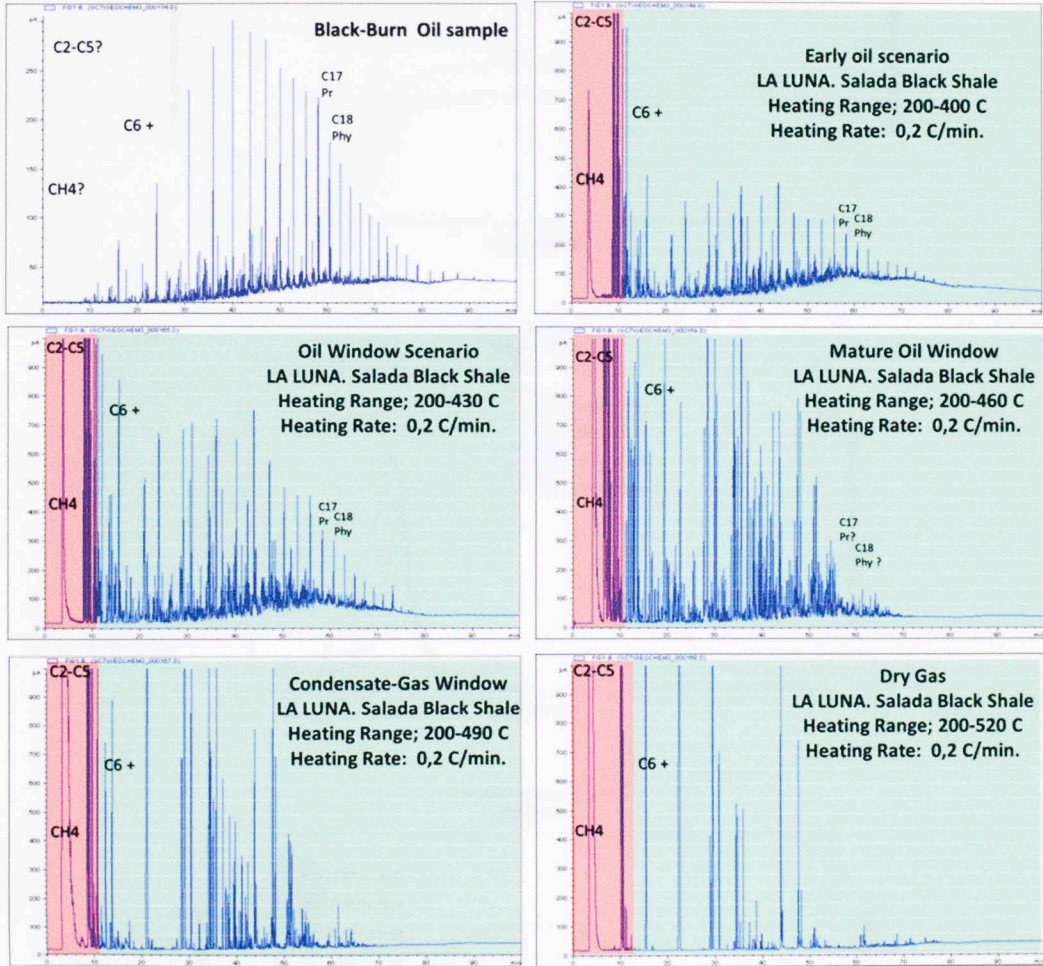
TOC%	S1	S2	S3	Tmax	%Ro Measured	%Ro Calculated	HI	OI	S2/S3	S1/TOC	PI
11.90	8.36	54.54	0.24	436	0.77	0.69	458	2	227	70	0.13

The integration of the generated peaks of methane, C<sub>2</sub>-C<sub>5</sub>, C<sub>6</sub>-C<sub>14</sub> and C<sub>15+</sub> was developed as the main input for the kinetic analysis and this generation ratios measured in the lab were related with the Schlumberger Petromod2012 petro-kinetics package for establishing a relation with the geological conditions of the study area, thus, obtaining the source rocks kinetics for the Salada member in OUTCROP B.

# Microscale Sealed Vessel-Pyro GC.

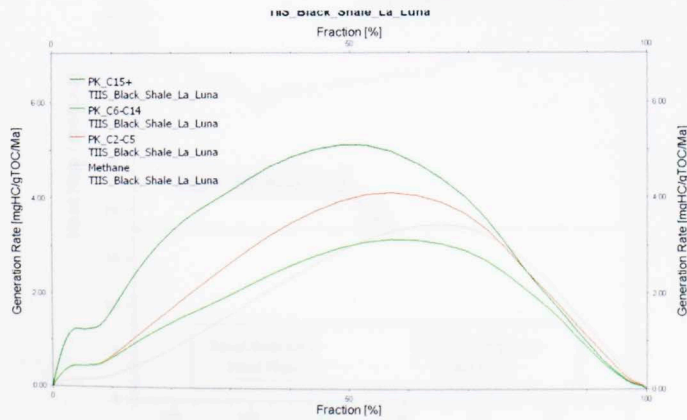
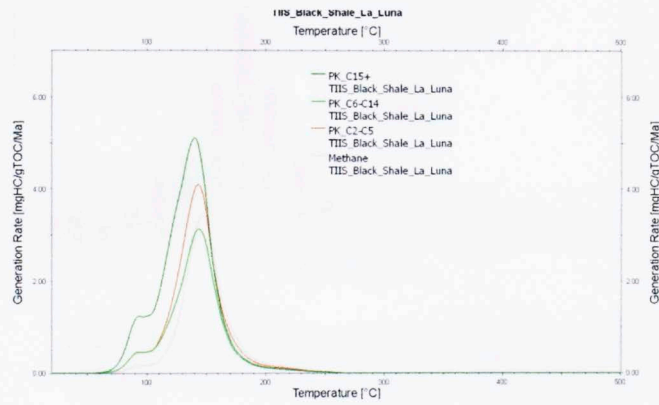
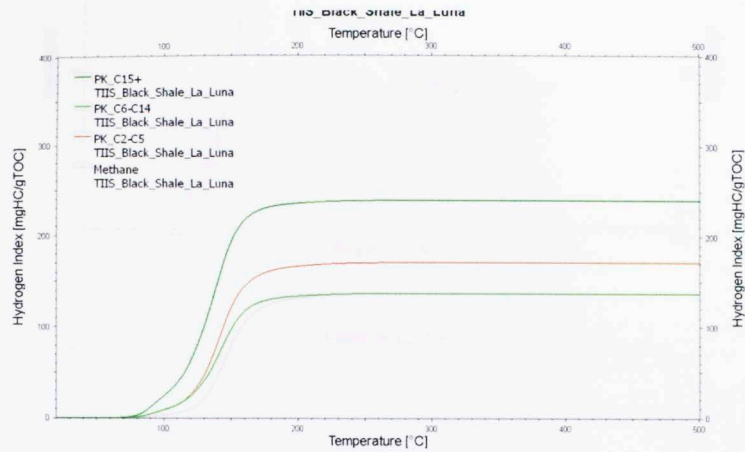
## CAR M-3, Salada member results.

Heating rate and ratio: 0.2 C/min. 200 °C to 520 °C.

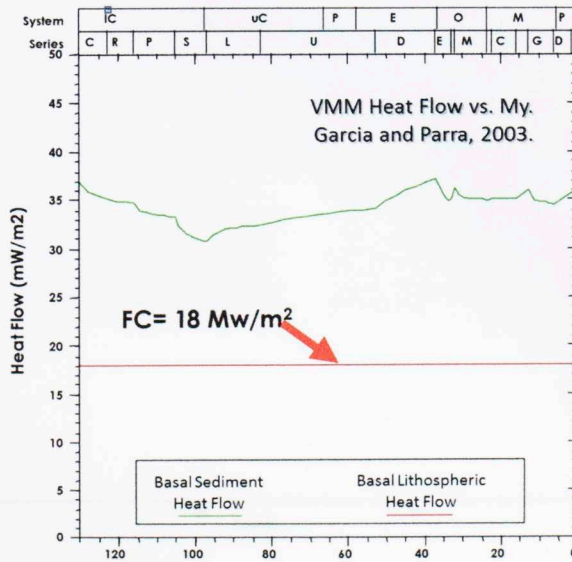
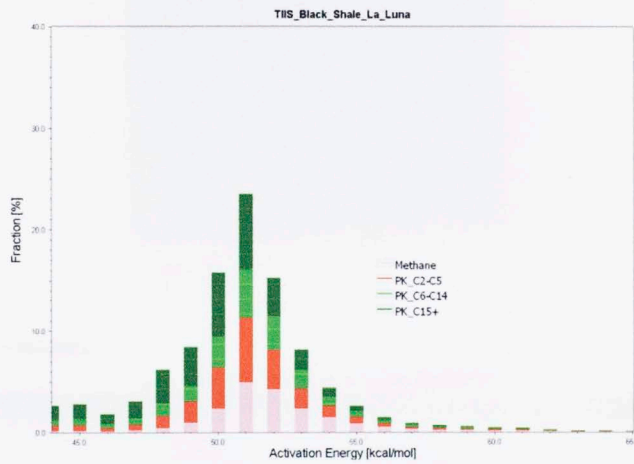
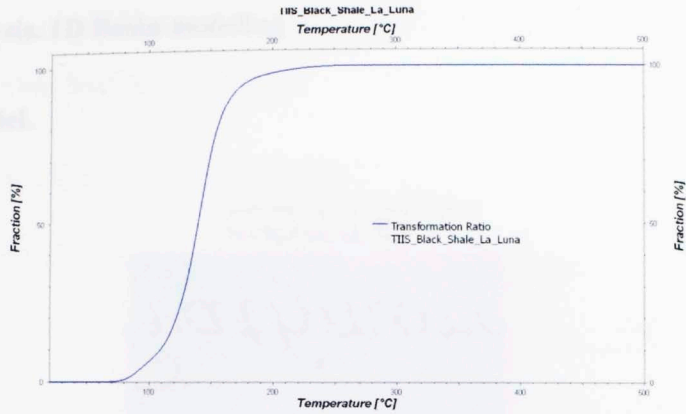


## Microscale Sealed Vessel. Kinetic Analysis.

Kinetic parameters calculation and analysis with Petromod 2012, PetroKinetics.

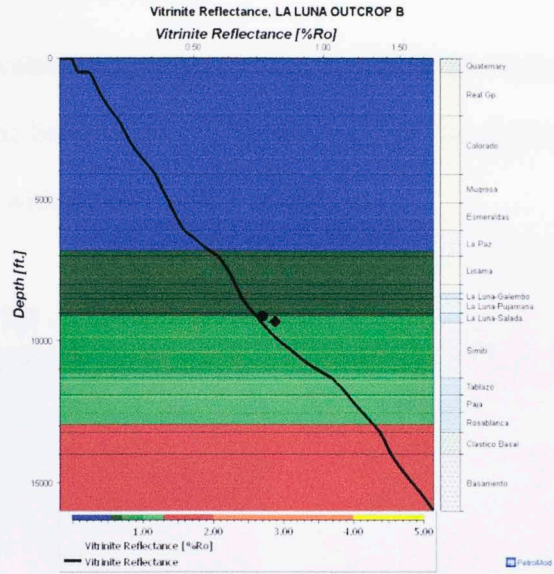




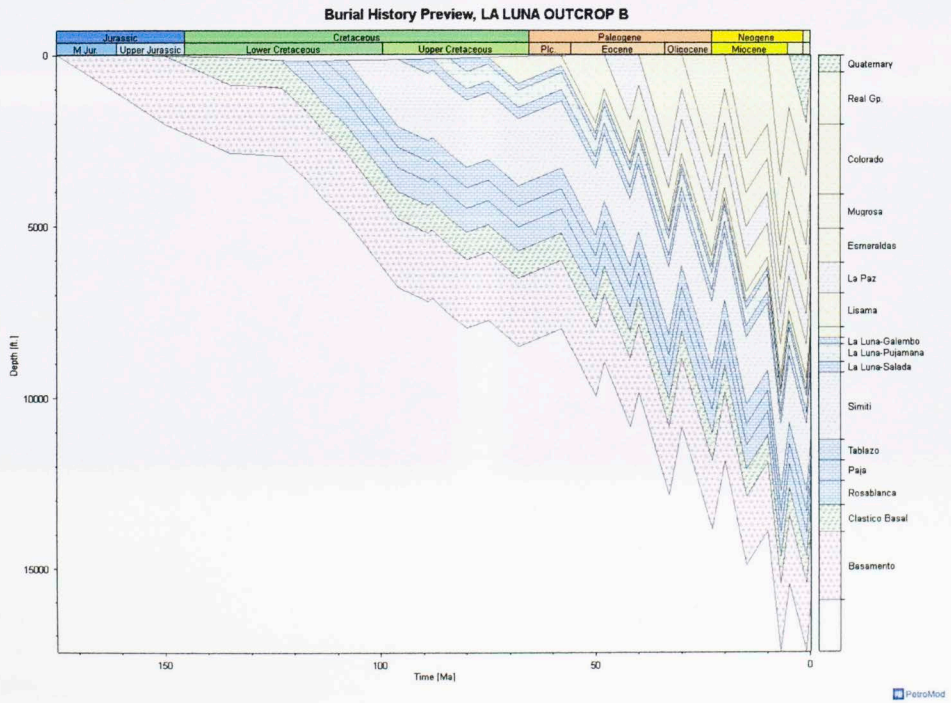


# Kinetic Analysis. 1D Basin modeling

## Maturity model.



## Burial History model



## APPENDIX II. Lithofacies Characterization

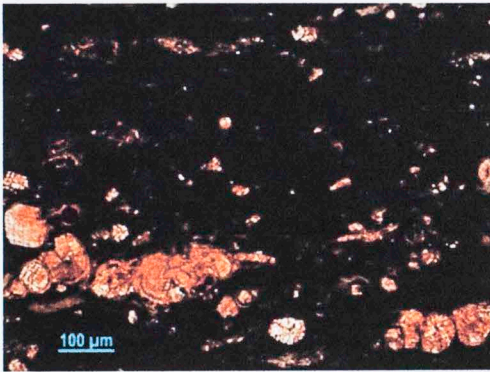
### Appendix II. Thin Section description

#### Facies S-i. CAR M-3 and CAR M4.

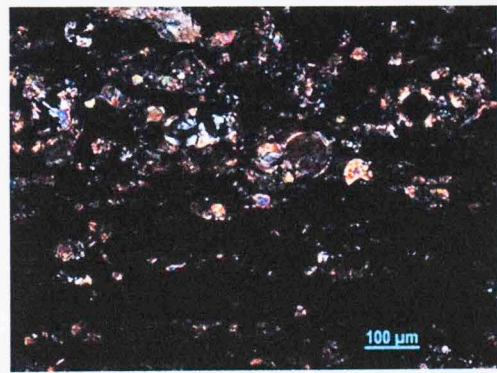
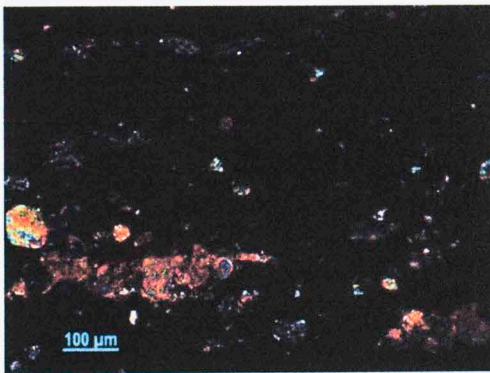
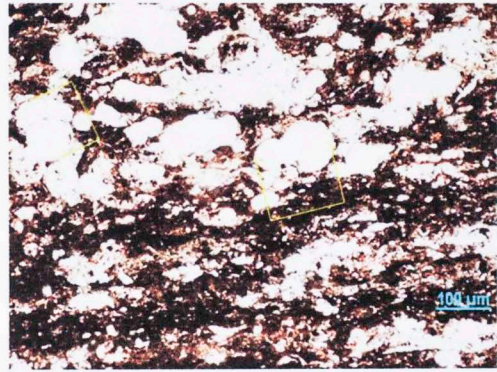
CAR M-3 is calcareous shale with abundant *Globigerina* replaced with calcite.

CAR M-4 is a micritic limestone with abundant *Globigerina* also replaced with calcite and matrix saturated with bitumen.

CAR M-3



CAR M-4

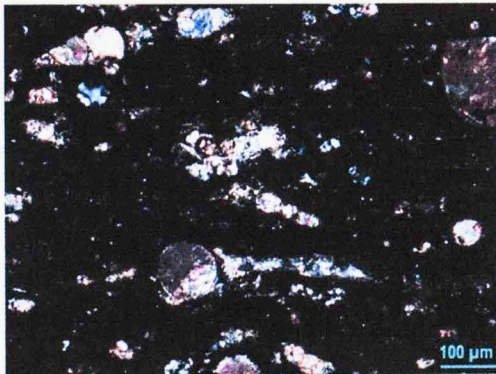
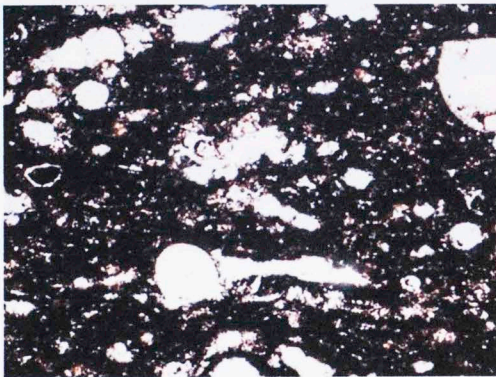




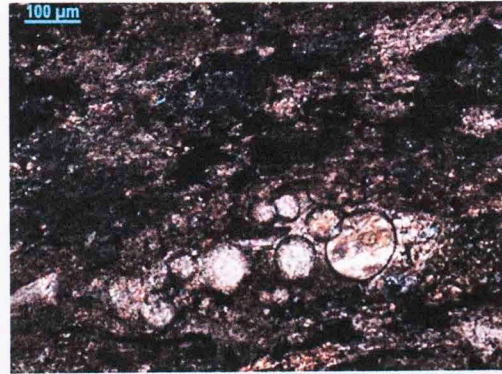
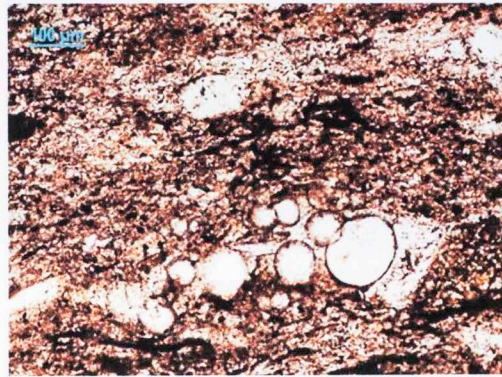
**Facies S-ii. CAR M-5 and CAR M13.**

CAR M-5 is calcareous shale with abundant *Globigerina* replaced with calcite, the matrix is saturated with bitumen. CAR M-13 is micritic limestone with abundant quartz content and also *Globigerina* replaced with calcite and matrix saturated with bitumen.

**CAR M-5**



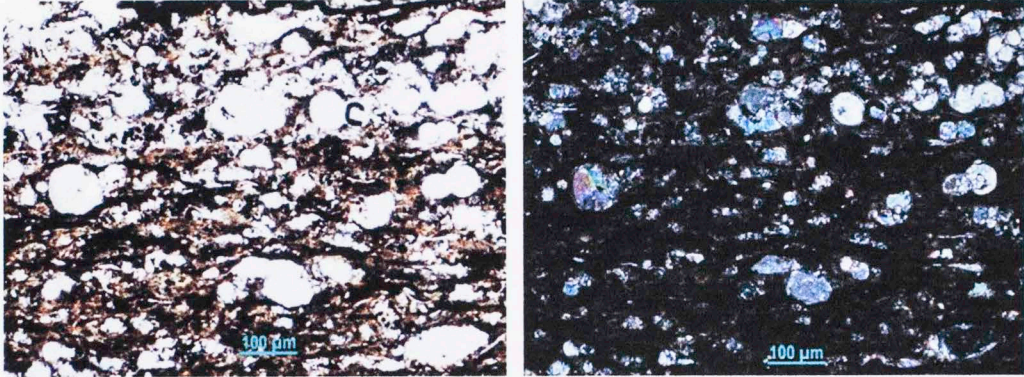
**CAR M-13**



**Facies P-iii. CAN M-5**

CAN M-5 is micritic limestone, with detrital quartz content and also *Globigerina* replaced with calcite and matrix saturated with bitumen.

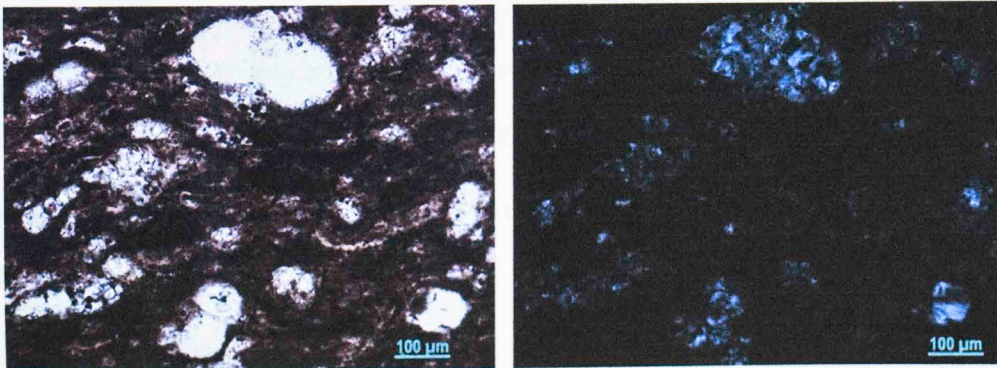
**CAN M-5**



**Facies P-iv. CAN M-8**

CAN M-8 is siliceous mudstone, with abundant quartz content and also *Globigerina* replaced with possible dolomite (replacement process) and matrix saturated with bitumen.

**CAN M-8**

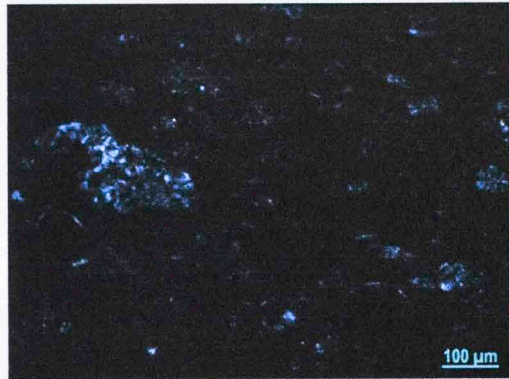
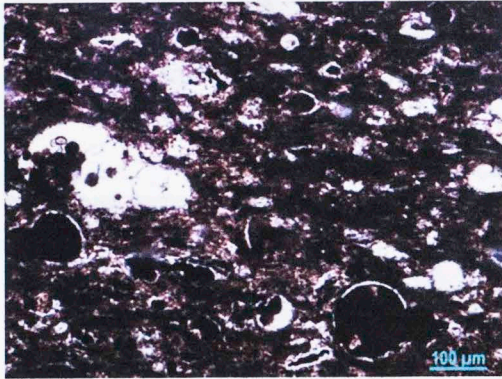




### **Facies P-v. CAN M-15**

CAN M-15 is black shale, with abundant quartz content and also *Globigerina* replaced with possible dolomite (replacement process) and filled with bitumen, the matrix is also saturated with bitumen.

### **CAN M-15**



### **Facies G-vi. QLS M-8.**

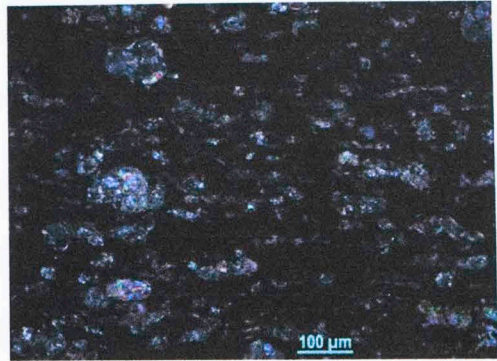
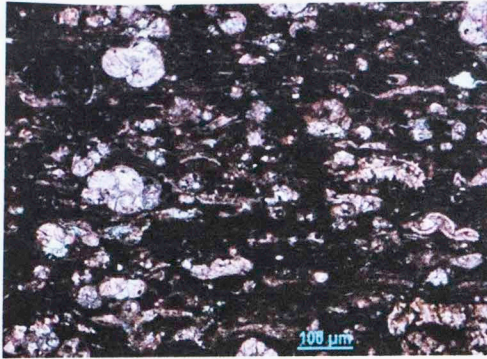
QLS M-8 is micritic Packstone, with quartz content and also *Globigerina* replaced with possible dolomite (replacement process) and filled with bitumen, the matrix is also saturated with bitumen.

### **Facies G-vi. QLS M-6 and QLS M-3.**

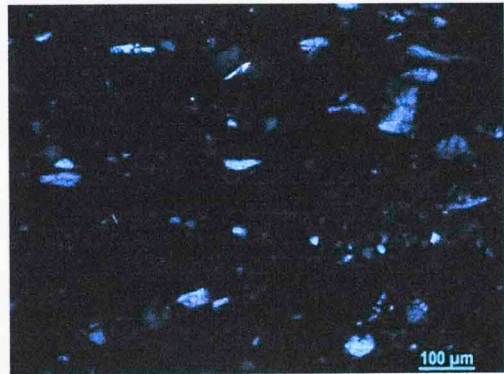
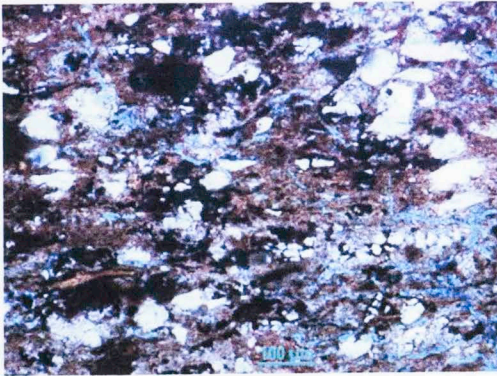
QLS M-6 is calcareous shale, with calcite fragments. Not observed any *Globigerina* fossils. Matrix is clay rich. QLS M-3 corresponds to black shale, with *Globigerina* replaced by calcite and filled with bitumen, the matrix is also saturated with bitumen.



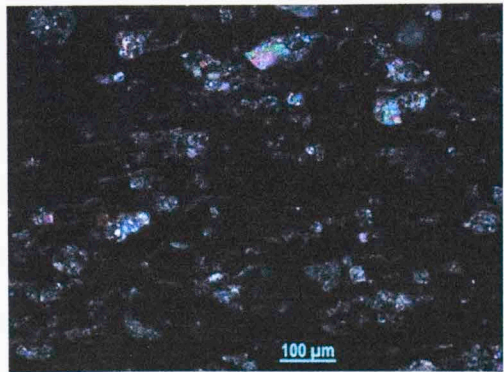
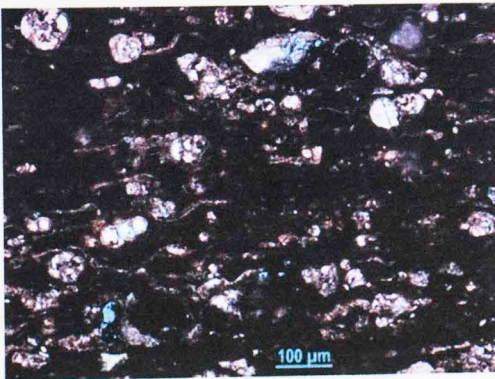
QLS M-8



QLS M-6



QLS M-3



### Appendix III

#### **Fecal Pellets and their significance in unconventional resource shales: Generation of hydrocarbons.**

Fecal pellets, the excrement of marine organisms containing both undigested organic matter and pores, are common in many shales and may provide a significant source of gas during burial. Such pellets are protected in the gut of animals by a membrane, which also helps preserve the contents from biological, geochemical, or physical disruption and dissolution (Porter and Robbins, 1981). The preservation of pellets in sediments occurs in low energy, anoxic or hypersaline environments which reduce or exclude benthic forms and minimize microbial activity.

Since single pellets cannot currently be isolated from shales, to test their potential as a gas source, experiments were conducted on fecal material from modern freshwater fish and shrimp using Micro-Scale Sealed Vessel analysis (MSSV), an artificial maturation technique that simulates petroleum generation from a source rock in a closed system (Horsfield et al., 1989). This method allows the oil and gas generation from the primary cracking of kerogen and the generation of gas from the secondary cracking of oil and bitumen. Primary products may be recombined by aromatization/condensation reactions into a gas-prone residue and the cracking at high maturity of pyrobitumen extends gas generation beyond the conventional secondary cracking window and provides significant quantities of methane.



For this specific case, simulations were run within the oil and gas generation windows. The primary cracking resulted in the release of significant C<sub>1</sub>-C<sub>5</sub> compounds and also C<sub>6</sub>-C<sub>20</sub> (liquid hydrocarbon traces). The secondary cracking process produced more methane and C<sub>2</sub>+ gases than liquids. The liquids that were produced suggest these modern animals don't provide a complete digestion process of proteins, carbohydrates, and lipids that constitute their primary food, thus these molecular constituents are incorporated into their excrement. If this analogy is correct, fecal pellets might be an important contributor to gas in unconventional resource shales.

### **Key words**

Source Rock, MSSV, pyrolysis, gas, liquids, fecal pellets.

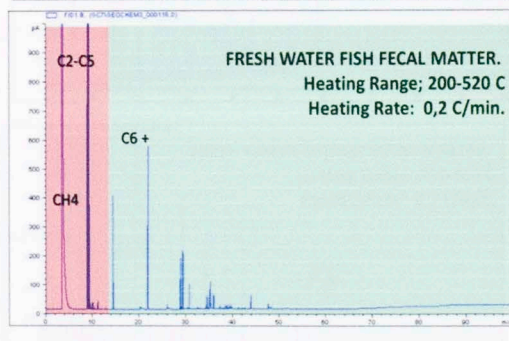
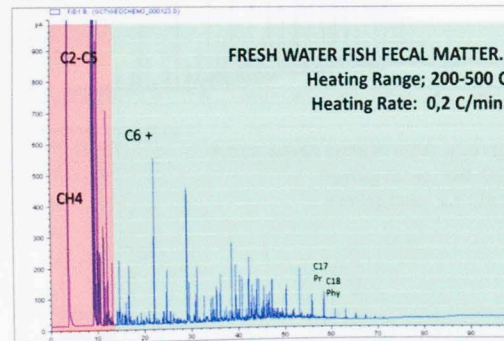
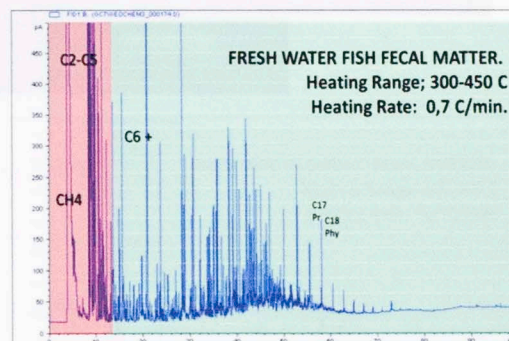
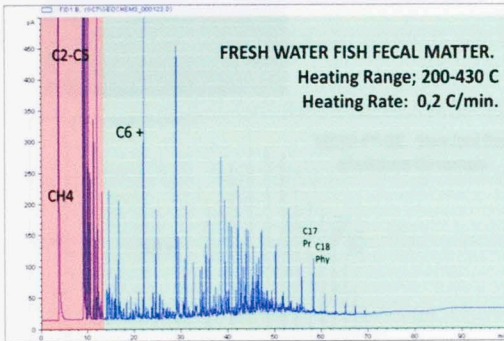
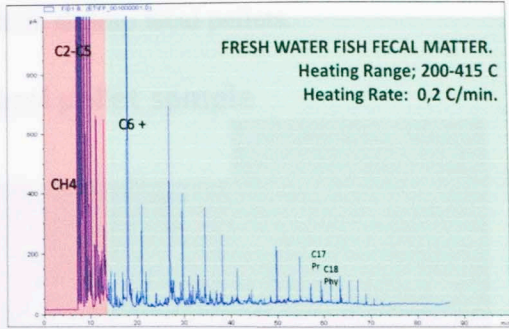
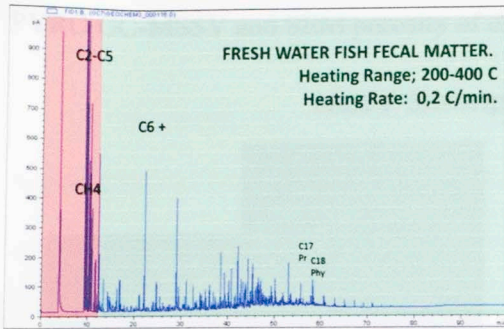
### **References**

Horsfield, B., U., Disko, F., Leistner, 1989, The microscale simulation of maturation: Outline of a new technique and its potential applications: *Geologische Rundschau*, v. 78, p.361-374.

Porter, K.G, & Robbins, E.I., 1981. Zooplankton fecal pellets link fossil fuel and phosphate deposits. *Science*, 212, 931-933.



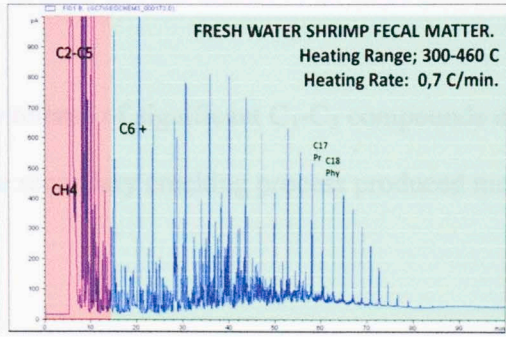
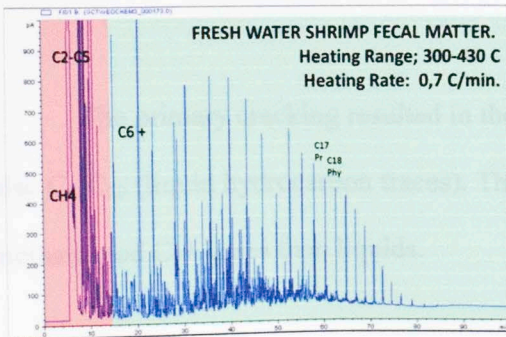
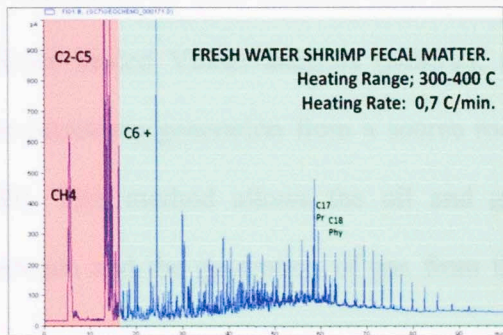
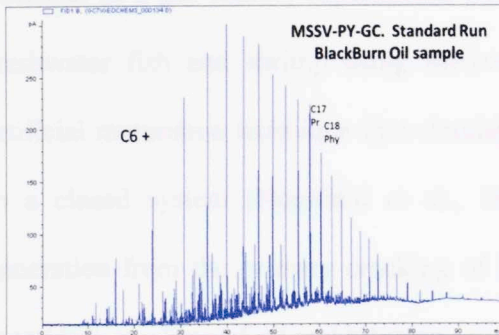
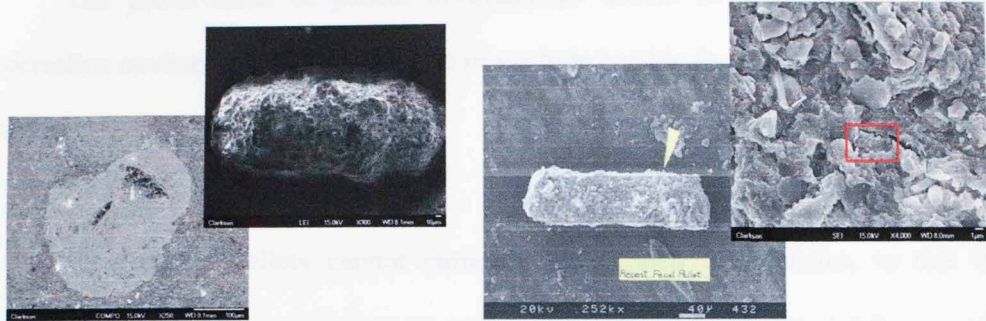
# Fish Fecal Pellet sample. MSSV-GC results.



## Shrimp Fecal Pellet sample. MSSV-GC results.

PYRO GC-MSSV and SEM porosity of daphnia shrimp fecal pellets.

### MSSV Shrimp fecal pellet sample



**Conclusions: Fecal Pellets and their significance in unconventional resource shales: Generation of hydrocarbons**

The preservation of pellets in sediments occurs in low energy, anoxic or hypersaline environments, which reduce or exclude benthic forms and reduce microbial activity.

Since single pellets cannot currently be isolated from shales, to test their potential as a gas source, experiments were conducted on fecal material from modern freshwater fish and shrimp using Micro-Scale Sealed Vessel analysis (MSSV), an artificial maturation technique that simulates petroleum generation from a source rock in a closed system (Horsfield et al., 1989). This method allows the oil and gas generation from the primary cracking of kerogen and the generation of gas from the secondary cracking of oil and bitumen.

The primary cracking resulted in the release of significant C<sub>1</sub>-C<sub>5</sub> compounds and also C<sub>6</sub>-C<sub>20</sub> (liquid hydrocarbon traces). The secondary cracking process produced more methane and C<sub>2</sub>+ gases than liquids.

The liquids that were produced suggest these modern animals don't provide a complete digestion process of proteins, carbohydrates, and lipids that constitute their primary food, thus these molecular constituents are incorporated into their excrement. If this analogy is correct, fecal pellets might be an important contributor to gas in unconventional resource shales.